IR 88-3791

CANCELLED

UNAVAILABLE FOR BINDING

NBSIR 88-3792

Investigation into the Ashland Oil Storage Tank Collapse on January 2, 1988

Center for Building Technology
National Engineering Laboratory

Metallurgy Division
Institute for Materials Science and Engineering

U.S. DEPARTMENT OF COMMERCE
NATIONAL BUREAU OF STANDARDS

NBSIR 88-3792

Investigation into the Ashland Oil Storage Tank Collapse on January 2, 1988

John L. Gross
Felix Y. Yokel
Richard N. Wright
A. Hunter Fanney

Center for Building Technology
National Engineering Laboratory

John H. Smith
George E. Hicho
T. Robert Shives

Metallurgy Division
Institute for Materials Science and Engineering

Issued June 1988

U.S. DEPARTMENT OF COMMERCE
NATIONAL BUREAU OF STANDARDS, Ernest Ambler, Director

ABSTRACT

On January 2, 1988, a four million gallon capacity oil storage tank at the Ashland Petroleum Company Floreffe Terminal near West Elizabeth, Pennsylvania, collapsed as it was being filled to capacity for the first time since it was reconstructed at the site. The tank had been dismantled in Cleveland, Ohio, after more than 40 years of service and reconstructed at the Floreffe site in 1986. The National Bureau of Standards (NBS) conducted an independent investigation of the physical causes of the Ashland Tank collapse. Data were obtained from NBS field observations, laboratory and analytical studies, from the investigation of the Pennsylvania Tank Collapse Task Force appointed by the Governor of Pennsylvania, and from the Battelle Columbus Division investigation sponsored by the Ashland Petroleum Company. The cause of the failure was determined to be brittle fracture, initiating from a flaw existing prior to the reconstruction of the tank. Complete rupture of the tank shell occurred because the steel of the shell was of inadequate toughness at the operating temperature to prevent brittle fracture propagation. The steel did not meet the fracture toughness requirements of the American Petroleum Institute Standard 650, 1984, "Welded Steel Tanks for Oil Storage," which was effective at the time of reconstruction of the tank. The collapse shows the importance of using steel with sufficient fracture toughness to prevent propagation of a brittle fracture in tanks whose sudden failure would mean unacceptable human, environmental or economic losses.

Keywords: Brittle fracture; collapse; failure investigation; fracture analysis; steel; tanks; welded steel tanks

EXECUTIVE SUMMARY

Introduction

On January 2, 1988, a four million gallon capacity oil storage tank at the Ashland Petroleum Company Floreffe Terminal near West Elizabeth, Pennsylvania, collapsed as it was being filled to capacity for the first time since it was reconstructed at the site. As a result of the collapse, about one million gallons of oil spilled into the Monongahela River approximately 25 miles upstream from Pittsburgh. The spill contaminated the water supply of many municipalities that draw their water from the Monongahela and Ohio rivers.

The Ashland tank that failed was a welded steel tank that was reported to have been in service near Cleveland, Ohio, for over 40 years. It was reported to have been dismantled in 1986, reconstructed at the Ashland Floreffe Terminal site, and placed in service in August 1987. The tank was 120 feet in diameter and 48 feet high and had a column-supported shallow conical roof and a flat bottom. The tank rested directly on a crushed limestone foundation and a compacted soil fill.

Congressman Doug Walgren, the Fire Marshal of Allegheny County, and the Governor of Pennsylvania requested the National Bureau of Standards (NBS) to conduct an independent technical investigation into the cause of the collapse. Data were obtained from: NBS field observations, laboratory and analytical studies; the investigation of the Pennsylvania Tank Collapse Task Force appointed by the Governor of Pennsylvania; and the Battelle Columbus Division investigation sponsored by the Ashland Petroleum Company.

The objective of the NBS investigation was to determine the most probable cause of failure of the tank. The investigation included: on-site investigation and debris identification, subsurface exploration and foundation evaluation, structural analysis, thermal analysis, materials characterization, fracture analysis, review of procedures and methods used in dismantling, transporting and reconstructing the tank, review of documentation related to terminal operation, review of eyewitness accounts of the collapse, review of applicable standards, and determination of conformance with them.

The NBS investigation was limited to the technical aspects of the failure and determination of properties, practices and procedures which may have contributed to the failure. Issues specifically not addressed in this investigation include assignment of responsibility for the failure, performance of the spill containment system, and conditions of other oil storage tanks.

Description of Conditions at Failure

The oil level in the reconstructed tank was reported never to have exceeded 37 ft prior to January 2, 1988 when the tank collapsed. On that morning Ashland personnel began to fill the tank to 46 ft. The Ashland terminal operator reported that at approximately 5 pm the level of oil in the tank was 45 ft 10 in. He then returned to the office when, within 5 minutes of taking the reading, the tank collapsed.

The NBS team of investigators arrived at the site of the collapse on January 6, 1988. The site appeared to be undisturbed, except for removal of spilled oil. The tank wall had split completely open and the once-cylindrical shell had unwrapped until it was nearly straight. The tank shell came to rest on top of a dike approximately 120 ft from its original location. The shell was separated from the tank bottom which, except for two large tears in the lap welded seams, remained relatively intact. The tank top was severely crumpled with several large tears but was in one piece. The top remained attached to the shell opposite the vertical split. Debris from the roof support system lay scattered mostly within the dike area.

The flat surface of the fracture of the shell indicated that it was a result of brittle fracture. Chevron-like markings were evident on the fracture surface. These pointed to a flaw extending about two-thirds of the way through the plate thickness and located about 8 ft above the base of the tank, just below the horizontal weld between the first and second shell courses, and just to the left (looking from the outside of the tank) of a vertical seam in the second course. The chevron markings, pointing to the flaw from above and below, are convincing evidence that the fracture of the shell initiated at this flaw.

Analysis Results

NBS metallurgical investigations defined the properties of the base metal of the shell steel (where it was unaffected by welding), the weld deposits from original construction and reconstruction, and the heat-affected zones of the base metal adjacent to welds.

Battelle conducted analyses of the material in the vicinity of the flaw and made results available to NBS. The flaw had a length of 0.74 in and was located in the base metal at the top of the first course of the shell just below the old weld deposit. The flaw lay near the interior surface of the shell, in a vertical plane perpendicular to the shell surface. A carburized layer on the surface of the flaw showed that it was created in a cutting operation; this indicates the flaw existed prior to the reconstruction at Floreffe. The base metal adjacent to the flaw showed a hardness substantially higher than that of normal base metal indicating embrittlement caused by the cutting that produced the flaw and by subsequent welding adjacent to the flaw.

Battelle made residual stress measurements in the base metal adjacent to a T-weld (intersection of a vertical and a horizontal weld) remote from the fracture but similar to the T-weld at which the fracture initiated. The maximum measured residual tensile circumferential stress was 15 kilo-pounds (thousand pounds) per square inch (ksi).

The stress in the tank shell at the flaw at the time of failure was about 30 ksi based on the measured residual stress and the stress NBS calculated from the level of oil in the tank. The upper limit would be the yield point of the steel, about 34 ksi, at which the steel would undergo large, inelastic deformations, and the lower limit about 15 ksi if the residual stress were extraordinarily small. According to NBS analysis, the temperature of the shell steel was about 32° F at the time of failure.

Prior experience with failures -- Liberty ships which split open in World War II and welded tank failures in the 1940s -- includes many brittle fractures initiated in steels similar to that of the Ashland tank at similar flaws and stresses. Extensive laboratory studies conducted in the United States, United Kingdom and Japan show that brittle fractures initiate at stresses well below

the yield point in base metal embrittled by welding near flaws of dimensions similar to that found in the Ashland tank. Stress in the Ashland tank at the flaw where the fracture initiated approached the yield point. Nearby stresses due to the oil in the tank were about half the yield point. These stresses are consistent with initiation of brittle fracture in the embrittled zone and continued fracture propagation beyond the embrittled zone because the shell temperature was far below its ductile to brittle transition temperature as determined by drop-weight nil-ductility and Charpy-V-notch tests.

Fracture mechanics analysis showed that the fracture toughness of the base metal exceeded the calculated stress intensity due to the flaw, the stresses due to oil in the tank and residual stresses. However, the increased hardness measurements in the heat-affected zone of the base metal adjacent to the flaw indicate a marked reduction of the fracture toughness from that of the unaffected base metal. This embrittlement allowed initiation of the fracture at the stress intensity in the vicinity of the flaw at the time of fracture.

Conformance with Standards

The nationally recognized current standard for above-ground, atmospheric, welded steel tanks is the American Petroleum Institute Standard 650, *Welded Steel Tanks for Oil Storage*, Seventh Edition, Revision 1, 1984 (hereafter denoted as API 650). API 650 does not explicitly address the reconstruction of existing tanks. It does, however, include provisions for the use of "materials on hand which are not identified as complying with any listed specification." In NBS's opinion, API 650 can be used for reconstruction of a tank when documentation is not available for the steel. In these circumstances, API 650 requires measurements of steel properties.

The steel of the tank shell did not conform to any of the steels allowed in API 650. Its chemical and mechanical properties correspond to ASTM A 283 grade D steel. API 650 allows use of ASTM A 283 grade C steel, which has a lower tensile strength. API 650 specifies toughness requirements. For the 5° F design temperature conditions of the Floreffe site, ASTM A 283 grade C steel should be semi-killed (deoxidized) and possess a Charpy-V-notch toughness of 15 ft-lb. The Charpy-V-notch toughness for specimens taken from the tank was 6 ft-lb or less for temperatures below 40° F. Thus, the toughness of the

material was seriously deficient.

Conclusions

The failure of the tank was caused by a brittle fracture that initiated at a flaw in the tank shell about 8 ft above the base and just below the horizontal weld between the first and second courses of steel. The fracture propagated to complete rupture of the tank shell because the steel lacked sufficient toughness to arrest a propagating fracture at the temperature and stresses existing in the tank shell.

Failure was reported to have occurred as the tank was being filled to capacity for the first time at the Floreffe site. The temperature of the shell was about 32° F, and the calculated stress at the initiating flaw about 13.7 ksi. These conditions are fully consistent with initiation and complete propagation of brittle fracture considering the flaw size, embrittlement of adjacent steel, presence of residual stresses, and the low fracture toughness of the shell steel at 32° F. The shell steel did not meet the fracture toughness requirements of API 650.

The flaw at which the fracture initiated was determined by Battelle to be present prior to the reconstruction of the tank at the Floreffe site. Deposits on the surface of the flaw indicate it was formed during a cutting operation.

Although the weld quality did not conform to API 650, the weld quality was not a contributing factor in the initiation or propagation of this fracture. However, welding adjacent to the flaw contributed to embrittlement of the metal.

Foundation conditions were investigated to determine if instability or irregular settlement of the foundation might have increased stresses in the shell. No evidence was found of foundation instability or excessive settlement.

Lessons Learned

This study focused on the tank that collapsed at the Floreffe Terminal on January 2, 1988, and on the standards applicable to its dismantling and reconstruction. In spite of this limited scope, lessons of general significance have been learned from this failure, and relearned from earlier, similar failures.

The catastrophic failure of the Ashland tank resulted from a flaw that might have been, but was not, detected in tests for welding quality, and the use of steel that did not possess sufficient fracture toughness to arrest a fracture that initiated at a localized flaw. While there are many reasons for control of weld quality, it is not feasible to guarantee the absence of localized defects by control of fabrication and detailed inspection for defects during fabrication. Neither is it feasible to guarantee the absence of localized defects during service by recurrent inspections. Therefore, it is advisable to use steel of adequate toughness to provide "leak before break" fail-safe behavior. If a crack is initiated, due to a flaw or local damage in service, in a tank with steel of adequate fracture toughness, the crack will arrest, the tank will leak, normal spill-control measures will confine the spread of contents, and the tank can be repaired, all without catastrophic consequences.

Available standards should be reviewed to identify those calling for sufficient fracture toughness to prevent catastrophic brittle fracture at design stresses and temperatures. This study found the provisions of API 650 (1984) to be sufficient for the structural steels in its Materials Group I. Compliance with sufficient fracture toughness provisions should be required for steel to be used in construction or reconstruction of tanks, or for changes in service conditions.

There is concern for the safety of existing tanks whose catastrophic failure would cause unacceptable human, environmental or economic losses. If documentation exists to show that the steel of an existing tank meets sufficient fracture toughness provisions, the concern will be alleviated. If documentation shows inadequate fracture toughness, remedial actions should be taken. Possible remedial actions include conversion to adequately high temperature service, retirement, or installation of crack arresters.

Test and assessment protocols should be developed for assessing the fracture safety of potentially hazardous existing tanks that lack adequate documentation for definition of the fracture toughness of their steel.

ACKNOWLEDGEMENTS

Special appreciation is extended to Mr. Leonard C. Smith, NBS Chief Metallographer for exceptional skill and care taken in the metallographic evaluation and hardness tests conducted for this investigation. In particular, the specific choice of areas in the microstructures to be examined and the skill and judgement used in presenting the results were a key factor in leading to the conclusions reached in this report.

Thanks also go to Dr. William Stone of the Structures Division of the Center for Building Technology for performing the computer modeling, analysis and post-processing of the symmetric model of the tank for the foundation settlement analysis.

A special thanks goes to Mr. F. Keith Mackley and Mr. Raymond J. Mele of the National Engineering Laboratory (NEL) Graphics for their work in producing the drawings and labeled photographs and for performing the layout for the report.

TABLE OF CONTENTS

LIST OF FIGURES

LIST OF TABLES

1.0 INTRODUCTION

1.1 Background

On January 2, 1988, a four million gallon capacity oil storage tank at the Ashland Petroleum Company Floreffe Terminal collapsed as it was being filled (see Figure 1.1). The Ashland Floreffe Terminal is located near West Elizabeth, Pennsylvania on the Monongahela River (see Figure 1.2). A plan of the terminal indicating the location of the collapsed tank relative to Route 837 and the shoreline of the Monongahela River is shown in Figure 1.3. As a result of the collapse, an estimated one million gallons of oil spilled into the Monongahela River approximately 25 miles upstream from Pittsburgh. The spill contaminated the water supply of many municipalities that draw their water from the Monongahela and Ohio Rivers.

The tank that failed was a reconstructed steel tank that had originally been in service near Cleveland Ohio for over 40 years. It had recently been dismantled and reconstructed at the Ashland Floreffe Terminal site near Pittsburgh. The tank was 120 ft in diameter and 48 ft high and had a column-supported shallow conical roof and a flat bottom. The tank rested directly on a crushed limestone and compacted fill foundation.

The tank was being used to store No. 2 fuel oil and had been in service at its new location since August of 1987. Oil was brought to the Ashland terminal by barge on the Monongahela River and pumped into the storage tank. The failure occurred as the tank was being filled to capacity for the first time.

Congressman Doug Walgren, the Fire Marshal of Allegheny County and the Governor of Pennsylvania requested the National Bureau of Standards (NBS) to conduct an independent technical investigation into the cause of the collapse. A team of NBS investigators arrived at the site of the collapse on January 6, 1988. (Access to the site prior to this date was not possible due to the presence of oil within the dike area surrounding the collapsed tank.) The investigation was conducted under public law which gives NBS the authority to conduct independent investigations into the causes of structural failures which affect the general public and which have broad importance.

1.2 Objective and Scope of Investigation.

The objective of this investigation was to determine the most probable cause of failure of the Ashland tank. The investigation included:

- o On-site investigation and debris identification
- o Sub-surface exploration and foundation evaluation
- o Materials characterization
- o Fracture analysis
- o Review of procedures and methods used in dismantling, transporting and reconstructing the tank
- o Review of documentation related to terminal operation
- o Review of eyewitness accounts of the collapse
- o Review of applicable codes and standards and determination of compliance with them.

The investigation was limited to the technical aspects of the failure and a determination of practices and procedures which may have been contributory to the failure. Issues not addressed in this investigation include:

- o Assignment of responsibility for the failure
- o Performance of the spill containment system
- o Recommendations for either new standards or changes to existing standards to prevent future occurences of this type of failure.

1.3 Cooperation with Other Organizations

Following the collapse of the oil storage tank, the Governor of the Commonwealth of Pennsylvania appointed a task force to investigate the collapse and make recommendations to prevent further occurrences of similar accidents. The Pennsylvania Tank Collapse Task Force (hereafter referred to as the Pennsylvania Task Force) worked closely with NBS and shared information related to the investigation. This information included: records provided to the Pennsylvania Task Force by Ashland Petroleum Company (hereafter referred to as Ashland); information obtained by staff investigators through personal interviews; and test data obtained from soil samples taken under the direction of the Pennsylvania Task Force. NBS also worked closely with the Advanced Technology for Large Structural Systems (ATLSS) Research Center at Lehigh University, which provided technical assistance to the Pennsylvania Task Force on the structural and metallurgical aspects of the tank failure.

In addition, Battelle Columbus Division (hereafter referred to as Battelle), contracted by Ashland to conduct an investigation into the cause of the collapse, provided valuable metallurgical data and characterization of the fracture surface. Under an agreement worked out among NBS, Ashland and Congressman Walgren, both fracture surfaces were shipped to Battelle for preservation and analysis. Thus, all information related to the fracture surface was provided to NBS by Battelle. NBS investigators personally observed the taking of samples by Battelle and the testing and fractography conducted at the Battelle laboratory.

1.4 Organization of the Report

Chapter 2 contains a description of the tank and its history including dismantling of the tank at its previous location and reconstruction at the Ashland Floreffe Terminal.

Chapter 3 is a description of the collapse including activities and conditions preceding the collapse, eyewitness accounts of the collapse, and observations of the debris made during the initial site investigation.

Chapter 4 contains a description of the foundation and site and describes the subsurface exploration and foundation analysis.

Chapter 5 presents the results of an analytical study to determine the stresses in the tank.

Chapter 6 addresses the prediction of the temperature in the tank wall at the time of collapse.

Chapter 7 presents the results of metallurgical tests conducted to characterize both the base metal and weld metal. The tests include chemical analyses, tensile tests, notch sensitivity tests, hardness tests, fracture toughness tests and residual stress determination.

Chapter 8 presents several fracture analyses, based on the metallurgical test results and tank shell stresses determined by analysis, to determine why the fracture of the tank shell initiated and why it propagated to complete rupture.

Chapter 9 addresses the issue of conformance with applicable codes and standards, limited to those aspects relevant to structural performance.

Chapter 10 presents NBS's findings regarding the cause of failure and lessons learned from the failure.

Figure 1.1 - Aerial View of the Ashland Tank Collapse, January 4, 1988.
(Photo Courtesy of Vince Musi -- Pittsburgh Press/SIPA)

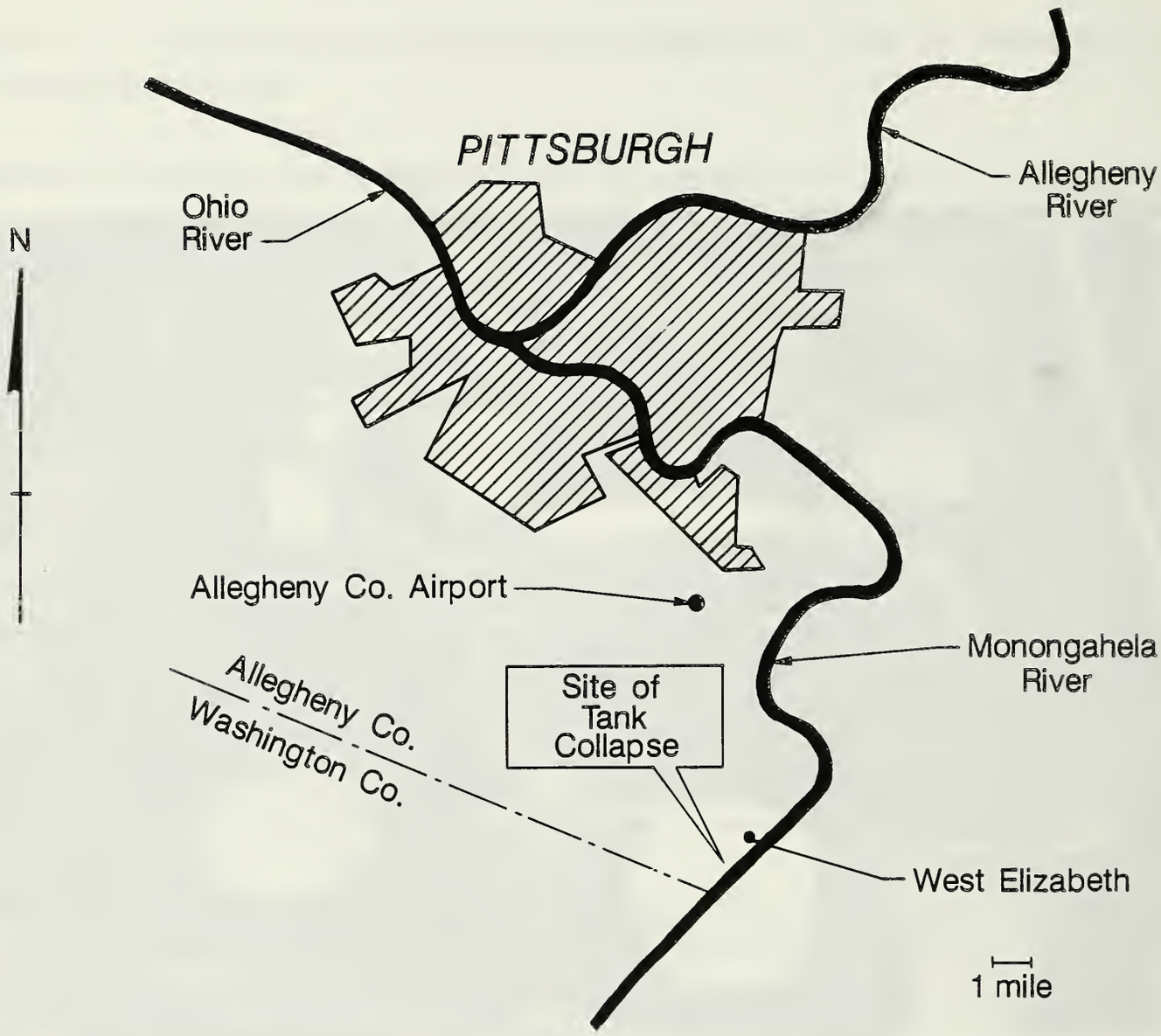

Figure 1.2 - Site of the Tank Collapse

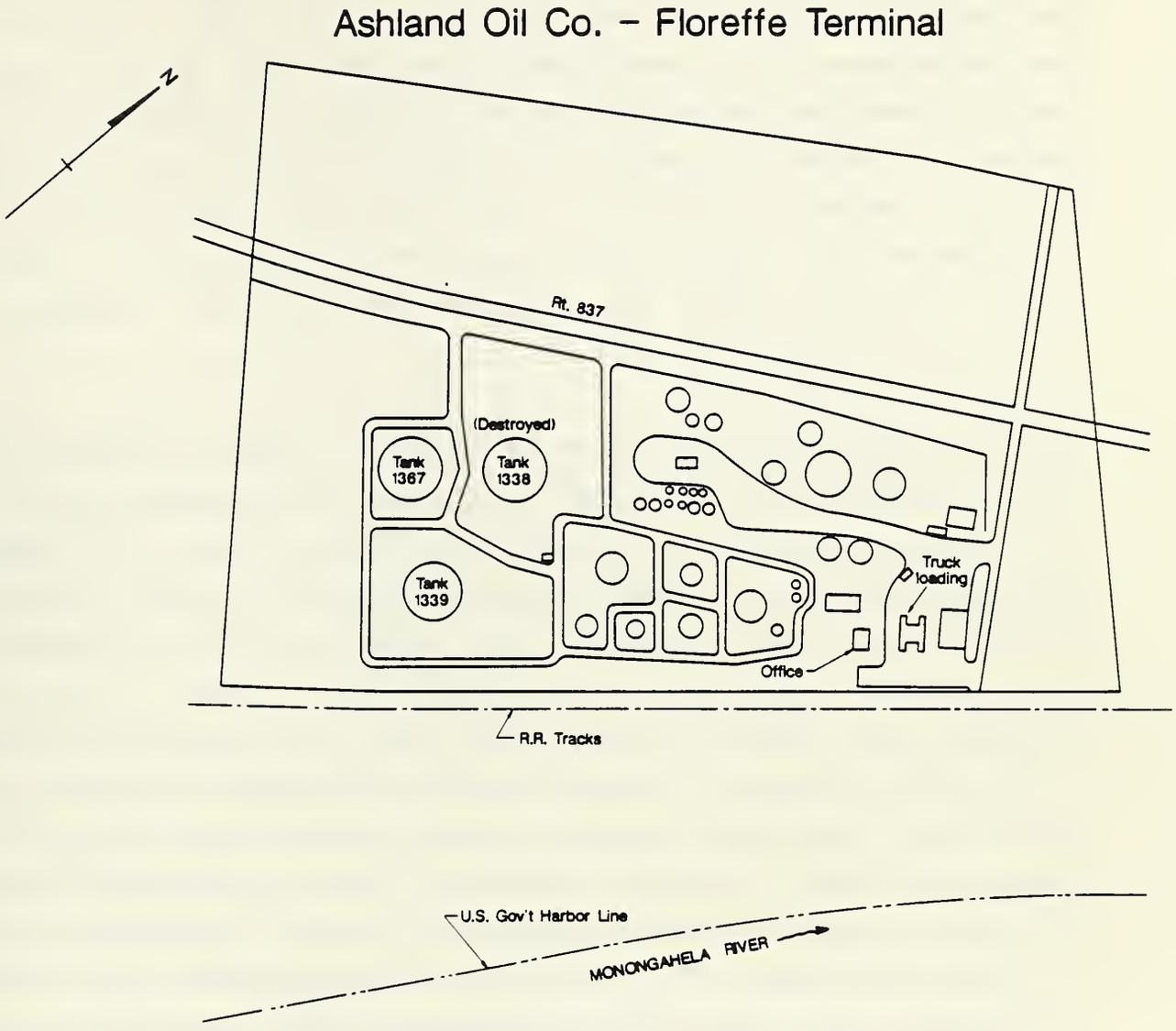

Figure 1.3 - Plan of the Ashland Floreffe Terminal

2.0 DESCRIPTION OF THE TANK

2.1 General Description

A description of the tank and details of its history were compiled from a variety of sources. Since no drawings of the tank were available, the physical description of the tank was reconstructed from examination and measurements of the debris. In addition, no cutting or welding specifications were available from the erector, therefore, the information which follows was obtained by interviewing individuals with first-hand knowledge of the procedures used in dismantling and reconstructing the tank. The Pennsylvania Task Force conducted the interviews and gave NBS access to all of their findings.

The Ashland tank had a nominal capacity of 96,000 barrels or four million gallons. It was a welded steel tank with a flat bottom and shallow conical roof (see Figure 2.1). The roof was 3/16-in plate with lap welded joints. It was supported by a system of rafters and girders which in turn were supported by columns resting on the tank bottom. The cylindrical shell was 120 ft in diameter and 48 ft high. It consisted of six shell courses, each approximately 8 ft high and 32 ft long, which were butt welded. The thickness of each shell course was measured by NBS and results are shown in Table 2.1. Corrosion of the tank wall occurred over the service life of the tank so the original plate thicknesses can only be assumed; Table 2.1 shows the assumed original plate thicknesses. The shell thicknesses shown in Figure 2.1 are the assumed original plate thicknesses before corrosion. The tank bottom was 1/4-in lap welded, steel plate which was attached to the first shell course by a double fillet weld (fillet welds on both sides of the shell).

A structural framework supported the shallow conical roof. The framework consisted of 120 roof rafters spanning in the radial direction, two rings of column-supported girders and the tank shell (see Figure 2.2). There were five columns supporting the inner ring of girders and 10 columns supporting the outer ring. The columns consisted of two channel sections welded together so that the flange of a 9-in channel was welded to the back of the web of a 12-in channel. The columns rested directly on the tank bottom and the load was

distributed by the "H" shaped column base shown in Figure 2.3. The girders comprising the rings consisted of 15-in channel sections which spanned between the columns. They were welded to a cap plate on top of each column as shown in Figure 2.4. The girders formed five- and ten-sided polygons for the inner and outer support ring, respectively. The rafters, which were 8-in channels, usually were connected to the girders by means of clip angles riveted to the girder (original construction) and welded to the rafter. The rafters were attached to the tank shell by means of plates as shown in Figure 2.5.

2.2 History of Operation

The tank that collapsed had been recently moved from a site near Cleveland, Ohio, and reconstructed at the Ashland Floreffe terminal. It replaced an aging tank designated as No. 1338. The old tank was approximately 115 ft in diameter and 40 ft high and had a capacity of 74,000 barrels. It was reported to be a riveted tank and had a recent history of leaking. An inspection by Ashland determined that the old tank would be too expensive to repair and it needed to be replaced.

A 96,000 barrel tank that was out of service was located at a site called Whiskey Island near Cleveland, Ohio. This tank, designated as No. 16, had been built about 1940 and had most recently been used to store No. 6 oil, a viscous petroleum product which is generally maintained at a temperature of approximately 150° F. The tank was covered with about 3 inches of foam insulation in 1981. In March 1986, the Whiskey Island tank was inspected to determine if it was in good enough condition to replace the aging 74,000 barrel tank at the Floreffe terminal. The tank was visually inspected and the thicknesses of the first and sixth shell courses were measured ultrasonically. The inspection report indicated that the tank shell was not severely corroded and could be re-used. The bottom plate, however, was found to be badly corroded and the report recommended that the bottom plate be replaced with new steel. The decision was therefore made by Ashland to scrap tank No. 1338 at the Floreffe site and replace it with tank No. 16 from the Whiskey Island site.

2.3 Dismantling of the Tank

Dismantling of tank No. 16 at Whiskey Island began in May 1986, and took less than four weeks. First the insulation was removed by hand along the weld seams. Then, starting from the bottom, the tank was cut into sheets. The cuts were made just to the right of the vertical welds, looking from the outside of the tank, and above the horizontal welds. For the vertical cuts, a series of cuts about two feet long were made and an uncut section of about three inches was left to hold the plates together. This remaining uncut portion of the tank wall was known by the welders as a "tack". For the horizontal cuts, a series of cuts was made, each four feet long, and again a three-inch "tack" was left. At the intersection of a horizontal and a vertical cut, a "tack" of about six inches was left to hold the plates together. After cutting the first shell course, the scaffolding was moved up to the second course and the procedure was repeated. This continued until all of the tank wall had been cut. Cuts were made manually with no guide using an acetylene torch. As each sheet was cut, the shell course number was marked on the inside of the plate and the edges were marked with an identifying seam number so the tank could be reassembled.

Next, a crane was set in place for dismantling the roof plate. While the piece to be removed was being hooked onto the crane, a welder made the final cut. The piece of the roof was then swung free and lowered to the ground. After the roof had been removed, a door opening was cut in the tank wall for the crane to drive through. The crane was then used from the inside of the tank to remove the rafters and girders. After the roof framing was removed, the welders removed the wall of the tank beginning with the top shell course. The piece to be removed was attached to the crane by two clamps spaced about eight feet apart. Working from the scaffolding on the outside of the tank, a welder cut the remaining "tacks" and the plate was swung free, lowered and stacked on the tank bottom.

The sheets cut from the tank still had insulation over most of their outer surface. To remove the remaining insulation, the sheets were placed on the ground, insulation side up, and a rubber-tired tractor with a scraper blade was used to remove the insulation. After the insulation was removed, the

sheets were loaded onto a flatbed truck and hauled to the Floreffe site.

2.4 Reconstruction of the Tank

Before the dismantled tank from Whiskey Island could be erected, the old tank that it was replacing had to be dismantled. This work began in June, 1986, and took several weeks. The old tank was hauled away and scrapped. A new foundation was built where the tank had been located. It consisted of two to three feet of compacted fill covered by a soil stabilization fabric, and 12 to 18 in of crushed limestone (a complete description of the tank foundation in given in Chapter 4). The fill was placed in 6 to 8 inch lifts and compacted. The foundation work was completed during the month of July 1986.

Reconstruction of the tank began in August, 1986. Work began by laying a new steel bottom. Lugs were welded to the tank bottom for aligning the first shell course and to hold the first course in place as it was being tack-welded. Once the first course was tack-welded, the vertical seams were welded from the outside. Next the horizontal seams were welded from the outside. Once the outside welds were complete, the root pass (first pass) was cut out from the inside of the tank and the inside welds were made.

Edge preparation prior to welding consisted of hand flame cutting with an acetylene torch to produce a bevel. It was very clear that the no attempt was made to remove the old weld. It was not possible to determine whether the flame cut edges had been ground prior to re-welding. It was reported that, at the intersection of the vertical and horizontal welds or "T-welds", extra weld passes were made (extra passes were observed at several T-welds during the site investigation). Inspection of the welds consisted of visual inspection or liquid penetrant inspection in which fuel oil was sprayed on the inside of the welds and the outside was checked for leaks. No radiographic inspection was performed while welding was in progress.

Radiographic inspection was conducted by an independent laboratory after the tank had been completely welded. A total of 39 radiographs were taken; 26 in vertical welds, 4 in horizontal welds and 9 in T-welds. Of the 39

radiographs, 22 were "rejected" in accordance with the criteria in ASME Section VIII, Paragraph UW-51 [2.1]. The defects reported by the radiographer include slag inclusion, lack of fusion and lack of penetration. The radiographer reported to Ashland that the defects "appeared to be in the old weld metal" which had not been removed prior to re-welding. No repairs were made to the defective welds. Tank erection was completed in mid-November 1986.

On March 12, 1987, elevation readings were taken on the lip around the bottom of the tank at the seams. By May 1987, all piping to the tank had been completed and the tank was partially filled with water to test for leaks. Water was supplied by the West Penn Water Company and the tank was filled using a fire hose placed into the top of the tank. It took approximately two days to fill the tank to the 5 ft-level. A gage on the side of the tank was used to measure how much water was in the tank. The water was then allowed to sit in the tank for several days and the tank was checked daily for leaks at the base and side. On June 11, 1987, elevations were again taken around the base of the tank. No leaks were observed and the water was emptied from the tank. In August 1987, Tank No. 1338 was put into service storing No. 2 fuel oil. Settlement readings were again recorded on August 25, 1987, when Ashland inventory records indicated 10 ft - 3 1/2 in of oil in the tank.

Table 2.1 - Shell Plate Thicknesses

	Plate Thickness (in)	
	Measured by NBS (to nearest 1/16)	Original (assumed)
Tank Bottom	1/4	1/4
Shell Course 1	7/8	7/8
Shell Course 2	11/16	3/4
Shell Course 3	1/2	5/8
Shell Course 4	3/8	1/2
Shell Course 5	1/4	3/8
Shell Course 6	3/16	1/4
Tank Roof	1/8	3/16

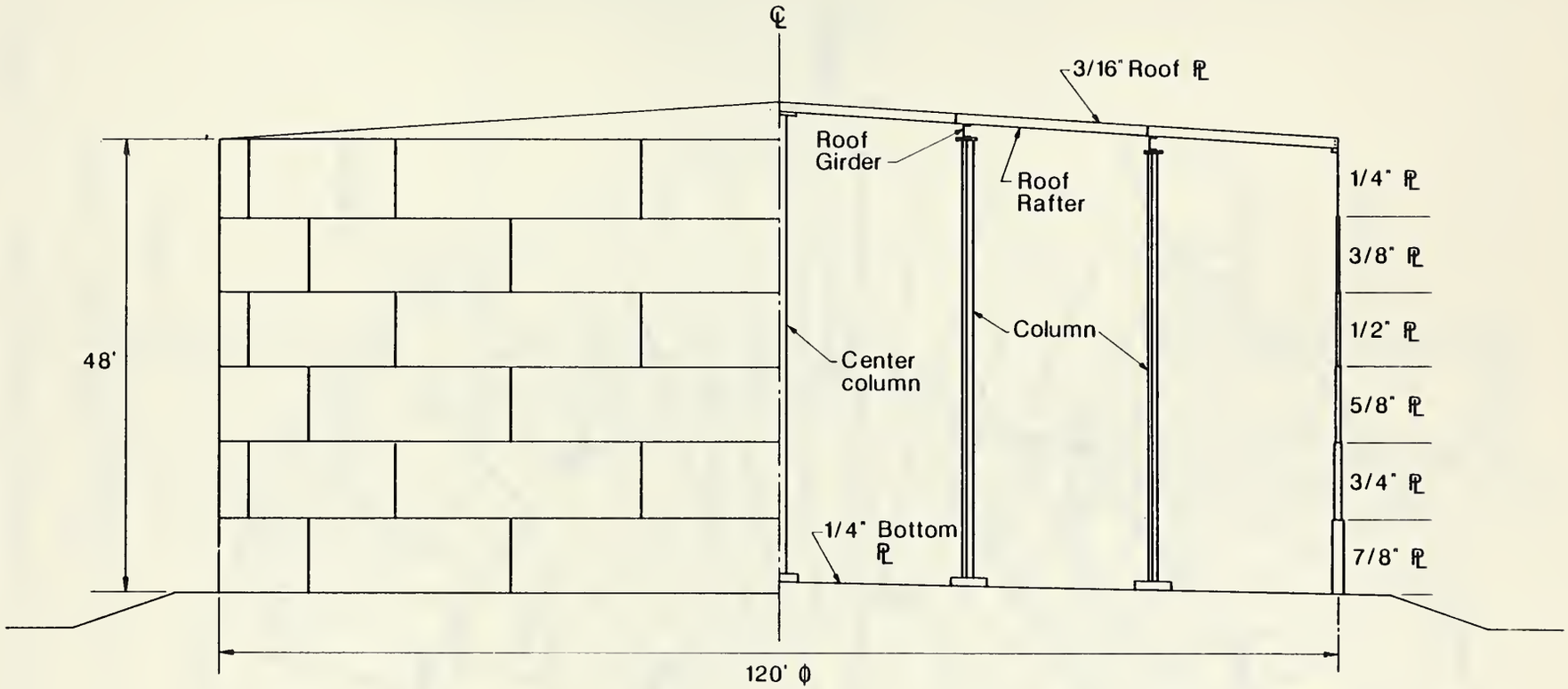

Figure 2.1 - General Description of the 96,000 Barrel Tank

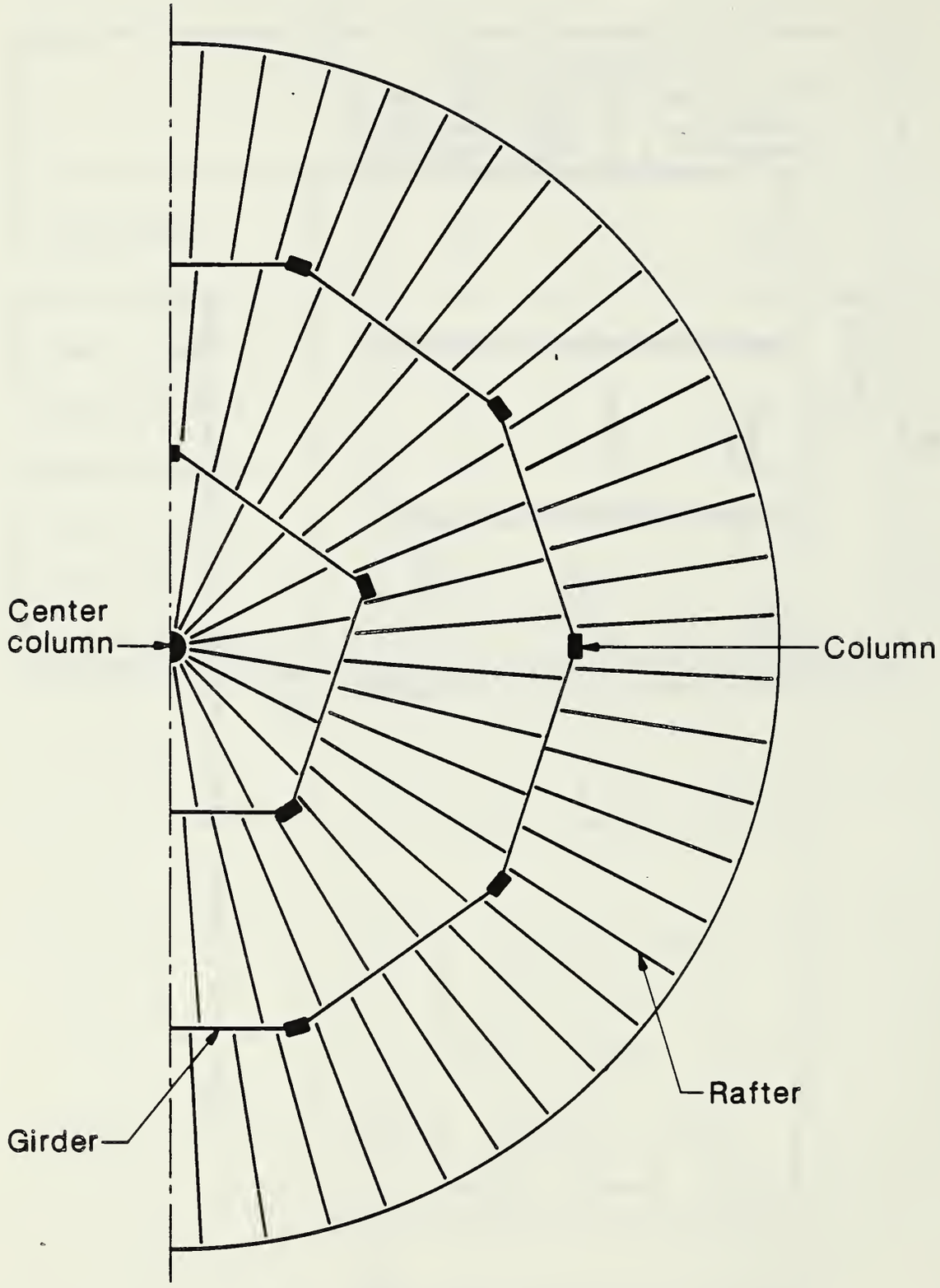

Figure 2.2 - Plan View of Roof Support System

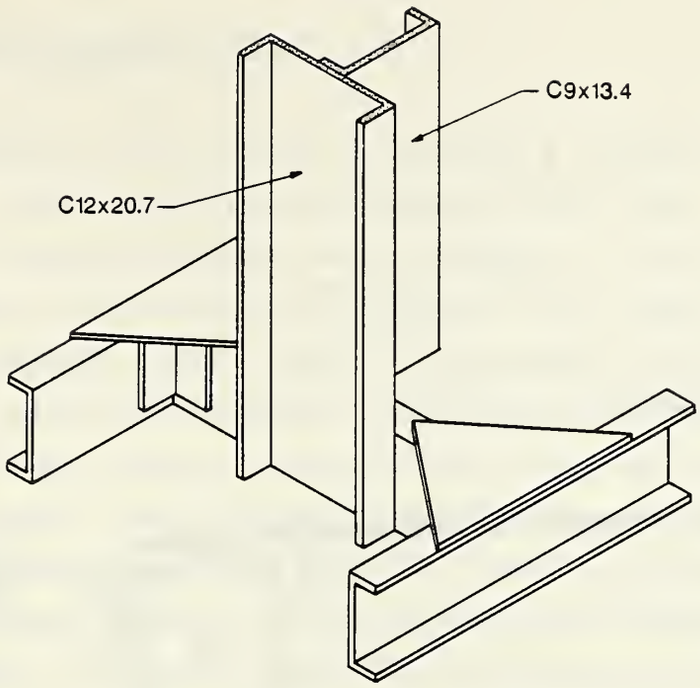

Figure 2.3 - Column Base Resting Directly on Tank Bottom

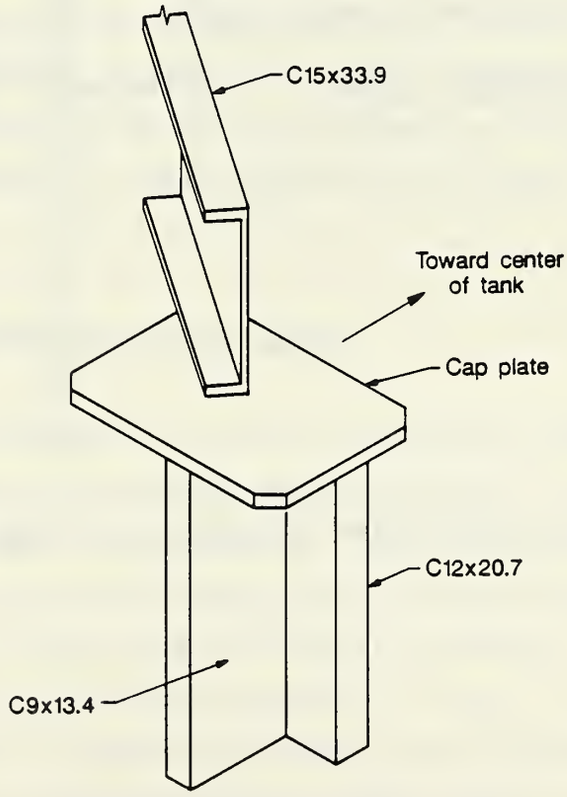

Figure 2.4 - Roof Girders Supported on Top of Columns

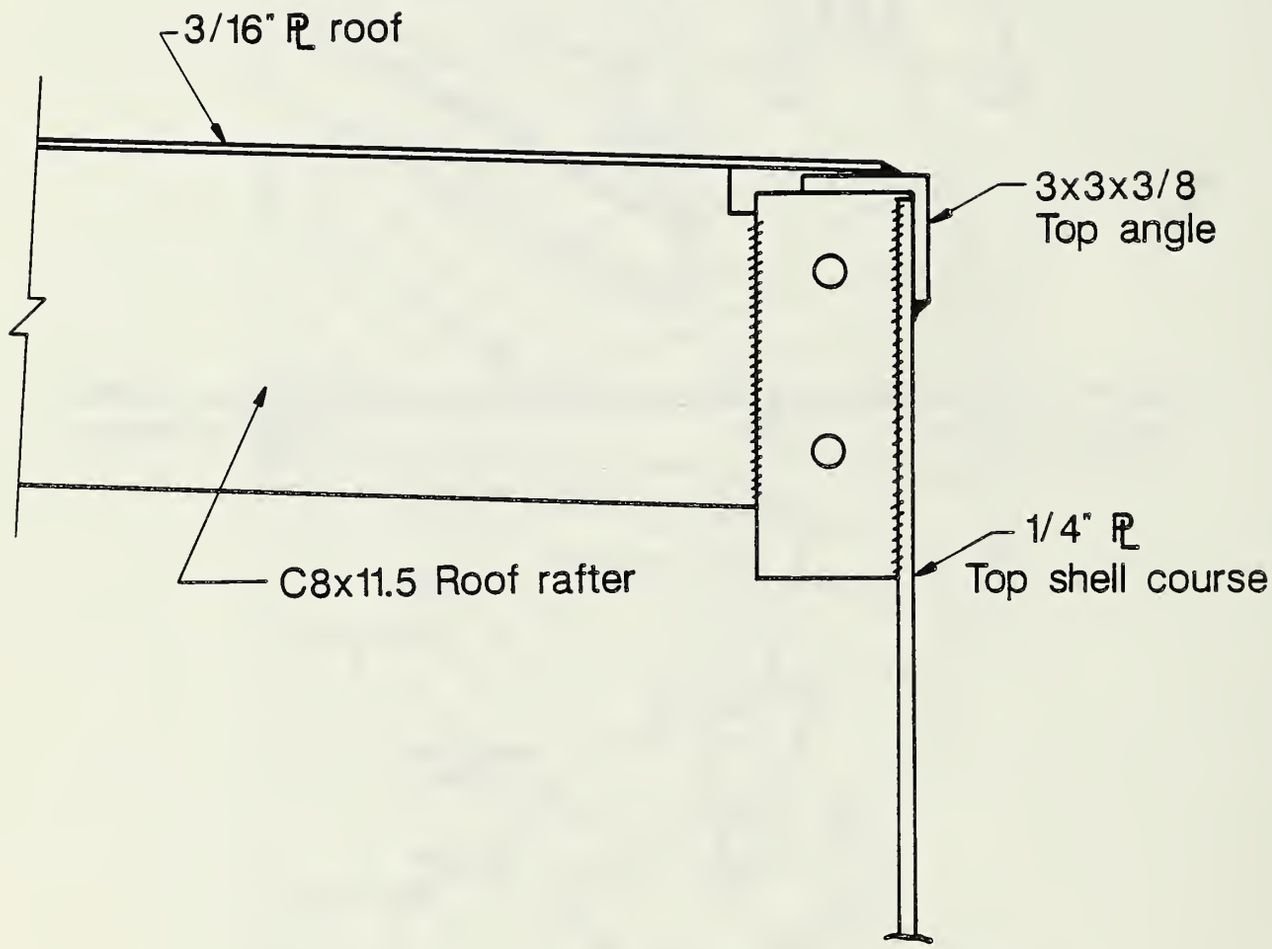

Figure 2.5 - Roof Rafter Attachment to Tank Shell

3.0 DESCRIPTION OF THE COLLAPSE

3.1 Operation of Tank No. 1338

Tank No. 1338 was put into service at Ashland's Floreffe Terminal in August, 1987, when No. 2 fuel oil was first added to the tank. The first entry in Ashland's Daily Inventory Report was on August 25, 1987, at which time the product level was 10 ft 3-1/2 in. Fuel oil was brought to the terminal by barge on the Monongahela River. The oil was pumped from the storage tank into tank trucks for local distribution. The level of oil varied from day to day as oil was added and removed. On the days that the Floreffe terminal was operating, the product level in each storage tank was recorded for inventory purposes. The product level for Tank No. 1338 is plotted in Figure 3.1 for the period beginning August 25, 1987, and ending January, 1, 1988, the day before the collapse. It can be seen that the product level had never exceeded the 37-ft mark prior to the day the tank collapsed.

The daily high and low temperature recorded at the Allegheny County Airport, which is approximately seven miles from the Floreffe Terminal (see map in Figure 1.2), is shown in Figure 3.2. The lowest temperature experienced during the history of operation of the reconstructed Tank No. 1338 was 12° F, which occurred on January 2, 1988, the day of collapse.

3.2 Conditions Preceding the Collapse

At about 4:30 am on January 2, 1988, two barges containing No. 2 fuel oil arrived by river tug at the Ashland terminal dock. An 8,500-barrel barge was the first to be unloaded into Tank No. 1338. Ashland personnel determined that there was more oil on the barges than could be put into Tank No. 1338. It was decided to fill the tank to the 46-ft mark -- six inches below the level at which the fire foam lines entered the tank. The 11,000-barrel barge containing No. 2 fuel oil began unloading into Tank No. 1338 at about 11:30 am. The pumping rate was approximately 2000 barrels per hour which, for a 120-ft diameter tank, translates to a fill rate of approximately 1 inch every 5 minutes. The level of oil was read every half hour using the gage on the

side of the tank. At about 4:00 pm, gage readings began to be taken every ten minutes. At approximately 5:00 pm the Ashland terminal operator recorded the level at 45 ft - 10 in. He determined that it would take approximately 10 more minutes of loading to reach the 46-ft level. He then returned to the office and, within 5 minutes after taking the reading, the tank collapsed.

At the time of collapse, it was still daylight (dusk), the weather report at the Allegheny County Airport indicated clear skies and the temperature was 26° F. The level of oil in the tank at the time of collapse was approximately 46 ft - 0 in.

3.3 Witness Accounts of the Collapse

Descriptions of the collapse of Tank No. 1338 were given by four witnesses. All of the witnesses, except the Ashland operator, were more than 500 yards from the tank at the time of collpase. None of these witnesses was looking at the tank at the instant of collapse. Rather, their attention was drawn to the tank by the sound of the collapse which was described as a "loud rumbling noise" similar to "thunder". Accounts indicated that the sound lasted between 3 seconds and 30 seconds. Witnesses saw the tank fall toward the north and a wave of "foam" or "white smoke" spill over Route 837. They also reported what was variously described as "green mist," "a green cloud" or "chemical cloud" which formed and then dissipated.

The Ashland operator who was standing next to the tank just minutes prior to the collapse had not observed any unusual circumstances such as leaking product or noises coming from the tank.

The accounts of the collapse can be summarized as follows:

- There were no warnings or evidence that a failure was imminent.
- The loud rumbling sound created by the collapsing tank lasted at least several seconds.
- There was no report of an explosion or fire.

3.4 Observations of the Debris

The NBS team of investigators arrived at the site of the collapse on January 6, 1988. Prior to that date, oil which had spilled from the tank flooded the dike area (see Figure 1.1) and prevented safe access. By January 6, 1988, most of the oil had been removed from the dike area of Tank No. 1338 as well as from the adjacent dike areas. The site appeared to be otherwise undisturbed at the time NBS investigators arrived.

As can be seen from the aerial view of the collapse site shown in Figure 3.3 (3.3), the tank wall had split completely open and the once-cylindrical shell had unwrapped until it was nearly straight. The tank shell came to rest on top of a dike approximately 120 ft and generally north of its original location. A description of the fractured tank wall is given in the next section. A composite photograph of the collapsed tank from within the dike area is shown in Figure 3.4.

The wall was completely separated from the tank bottom. Figure 3.5 shows the tank bottom in the foreground and the tank wall and portions of the roof in the background. The bottom tore at the toe of the inside fillet weld attaching the first shell course to the bottom plate leaving a 3-inch "lip" attached to the tank wall (see Figure 3.6). This tear was ductile as evidenced by the approximately 45° failure plane. The tank bottom remained relatively intact except for two large tears in the lap welded seams. The edge of the bottom plate where the tank wall tore away had a "scalloped" appearance as shown in Figure 3.5.

The tank roof was severely crumpled with several large tears but otherwise was in one piece. The tank wall had torn away from the roof as it "unwrapped" except for a portion which remained attached to the wall opposite the vertical split. The tear was generally at the weld between the roof plate and the top angle and was also generally ductile.

Debris from the roof support system lay scattered mostly within the dike area as can be seen in Figure 3.3. A closer view of some of the debris on the tank bottom is shown in Figure 3.7. The roof framing members were severely twisted

and many of the welds had failed.

Tank No. 1367, which was empty at the time of the collapse, was severely dented on the side facing Tank No. 1338. Tank No. 1367 is partially in view at the left in Figure 3.4 and is shown in Figure 3.8. An oil stain was evident on this tank and on Tank No. 1339 extending as high as the roof line which was approximately 48 ft for both tanks.

3.5 Description of the Tank Wall Fracture

One side of the fracture in the tank wall came to rest inside the dike area near Tank No. 1366. It is shown in Figure 3.9. The fracture surface was flat and perpendicular to the tank wall indicating that it was a brittle fracture. Chevrons were evident on the fracture surface (see Figure 3.10). The chevrons pointed to a dark area extending about two-thirds of the way through the plate thickness (see Figure 3.11). The location of this dark area is just below the horizontal weld, between the first and second shell courses, and just to the left (looking from the outside of the tank) of a vertical seam in the second course. The fracture was believed to have initiated at this point and extended to the top and bottom of the tank wall. A diagram showing the path of the fracture is shown in Figure 3.12. Note that the fracture neither started nor propagated in the welds.

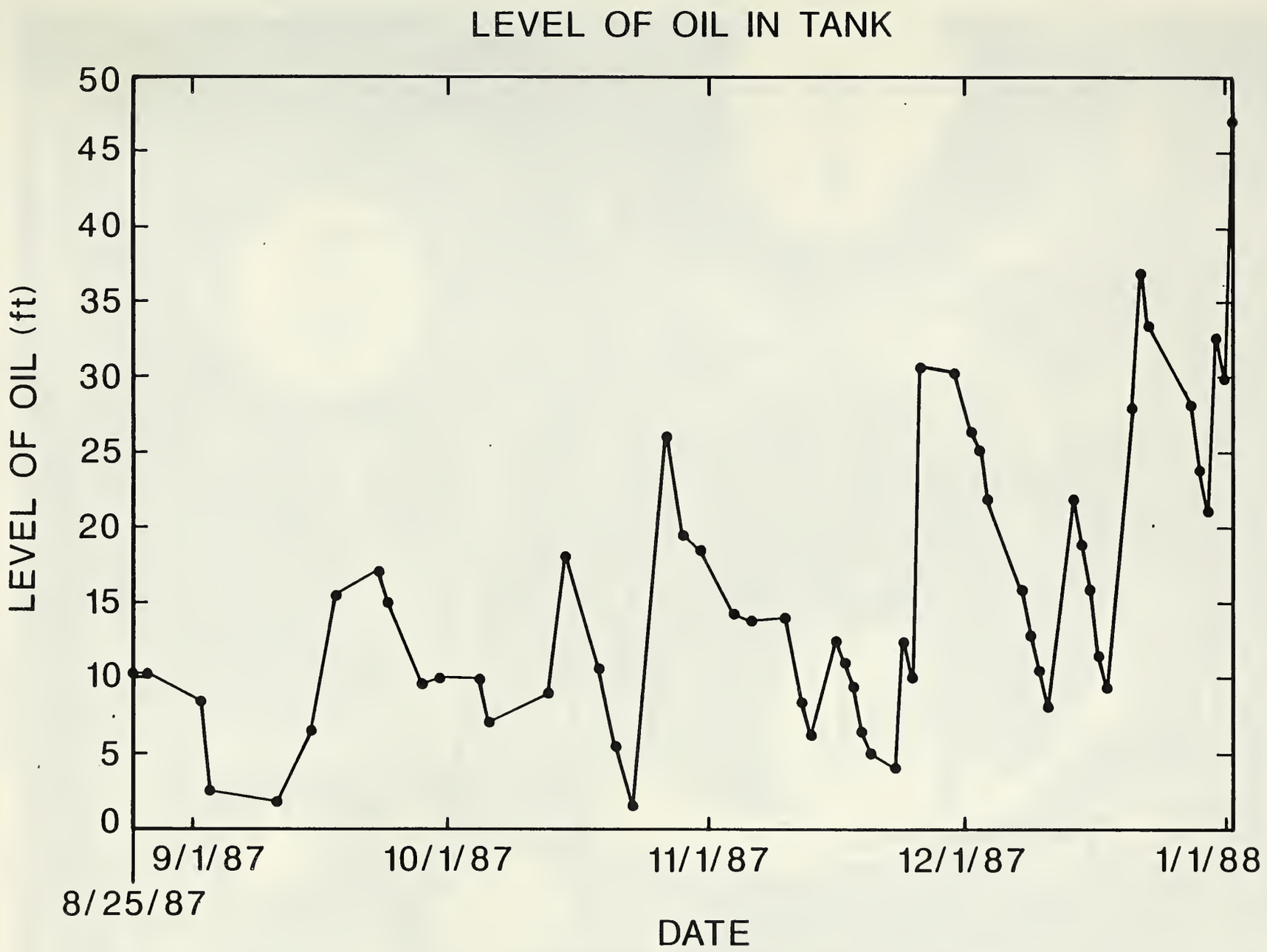

Figure 3.1 - Product Level in Tank No. 1338

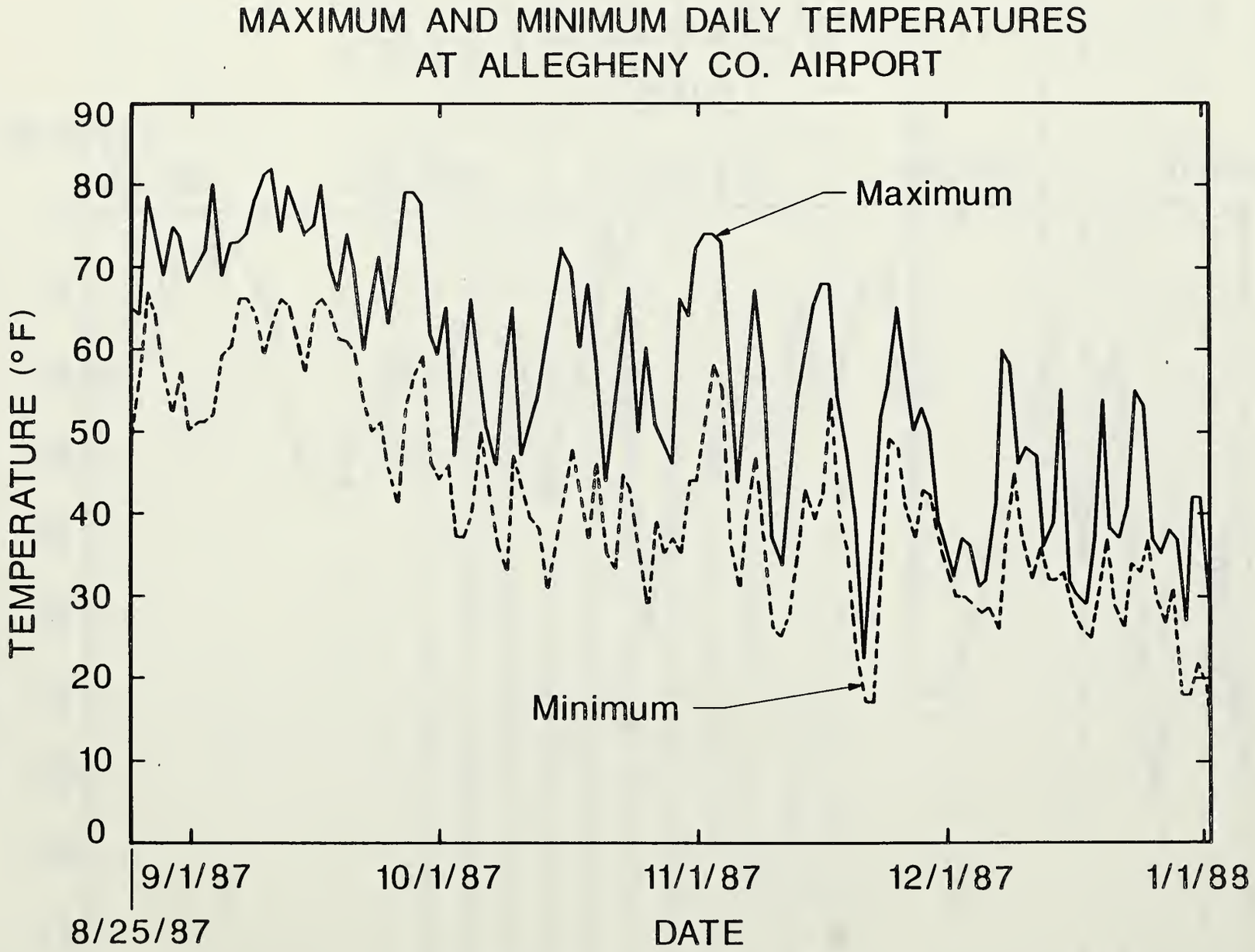

Figure 3.2 - Maximum and Minimum Daily Temperatures at Allegheny County Airport

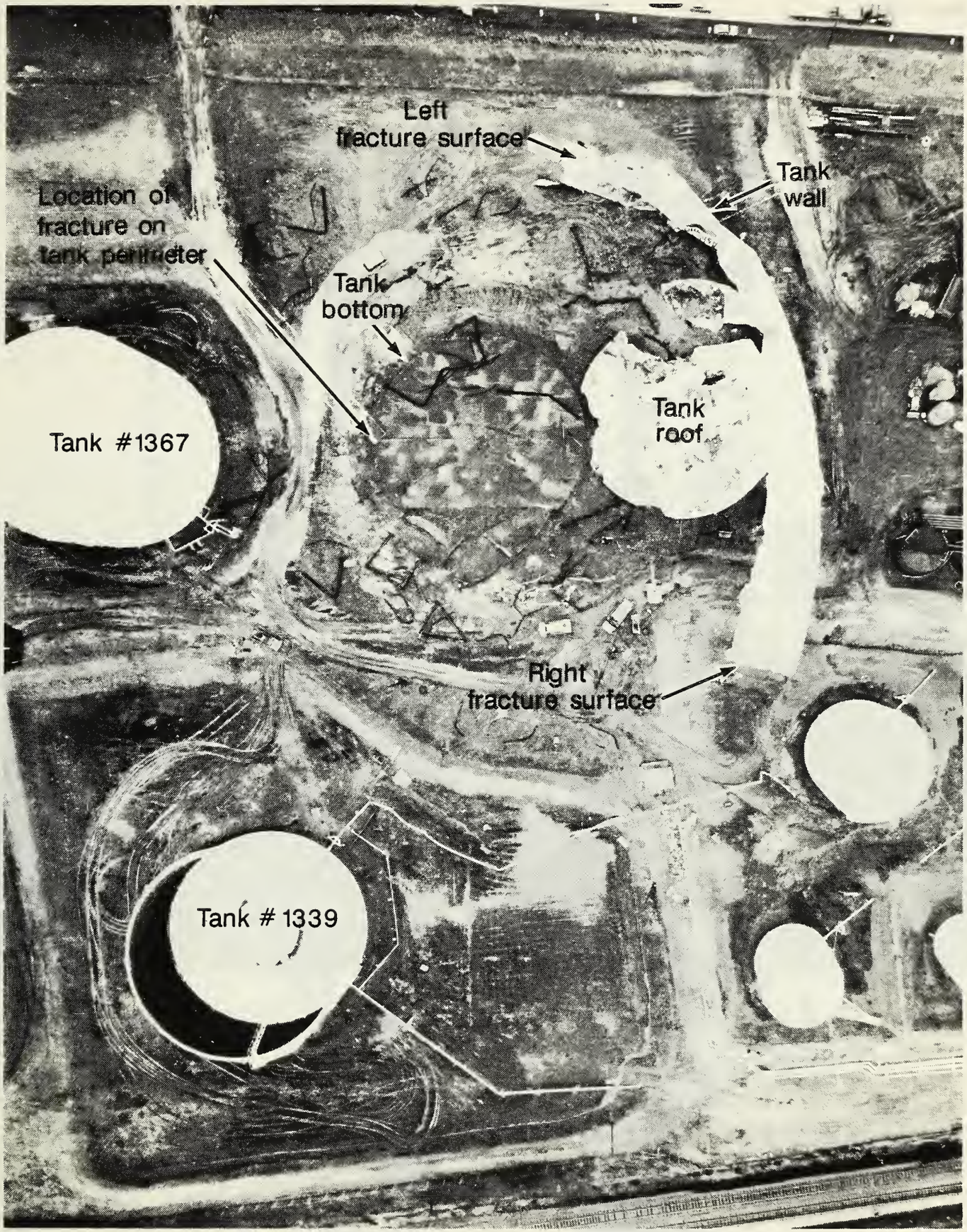

Figure 3.3 - Aerial View of the Collapse Site
(Photo by Pennsylvania Task Force)

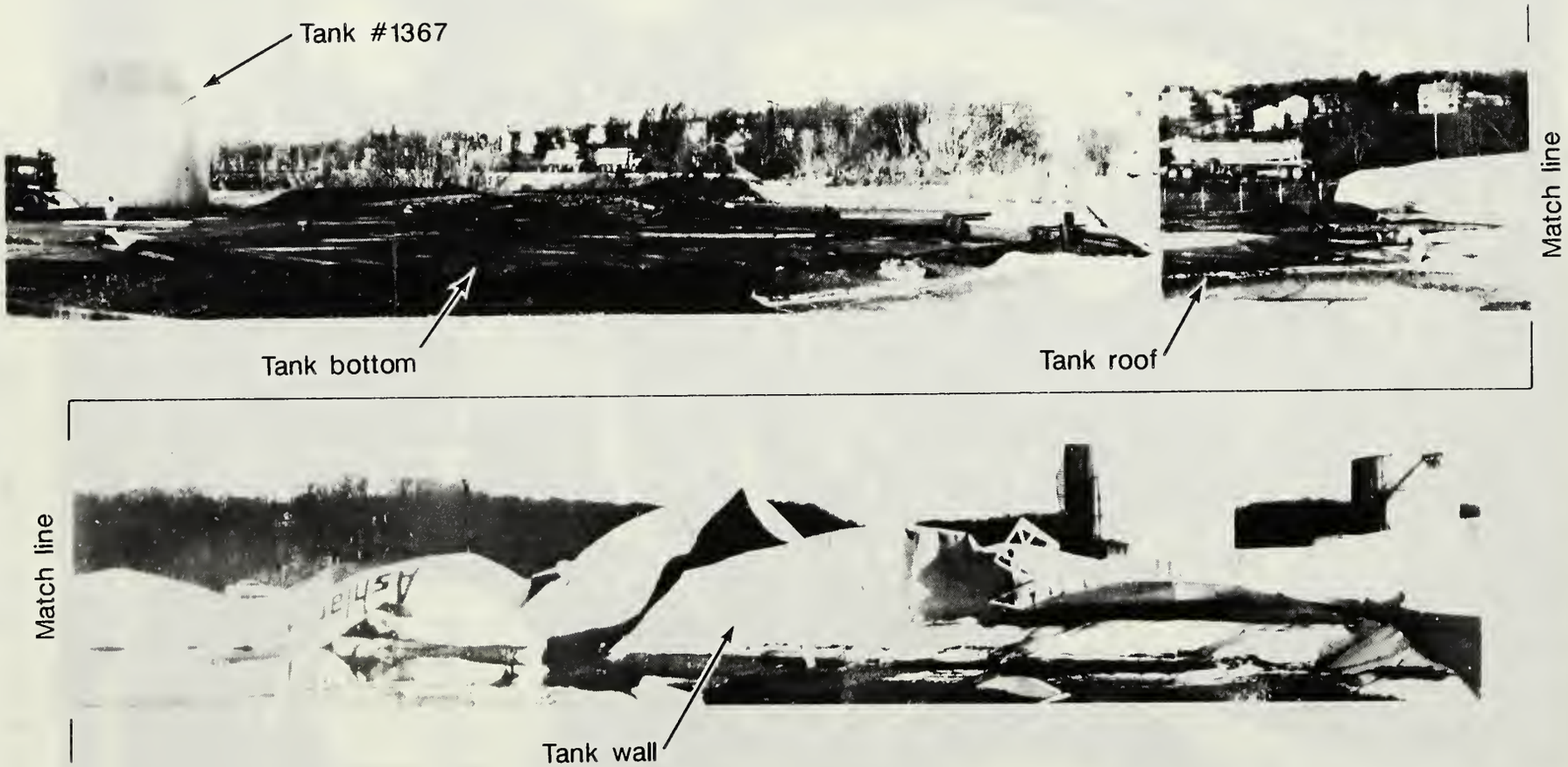

Figure 3.4 - View of Collapsed Tank No. 1338 from Ground Level

Figure 3.5 - View of Tank Bottom with Tank Wall and Roof in Background

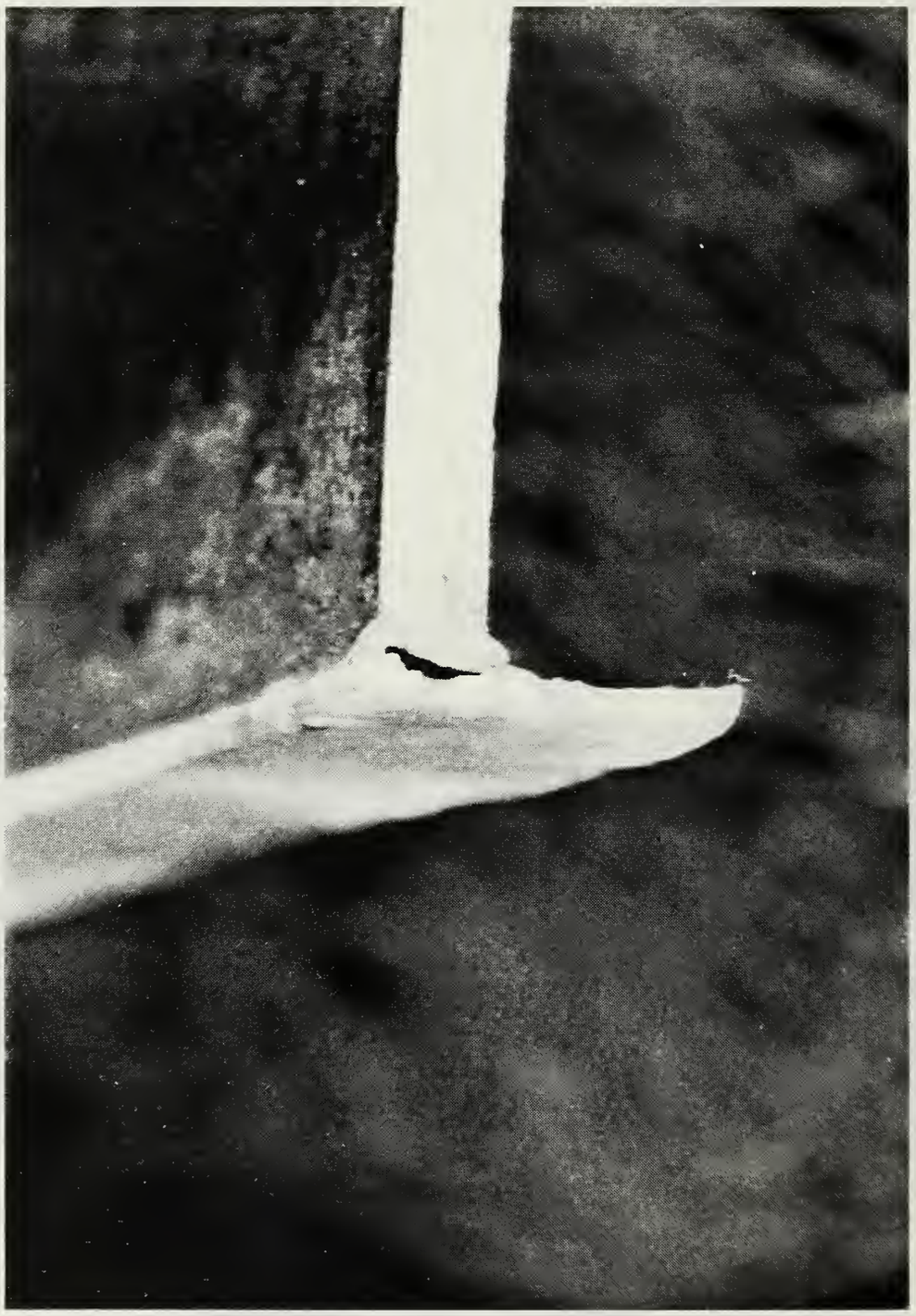

Figure 3.6 - Tear in Tank Bottom at Inside Fillet Attaching First Shell Course and Bottom Plate

Figure 3.7 - Roof Framing Debris Scattered on Tank Bottom

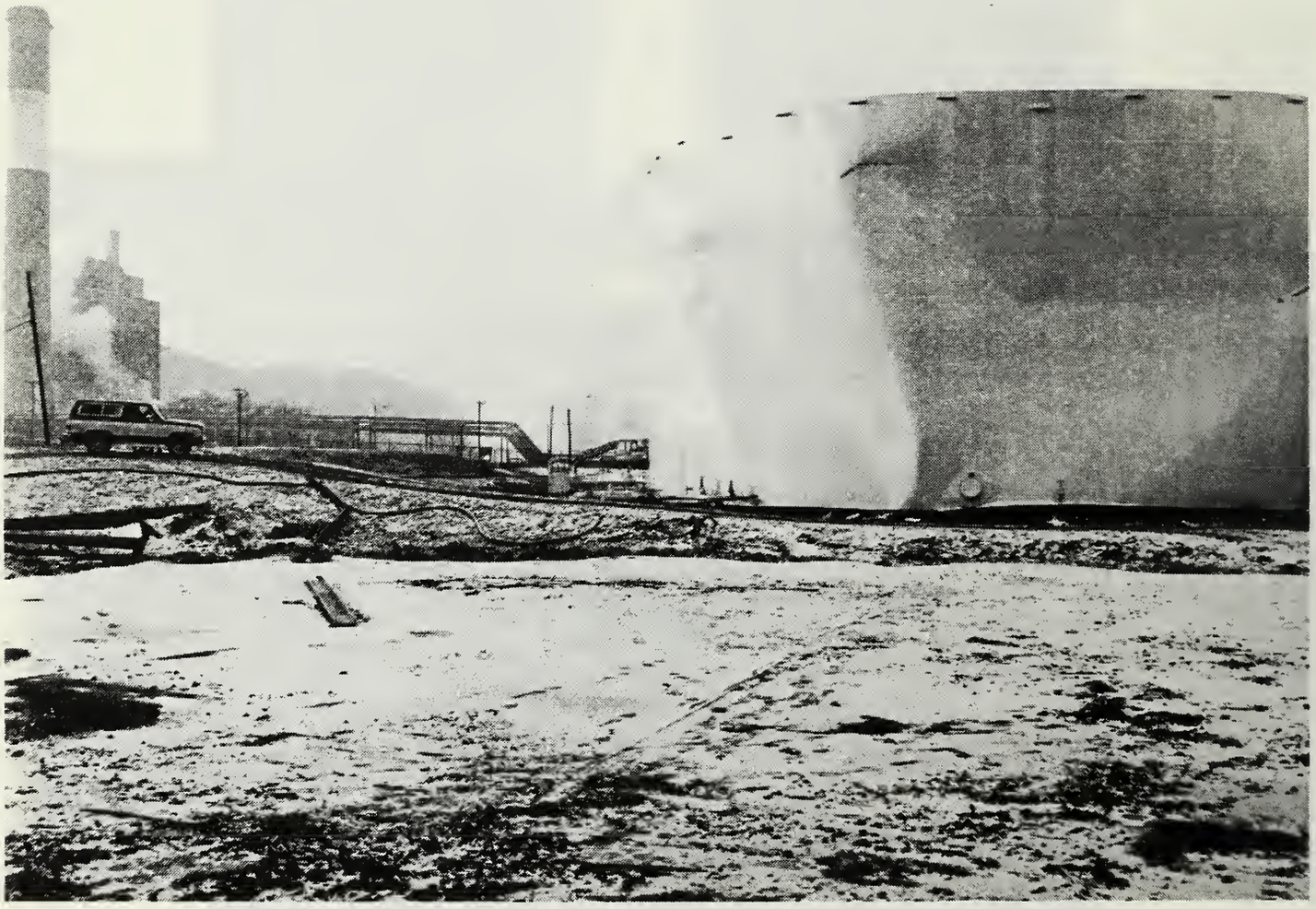

Figure 3.8 - Tank No. 1367 Dented in the Collapse of Tank No. 1338

Figure 3.9 - Right Side of Fracture

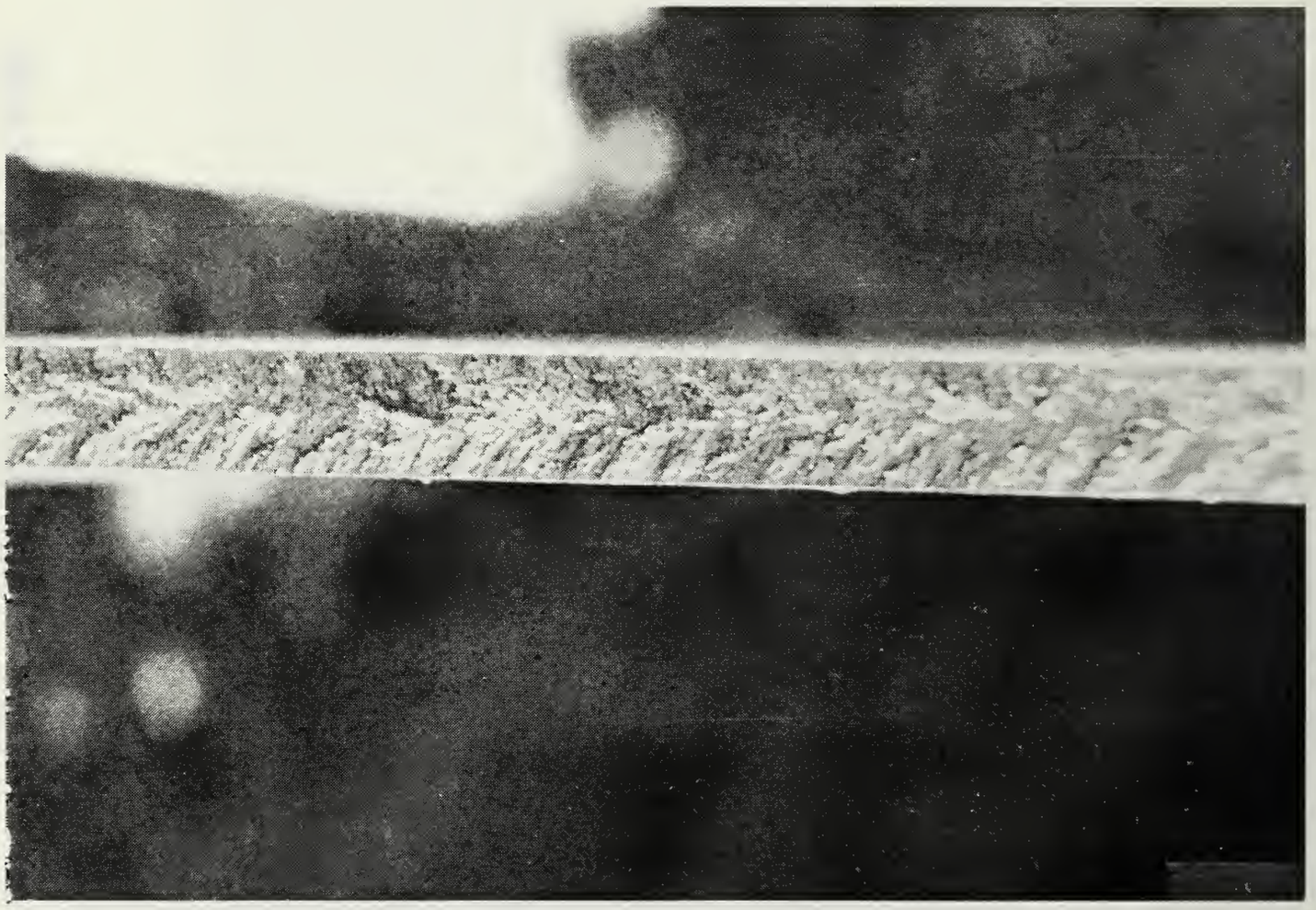

Figure 3.10 - Chevrons in Fracture Surface

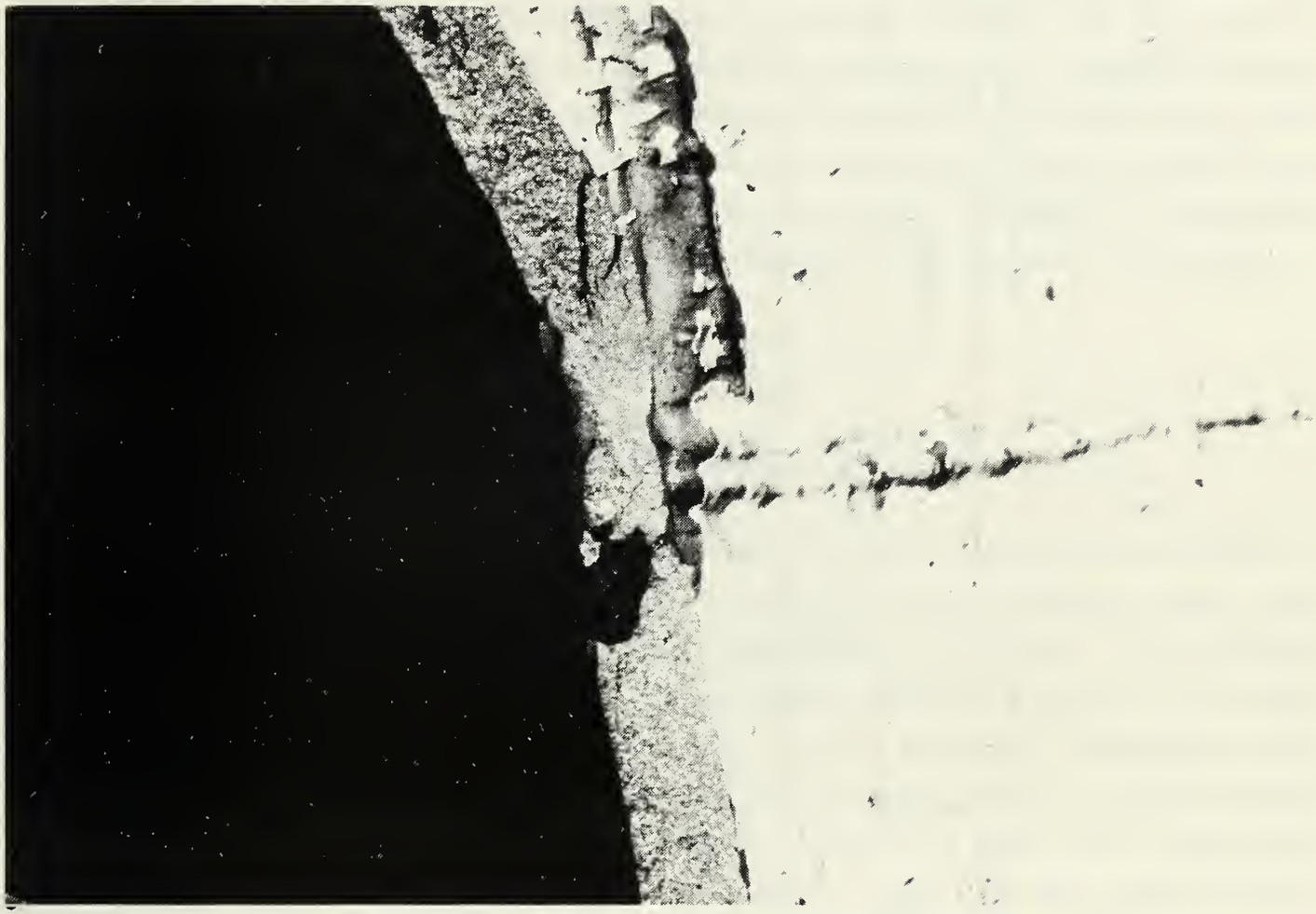

Figure 3.11 - Dark Area on Right Fracture Surface

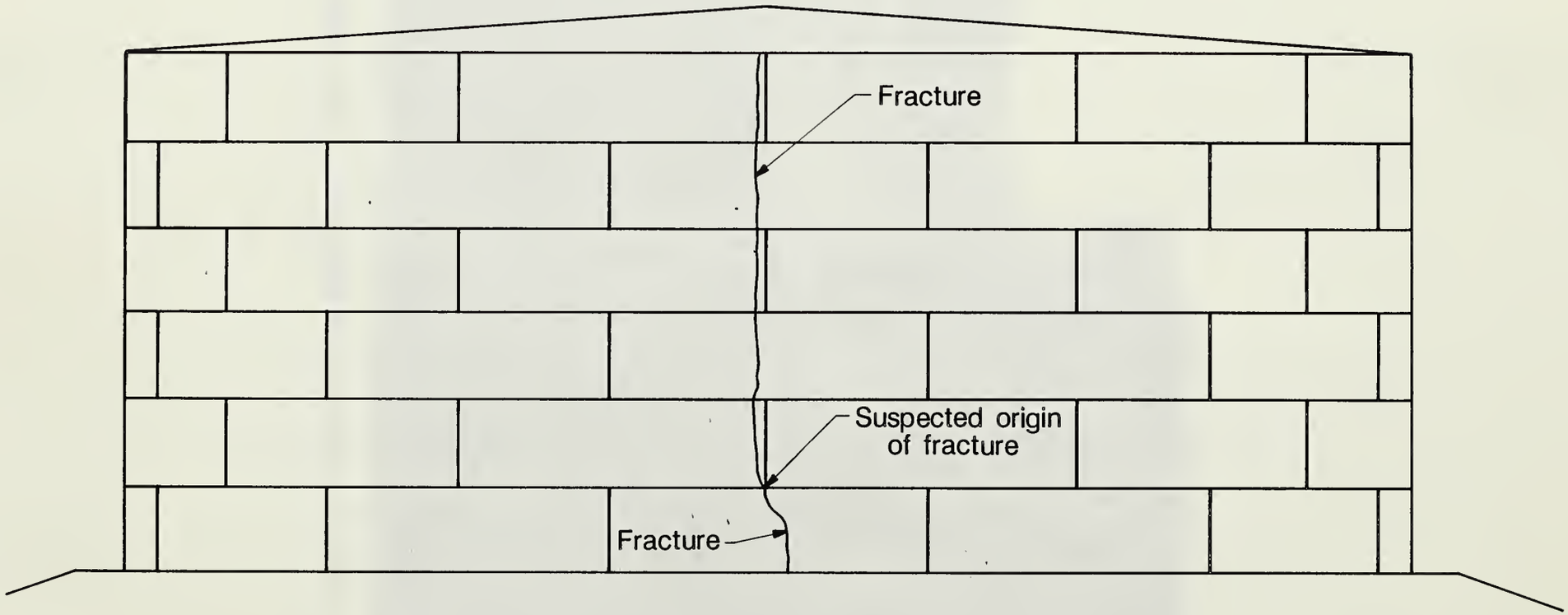

Figure 3.12 - Approximate Path of Fracture in Tank Wall

4.0 FOUNDATION STUDY

4.1 Objective of Foundation Study

The observations of the debris of Tank No. 1338 described in Section 3.3 indicate that the tank shell had split and was separated from the tank bottom plate by a bottom-plate failure adjacent to the weld between the bottom plate and the shell. There were also tears in some lap welded seams of the bottom plate which appear to have originated near the seam between the shell and the bottom plate. The objective of the foundation study was to determine whether a foundation stability failure or excessive foundation settlements could have caused a failure of the bottom plate and its separation from the shell, and whether shell distortions introduced by non-planar foundation settlements along the tank perimeter could have contributed to the failure of the shell.

4.2 Description of Foundation and Site

4.2.1 Sources and Scope of Information

Information for the foundation study was derived from data provided by Ashland, including construction drawings, records of field density tests taken during the construction of a raised compacted fill base, and elevation readings along the rim of the tank taken during partial filling of the tank, and data provided by the Pennsylvania Task force, including topographic data for the site and elevations of the foundation surface taken in a field survey after removal of the bottom plate of Tank No. 1338, and data from a subsurface exploration conducted after the tank collapse. The site was also visually inspected by the NBS investigation team prior to, and during the subsurface exploration.

The soil exploration and laboratory testing data used in the foundation analysis were provided to NBS by the Pennsylvania Task Force. Boring logs, oedometer tests from boring B-4 and B-5, and data from unconsolidated undrained triaxial compression tests are presented in the Appendix. All other data can be obtained fron the Pennsylvania Task Force.

Since there was concern that drilling through the tank foundation might cause groundwater contamination by residual fuel oil from the spill, the soil exploration methods had to be modified to prevent any infiltration of fuel oil into the ground water. As a consequence, the borings through the tank foundation itself were not carried to bedrock. However, two borings through dikes in the vicinity of the tank foundation were carried into bedrock and thus provide more complete information on the stratigraphy of the unconsolidated deposits.

4.2.2 Foundation Description

Figure 4.1 shows a cross section of the tank foundation taken from the construction plans provided by Ashland. The bottom plate of the tank was supported by a crushed limestone pad varying in thickness from 1 ft at the center to 1.5 ft at the tank perimeter. The top surface of the crushed stone pad was to be graded to slope from the center of the tank to its perimeter, with the center 0.5 ft higher than the perimeter. The crushed stone pad in turn was supported by a compacted fill base which was constructed above the natural grade to a height of approximately three feet.

A geotextile (reinforced plastic) blanket was inserted between the crushed stone pad and the compacted fill base. The raised foundation had a diameter of 130 ft at the top and had sides which, according to the plans, sloped at a ratio of 3:1 toward the natural grade. The distance from the tank perimeter to the upper edge of the slope was to be 5 ft.

4.2.3 Foundation and Site Conditions

Past Loading History

Prior to the reconstruction of Tank No. 1338, the site supported a tank 115 ft in diameter and 40 ft high. The center of the foundation of this old tank was approximately 27 ft from the center of Tank No. 1338. Thus a substantial portion of the foundation of Tank No. 1338 was pre-loaded by the previous tank. There is no evidence that the previous tank experienced any foundation problems.

Construction Records

Records are available from the construction of the compacted fill base. Solar Testing Laboratories, Inc. of Pittsburgh issued six inspection reports between July 2 and July 25, 1986 during the construction of the compacted fill. The reports indicate that the soil was to be compacted to a Standard Proctor (ASTM D 698) density of 95%. A soil sample taken from the borrow area prior to the construction of the fill was described as a "reddish-brown sandy silt with clay and rock fragments" with a maximum (ASTM D 698) dry density of 117.2 pcf and an optimum moisture content of 12.4%. The inspection reports indicate that the original grade prior to the placement of fill had some wet spots. The muddy areas were to be skimmed and the site was to be proof-rolled prior to placement of the fill. There is no evidence indicating that the inspection laboratory confirmed that this was done.

The fill was placed in four 8-inch layers and nuclear density tests were performed at several locations for each layer to determine dry density. Most of the teste points met or exceeded the specified density. However, some test points were somewhat deficient. Corrective actions were recommended by the inspection laboratory. While the foundation contractor stated that corrective actions were taken, there is no documented evidence that the deficient areas were re-tested to confirm that the in-place density of the fill is adequate. The available records, discussed above, indicate that the fill probably was constructed in accordance with specifications.

Foundation Surface

The foundation surface was visually inspected by the NBS team after removal of the bottom plate of the ruptured tank, and level readings were taken to document its topography. The level readings are shown in Figure 4.2. These can be compared with Figure 4.3 which shows part of an aerial photograph taken by the Task Force after the collapse. It is important to recognize that, at least in part, the deviations of the level readings from the planned foundation profile shown in Figure 4.1 are attributable to disturbances that occurred during the collapse.

It is apparent from the elevation readings that there was no recognizable overall planar tilt of the tank foundation. There are, however, three areas, marked in figure 4.2 and 4.3 as A, B and C, where the topography shows localized depressions resembling the effects of local stability failures (edge failures). In all three of these areas bottom plate failures other than the separation of the bottom plate from the shell of the tank occurred. The aerial photograph shown in Figure 4.3 also shows some dark areas where oil was ponding on the bottom plate. Visual inspection of the foundation pad after removal of the bottom plate indicated some localized depressions at these locations. These depressions could conceivably be indicative of localized settlements which may have preceded the tank failure. In addition to the depressions at points A, B, and C there is some variation in the elevations around the tank perimeter. While these variations are not necessarily an indication that non-planar shell settlements of a similar magnitude took place prior to the collapse, records of level readings taken during partial filling of the tank after its construction give an indication that there were some non-planar shell settlements. These will be discussed later in this chapter.

Because no documents on the as-built foundation-pad profile are available, no definitive conclusions can be drawn about possible overall residual settlements from the difference between the level readings and the planned foundation pad profile which specified a difference of 0.5 ft between the elevation at the center of the tank and that at the rim. However, it appears that the difference between the elevation at the center of the tank and those at the rim is typically 0.3 ft, and thus may have decreased by approximately 0.2 ft from that specified.

An examination of the area surrounding the elevated foundation pad gave no indication of any heave such as that resulting from a rotational slide opposite areas A, B, and C.

In areas A and B some soft, clayey silt was encountered near the surface of the depressions. Test pits dug to explore the extent of the soft material showed that soft material only occurred in small, localized pockets. It is, therefore, reasoned that the pockets of soft material are attributable to disturbance of the compacted fill and mixing with oil as a result of oil

spills. It was also observed that the surface of the fill under the geotextile blanket was covered with a thin film of oil.

Compacted Fill

Data on the condition of the compacted fill are available from sixteen shallow borings (M1-M16), three compaction tests from bag samples (D1, D2, D3), and three undisturbed (Shelby Tube) samples (S1, S2, S3) which were subsequently tested in the laboratory (refer to location map in Figure 4.4). The bag samples were combined and re-constituted in the laboratory to two dry densities (111.9 pcf @ w = 16.8%; and 116.4 pcf @ w = 14.3%; where w = water content) in order to perform triaxial compression tests for the range of densities encountered in the compacted fill.

The shallow borings ranged in depth from 1.4 ft to 1.85 ft below the top surface of the crushed stone pad. The borings were advanced by continuous Standard Penetration Test (SPT) sampling (ASTM D 1586), using a rope and cathead assembly and a donut hammer. Blowcounts ranged from 14 to 30 blows per ft and tended to be higher near the bottom of the borings. The water content of the samples retrieved ranged from 12.9 to 18.1 percent. In the laboratory the samples from the shallow borings were identified as "Brown Sandy Lean Clay (CL)" with plasticity indices ranging from 10.4 to 13.7%.

Bag samples taken from the field density tests were identified as "Brown Clayey Sand" (SC). Compaction tests (ASTM D 698) performed on these samples indicate a maximum dry density of approximately 117 pcf at an optimum moisture content of 14%. This compares with a reported maximum dry density of 117.2 pcf at an optimum moisture content of 12.4% determined from a sample taken at the borrow site prior to the construction of the fill.

Dry densities determined from the undisturbed samples (S1, S2, S3) ranged from 106 to 119 pcf and water contents from 14% to 22%. The data indicate that five out of the six samples tested had dry densities in excess of the specified dry density of 111.3 pcf.

Results of the two unconsolidated undrained triaxial compression test of the remolded samples indicate the following strength values:

112 pcf density sample: c_a = 1.3 ksf; ϕ_a = 14.5°
116 pcf density sample: c_a = 2.0 ksf; ϕ_a = 26.0°

where, c_a = apparent cohesion
ϕ_a = apparent angle of friction for total stress envelope.

These samples were not saturated (83% to 86% saturation) and, therefore, the tests do not provide a measure of the undrained shear strength in a saturated condition. It is reasonable to assume that, at the time of the tank failure, the compacted fill was also not saturated since it is elevated above the surrounding area.

It is concluded from the above information that the compacted fill was constructed in accordance with the specifications, and had a wet unit weight of approximately 134 pcf and a shear strength under prevailing loading (refer to 4.3.2) and drainage conditions at the time of collapse of approximately 2 ksf.

Subsurface Conditions

The site was explored by five deep borings (B1 through B5). In addition, four undisturbed samples (S4, S5, S5A, and S6) were taken at a shallow depth immediately below the compacted fill. The boring and sampling locations are shown in Figure 4.4.

The borings were advanced by continuous SPT sampling (ASTM D 1586). The rope and cathead method was used to drop a 140-lb donut hammer from a height of 30 inches to advance a 2-inch O.D. 1 3/8 inch I.D. split spoon sampler without a plastic liner. The sampler was followed by a 3.5 inch I.D., 7.5 inch O.D. hollow-stem auger which was used to support the sides of the drill hole. Rock coring was performed with an NX double core barrel sampler which took 3-inch diameter rock cores. The recorded data include blow count for 6-inch depth increments, soil type by visual-manual identification, sample recovery in

inches, pocket penetrometer readings on the split spoon samples, and Shelby Tube and rock core recovery. The undisturbed and split-spoon samples were preserved for laboratory testing.

To prevent groundwater contamination all boreholes were filled with cement grout after completion of the boring. Special precautions were taken in the area of the tank foundation (B3, B4, and B5). For these borings a 16-inch diameter hole was first drilled to a depth of 4 to 6 ft. Then a 12-inch O.D. casing was placed in the drillhole and driven 6 inches into the bottom of the 16-inch hole. The space between the casing and the borehole was subsequently filled with cement grout. Then a boring was advanced from the bottom of the casing, using continuous sampling and a hollow-stem auger as described previously . At the end of each working day, the drill rod and the hollow-stem auger were withdrawn regardless of the depth to which the boring advanced during the day and the borehole was filled with cement grout. As a result of the time restraints imposed by this procedure, the borings located in the area or immediate vicinity of the tank foundation had to be terminated in soft material and the unconsolidated deposits were not explored to their full depth.

Laboratory tests included soil classification in accordance with ASTM D 2487, and oedometer and unconsolidated undrained triaxial compression tests of undisturbed samples. Most of the undisturbed samples were not saturated, and thus the undrained-unconsolidated tests did not provide definitive information on the undrained shear strength. However, an attempt was made to saturate samples from borings S4 and S5 by applying a back pressure in excess of 11 ksf before performing unconsolidated undrained triaxial tests. A set of consolidated undrained tests was also performed on an undisturbed sample taken from boring S6.

In order to assess the subsurface conditions to the full depth of the unconsolidated deposits it is necessary to interpolate between borings B1 and B2 which were carried to bedrock. Boring B1 is 200 ft from the centerline of the tank in a Southeasterly direction and was carried 7 ft into bedrock to elevation 719. Boring B2 is approximately 215 ft from the center of the tank in a Northwesterly direction and was carried 10 ft into bedrock to elvation

726. Between these two borings are borings B3, B4, and B5. Boring B5 is in the center of the tank and extends to a depth of approximately 24 ft below the compacted fill. Boring B3 is on the tank perimeter in a Northwesterly direction from the tank center and extends to a depth of approximately 18 ft below the compacted fill. Boring B4 is approximately 85 ft from the centerline of the tank in a Southeasterly direction, it is approximately 25 ft outside the perimeter of the tank, and it extends to a depth of 36 ft into the natural ground. While not extending to bedrock, boring B4 traverses all the compressible layers and extends approximately 6 ft into a layer of dense silty sands and sandy silts.

Comparison between adjacent borings indicates that the stratification of the compressible layers is approximately horizontal. Figure 4.5 shows an idealized schematic soil profile based on the available information. The upper soil layer extending approximately to elevation 757 is identified as a stiff moist silty clay. Several undisturbed samples were taken from this layer, providing information on compressibility and undrained shear strength. The undrained shear strength (s_u) given in figure 4.5 is based on the lowest strength recorded for a sample from boring S4 which was saturated in the laboratory (this is a lower limit, because it is unlikely that the soil was saturated at the time of collapse). This upper layer is underlain by sandy silty clays and sandy clayey silts to approximate elevation 745. Part of this second layer, below approximate elevation 751, is saturated. Below this second layer is a layer of saturated loose silty sands and sandy silts. Below approximate elevation 740 is a layer of dense clayey silty sands with rock fragments which extends to bedrock. It can be seen from the recorded plasticity indices (P.I.) that the boundaries between the layers above the dense clayey silty sands are artificial and predicated on the soil classification method used. Actually, the deposits become gradually more coarse-grained with depth, their clay fraction gradually decreases with depth, and there is a gradual transition from clays to silts to silty sands.

4.3 Foundation Analysis

4.3.1 Failure Limit States

On the basis of past performance of oil tanks with similar foundations, several possible foundation-induced failure limit states have been identified. These are: stability failures which include base shear failures (bearing capacity failure or planar tilt) and edge shear failures (local stability failure); and settlement-induced failures which include bottom plate or bottom plate connection failure induced by excessive differential settlements and excessive stresses induced in the shell by non-planar shell settlements along the tank perimeter (shell distortion). In addition to the possibility that the overall tank failure may have been triggered by foundation instability or excessive settlements, NBS investigated the possibility that settlement-induced shell distortions could have contributed to the tank failure by increasing the circumferential tensile stress in the shell at the location where the brittle fracture originated. It is important to consider the fact that prior to the erection of Tank No. 1338, the site supported a somewhat smaller tank which exerted foundation loads of approximately 80 percent of the load acting at the time of collapse. No foundation failures were reported for this old tank.

4.3.2 Stability

Duncan and D'Orazio (1984) [4.1] studied available documented information on steel tank foundation shear failures and developed empirically-based criteria for foundation stability. The safety factors against base and edge shear failure calculated herein are based on these criteria.

Using an oil depth in the tank of 46 ft and a specific gravity of the oil of 0.87, the oil pressure on the bottom of the tank at the time of failure was approximately 2.5 ksf. If it is assumed that the bottom plate was 1/4 inch thick, the roof plate was 1/8 inch thick, the average thickness of the shell was 1/2 inch, and an allowance is made for the columns and beams supporting the roof, the total weight of the tank is calculated to be approximately 630 kip. If, for the purpose of base stability calculations, it is assumed that

the tank weight is evenly distributed over the base, it would contribute approximately 0.06 ksf to the pressure at the base of the tank, for a total base pressure of 2.56 ksf. If it is assumed that the crushed stone pad had a unit weight of 140 pcf and the compacted fill had a unit weight of 134 pcf, the pressure at the base of the fill was approximately 3 ksf, spread over the equivalent diameter , D_e = 124 ft.

It is assumed that a shear failure would not extend below the surface of the dense silty sand at elevation 740. Thus the thickness of the soft material, T, is approximately 28 ft. Therefore,

$$D_e/T = 124/28 \simeq 4.43 \text{ and } N_c = 6.1 \quad \text{(Reference [4.1])}$$

where, N_c = dimensionless bearing-capacity factor for base shear.

No triaxial test information for the U2 undisturbed samples, which were below the groundwater table at elevation 751, is available. It is assumed that the undrained shear strength of these saturated deposits is lower than that of the partially saturated deposits above them after their saturation in the laboratory. Using an estimated average undrained shear strength of 1 ksf for the entire depth of the soft layer, the factor of safety against base shear, F_b, can be calculated:

$$F_b = (1)(6.1)/3 = 2.03$$

This estimate is conservative, because it is based on the lowest undrained shear strength obtained for a saturated soil condition. At the time the borings were taken the soil was only partially saturated above elevation 751, and it is unlikely that at the time of the collapse the upper soil layer was saturated. The estimated minimum factor of safety against base failure in excess of 2 corroborates the findings from the level survey of the foundation surface which indicate the absence of any recognizable planar tilt.

In order to calculate the factor of safety against edge shear failure it is necessary to make an assumption with regard to the size of the area that failed, or else find the area with the lowest factor of safety. A failure

associated with areas A, B, and C outlined in Figure 4.2 would involve a segment of the tank bottom of approximately 20 ft width in a radial direction (refer to foundation surface topography, figure 4.2). The possibility of a slope failure involving an even smaller bottom plate segment (essentially a failure of the compacted fill slope) is considered unlikely because the shell would bridge over such a small perimeter segment and thus transfer the load in case of a foundation movement.

The following expression suggested by Duncan, et al [4.1] for bearing-capacity factors for edge failures was derived from values suggested by Bjerrum and Overland [4.2]:

$$N_e = 5.2 + B/D$$

where, N_e = dimensionless bearing capacity factor for edge shear
B = radial width of failed bottom segment.
D = diameter of tank

Safety factors against edge shear failure were calculated in accordance with methods recommended in Reference 4.1, assuming an undrained shear strength of 2 ksf for the compacted fill, an angle of internal friction of 40° for the crushed stone pad, and an undrained shear strength of 1.2 ksf for the material underlying the compacted fill. As recommended in Reference 4.1 the shear resistance of the pad and compacted fill was considered in the calculations, and a bearing pressure of 2.8 ksf at the base of the crushed stone pad was assumed. For these assumptions it was found that the factor of safety against edge failure is 2.2 or larger.

4.2.3 Settlements

Differential Settlements

Steel tanks can tolerate large differential settlements when compared to other structures. However, there are records of tanks which ruptured as a result of excessive differential settlements. D'Orazio and Duncan (1987) [4.3] summarize available records on settlement characteristics and tolerances of

steel tanks available before December 1986. On the basis of these records, methods for predicting settlement profiles and tolerances are recommended. The paper addresses differential settlements in the radial direction only, which are associated with failure of the bottom plate, or its connection to the shell.

Bottom-plate failures could also include failure of the fillet welds connecting individual plates similar to that observed between points A and B in figure 4.3.

The shape of the settlement profile of steel tanks depends on the depth and stiffness of the underlying soft soil layer, and can be predicted on the basis of two parameters: the D/T Ratio, which in this case is 4.43; and the factor of safety against stability failure (base or edge) which in this case is larger than 2. In accordance with Reference 4.3, the shape of the predicted settlement profile falls within the limits shown in Figure 4.6 (profile-shape B in Reference 4.3). The effect of subsurface characteristics on profile shapes suggested in Reference 4.3, which is based on empirical data, was also corroborated by some finite-element studies by the authors of ref.[4.3]. For the profile-shape limits shown in Figure 4.6 the following differential settlement tolerance is recommended in reference 4.3 to prevent bottom plate rupture:

$$(\rho_c - \rho_e) / D = 0.015$$

where, ρ_c = settlement under center of tank

ρ_e = settlement under edge of tank.

The settlement itself has two components: a settlement caused by the distortion in the foundation soil due to shear strains and a consolidation settlement. The settlement caused by the distortion in the foundation soil occurs immediately since the shear distortion is not associated with volume changes and thus requires no pore water displacement. The consolidation settlement is time dependent because it requires volume change in the subsoil and thus displacement of pore water. In the case of saturated clay, only very small consolidation settlements could occur during the time frame of the

loading of the tank prior to failure. For the conditions at the site, however, part of the consolidation settlement could have occurred, because: 1) the silty clays and silts above elevation 751 were not fully saturated (about 83 to 85% saturation) and volume change could occur by the compression of the air space in the pores; and 2) soil permeability is increasing with depth, and the clayey silts and silty sands below elevation 750 could have experienced some instantaneous volume changes. An upper limit of the consolidation settlement is therefore calculated and compared with the failure criterion.

The instantaneous shear-strain induced settlement can be calculated by the following equation ([4.3]):

$$\rho_i = (I_p q D_e)/2E$$

where: ρ_i = instantaneous settlement
q = foundation pressure = 3 ksf
D_e = diameter of loaded area = 124 ft
E = average value for Young's modulus of the soil
I_p = dimensionless influence factor, depending on D_e/T and r/R (radial distance from center divided by radius).

A lower limit for Young's modulus is estimated to be 640 s_u = 770 ksi [4.3]. Influence factor I_p is estimated to be 0.15 in the center of the tank and 0.08 at the perimeter. Thus the instantaneous shear-strain induced settlement is of the order of 0.04 ft. in the center and 0.02 ft on the perimeter of the tank.

An upper limit for the consolidation settlement calculated from the oedometer test results (assuming that all the pore water was displaced prior to the failure) is 0.3 ft at the center of the tank and 0.16 ft at the tank perimeter (actual settlements conservatively estimated to have occurred within the time frame of the failure are on the order of 0.18 ft in the center and 0.1 ft at the perimeter). Thus using the upper limit:

$$(\rho_c - \rho_e)/D \simeq 0.0013 << 0.015$$

Thus the differential settlement in the radial direction at the time of the tank failure is estimated to have been more than an order of magnitude smaller than the differential settlement that could have caused a rupture in the bottom plates of the tank or the fillet weld connecting the bottom plates.

Non-Planar Shell Settlements

Unlike differential settlements in the radial direction, non-planar shell settlements cannot be predicted on the basis of the stiffness and depth of compressible soil layers, even though some estimates could conceivably be derived from changes in soil characteristics between adjacent borings. For this reason information is usually obtained by monitoring shell elevations around the tank perimeter when the tank is first filled with water to test its integrity.

There are three possible reasons for non-planar shell settlements: 1) differential foundation settlements during the filling of the tank or after the tank is filled; 2) irregularities in the foundation pad; and 3) irregularities in the tank geometry. Differential foundation settlements tend to increase gradually while the tank is filled and may increase with time after the tank is filled. Irregularities in the foundation pad and tank geometry, on the other hand, could cause initial seating displacements which do not increase when additional fluid is added.

Two questions need to be addressed in this analysis: 1) Could shell distortions have caused a structural failure of the shell? 2) Could shell distortions have contributed to the shell fracture by increasing the circumferential tensile stress at the flaw where failure originated?

Records of shell displacements are available for an initial filling with 5 ft of water on June 11, 1987, corresponding to a foundation live load of 0.312 ksf, and a subsequent filling with 10 ft of oil on August 25, 1987 corresponding to a foundation live load of 0.542 ksf. The foundation live load at the time of the failure was 2.5 ksf or 4.6 times the maximum load for which data on non-planar shell settlements are available.

Table 4.1 shows level readings, recorded to the nearest 0.01 ft, which were taken at 12 points on the perimeter of the tank, representing twelve 30° tank segments with a distance of 31.59 ft along the arc between measuring points. Another reading was taken between points 11 and 13. The reading is not shown in the table because there was no shell distortion between points 11 and 13. The readings taken on 3/12 are for the empty tank, those taken on 6/11 are for a 5-ft water level, and those taken on 8/25 for a 10-ft oil level. Column 5 shows elevation changes for the water filling and column 6 for the oil filling. Column 7 shows the estimated out-of-plane settlements for the oil filling. The estimated out-of-plane settlements were calculated assuming a planar settlement of 0.02 ft and no planar tilt. Hypothetical out-of-plane settlements at the time of the failure are listed in column 8. These settlements were calculated by linear extrapolation of the out-of-plane settlements calculated from the data for the 10-ft oil filling. They are thought to represent an estimated upper bound, because the time-element required for consolidation settlements was not taken into consideration. It is also important to realize that large errors in the estimate of these hypothetical settlements may exist because the precision of the recorded settlements is only 0.01 ft and initial seating settlements are not considered. Thus the out-of-plane settlements in column 8 are at best a very rough estimate.

There are criteria for non-planar shell settlements of floating-roof tanks [4.4, 4.5, 4.6]. These settlements cause out-of-plane deformations in the shell which in turn distort the geometry at the top of the tank, causing problems with the floating roof. The criteria are intended to keep the deformations of the top of the tank within acceptable tolerances and are not related to stresses induced in the shell. A criterion related to shell stresses, which would be applicable to conical-roof tanks, was proposed by Marr et al.(1982) [4.7]. The latter criterion was derived from "beam theory" and thus assumes that no horizontal deformations occur in the shell. Therefore the shell stiffness, and consequently the induced circumferential stresses are overestimated; as a result the criterion is overly conservative with respect to circumferential stresses. The criterion can, however, be considered a lower bound for estimating the magnitude of potentially harmful distortions with respect to induced circumferential stresses. The criterion

ignores potential effects from induced vertical stresses resulting from horizontal bending of the shell out of its plane. There are no documented cases where shell distortion caused structural failure of the shell. This may indicate that vertical shell distortions, while causing out-of-plane deformations, do not tend to overstress the shell. Reference 4.7 notes that three tanks which experienced shell distortions greater than those permitted in the proposed criterion did not exhibit shell damage. The following criterion for maximum tolerable out-of-plane settlements has been proposed in 4.7:

$$\Delta s_i \leq 11(\sigma_y)(\ell^2)/[(E)(H)]$$

where, $\Delta s_i = s_i - 0.5(s_{i-1} + s_{i+1})$ = distortion of tank wall at point i

s_i = out-of-plane settlement at point i

σ_y = yield stress of steel

ℓ = length of shell between observation points i and i $\pm$ 1

E = Young's Modulus of steel

H = height of tank

The criterion is to prevent yielding of the shell by circumferential stresses. For a ductile steel, actual rupture would occur at considerably larger deformations. Assuming a steel yield stress of 34 ksi, a length between gage points of 31.59 ft and a tank height of 48 ft, the allowable limiting value of Δs_i according to this criterion can be calculated as, :

$$\Delta s_i = 11(34)(31.59^2)/[(29000)(48)] = 0.268 \text{ ft.}$$

The highest value of Δs_i for the 10 ft oil level occurs at point 7 and is calculated at:

$$\Delta s_i = 0.01 - 0.5(0-0.01) = 0.015 \text{ ft}$$

if this value is linearly extrapolated to the 46 ft oil level at the time of failure, it results in a Δs_i value of 0.069 which is only approximately 1/4 of the lower bound for settlement distortions, which could induce circumferential yield stresses in the tank shell.

Thus it is unlikely that non planar shell settlements could have induced critical circumferential stresses in the tank shell.

Possible effects of the shell distortion on circumferential stresses at the location of the flaw are approximately assessed in Section 5.2 by a finite element study of the effect of an induced vertical sinusoidal shell deformation at the foundation level. It is concluded that the out-of-plane shell distortions did not significantly affect the magnitude of the circumferential stress at the locetion of the flaw.

4.3 Summary

An analysis of available data on subsurface conditions, foundation loads at the time of failure, and foundation displacements indicates that it is unlikely that the base of the tank ruptured as a result of instability or excessive differential settlements. Based on an analysis of the observed effects of a 10 ft oil level to estimate shell distortions at the time of the failure, it is concluded that shell distortions caused by foundation displacements did not contribute to the tank failure.

Table 4.1 - Shell Displacements

(all dimensions in ft)

Point/Date	3/12	6/11	8/25	ρ_1	ρ_2	s_2	s_f
1	96.81	96.79	96.70	.02	.02	0	0
2	96.89	96.87	96.87	.02	.02	0	0
3	96.95	96.93	96.93	.02	.02	0	0
4	96.94	96.93	96.92	.02	.02	0	0
5	96.95	96.93	96.92	.02	.03	-.01	-.046
6	96.98	96.96	96.95	.02	.03	-.01	-.046
7	96.91	96.91	96.90	.00	.01	+.01	+.046
8	96.95	96.94	96.93	.01	.02	0	0
9	97.04	97.03	97.02	.01	.02	0	0
10	97.09	97.09	97.08	0	.01	+.01	+.046
11	96.98	96.98	96.96	0	.02	0	0
13	96.91	96.91	96.90	0	.01	+.01	+.046

ρ_1 = total settlement on 6/11/87

ρ_2 = total settlement on 8/25/87

s_2 = out-of-plane settlement on 8/25/87

s_f = hypothetical out-of-plane settlement at failure

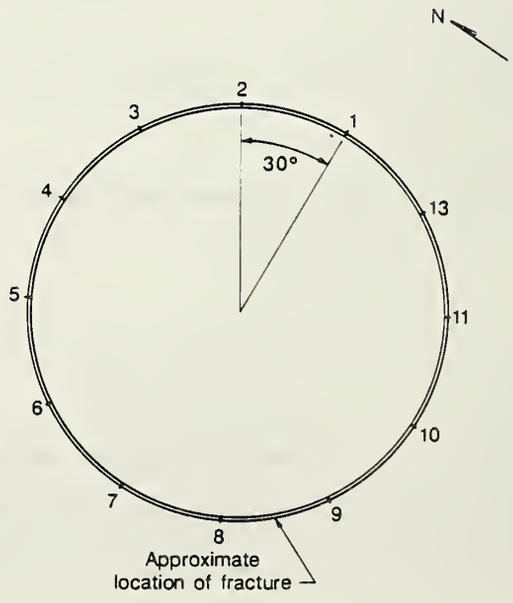

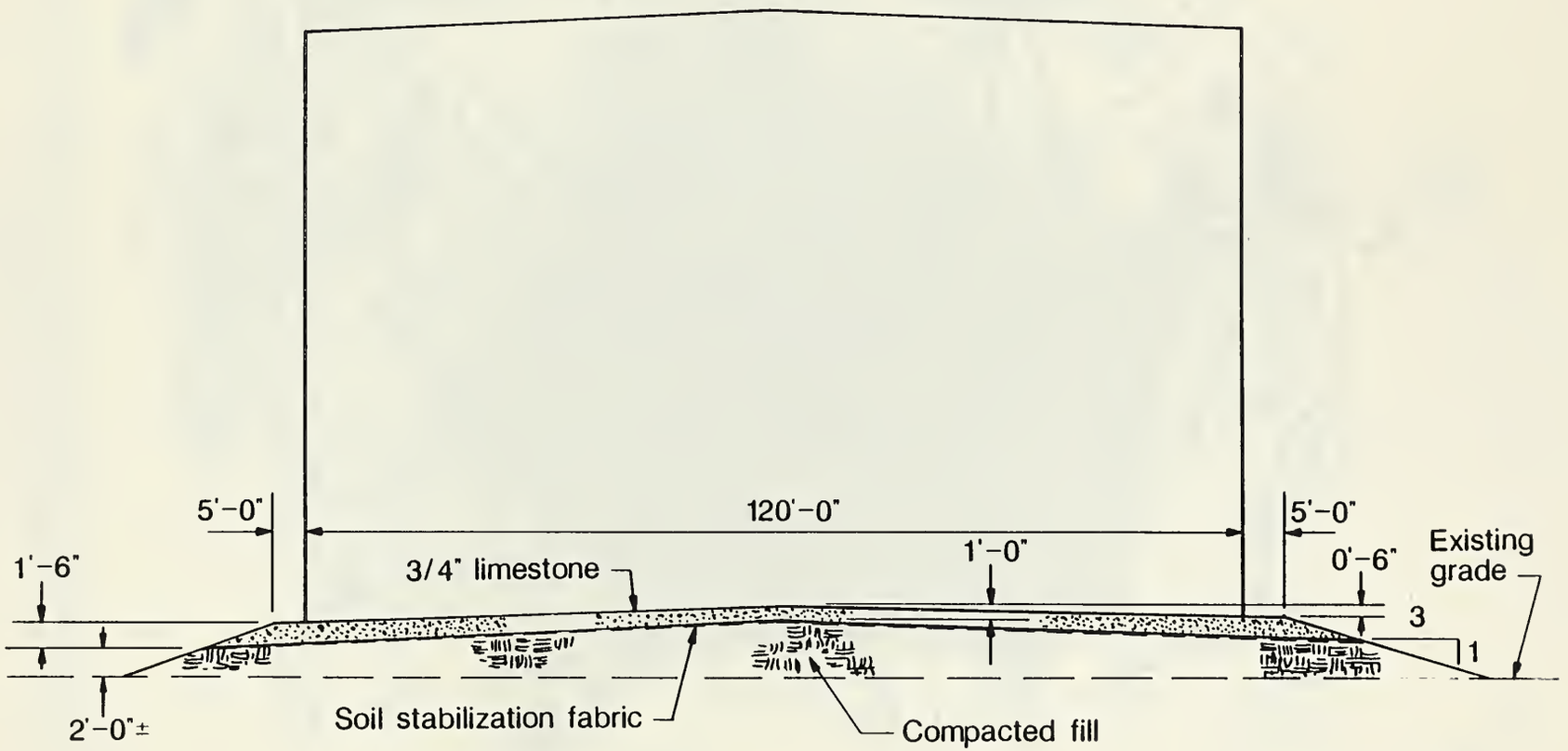

Figure 4.1 - Cross Section of Tank Foundation

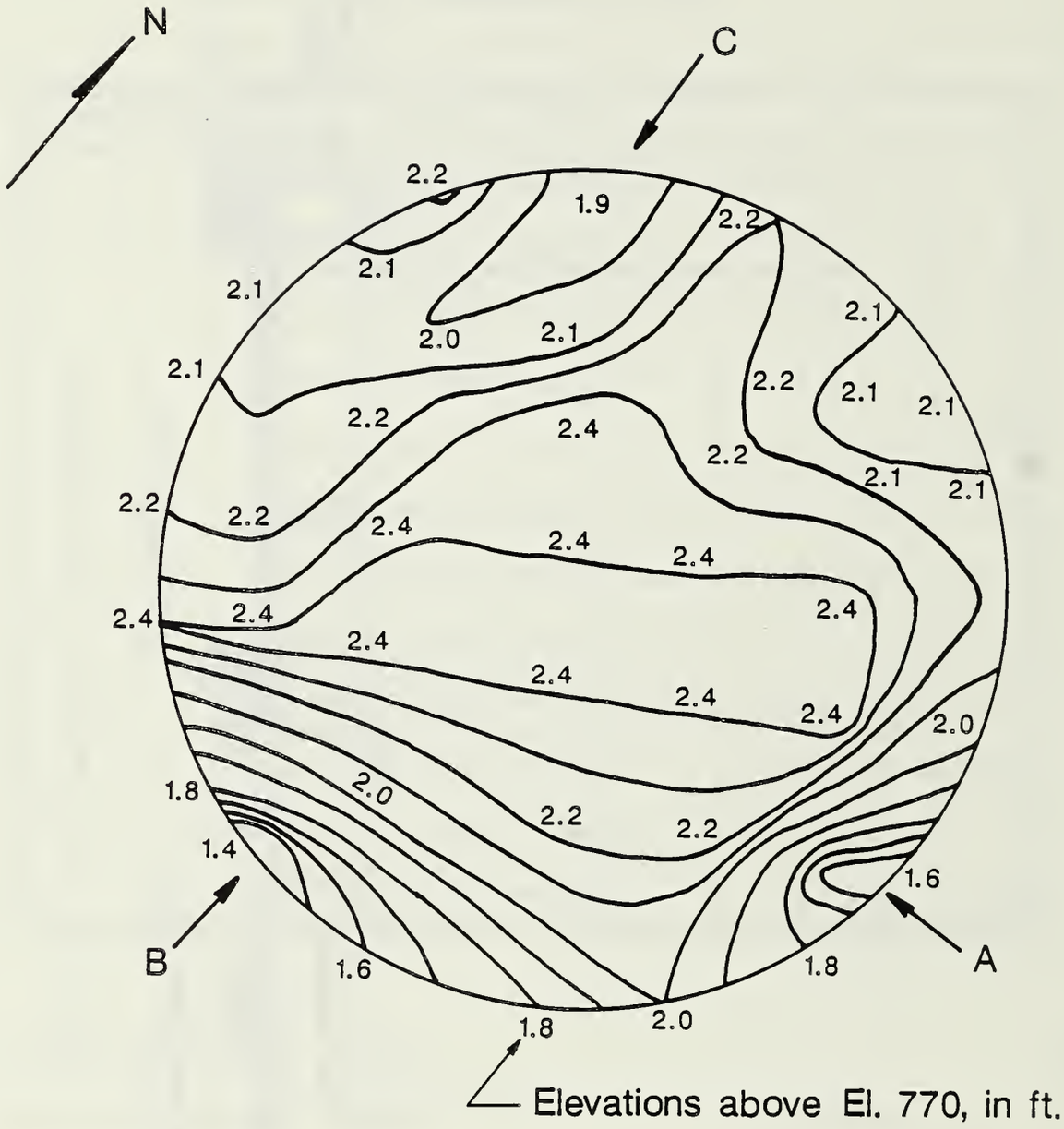

Figure 4.2 - Topography of Foundation Surface Surveyed After Removal of the Base Plate. (Provided by the Pennsylvania Task Force)

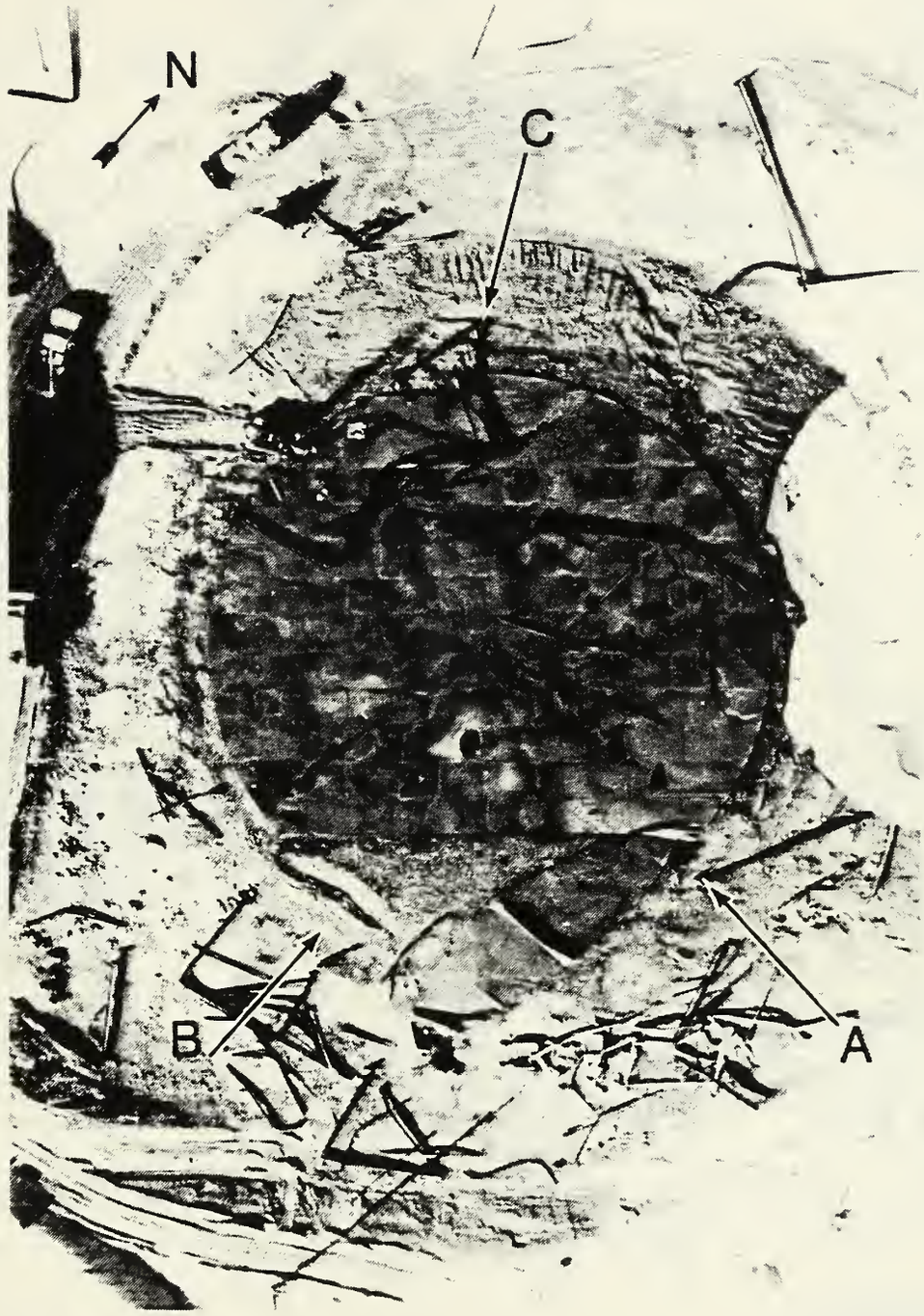

Figure 4.3 - Aerial Photograph of Tank Foundation Taken Prior to Removal of the Base Plate. (Provided by the Pennsylvania Task Force)

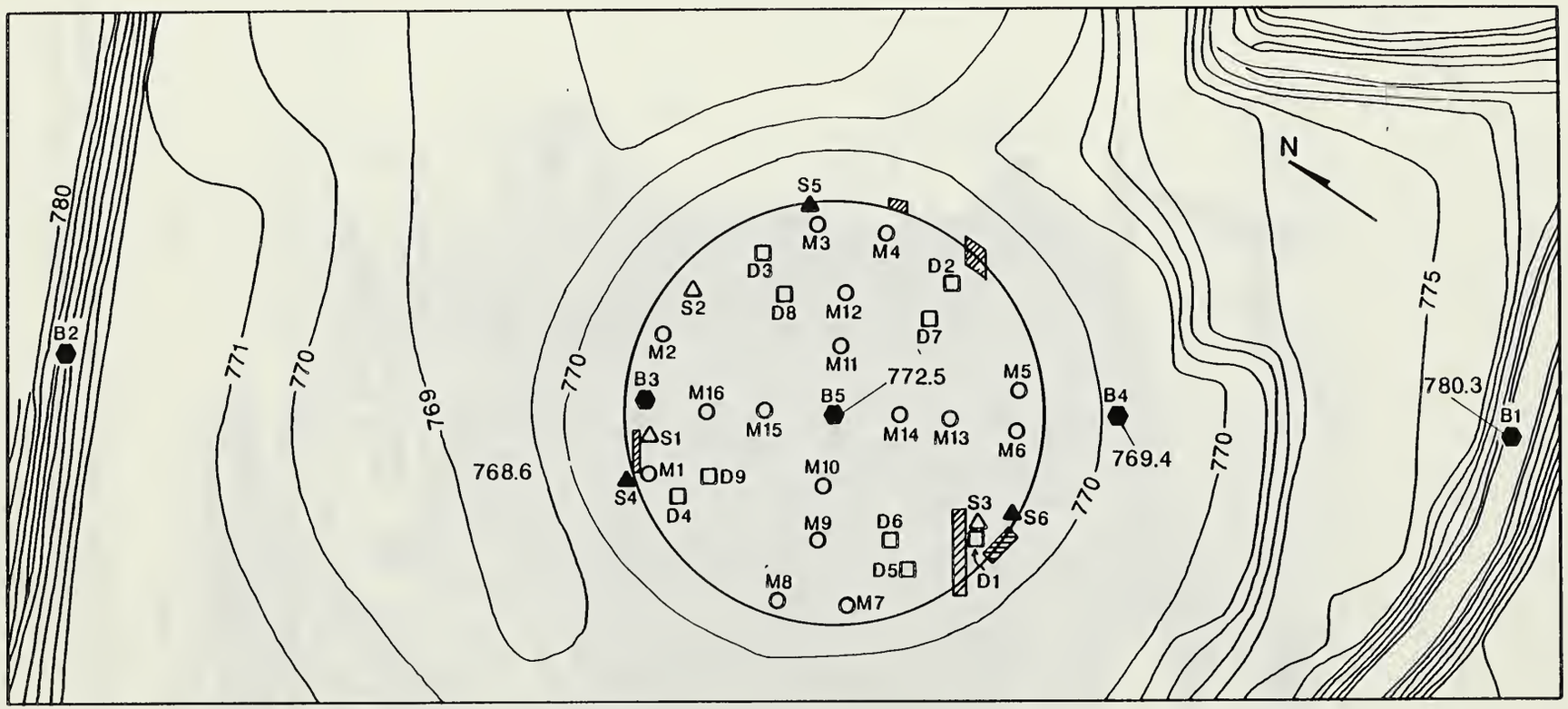

Figure 4.4 - Location Map for Soil Exploration. (From information provided by the Pennsylvania Task Force)

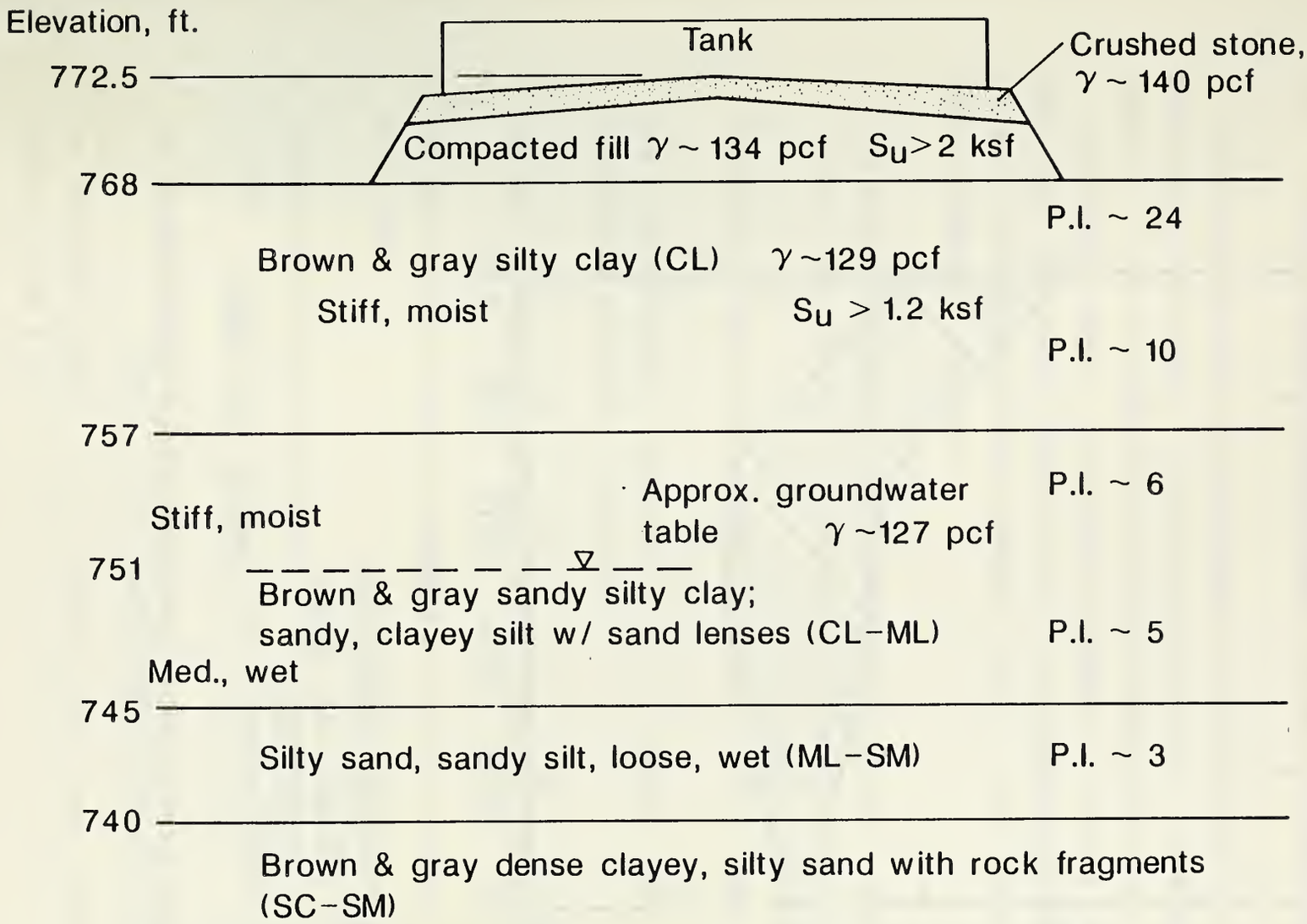

γ = in-place unit weight of soil, pcf
P.I. = plasticity index, percent
S_u = undrained shear strength
CL,ML,SM, are soil classification symbols (ASTM D2487)

Figure 4.5 - Schematic Drawing of Soil Profile Developed by Interpolation Between Borings. (Based on subsurface data supplied by the Pennsylvania Task Force)

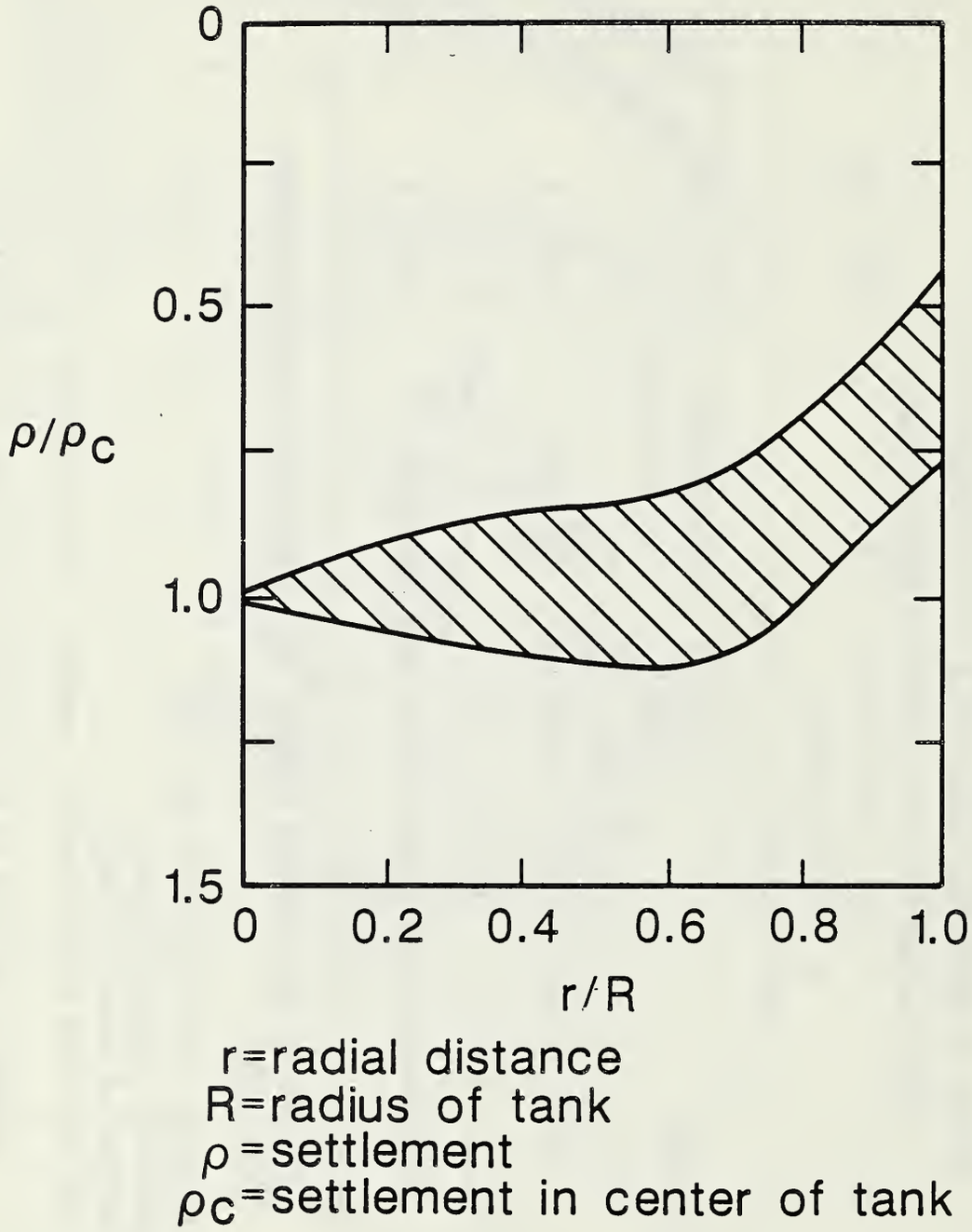

Figure 4.6 - Assumed Shape of Normalized Settlement Profile of Tank. (Profile-shape B from D'Orazio et al., 1987)

5.0 STRUCTURAL ANALYSIS

5.1 Stress Analysis of the Tank

A structural analysis was performed to determine the stresses in the tank at the time of collapse. The cylindrical wall of the tank was modeled (see Figure 5.1) and analyzed by the finite element method for the loading produced by the static head of the stored product. Pre- and post-processing of the data were done using PATRAN [5.1]. An axisymmetric analysis was performed using 4-node quadrilateral elements [5.2]. The following assumptions were made in modeling the tank:

- The plate thicknesses were assumed to be the nominal plate thicknesses (shown in Figure 2.1) less an average corrosion of 1/16 in.
- The shell courses were assumed to be 8 ft - 0 in high.
- The welds between successive shell courses were modeled as smooth transitions as shown in Figure 5.1.
- The tank bottom and roof were not included in the model.
- The base of the tank was modeled as fixed in the radial direction but free to rotate.
- The top of the tank was modeled as free in the radial direction and free to rotate.
- The height of the stored product was assumed to be 46 ft - 0 in.
- The specific gravity of the stored product was assumed to be 0.87 for a density of 54.3 pcf.

Two elements were used through the shell thickness and the aspect ratio of the elements was no greater than 1:1.5. This produced a model of the full height of the tank consisting of 5913 nodes and 3940 elements.

The circumferential membrane stress (the normal stress in the circumferential direction reported at the tank wall centerline) is plotted in Figure 5.2. The circumferential membrane stress is zero at the tank base (the base is radially restrained) and reaches a maximum of 15.1 ksi in the first shell course at a height of approximately 40 in. The circumferential membrane stress at the juncture of the first and second shell courses is approximately 13.7 ksi.

The effect of a rotational restraint at the base of the tank was also investigated. The analysis described above was repeated except that the base was restrained against both translation and rotation. The meridional bending stress (vertical stress at the outer surface) in the first two shell courses is shown in Figure 5.3. The rotational restraint produces a significant meridional bending stress at the base of the tank but the effects of the restraint diminish rapidly with increasing height. At the juncture of the first and second shell courses (8 ft), there is essentially no difference in the meridional bending stress between the rotationally restrained and rotationally free cases. In addition, the meridional bending stress at this elevation, resulting from the discontinuity in plate thickness, is shown to be approximately zero. Thus, the stress at the juncture of the first and second shell courses is essentially the circumferential membrane stress and is independent of the base fixity condition.

5.2 Foundation Settlement Analysis

To evaluate the stresses in the tank resulting from differential foundation settlement, a finite element analysis was made for an assumed displacement profile. The following assumptions were made in modeling the tank:

- The plate thicknesses were assumed to be the nominal plate thicknesses (shown in Figure 2.1) less an average corrosion of 1/16 in.
- The shell courses were assumed to be 8 ft - 0 in high.
- The welds between successive shell courses were not modeled.

o The tank bottom and roof were not included in the model.

One half of the tank wall was modeled using 8-node quadrilateral shell elements. Each element was uniform in size and measured 24 in high by 23.52 in wide. This resulted in 24 elements along the height of the tank and 96 around one half of the circumference for a total of 2304 elements. A diagram of the finite element model is shown in Figure 5.4.

Symmetry was accounted for in the boundary conditions along the tank centerline. The top of the tank wall was restrained in the radial direction only to account for the restraint provided by the roof. The base of the tank was restrained radially and subjected to an assumed displacement profile in the vertical direction, $v_0(\theta)$, given by

$$v_0(\theta) = 0.06 \cos(6\theta) + 0.06 \quad \text{for} \quad 0° \leq \theta \leq 30°$$
$$v_0(\theta) = 0.0 \quad \text{for} \quad 30° < \theta \leq 180°$$

This displacement profile is symmetric about the tank centerline, has a maximum displacement of 0.12 in (0.01 ft), and has a zero slope at 0° (tank centerline) and 30° (extent of localized differential settlement). This profile was selected to represent a differential displacement of 0.01 ft in a 60° arc corresponding to level readings taken at 12 locations around the tank base.

The maximum meridional membrane stress was approximately 3 ksi. Of more interest is the circumferential stress at the juncture of the first and second shell courses (height above tank bottom of the flaw). The membrane circumferential stress, plotted as a function of θ, is shown in Figure 5.5. As can be seen, the maximum tensile stress is approximately 120 psi and the maximum compressive stress is approximately 200 psi. The stresses are seen to decay to zero within 90°. From this analysis, it is seen that locallized differential settlements on the order of 0.04 ft (approximately 0.5 in) would produce tensile membrane stresses in the vicinity of the flaw of only 500 psi. Thus, it is unlikely that any differential foundation settlements contributed significantly to the tensile stress normal to the flaw.

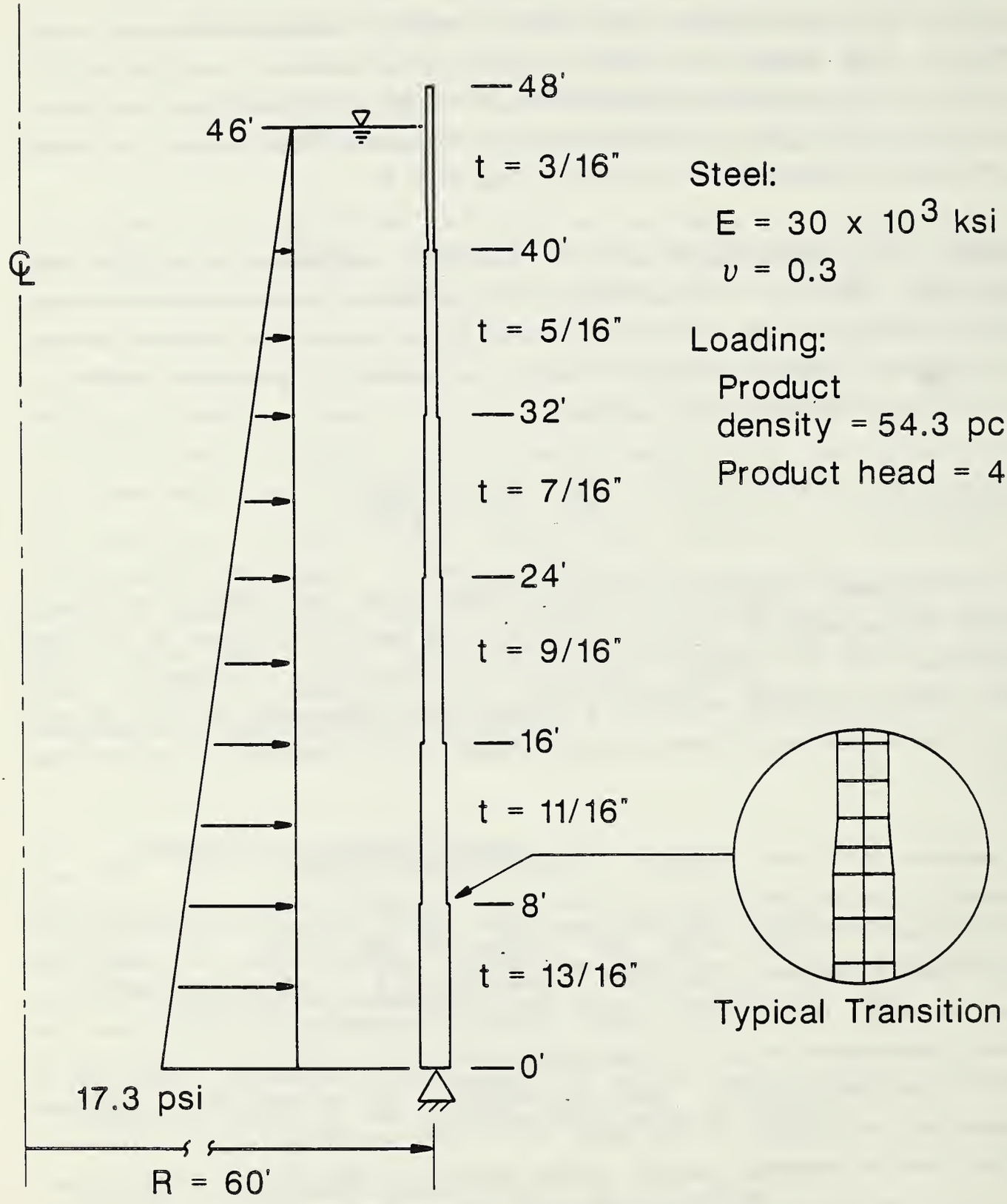

Figure 5.1 - Axisymmetric Analysis Model of Tank Wall

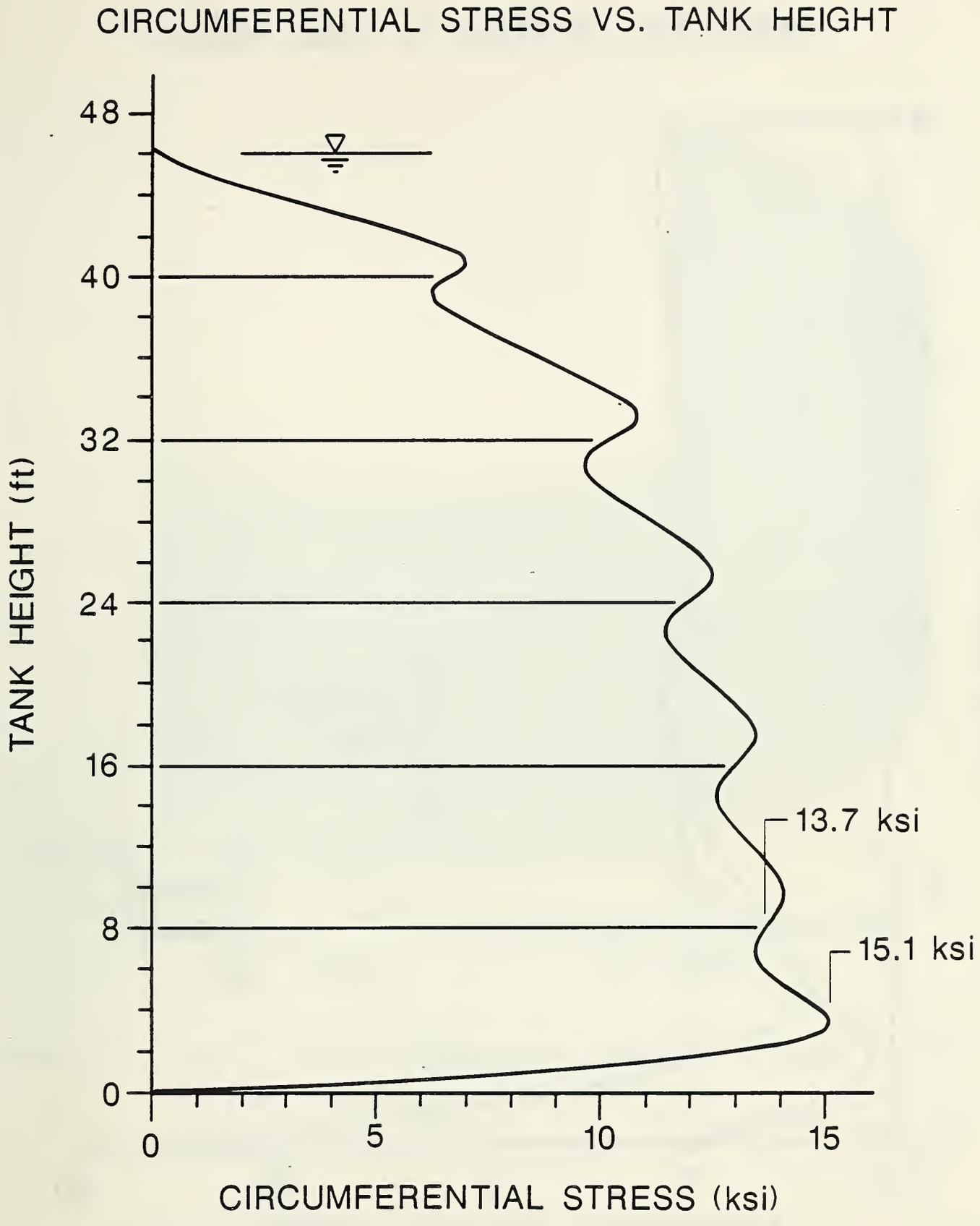

Figure 5.2 - Circumferential Membrane Stress in the Tank Wall

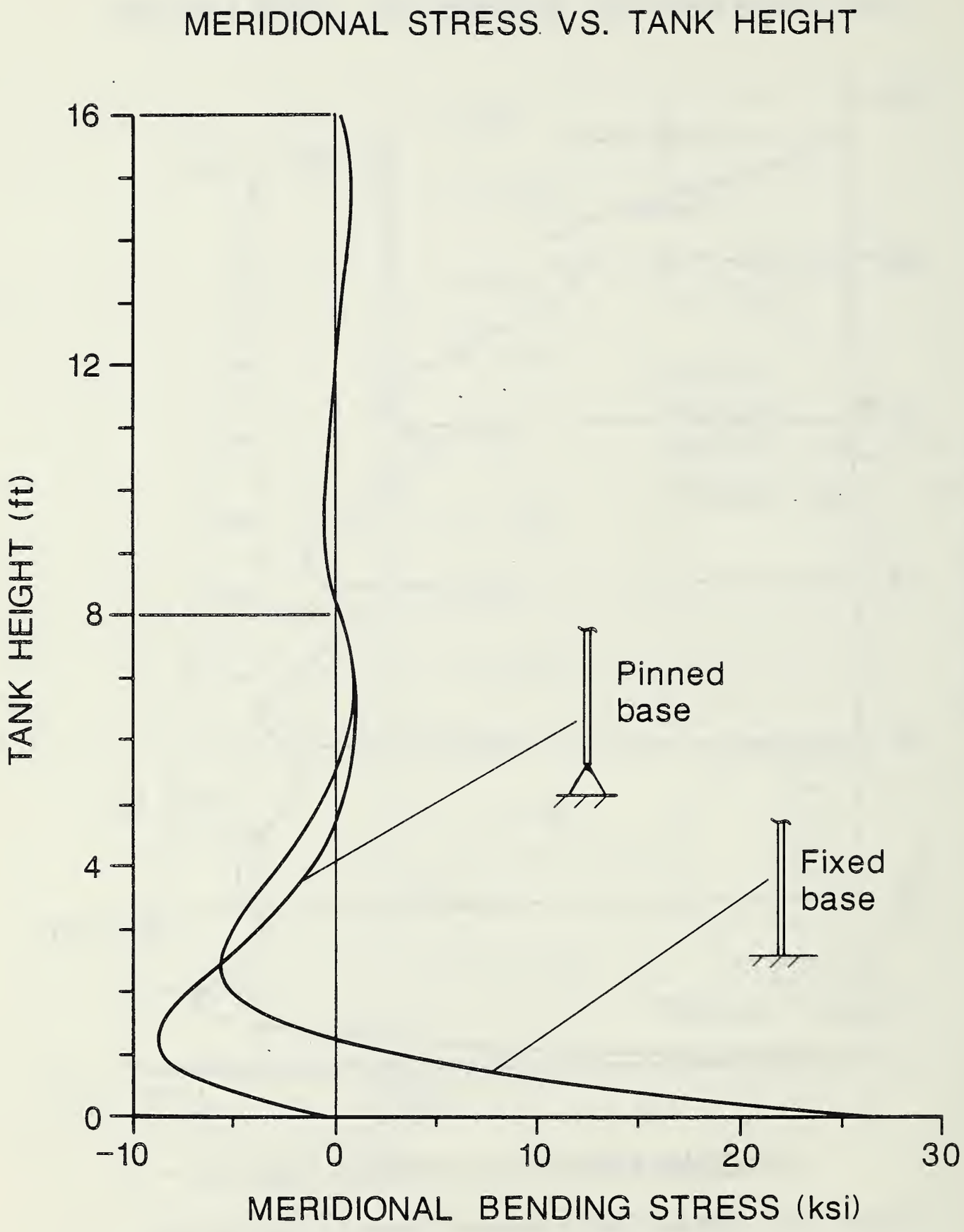

Figure 5.3 - Meridional Bending Stress in the First Two Shell Courses

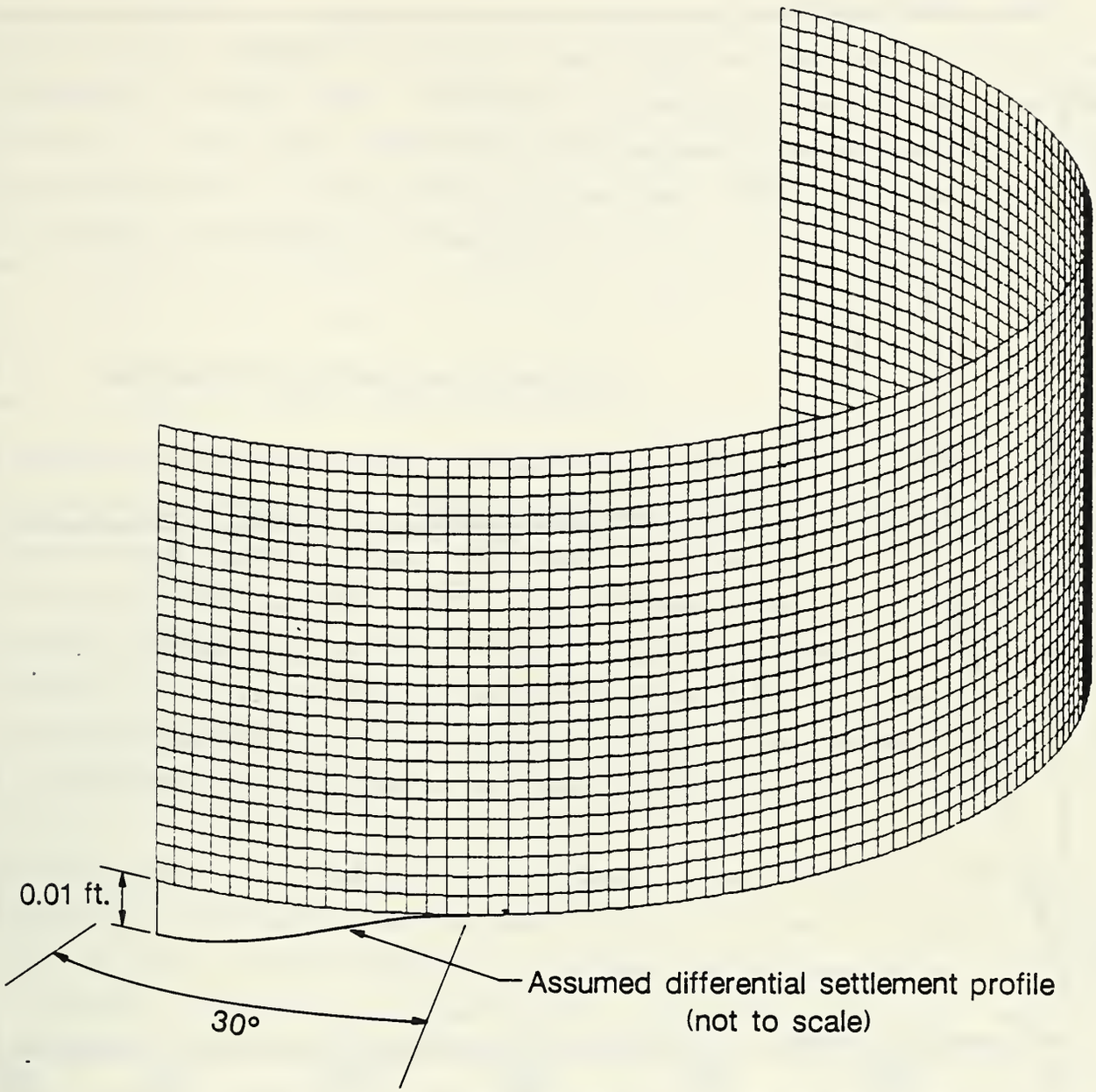

Figure 5.4 - Symmetric Model of Tank Wall for Foundation Settlement Analysis

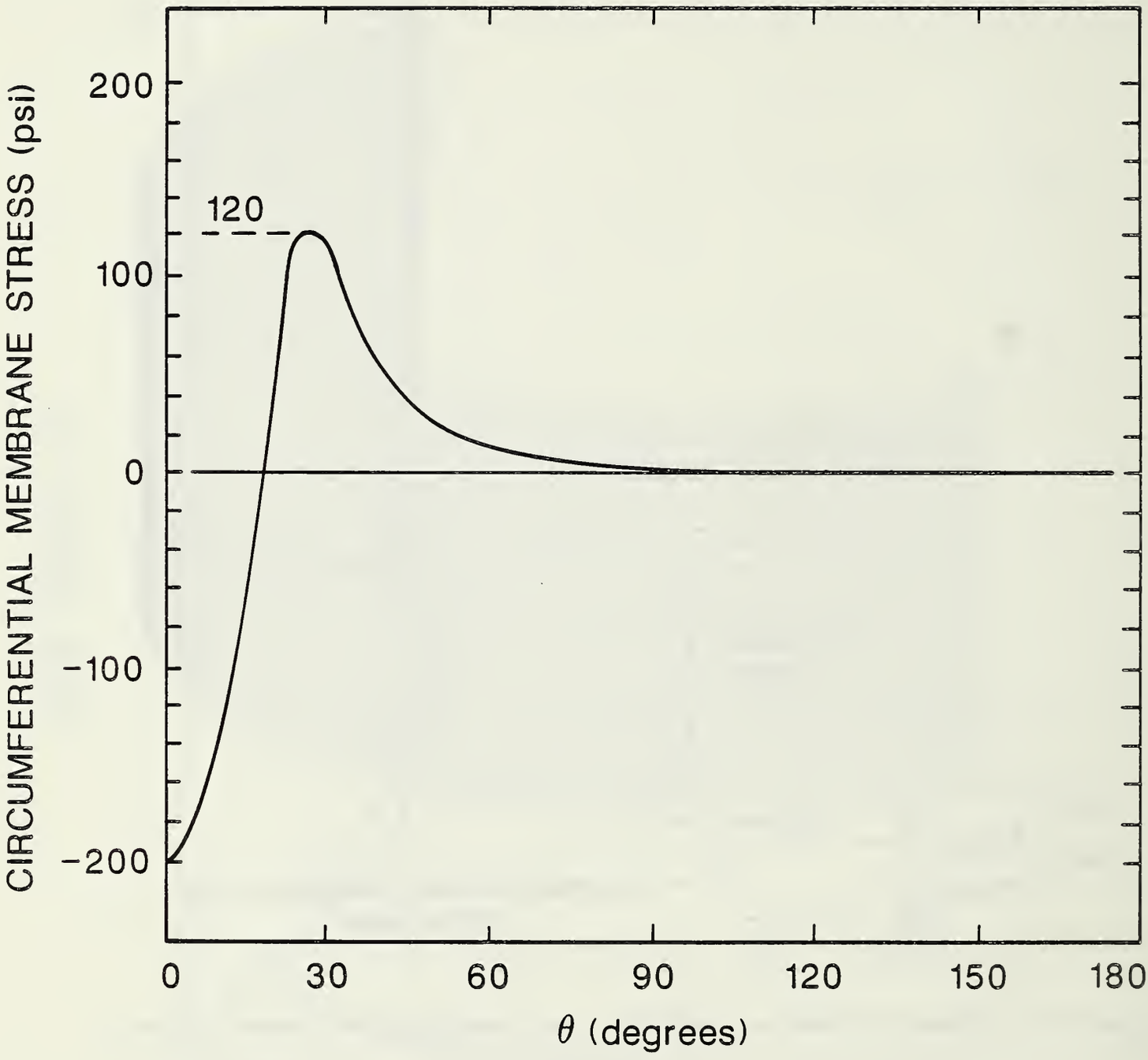

Figure 5.5 - Circumferential Stresses in the Tank Wall at a Height of 8 ft due to an Assumed Differential Settlement of 0.01 ft

6.0 THERMAL ANALYSIS OF THE TANK WALL

6.1 General

The fracture toughness of carbon steel, such as that used in this tank, is dependent on temperature. Therefore, to determine the fracture toughness of the steel at the time of collapse, it is necessary to estimate the temperature of the tank wall in the vicinity of the flaw. This information will be used in the fracture analysis in Chapter 8.

6.2 Ambient Temperature and Wind Data

Surface weather observations for January 2, 1988, the day of the collapse, are presented in Table 6.1. These data were recorded at the Allegheny County Airport (see map in Figure 1.2) located approximately seven miles from the Ashland Floreffe terminal. At the approximate time of collapse (16:57), the recorded temperature was 26° F. As indicated in Table 6.1, the temperature was 26° F for the preceeding two readings as well. Due to the proximity of the Ashland terminal to the Allegheny Airport, it was assumed that the ambient air temperature at the time of collapse was 26° F.

The wind speed recorded at the Allegheny County Airport at the approximate time of collapse was out of the south-west at 8 knots or slightly more than 9 mph. To translate this information to the tank collapse site, the difference in surface terrain between that at the airport where the data were recorded and that at the collapse site must be considered. The variation in wind speed with terrain roughness is well documented [6.5]; at equal elevations, the mean wind speed will be less over the rougher terrain. Additionally, there is a variation in wind speed with height above the ground. The relationship between mean wind speed, height above ground and roughness of the terrain is [6.5],

$$\frac{u(z)}{u(z_r)} = \frac{\ell n \frac{z}{z_0}}{\ell n \frac{z_r}{z_0}}$$

where,

u = mean wind speed

z = height above ground

z_r = reference height

z_0 = roughness length

Roughness lengths for various terrain categories have been compiled [6.5]. If the airport is categorized as "open" terrain (z_0 = .230 ft) and the Ashland terminal as "sparsely built up" terrain (z_0 = .989 ft), then for a wind speed of 9 mph recorded at height of 20 ft (assumed), the mean wind speed at a height above ground of 8 ft (top of first shell course) is calculated to be between 4 and 5 mph.

6.3 Temperature of the Oil in the Tank

The temperature of the oil was recorded by Ashland personnel at the time the product level readings were taken. A graph showing the temperature of the fuel oil in Tank No. 1338 for the period August 25, 1987 through January 1, 1988 is presented in Figure 6.1. The temperature of the oil in Tank No. 1338 on the day before the collapse (the last date on which the temperature was recorded) was 46° F. The temperature of the oil pumped into Tank No. 1338 on the day of collapse was reported to be 46° F as well. Assuming that the recorded temperature of the oil, both in the tank and on the barges, was representative of the stored product (i.e., no stratification had occurred), and that complete mixing occurred as a result of the introduction of the fuel oil into Tank No. 1338, a reasonable estimate of the oil temperature at the time of collapse is 46° F.

6.4 Thermal Analysis

The steady-state heat transfer through the wall of the storage tank may be expressed as

$$q = \frac{T_{oil} - T_A}{\frac{1}{h_i A} + \frac{\Delta x}{kA} + \frac{1}{h_o A}}$$

where

T_{oil} = temperature of the oil within the storage tank, °C

T_A = surrounding ambient temperature, °C

h_i = inside surface heat transfer coefficient, $W/m^2 \cdot °C$

h_o = outside surface heat transfer coefficient, $W/m^2 \cdot °C$

k = thermal conductivity of the storage tank wall, W/m°C

Δx = thickness of the storage tank wall, m

A = heat transfer area, m^2

In accordance with Reference 6.1, the inside surface heat transfer coefficient, h_i, due to free convection may be evaluated using,

$$Nu_{y,f} = .59 \left(Gr_{y,f} \, Pr_f\right)^{.25}$$

where

$Nu_{y,f}$ = local Nusselt number evaluated at the interior film temperature, $(T_i + T_{oil})/2$ where T_i is the inside surface temperature, and at the juncture of the first and second shell courses (dimensionless),

$Gr_{y,f}$ = local Grashof number evaluated at the interior film temperature and at the juncture of the first and second shell courses (dimensionless), and

Pr_f = Prandtl number evaluated at the interior film temperature (dimensionless).

The inside surface heat transfer coefficient is computed from the relationship

$$h_i = \frac{Nu_{y,f} \, k_f}{y}$$

where

k_f = thermal conductivity of the oil evaluated at the interior film temperature, W/m°C, and

y = height of the first shell course, m.

The required thermal properties were taken from Spiers [6.2]. The outside heat transfer coefficient is computed using the Jurges correlation presented in McAdams [6.3],

$$h_o = 5.7 + 3.8V$$

where

V = wind speed in m/s.

The thermal conductivity of the steel wall is taken as 54 W/m•°C which corresponds to a 0.5% carbon steel [6.4]. The inside and outside surface temperatures are computed as

$$T_i = T_{oil} - \frac{q}{h_i}$$

and

$$T_o = T_A + \frac{q}{h_o}$$

Because the properties used to compute the inside surface heat transfer coefficient are evaluated at the interior film temperature which in turn is dependent on the inside surface temperature, the solution requires an iterative approach. An initial guess is made to approximate the inside surface temperature. The inside heat transfer coefficient, heat transfer, and accompanying inside and outside surface temperatures are then computed. The interior film temperature is computed from the resulting inside surface temperature. The computations are repeated using the computed inside surface temperature. This procedure is repeated until the interior film temperature converges to within 0.01°C.

The heat transferred through the tank wall was computed using the values for the temperature of the oil in the tank, ambient air temperature, and wind speed determined in the previous sections and converted to the appropriate units. It was found that the temperature gradient through the tank wall at a height of 8 ft was almost negligible, being less than one half a degree. Therefore, the average of the outside and inside wall temperatures is reported. For an oil temperature of 46° F, an outside ambient temperature of 26° F and a wind speed of 5 mph, the average wall temperature of the tank, at

a height of 8 ft, was approximately 32° F.

To illustrate the effects of the oil temperature and wind speed on the temperature of the tank wall, heat transfer calculations were made for oil temperatures ranging from 35 to 55° F and wind speeds from 0 to 10 mph. Results are given in Table 6.2.

Table 6.1 - Surface Weather Observations - January 2, 1988
(Allegheny Co. Airport)

Time	Temperature (° F)	Wind Speed (knots)	Wind Direction (deg from North)
00:50	18	7	290
01:50	16	7	290
02:50	16	10	290
03:50	14	7	270
04:50	13	6	270
05:50	13	5	270
06:50	12	4	300
07:45	12	6	300
08:45	14	4	270
09:50	15	6	180
10:50	17	9	170
11:50	20	5	230
12:50	22	0	000
13:50	24	6	230
14:50	26	6	240
15:50	26	8	220
16:57	26	8	230
17:51	24	5	210
18:50	24	6	230
19:55	23	5	190
20:55	22	6	200
21:55	21	6	200
22:55	21	6	200
23:55	20	5	180

Table 6.2 -Average Tank Wall Temperature at Elevation 8 ft

Wind Speed (mph)	Oil Temperature (° F)				
	35°	40°	45°	50°	55°
0	30.2	33.0	36.0	39.3	43.0
1	29.7	32.2	34.9	37.9	41.2
2	29.3	31.5	34.0	36.7	39.8
3	29.0	31.0	33.3	35.8	38.6
4	28.7	30.6	32.7	35.0	37.6
5	28.5	30.2	32.2	34.3	36.8
6	28.3	29.9	31.7	33.8	36.0
7	28.1	29.7	31.4	33.2	35.4
8	28.0	29.4	31.0	32.8	34.8
9	27.9	29.2	30.7	32.4	34.3
10	27.8	29.0	30.5	32.1	33.9

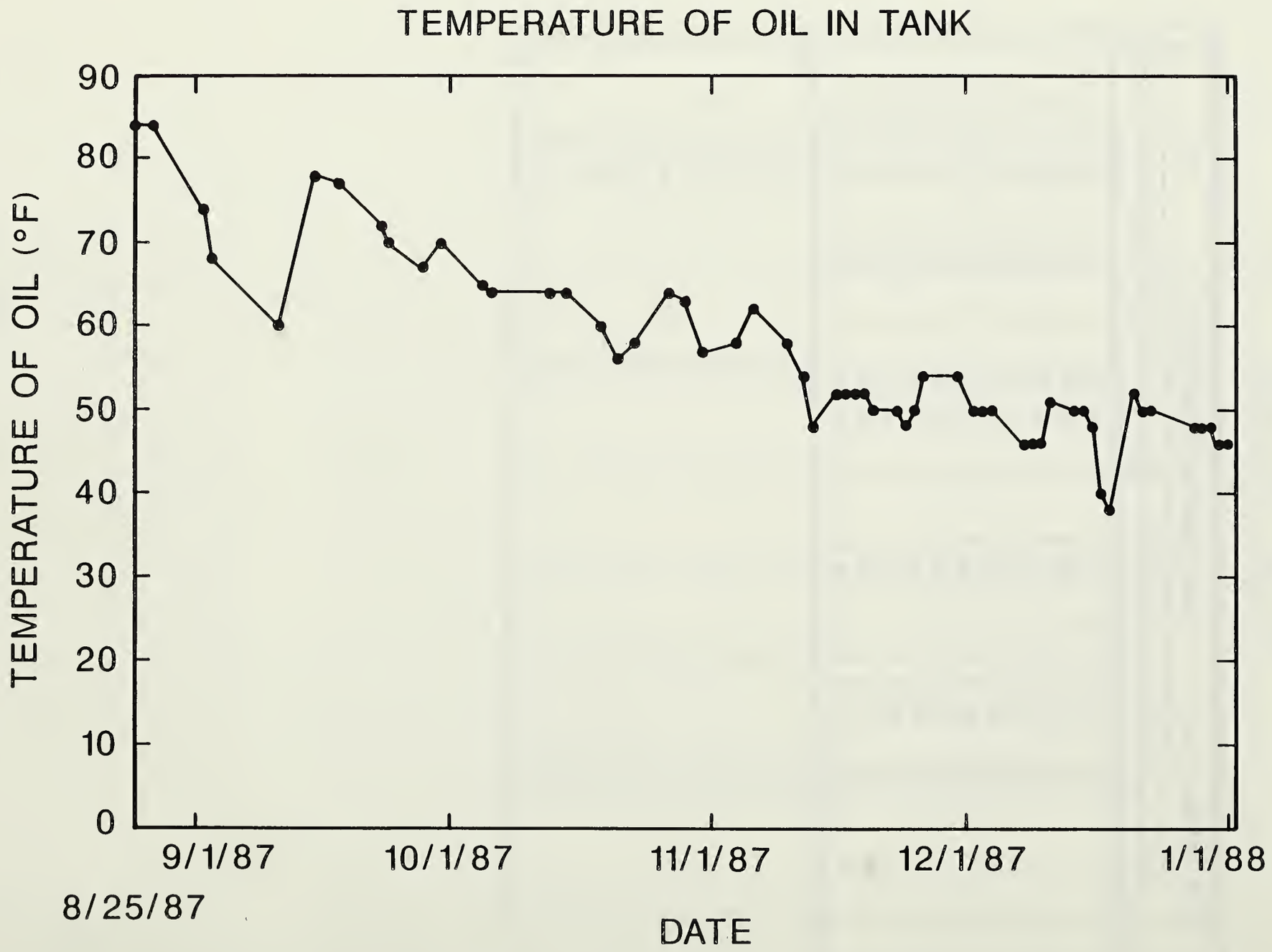

Figure 6.1 Temperature of the Oil in Tank No. 1338

7.0 METALLURGICAL INVESTIGATION

7.1 Introduction

The NBS metallurgical investigation consisted of examination of the failed tank at the field site of the failure, selection of samples from the tank to be used for characterizing material properties, identification of possible failure modes and causes, detailed examination of the fracture surfaces, and failure analysis based on fracture mechanics principles. In addition, a detailed fractographic analysis of the fracture surface and the defect found on the fracture surface was conducted by Battelle. The results were made available to NBS and are included in this report.

As described in detail in Chapter 2 of this report, the tank was constructed of steel plates that were nominally 8 ft wide and 32 ft long. The tank consisted of 6 shell courses each approximately 8 ft high. The bottom, or first, shell course was nominally 7/8 in thick, the next higher or second course was 1/8 in thinner i.e. 3/4 in thick, and each subsequent shell course was nominally 1/8 in thinner than the next lower shell course. The highest or sixth course was 1/4 in thick. A primary fracture was found that had propagated vertically through all six shell courses and split the tank from top to bottom as shown in Figure 7.1. Visual observation at the field site showed that this fracture was flat and perpendicular to the plate surface over its entire length (see Figure 3.10) with no evidence of tearing or shear fracture. Chevron markings on the fracture surface pointed to a defect on the fracture surface that was identified as the point of initiation of the fracture. This defect was near the top of the first shell course just below the horizontal weld between the first and second shell courses and just below the vertical weld between two plates in the second shell course.

As shown in Figure 7.1, test specimens were taken from the first and second shell courses to evaluate the typical properties of the steel plates in the tank. Test specimens were taken from typical regions of vertical, horizontal, and T weld sections to evaluate the welds in the tank. The laboratory tests conducted to evaluate the properties of the tank steel were tensile tests to determine strength and ductility, various fracture toughness and notch

sensitivity tests to determine the susceptibility to fracture initiation, propagation, and arrest, and metallography and hardness tests.

7.2 Materials Properties Characterization

7.2.1 Location of Test Specimens

Samples were taken by Ashland from the failed tank to evaluate the properties of the steel from which the tank was constructed. Test samples approximately 2 ft by 3 ft size were taken for the NBS from the steel plate in the first and second shell courses of the tank near the vertical fracture surface as shown in Figure 7.1. Test sample 5E was a base metal sample from the first shell course of the tank approximately 4 ft from the vertical fracture. Test sample 3E was a base metal sample from the second shell course of the tank approximately 4 ft from the vertical fracture. Test sample 4E included the horizontal weld between the first and second shell courses of the tank. Test sample 9 was a T weld at the junction of two plates in the second shell course and a plate in the first shell course of the tank approximately 60 ft from the vertical fracture. The identity and location of specific material properties test specimens taken from each of the test samples are shown in Figures 7.2, 7.3, 7.4 and 7.5. For the plates in the first and second course of the tank, the rolling direction was parallel to the long (32 ft.) dimension of the plate. The orientation of the plate (relative to the rolling direction) was maintained and taken into account for all specimens used for mechanical properties tests and for fracture toughness tests.

7.2.2 Chemical Composition

To identify the plate steel used in the tank, samples for chemical analysis were taken from the first and second shell course plates. The chemical analysis was performed by emission spectroscopy following ASTM Standard E-415-85 [7.1]. Quantitative analysis was performed to determine the amount of C, P, S, Mn, Si, Ni, Cr, V, Ti, Mo, Cu, Co, and Al in each sample.

Chemical analyses were performed on three locations in the base metal specimen from the first course (sample 5-3). As shown in the micrograph in Figure 7.6,

the first shell course base metal showed substantial evidence of "banding" due to chemical segregation in the steel plate. Therefore, chemical analyses were taken in three locations as shown in Figure 7.6 to determine the extent of the chemical segregation. The chemical analyses were performed four times at each location. The results (average of four determinations) are shown in Table 7.1 as samples 5-3-1, 5-3-2, and 5-3-3 corresponding to the locations shown in the micrograph in Figure 7.6. Chemical analyses were performed on one location in the base metal specimen from the second shell course (sample 3-2). The sample was analyzed four times. The results of the chemical analyses are shown in Table 7.1 as sample 3-2.

The tank was probably constructed of steel made to the ASTM standard A-10-39 for Mild Steel Plates [7.2]. This ASTM Standard has been replaced by Standard A-283-84 [7.3] for Low and Intermediate Tensile Strength Carbon Steel Plates, Shapes, and Bars. The very limited specifications for chemical composition of the steel are identical in both Standards A-10-39 and in A-283-84. The only chemical composition limits specified in either standard are that the maximum phosphorus content should be less than 0.040 percent, the maximum sulfur content should be less than 0.050 percent, and. if copper is specified, the minimum copper content should be greater than 0.20 percent. No specific carbon content or amount of any alloying element is specified in either of the referenced standards.

Table 7.1, shows that the steel plates from both the first shell course (sample 5-3) and from the second shell course (sample 3-2) satisfy the chemical composition requirements of both the ASTM A-10-39 and A-283-84 Standards. Steel made to the ASTM Standard A-283-84 (Grade C strength level) is one of the types of steels permitted for construction of oil storage tanks by the current version of the American Petroleum Institute Standard 650, *Welded Steel Tanks for Oil Storage* [7.4].

The steel plates from this tank are identified as plain carbon steels typical of common structural steels. No additional alloying elements were present in amounts above the levels normally considered as residual levels. The ratio of the manganese to carbon in these steel plates was less than three. To reduce the tendency for brittle fracture, current steels for welded construction are

specified to have a ratio of manganese-to-carbon of not less than three [7.5]. The significance of this manganese to carbon ratio was not known or used at the time this tank was originally constructed.

The very low silicon content (less than 0.001 percent) in sample 3-2 from the second shell course indicates that this steel plate probably was produced as a "rimmed" steel. The slightly higher, silicon content (0.026 percent) of the steel plate from the first shell course (sample 5-3) is still quite low for steels of this type and indicates that this steel plate also probably was produced as a "rimmed" steel. The present API 650 permits ASTM A-283 (Grade C) steel to be used as a Group I steel for oil tank construction, but requires that the steel be produced as a semi-killed steel when fracture toughness criteria apply. "Rimmed" steel is not allowed and therefore the steel in this tank does not meet the requirements of the present API 650.

Chemical analyses were performed at 8 locations within the specimen taken from a section of the horizontal weld (test sample 4E) as shown in Figure 7.6. The results of these chemical analyses are shown in Table 7.1 identified as samples 1 through 8. Sample location 1 was in the base metal from the second shell course. The chemical composition at this location is consistent, within the expected normal variability in composition, with the chemical composition of the same base metal plate (sample 3-2) at a different location. Sample locations 2, 3, and 4 are in the base metal from the first shell course. The chemical compositions at these three locations (2, 3,and 4) are consistent with the chemical compositions determined in corresponding locations in the base metal sample from the first shell course (test sample 5-3). Although the base metal from the first shell course showed significant banding in the microstructure (Figure 7.6), no evidence of significant segregation was shown by the chemical analyses.

The chemical composition was determined for selected areas in the horizontal weld (test sample 4E). Areas of "new" weld deposited when the tank was reassembled at the Floreffe site were identified by metallographic examination of the weld metal and could be distinguished from the "old " welds deposited when the tank was originally constructed near Cleveland.

Locations 6 and 8 in the weld metal sample (Figure 7.6) have been identified to be in the "new" weld metal (the weld made when the tank was reassembled at the Floreffe site). The chemical composition of the weld metal at locations 6 and 8 are considered to be equivalent within the expected range of variability for chemical composition of weld metal. Locations 5 and 7 in the weld metal sample (Figure 7.6) have been identified to be in the "old" weld metal that was deposited when the tank was originally fabricated at the site near Cleveland. The chemical composition at locations 5 and 7 are considered to be equivalent within the normally expected range of variability for chemical composition of weld metal.

The chemical composition of the "new" weld metal is significantly different from the chemical composition of the "old" weld metal. This indicates that the "new" welds most likely were made with a different type welding electrode and/or by using a different welding process than the "old" welds. The significant difference in chemical composition is that the "new" weld metal had a nominal chemical composition 0.90 per cent manganese and 0.40 per cent silicon whereas the "old" weld metal had a nominal chemical composition of 0.50 percent manganese and 0.16 per cent silicon. No attempt was made to identify the specific type of welding electrode used from the chemical composition.

7.2.3 Tensile Tests

Standard, round (0.500 in diameter) tensile test specimens made according to ASTM Standard E-8-86 [7.6] were taken in the longitudinal (parallel to the plate rolling direction) and transverse (perpendicular to the plate rolling direction) orientations from test sample 5E (the first shell course) and from test sample 3E (the second shell course) to evaluate the strength and ductility of the steel in the tank at room temperature. The results of these tests are summarized in Table 7.2. All tests were conducted according to the procedures specified in ASTM Standard E-8-86. At least three specimens were tested from each of the two shell courses in each of the two specimen orientations. No significant differences were found in the tensile strength, yield strength or elongation between specimens taken from the first shell course and specimens taken from the second shell course. No significant

effect of orientation relative to the plate rolling direction was found for the properties determined from the tensile tests.

Because there was no significant effect of specimen orientation and shell course plate found in the tensile tests results, the average value from all test specimens will be used for the calculations shown in later sections of this report. The value used for the yield strength is 34,000 psi and the value used for the tensile strength is 67,100 psi.

The tensile properties determined for the steel from both the first and second shell course of the tank meet the requirements specified in current ASTM Standard A-283-84 for Grade D and of the previous ASTM Standard A-10-39 in use at the time the tank was originally built. The current ASTM Standard A-283-84 specifies that for Grade D material, the tensile strength should be between 60,000 and 72,000 psi and the yield strength should be greater than 33,000 psi. However, API 650 only allows ASTM A-283 Grade C steel which has an allowed tensile strength range of 55,000 to 65,000 psi. Therefore, the steel in this tank does not meet the requirements for a ASTM A-283-84 Grade C steel that is permitted by API 650. The average elongation of 34.4 percent determined from these tensile tests exceeds the minimum of 23 per cent required by the current ASTM Standard A-283-84.

7.2.4 Charpy-V-Notch Tests

Charpy-V-notch tests were conducted on material from the first shell course (test sample 5E) and from the second shell course (test sample 3E). Standard, full size (10 x 10 mm) Charpy-V-notch specimens were made and tested according to ASTM Standard E-23-86 [7.7]. Specimens were taken from each plate in the longitudinal orientation (with the axis of the specimen parallel to the rolling direction of the plate) and in the transverse direction (with the axis of the specimen perpendicular to the rolling direction of the plate). All specimens were notched in the through thickness direction, that is with the axis of the notch perpendicular to the plate surface. At least two specimens from each plate in each orientation were tested at each of the selected test temperatures. The tests were conducted at nominal temperatures of 20° F, 40° F, 60° F, 80° F, 120° F and 160° F to determine the full transition

temperature curve for the steel plates. For each test specimen, the energy absorbed, lateral expansion, and percent shear fracture appearance were determined.

The results of the Charpy-V-notch tests for each plate and each orientation are summarized in Tables 7.3, 7.4, 7.5 and 7.6 and the values of the energy absorbed are shown Figures 7.7, 7.8, 7.9, and 7.10. For test temperature below 60° F all specimens exhibited low property values as determined by the Charpy-V-notch specimens. At all temperature of 55° F and below in each of the plates tested, the energy absorbed was less than 10 ft-lbs, the lateral expansion was 15 mils or less, and the amount of shear fracture was less than 30 per cent This indicates substantial tendency for brittle fracture at temperatures of 55° F and below. The energy absorbed and lateral expansion were essentially the same at 20° F as at 40° F indicating that the steel was operating in the "lower shelf" region as determined by the Charpy-V-notch tests. The steel plates did not exhibit significant toughness, as measured by the Charpy-V-notch tests until temperatures of 100° F and above. Specimens exhibited greater than 50 per cent shear fracture appearance only above a temperature of 95° F.

The plates from the first shell course (test sample 5E) and from the second shell course (test sample 3E) do not show significant differences in properties determined from the Charpy-V-notch tests at temperatures below 60° F. At higher temperatures, the plate from the first shell course (test sample 5E) appears to be slightly tougher than the plate from the second shell course (test samples 3E). At temperatures below 60° F, the orientation of the test specimens with respect to the rolling direction of the plate does not significantly affect the properties determined by these tests. At higher temperatures, the specimens oriented in the longitudinal direction are slightly tougher in both of the test plates.

The ductile-to-brittle transition temperature can be determined from the Charpy-V-notch tests results. A different value of the transition temperature is estimated depending on the choice of parameter used to define the transition temperature [7.8]. The transition temperature can be defined as (1) the temperature at which the energy absorbed exceeds 15 ft-lbs, (2) the

temperature at which the lateral expansion exceeds 15 mils, or (3) the temperature at which the shear fracture appearance is greater than 50 percent. Each of these measures of the transition temperature has been found to correlate with service experience or to predict failure for specific types of steels or structures. The most commonly used transition temperature criterion for low strength steels is the 15 ft-lbs absorbed energy. The 15 ft-lb criterion is used in API 650 to specify the transition temperature of steels.

A summary of the transition temperature for steel plates from the first and second shell courses is shown in Table 7.7. It should be noted that the transition temperature for the steel plates in this tank was well above the operating temperature of the tank by all of the criteria used to define transition temperature. This means that the tank was definitely operating at a temperature at which the steel is expected to be brittle.

7.2.5 Drop-Weight Nil-Ductility (NDT) Tests

Drop-weight tests were conducted to determine the nil-ductility transition (NDT) temperature for specimens taken from the first shell course (sample 5E) and from the second shell course (sample 3E). The specimens were prepared and the tests were conducted according to ASTM Standard E-208-85 [7.9]. Standard Type P-2 specimens (3/4 in thick by 2 in wide by 5 in long) were prepared from the first and second shell course plates. In addition, subsize Type P-3 specimens (5/8 in thick by 2 in wide by 5 in long) were tested from the first shell course plates to determine if specimen size had a significant effect on the NDT temperature. Tests were conducted at temperatures in the range of 40° F to 80° F to determine the nil-ductility transition (NDT) temperature.

The results of the test are shown in Table 7.8 for all plates tested. The NDT temperature for the plate from the first shell course (test sample 5E) was +60° F for the standard Type P-2 specimens and was +50° F for the subsized Type P-3 specimens. This difference in NDT temperature between the two different specimen sizes is not considered to be significant. For purpose of analysis the NDT temperature of the first shell course plate will be taken as +60° F. The NDT temperature for second shell course plate (test sample 3E) was determined to be +70° F.

The NDT temperature is defined as the maximum temperature where a standard drop-weight specimen breaks. This represents the temperature at which fracture in the structure can be initiated by a small flaw (length less than one inch) when stresses are at yield point levels. This temperature is significant because at temperatures below the NDT temperature, fracture initiation from relatively small flaws is possible and fracture arrest is unlikely to occur once the fracture is initiated. The NDT temperature is one measure of the temperature below which the structure behaves in a substantially brittle manner. The operating temperature of the tank at the time of failure was estimated to be approximately 32° F. Therefore, these test show that the tank was operating at a temperature substantially below the NDT temperature of the steel plates in the tank.

7.2.6 Fracture Toughness Tests

The fracture toughness was determined for the steel plate from the first shell course (test sample 5E) and from the second shell course (test sample 3E). The fracture toughness measured from these samples is representative of the fracture toughness of the base metal in the tank. The fracture toughness was determined using the ASTM E-813-87 "Standard Test Method for J_{IC}, a Measurement of Fracture Toughness" [7.10]. Standard 1T size compact tension test specimens were used to determine the fracture toughness. The single specimen, compliance test method option was used for determining the J_{IC}. All specimens were in the LT orientation as defined by ASTM Standard E-399-83 [7.11], that is the specimen was notched so that the crack propagated transverse to the rolling direction of the plate. This orientation matches the direction of crack propagation of the primary fracture in the ruptured tank. The specimens from the first shell course plate (test sample 5E) were nominally 0.750 in thick with side grooves to a depth of nominally 0.075 in on each side of the specimen. The specimens from the second shell course plate (test sample 3E) were nominally 0.625 in thick with sides grooves nominally 0.075 in deep on each side of the specimen.

The fracture toughness was determined over the temperature range of 20° F to 105° F. At least two test specimens from each plate were tested at each temperature from 20° F to ambient temperature (about 70° F). The fracture

toughness test results are summarized in Table 7.9.

The fracture toughness was determined according to the ASTM Standard test method E-813-87 instead of according to the ASTM Standard test method E-399-83 for Plane-Strain Fracture Toughness (K_{IC}) of Metallic Materials because preliminary calculations based on the estimated K_{IC} and the yield strength of the steel plates indicated that test specimens sufficiently thick to meet the validity requirements of E-399-83 could not be obtained from the available steel plates. The ASTM E-813-87 test method determines the property J_{IC} which is a measure of the toughness of the material at the onset of crack extension.

The requirements for the provisional value of J_Q to be considered a valid J_{IC} are specified in the ASTM Standard E 813-87. The requirements are:

1) The specimen thickness B is > 25 J_Q/σ_y,

2) Initial specimen ligament, b_o is > 25 J_Q/σ_y,

3) The slope of the power law regression line, dJ/da, evaluated at Δa_Q is less than σ_Y,

4) No specimen demonstrates brittle cleavage fracture at the applicable test temperature and rate,

5) None of the nine physical measurements of the crack size differ by more than 7% from the average physical crack size,

6) Neither of the two near surface crack extensions measurements or surfaces of plane sided specimens differs from the crack extension at the center by more than .02W.

7) The difference between the crack extension predicted by elastic compliance (or other method) at the last unloading and the average physical crack extension, Δa_p, does not exceed 0.15 Δa_p for crack extensions less than Δa_p(max) and 0.15 Δap(max) thereafter. E_M must not differ from E by more than 10%.

The total J integral is made up of two components, the elastic part identified as J_{el}, and the plastic part identified as J_{pl}. The elastic part is defined as:

$$J_{el} = \frac{[K_{(i)}]^2[1-\upsilon^2]}{E}$$

where

$$K_{(i)} = \left[\frac{Pi}{(B\ B_N\ W)^{1/2}} \right] f(a_o/W)$$

$f(a_o/W)$ is the compliance calibration for the specimen used

$$J_{PL} = \frac{\eta\ A_{PL}(i)}{(B_N)(bo)}$$

where

B_N = net specimen thickness

b_o = uncracked ligament, and

η = $(2 + 0.522\ b_o)/W$

In the tests conducted here, the J_{IC} tests did not give completely valid J_{IC} values at the lowest test temperatures (20° F, 40° F and 70° F) because there was little or no physical crack growth prior to failure of the specimens and the specimens failed almost completely by cleavage fracture. In these cases, as described in reference [7.12], a Jc value is obtained by taking the J integral at the point of crack initiation or instability to be the elastic component (Jel) as described above.

For specimens tested at 20° F, 40° F, and 70° F, the J versus crack growth curve did not show significant stable crack growth. This was confirmed after the test by cooling the specimen to liquid nitrogen temperature and then breaking the specimen open to examine the appearance of the fracture surface for evidence of stable crack growth prior to final fracture. No significant stable crack growth was found and the fracture surface was entirely brittle in appearance for all specimens tested at 20° F, 40° F, and 70° F.

The only completely valid J_{IC} that met all of the requirements shown above was obtained for the specimen tested at 105° F. This was the only specimen that showed sufficient stable crack growth prior to final fracture of the specimen.

The measured values of J_{IC} or J_C were used to estimate the plane strain fracture toughness (K_{IC}) or the plane stress fracture toughness (K_C) of the steel plates using the following relationship from reference [7.13]:

$$(K_C)^2 = (Jc)(E)$$

where

E = Young's modulus

The estimated values of Kc are reported in Table 7.9 and are used in the fracture analysis shown later in this report.

The fracture toughness of the first shell course plate (test sample 5E) was not significantly different from the fracture toughness of the plate from the second shell course (test sample 3E). The main interest of this study is focused on the toughness of the plate from the first shell course because that is where the fracture is believed to have originated. The fracture toughness in the plates from the first shell course was about 48 ksi$\sqrt{in}$ at 40° F and was 47 ksi$\sqrt{in}$ at 20° F. At 70° F, the fracture toughness was slightly higher, about 51 ksi$\sqrt{in}$.

7.2.7 Notched Bend Tests

A region of hardened metal with a maximum hardness on the Rockwell C scale (HRC) of 40 and a depth of 0.050 in was found around the defect on the fracture surface that was believed to be the origin of the fracture [7.14]. This region was expected to have a toughness less than the toughness of the normal steel plates in the tank. To verify this, special tests were conducted to simulate the effect of a defect located in heat affected or embrittled region. Single edge notched bend specimens were prepared from the first shell course plate steel. The specimens were nominally 3/4 in by 1 inch in cross section and 10 in long. A notch to simulate a defect was put in the center of the specimen as shown in Figure 7.11. The notch was made by electrodischarge

machining. The notch was 0.100 in deep, 0.010 in wide with an 0.005 in root radius. Some of the specimens were embrittled to simulate a heat affected zone by heating the surface of the specimen with gas-tungsten-arc (GTA) welding torch without melting the surface of the metal. This was done both before and after notching. As seen in Figure 7.12, heating with the welding torch produced an altered microstructure and hardened zone similar to the heat affected region found around the fracture surface defect described below.

The specimens were tested in three-point bending. The loading rate was held constant at 0.01 in/minute. Knife edges were attached to the mouth of the notch to monitor the notch-mouth-opening displacement. An environmental chamber was used to maintain the test temperature at 40° F. A load versus notch-mouth opening displacement curve was determined for each test specimen. One specimen with only a notch (without heating to cause embrittlement) was tested at room temperature (70° F). This specimen did not fail in a brittle manner but instead became fully plastic and did not fracture.

The results of additional specimens tested at 40° F are summarized in Table 7.10. A typical load versus notch-mouth-opening displacement curve for a notched only and notched plus heated specimen are shown in Figure 7.13. For each specimen, the maximum load at final fracture, the load at the onset of plastic deformation (yield load), and the notch-mouth-opening displacement at maximum load were determined. The area under the load versus displacement curve up to the point of fracture (maximum load) was calculated as a measure of the energy (expressed in ft-lbs) to initiate fracture in the specimen. A distinct brittle fracture occurred for each of the specimens tested at 40° F.

The specimen that was notched only, to simulate a defect in unaltered base metal, had a maximum load at the onset of fracture about 20 percent higher than the specimens that had a notch located in an embrittled and hardened region to simulate a defect in a heat affected region. The notch-mouth-opening displacement was more than twice as large for the specimen that only had a notch as for the specimens that were notched and heated. The total energy required to initiate fracture, taken as the area under the load-displacement curve, was more than twice as large (21.7 ft-lbs) for the notched only specimen as for the notched plus embrittled specimens (9.0 and 9.7 ft-

lbs). No significant difference was found between the specimens that were heated first and then notched and the specimens that were first notched and then heated.

These results show that it is much easier to initiate fracture at a defect in the steel base metal plate used in this tank if the defect is in a region that has been hardened and embrittled by heating. These results indicate that the toughness of the hardened and embrittled region may be less than one half the toughness of the normal steel plates.

7.3 Metallographic and Hardness Evaluation

7.3.1 Base Metal Evaluation

Additional characterization of the steel plates from the first and second shell courses was conducted by hardness tests and metallographic examination. The results of hardness tests on several samples are summarized in Table 7.11. The average hardness of the first shell course plate was 70 HRB (Rockwell B scale) and the average hardness of the second shell course plate was 71 HRB. These values are consistent with the measured tensile strength of approximately 67,000 psi. Typical microstructures of samples taken from the first and second shell course plates are shown in Figure 7.14. The microstructure consists of a uniform distribution of ferrite and pearlite, which is typical of low strength carbon steel. The ferrite grain size was determined to be ASTM grain size number 7.

7.3.2 Evaluation of Welds

The horizontal weld (test sample 4E) and the T-weld (test sample 9) were radiographed and then were evaluated by metallographic, hardness and Charpy-V-notch tests. The radiographic examination showed that the entire length of the horizontal weld from test sample 4E contained many weld defects including lack of fusion, nearly continuous lack of penetration, and extensive areas of porosity. The horizontal weld section was radiographed a second time after being ground from the original thickness of 7/8 in to a thickness of 1/2 in to

remove the weld crown and to attempt to remove the regions of lack of penetration. The second radiograph of the horizontal weld, shown in Figure 7.15, still shows extensive areas of porosity and lack of penetration. These results are confirmed by the metallographic examination results discussed below. The radiograph of the T-weld section (test sample 9), which includes the only section of vertical weld available for this investigation, showed similar extensive areas of weld defects such as lack of fusion, lack of penetration, and porosity. No attempt was made to determine from the radiographs if the defects found were located in the "old" welds used to fabricate the original tank or if the defects were in the "new" weld used to reassemble the tank at the Floreffe site. Although a detailed assessment was not made of the radiographs from this limited weld sample, the quality of the welds examined here would not satisfy the requirements of the current (1984) version of API 650.

Transverse sections of the welds were taken in the as received condition from nine different locations along the horizontal weld in test sample 4E. Photomicrographs were taken of each section to characterize the weld metal and to determine the type and number of weld defects in each specimen. Hardness measurements (Rockwell B hardness) were taken on each specimen at several locations within the old weld, new weld, and heat affected zones. Similar sections taken from four locations in the horizontal weld from test sample 4E (after the sample had been ground to a thickness of 1/2 in to remove the weld crowns) were evaluated in the same manner. Four transverse sections of the vertical weld in the test sample 9 containing the T-weld were taken to characterize the vertical weld.

Figure 7.16 shows a typical transverse section of the horizontal weld. The old weld is identified as the weld metal connected to the first shell course (the right side in Figure 7.16) and the new weld metal is connected to the second shell course. In this weld section, a significant area of lack of penetration is found at the junction between the old weld metal and new weld metal. This defect extends to a depth of about 40 percent of the thickness of the plate. A large area of porosity was found in the center of the old weld metal and numerous areas of small porosity were found in the upper part of the new weld metal.

Numerous hardness measurements were taken on this weld sample at location in the base metal, old and new weld metal, and heat affected zones of the old and new weld metal. As shown in Figure 7.16, the base metal had a Rockwell B (HRB) hardness of 81 in the first shell course plate and a hardness of 72 in the second shell course plate. The hardness of heat affected zones and old and new weld metals ranged from HRB 85 to HRB 96. A hard spot, believed to be an arc strike was found on the surface of the second shell course plate and had a Rockwell C (HRC) hardness of 33. Another hard spot with a hardness of HRC 28 was found in the surface "cap" pass of the weld and a very hard spot of HRC 43 was found in the vicinity of the lack of penetration defect. High magnification micrographs of the weld metal, heat-affected zones, and hard spots are shown in Figure 7.17. The microstructure were typical of weld metal and heat-affected zones in welds of this type of steel. There was evidence of martensite in the hardened regions. The microstructures, hardness values, and weld defects found in this specimen are typical of the those found in all of the transverse weld specimens that were evaluated.

Additional specimens from the horizontal weld are shown in Figures 7.18 and 7.19. These specimens are shown to indicate the type and extent of weld defects that were found in the horizontal weld. Numerous areas of porosity and lack of fusion were found in nearly all of the weld specimens. Hardness values (HRB) for the weld metal and base metals are shown on each of the specimens in Figures 7.18 and 7.19.

Specimens taken from the vertical weld (test sample 9) are shown in Figure 7.20. These specimens show a region identified as base metal separating the old weld metal from the new weld metal. This indicates that the old weld was not fully removed when the tank was dismantled and reassembled. The microstructure and hardness values in this vertical weld were similar to those found in the horizontal weld described above. Numerous weld defects, particularly lack of fusion, are found in all specimens of the vertical weld shown in Figure 7.20.

An attempt was made to evaluate the toughness of typical weld metal using Charpy-V-notch tests of specimens taken from the horizontal weld (test sample 4E). The samples were taken from the best portion of the weld identified by

radiography on the weld that had been ground to 1/2 in thick to remove the weld crown. The Charpy-V-notch specimens were etched before being notched and the notch was located in either the old weld metal, the new weld metal, or the new weld metal heat affected zone. The weld defects, particularly porosity, were so extensive that several of the specimens broke at the defect rather than at the notch of the Charpy specimen and valid results of the test could not be obtained. The results of satisfactory tests conducted at 40° F and at room temperature (71° F) are shown in Table 7.12.

These results show that the toughness of the weld metal at both room temperature and at 40° F is significantly better than the toughness of the steel plates from which the tank was fabricated.

7.4 Characterization of the Fracture Surface Defect

All characterization of the fracture surface defect was done by Battelle and the results reported here and all photographs of the deferct were supplied to the NBS by Battelle [7.15]. The NBS reviewed all test procedures with Battelle before the characterization of the defect was started and subsequently examined all test specimens used in the characterization.

A defect that extended part way through the wall of the tank was found on the surface of the major vertical fracture in the tank. This defect was on the inside of the tank in the first shell course plate at a location just below the junction of a T-weld joint as shown in Figure 7.21. This defect is believed to be the origin of the major vertical fracture in the tank because "chevron" markings on the surface of the fracture point to this defect from above and below the defect, as shown in Figure 7.22. No chevron markings or other defects were found elsewhere on the fracture surface that would indicate another origin of the fracture so it was concluded that this defect was the origin of the vertical fracture in the tank. When present, these chevron markings have been identified as one method of determining the origin of fracture in steel plates. Test samples, as shown in Figure 7.23, were cut out of the tank in the vicinity of this defect for detailed investigation of the exact location and features of this defect.

The location of the defect on the fracture surface is shown at a magnification of 4X in Figure 7.24. This figure shows that the defect was located in the first shell course plate on the inside of the tank, below the horizontal weld. The size of the defect was determined from Figure 7.24 and is shown on the Figure. These are the dimensions of the defect that were used in the fracture analysis shown in Chapter 8. Other features of the defect and the fracture surface that were determined by examination with the scanning electron microscope are shown on Figure 7.24.

To determine the exact location of the defect with respect to the new weld metal, old weld metal, and first shell course plate, the sample shown in Figure 7.24 was sectioned as shown in Figure 7.25. The sections were cut using a fine wire electrodischarge machine. Eight specimens were cut at intervals of 0.080 in starting from the inner surface of the tank. These specimens were then examined metallographically to permit a 3-dimensional reconstruction of the defect to be made and to determine the exact location of the defect. An example of one of these sections is shown in Figure 7.26. This figure shows that the defect was located entirely in base metal from the first shell course. The edge of the defect extended just to the edge of the heat affected zone of the old weld metal.

Battelle concluded that the weld metal at the edge of the defect was "old" weld metal rather than "new" weld metal and therefore that the defect was present prior to dismantling the tank for reconstruction at the Floreffe site [7.15]. Battelle based this conclusion on the following evidence: (1) In the horizontal weld, the old horizontal weld metal was always found to lie below (that is, on the first shell course side) the new horizontal weld metal, (2) a slice (sectioned similarly to the slices shown in Figure 7.25) that was taken from a region of the horizontal weld about 1 inch from the location of the defect had a chemical composition and microstructure representative of the old weld metal rather the new weld metal (see Table 7.1) and (3) as shown in Figure 7.26, the heat-affected zone surrounding the defect did not go through or alter the heat-affected zone of the weld metal adjacent to the defect. The NBS did not have access to material in the vicinity of the defect to independently verify this conclusion. However, the NBS did examine the metallographic specimens prepared by Battelle as well as do an independent

evaluation of typical horizontal welds. From these observations, the NBS did not find any evidence to conflict with the Battelle conclusion that the defect was below old weld metal and therefore was present prior to the dismantling of the tank.

As seen in Figure 7.26, a dark etching region is present surrounding the defect below the fracture surface. This dark etching region is believed to represent a region of heat-affected zone caused by heating of the metal, probably at the time the defect was formed. Hardness measurements made by Battelle showed that this heat-affected zone had a maximum hardness of slightly in excess of 400 Knoop (HKN) (equivalent to a Rockwell hardness of HRC 40) at the edge of the defect and that the hardness decreased with distance below the defect until a hardness of about HRB 85 was reached at a distance of about 0.050 in below the edge of the defect. The hardness of HRB 85 is representative of the hardness of the base metal plate. Chemical analyses using the electron microprobe and secondary electron emission imaging were conducted on the surface of the defect and in the heat-affected zone below the defect. A heavily carburized layer was found near the surface of the defect at the location showing the maximum hardness. Formation of such a carburized layer can only occur from a combination of high temperature and excess carbon in the atmosphere. This is the primary evidence for concluding that the defect was formed by a cutting torch.

7.5 Stress Analysis

A detailed analysis of the stresses in the tank at the time of failure was conducted to obtain the stresses necessary for the fracture analysis of the tank. The stress analysis, described in section 5.1 of this report, was performed on the tank to determine the stresses in the tank wall at the time of failure.

From the stress analysis the maximum stress at the top of the first shell course due to the hydrostatic pressure of the oil was calculated to be a circumferential membrane (hoop stress) of 13.7 ksi. Additional stresses due

to settling of the tank or thermal effects were not found to be of a significant magnitude and are not included in the stresses used for the fracture analysis.

Residual stresses were measured by Battelle using the chip removal method [7.16]. A typical T-weld joint removed from a location remote from the primary vertical fracture was used for the residual stress measurements. The results are considered to be representative of the residual stresses in the vicinity of the defect in the primary fracture but may not represent the exact stresses in the specific T-weld region near where the defect was located. The maximum residual stress measured was a tensile circumferential membrane stress of 15.1 ksi. Residual stresses as high as the yield strength of the base metal have often been found to be present in the vicinity of welds in steel plates [7.17].

For the fracture analysis shown in Chapter 8, the stresses at the location of the defect were taken to be:

Circumferential membrane stress due to the oil = 13.7 ksi

Circumferential residual stress = 15.0 ksi

Stress at the yield strength of the metal = 34.0 ksi

These stresses are used alone and in combination in the fracture analysis shown in Chapter 8.

Table 7.1 - Chemical Composition of Tank Steels and Weld Metal

Sample	*Location*	*Value in Percent (By Weight)*												
		C	*P*	*S*	*Mn*	*Si*	*Ni*	*Cr*	*V*	*Ti*	Mo	Cu	Co	Al
5-3-1	1st Course	.232	.016	.028	.531	.026	.030	.032	.0002	--	--	.025	.0050	.008
5-3-2	1st Course	.237	.016	.033	.538	.025	.030	.032	.0002	--	--	.025	.0049	.006
5-3-3	1st Course	.258	.017	.031	.540	.025	.031	.034	.0004	--	--	.025	.0049	.006
3-2	2nd Course	.299	.011	.017	.509	<.001	.016	.042	--	--	.0013	.026	.0046	--
1	2nd Course	.232	.007	.018	.486	.002	.015	.039	--	--	.016	.025	.0046	--
2	1st Course	.218	.014	.028	.532	.026	.028	.030	--	.0002	--	.024	.0040	.009
3	1st Course	.207	.015	.028	.517	.028	.029	.030	--	.0002	--	.024	.0050	.010
4	1st Course	.219	.014	.027	.529	.028	.029	.031	--	.0002	--	.024	.0042	.010
5	Old Weld	.100	.009	.023	.479	.162	.028	.024	.0006	.0140	.0038	.018	.0025	--
6	New Weld	.093	.007	.013	.896	.361	.030	.033	.0012	.0005	.0007	.022	.0045	--
7	Old Weld	.082	.010	.022	.520	.157	.023	.025	.0006	.0090	.0015	.034	.0031	--
8	New Weld	.079	.006	.012	.871	.395	.027	.036	.0012	.0008	.0020	.019	.0046	--

Table 7.2 - Tensile Properties of Plate Steels

Shell Course	Specimen Orientation	Tensile[1] Strength (psi)	Yield[1],[2] Strength (psi)	Elongation[1] in 2-inches (%)
First	Transverse	66,900	33,400	33.8
First	Longitudinal	66,900	34,500	34.2
Second	Transverse	67,300	33,000	34.6
Second	Longitudinal	67,200	34,900	34.8

(1) All values are the average of 3 or more specimens

(2) 0.2% offset yield strength

Table 7.3 - Summary of Charpy-V-Notch Test Results

First Shell Course - Transverse Orientation(1)

Average Temperature (F)	Absorbed Energy (ft.-lbs.)	Lateral Expansion (mils)	Shear Fracture (%)
160	37.5	34.4	80
121.5	27.5	26.9	70
79.7	17.3	22.0	40
57.7	9.0	15.8	25
40.1	5.5	12.7	13
20.8	4.0	11.5	0

(1) All values are the average of 2 or more specimens

Table 7.4 - Summary of Charpy-V-Notch Test Results

First Shell Course - Longitudinal Orientation(1)

Average Temperature (F)	Absorbed Energy (ft.-lbs.)	Lateral Expansion (mils)	Shear Fracture (%)
160.1	53.5	40.0	85
121.5	33.5	30.5	75
80.4	13.0	18.9	38
57.5	8.8	15.4	30
39.8	6.2	13.6	20
21.2	6.1	12.8	0

(1) All values are the average of 2 or more specimens

Table 7.5 - Summary of Charpy-V-Notch Test Results

Second Shell Course - Transverse Orientation(1)

Average Temperature (F)	Absorbed Energy (ft.-lbs.)	Lateral Expansion (mils)	Shear Fracture (%)
160.2	32	30.2	70
121.4	21	23.3	50
80.0	9.8	17.0	30
55.4	6.0	13.2	20
40.3	4.8	13.5	10
20.0	4.2	11.5	0

(1) All values are the average of 2 or more specimens

Table 7.6 - Summary of Charpy-V-Notch Test Results

Second Shell Course - Longitudinal Orientation(1)

Average Temperature (F)	Absorbed Energy (ft.-lbs.)	Lateral Expansion (mils)	Shear Fracture (%)
160	38.5	33.0	60
121.5	20.3	21.9	50
80.4	11.5	17.0	30
57.8	6.4	13.5	15
40.2	4.4	11.7	10
20.2	3.7	10.8	0

(1) All values are the average of 2 or more specimens

Table 7.7 - Ductile-to-Brittle Transition Temperatures Determined from Charpy-V-Notch Tests

Shell Course	Specimen Orientation	15 ft-lb (F)	15 mils Lateral Expansion (F)	50% Shear Fracture Appearance (F)
First	Transverse	80	55	95
First	Longitudinal	100	55	95
Second	Transverse	90	68	120
Second	Longitudinal	100	68	120

Table 7.8 - Drop-Weight (NDT) Test Results

Shell Course	Specimen Type	Temperature (F)	Test Results
First	P-2	40.0	Break
		60.2	Break
		60.0	Break
		70.0	No Break
		70.0	No Break
NDT Temperature for first shell course = + 60F			
First	P-3	40.4	Break
		49.0	Break
		49.4	Break
		58.8	No Break
		59.0	No Break
NDT Temperature for first shell course = + 50F			
Second	P-2	40.6	Break
		61.0	No Break
		60.4	Break
		71.0	No Break
		69.0	Break
		80.2	No Break
		80.2	No Break
NDT Temperature for second course = + 70F			

Table 7.9 - Summary of Fracture Toughness Test Results

Specimen No.	Shell Course	Temperature (F)	J_C (in-lb/in^2)	K_C(1) (ksi$\sqrt{in}$)
5LT-9	First	20	72	46.5
5LT-17	First	20	72	46.5
5LT-13	First	40	76	47.7
5LT-16	First	40	83	49.9
5LT-18	First	40	68	45.2
5LT-14	First	69	92	52.5
5LT-15	First	69	85	50.5
5LT-20	First	71	83	49.9
5LT-21	First	105	1011	174.2
3LT-1	Second	40	72	46.5
3LT-8	Second	40	69	45.5
3LT-7	Second	69	84	50.2
3LT-6	Second	69	81	49.3

(1) $K_C^2 = J_C E$

Table 7.10 - Summary of Notched-Bend Test Results

Specimen Condition	Maximum Load (lbs.)	Yield Load (lbs.)	Displacement at Maximum Load (in.)	Energy Absorbed to Maximum Load (ft.-lbs.)
Notched only	4748	2783	0.072	21.7
Notched, then Heated	4037	2904	0.034	9.0
Heated First, then Notched	3826	2662	0.035	9.7

Table 7.11 - Summary of Hardness of Steel Plates

Sample Number	Hardness (HRB)(1)	
	First Shell Course	Second Shell Course
421	73	69
422	71	71
423	72	73
424	65	70
4141	69	73
4142	68	71
4143	69	71
4144	69	72
Average Hardness	69.5 HRB	71.3 HRB

(1) Rockwell B Hardness

Table 7.12 - Charpy-V-Notch Results from Weld Metal

Sample Number	Location (1)	Temperature (F)	Energy Absorbed (ft.-lbs.)
2,3,4	New W.M.	40	All failed outside notch
5	New W.M.	71	85
6	New W.M.	71	117
7	New W.M.	71	57
			Average 86
14	Old W.M.	40	21
15	Old W.M.	40	37.5
16	Old W.M.	40	7
			Average 21.8
17	Old W.M.	71	17
18	Old W.M.	71	23
19	Old W.M.	71	29.5
			Average 23.2
--	First Course B.M.	40	Average 5.9
--	First Course B.M.	60	Average 9.0
--	First Course B.M.	80	Average 17.3

(1) W.M. - Weld Metal
B.M. - Base Metal

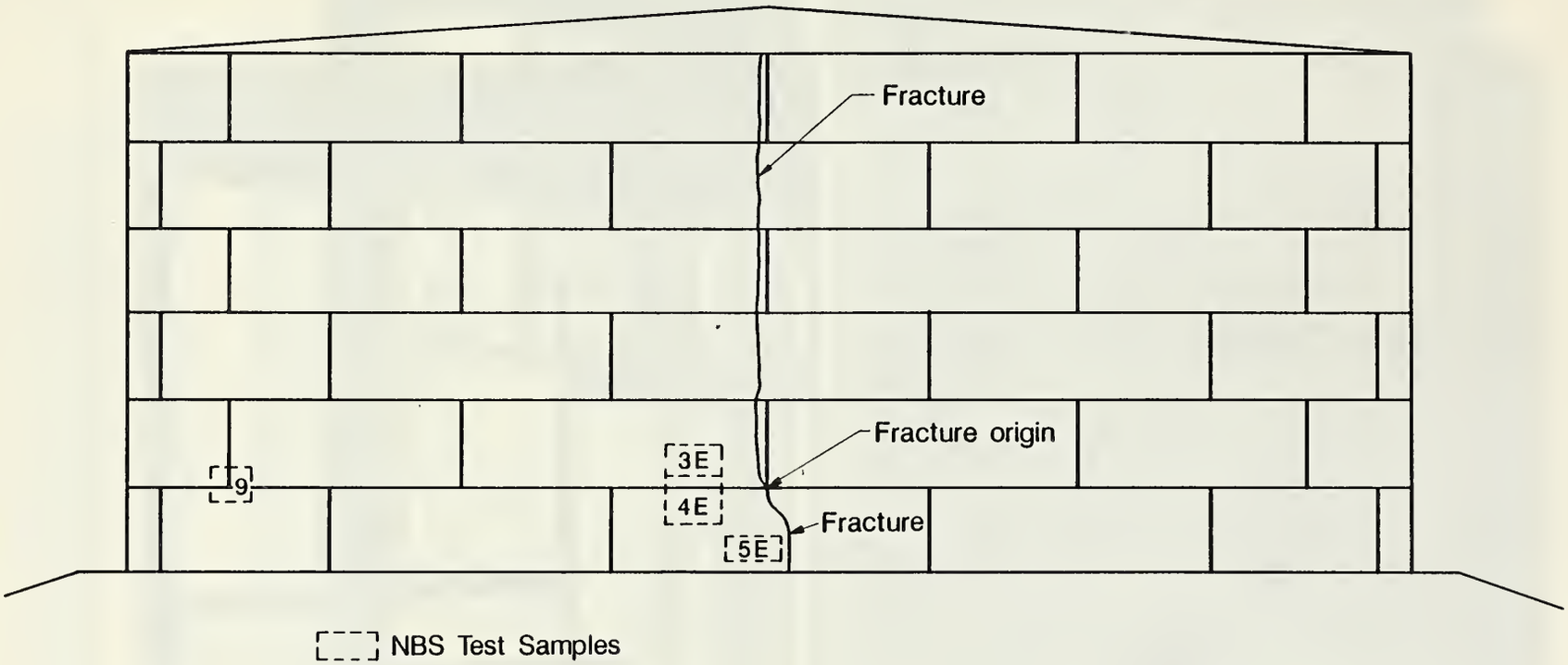

Figure 7.1 - Location of Primary Vertical Fracture and NBS Test Samples

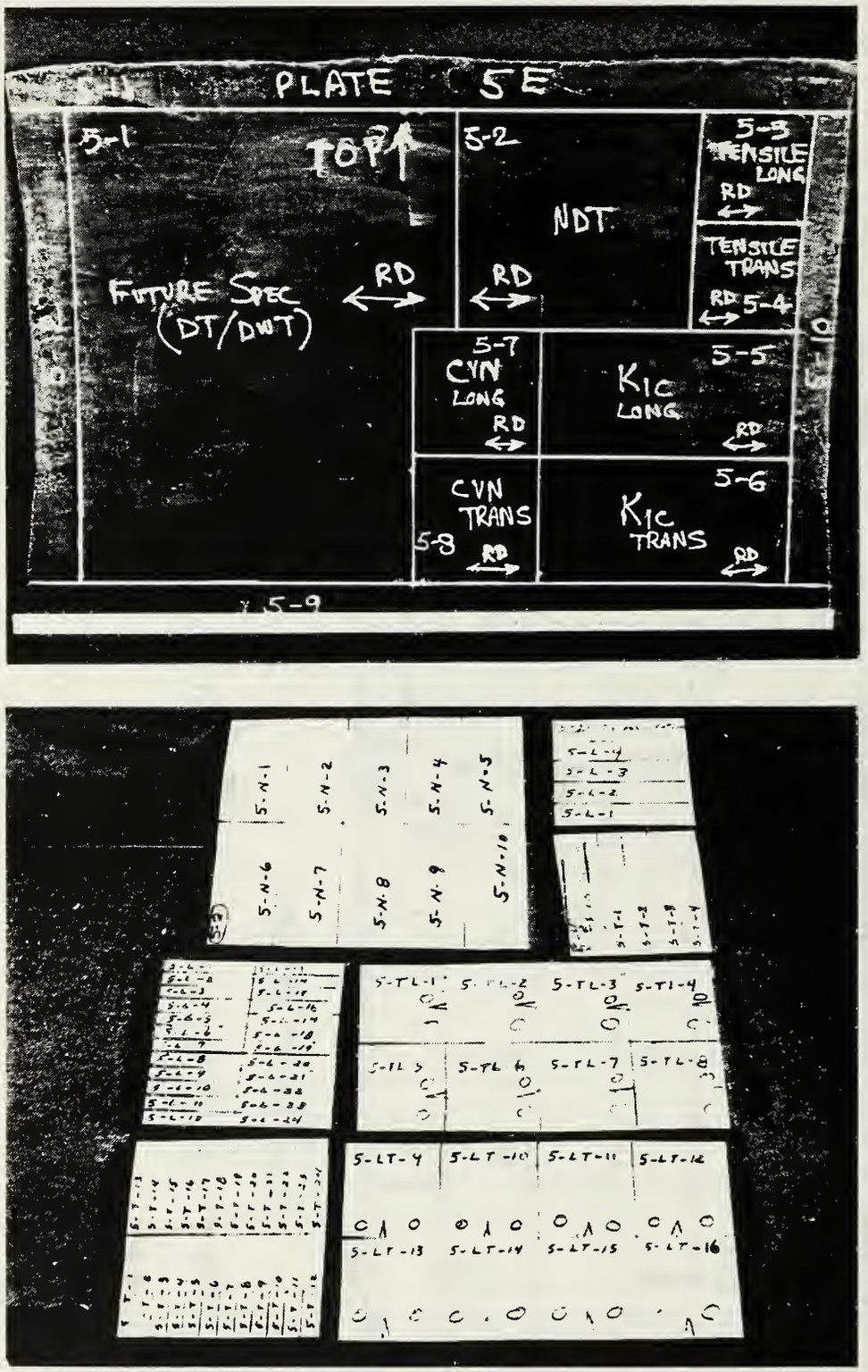

Figure 7.2 - Location of Test Specimens from First Shell Course

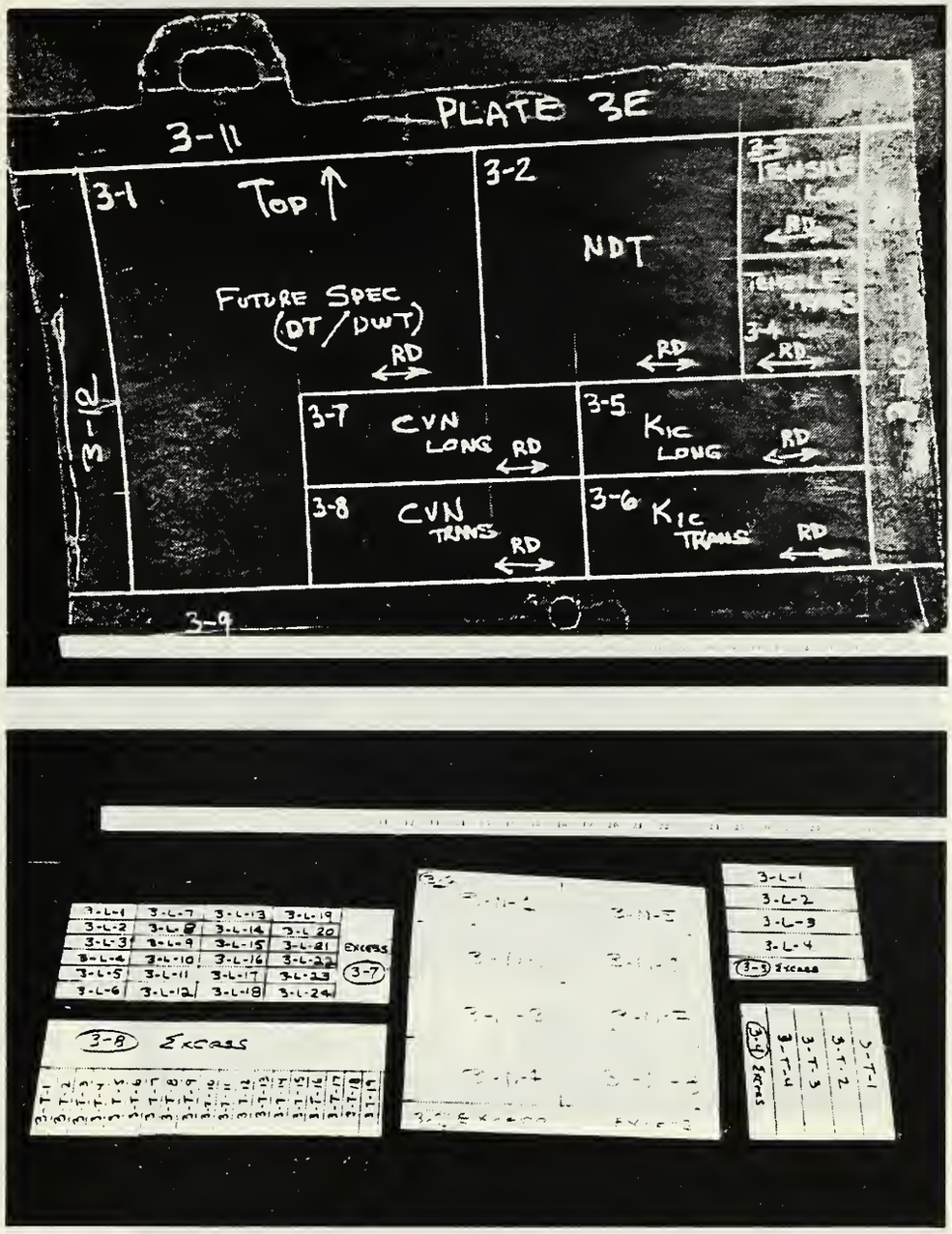

Figure 7.3 - Location of Test Specimens from Second Shell Course

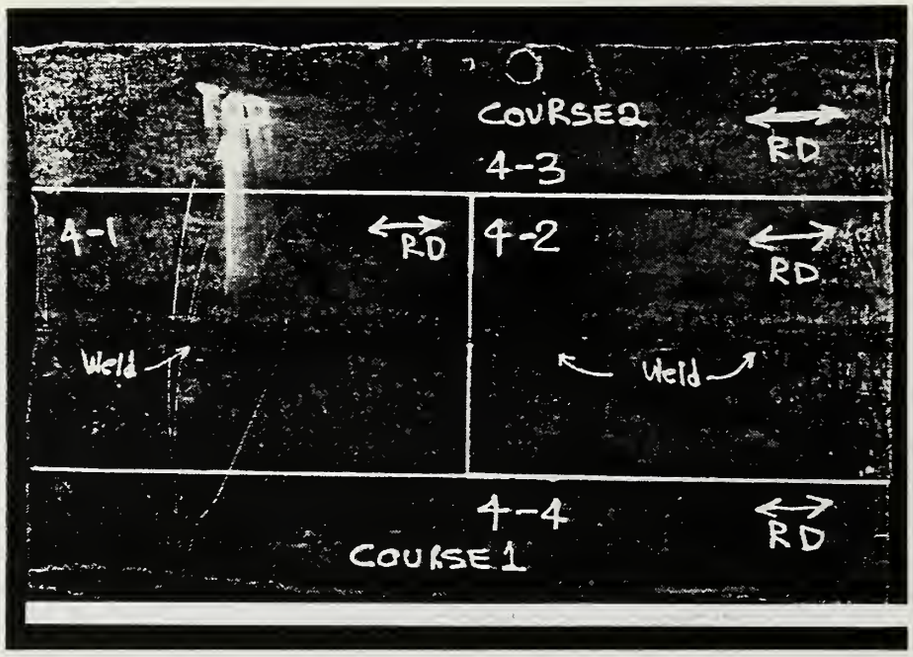

7.4a - Overall Location of Specimens

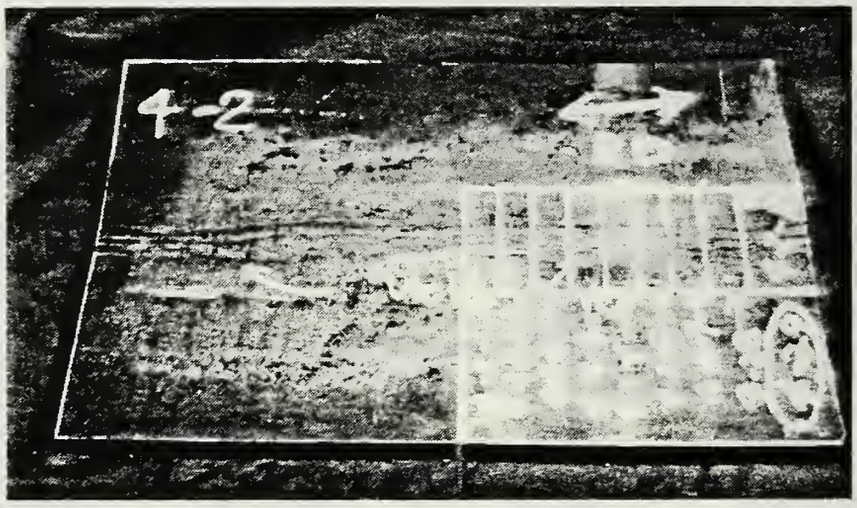

7.4b - As Received Weld Sample

7.4c - As Ground Weld Sample

Figure 7.4 - Location of Test Specimens from Horizontal Weld

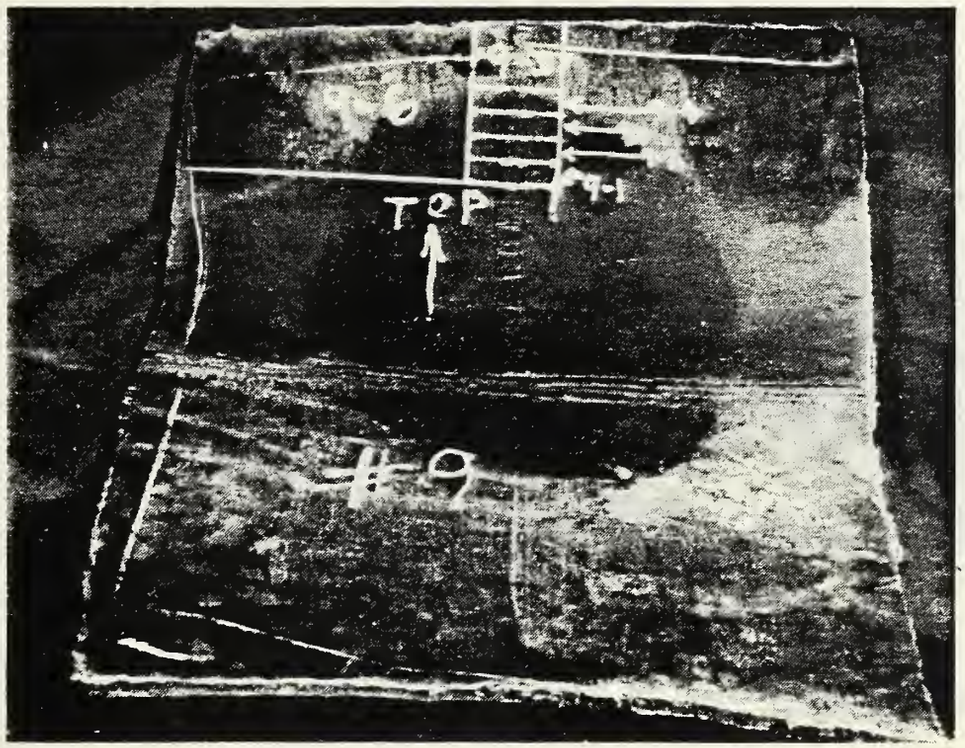

Figure 7.5 - Location of Test Specimens from Vertical Weld

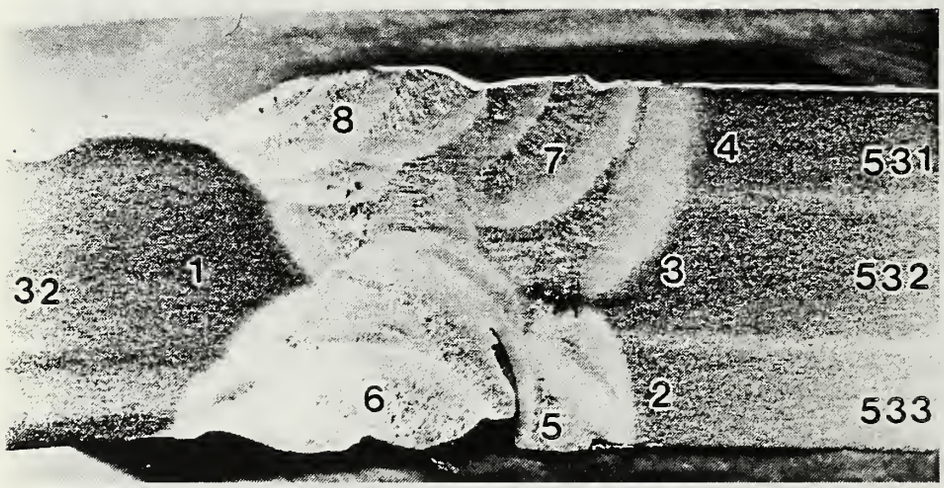

Figure 7.6 - Location of Samples for Chemical Analysis

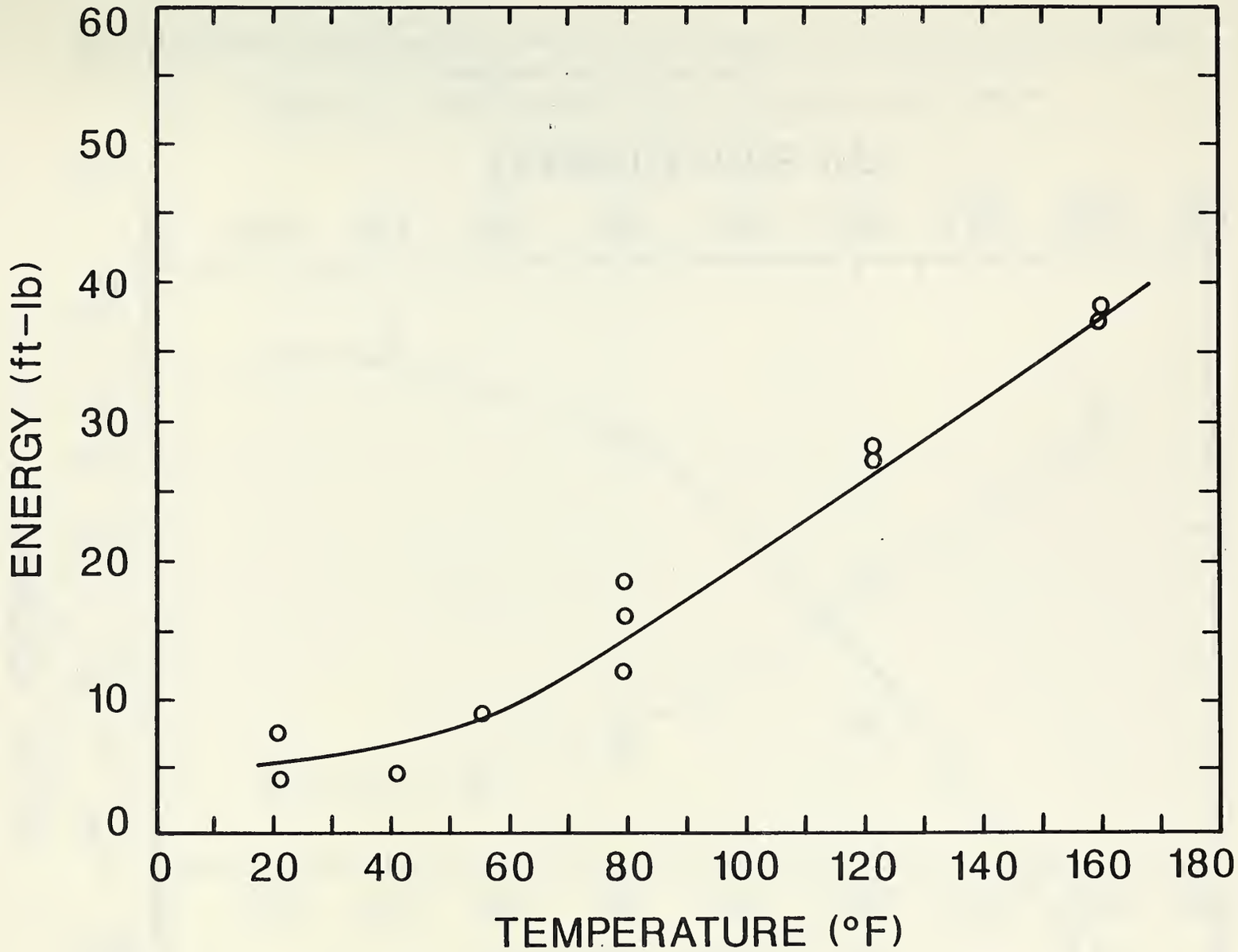

Figure 7.7 - Charpy-V-Notch Tests for First Shell Course - Transverse Orientation

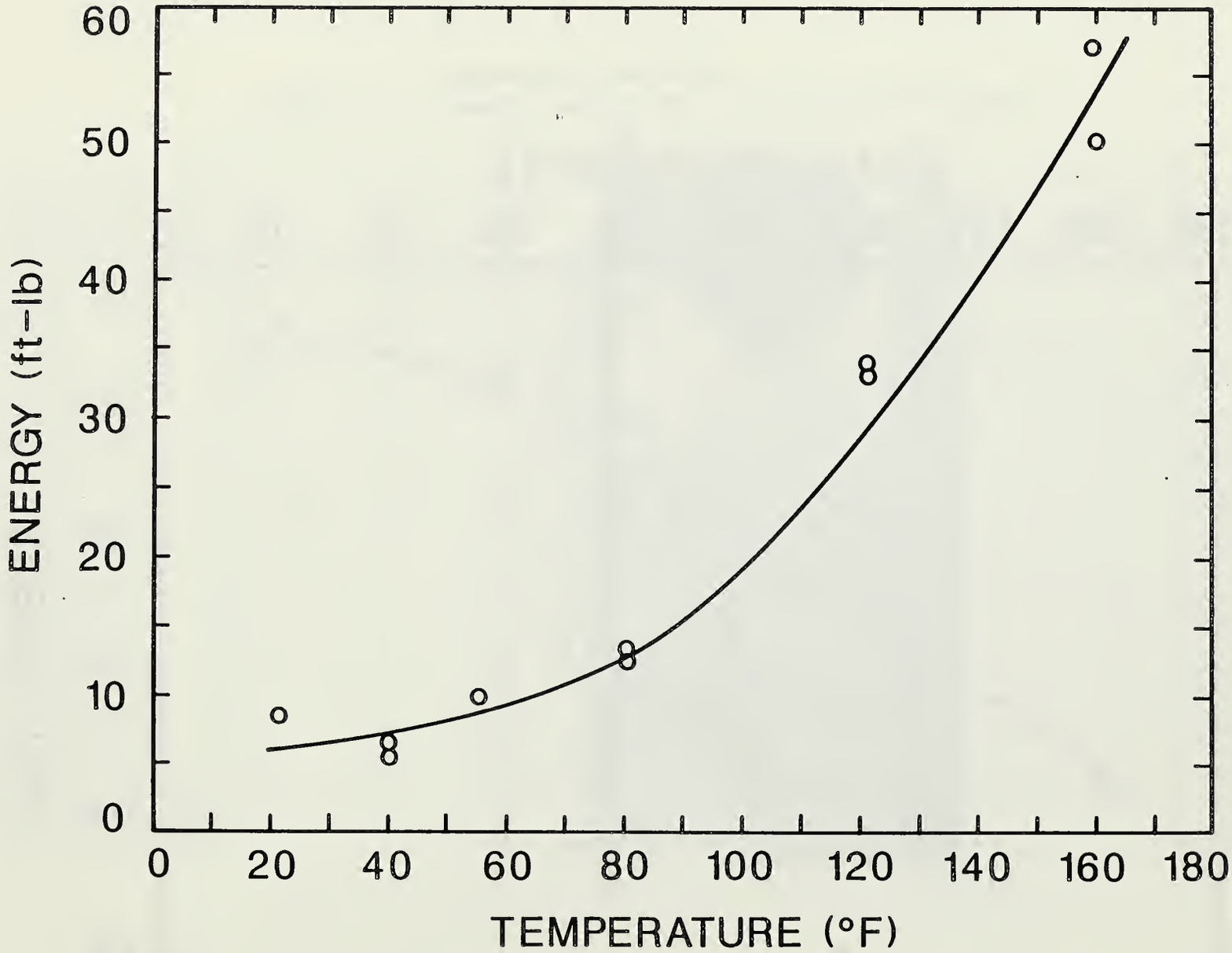

Figure 7.8 - Charpy-V-Notch Tests for First Shell Course - Longitudinal Orientation

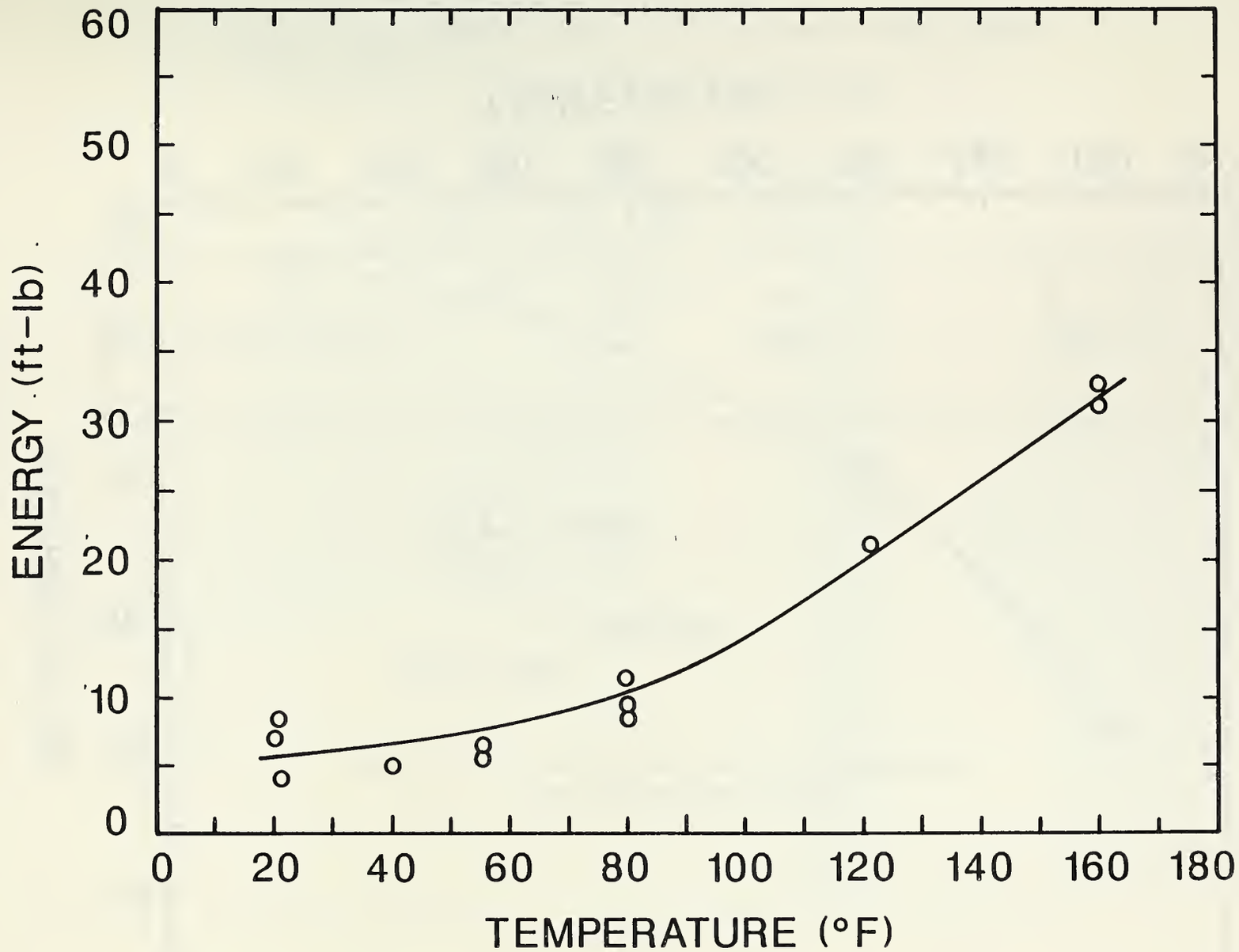

Figure 7.9 - Charpy-V-Notch Tests for Second Shell Course - Transverse Orientation

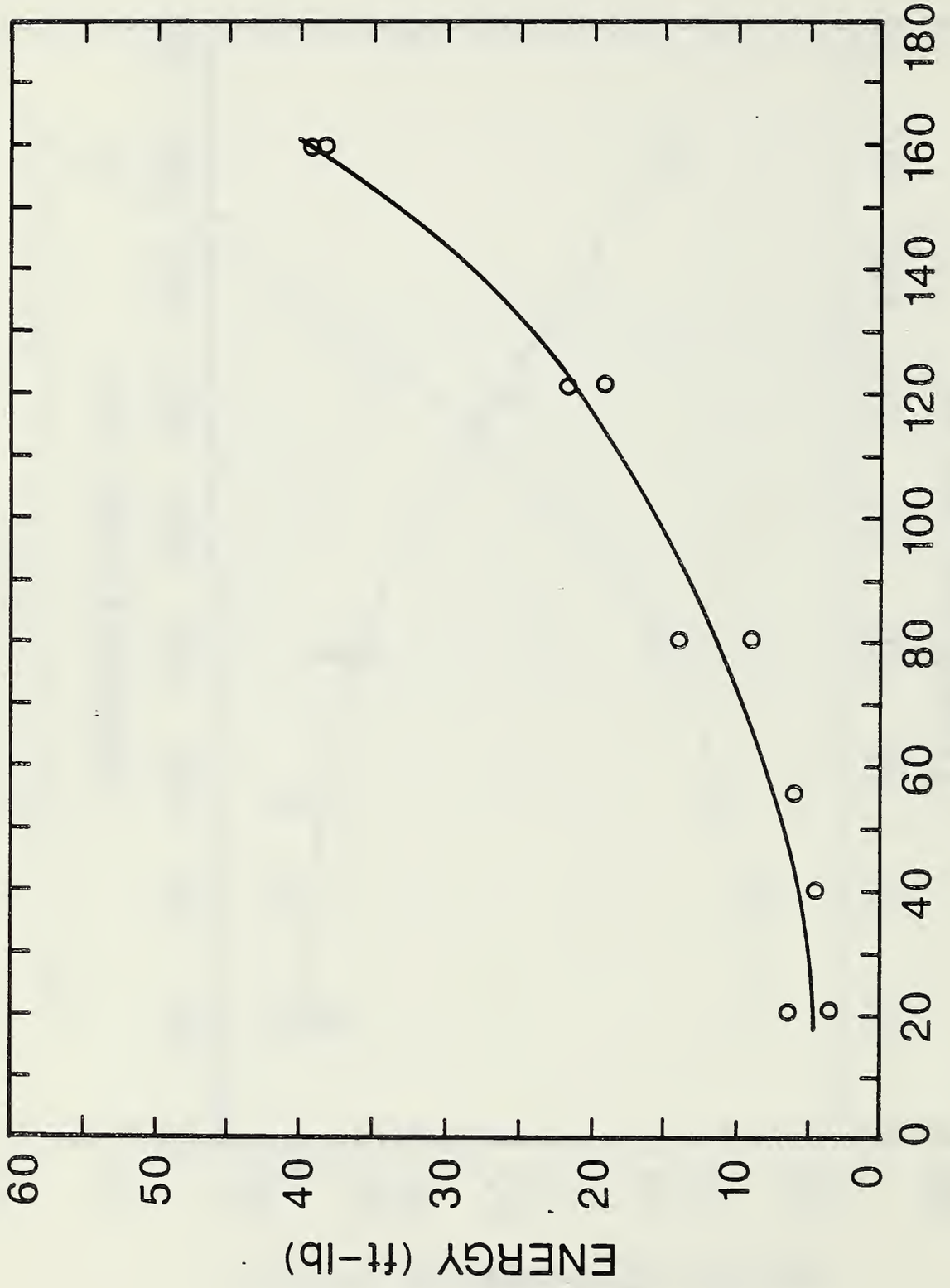

Figure 7.10 - Charpy-V-Notch Tests for Second Shell Course - Longitudinal Orientation

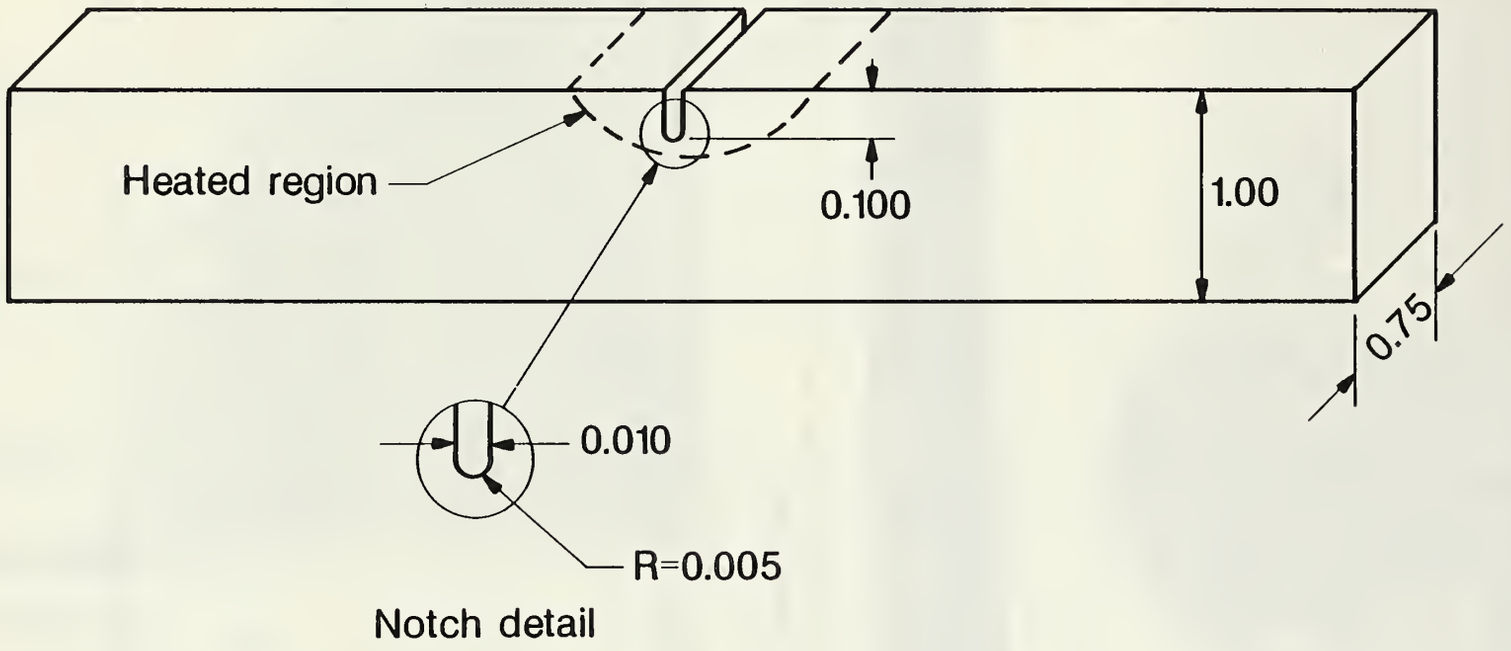

Figure 7.11 - Single Edge-Notch Bend Specimen
for Embittlement Study

Figure 7.12a - Embrittlement Zone at Notch Tip in Single-Edge Notch Bend Test

Depth (in)	Hardness
0.020	HRC 35
0.040	HRC 36
0.060	HRC 37
0.080	HRC 43
0.100	HRC 31
0.120	HRC 27
0.140	HRB 85
0.160	HRB 80

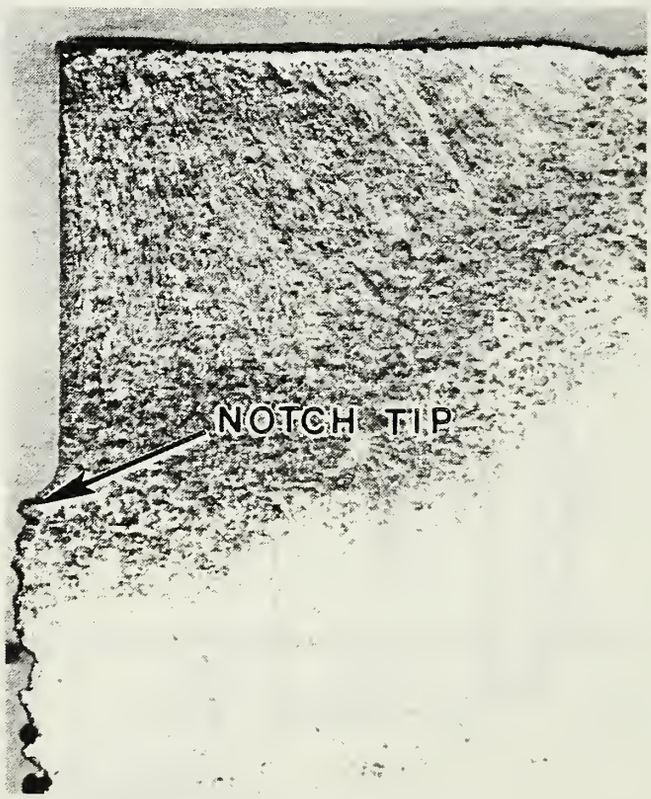

Magnification: 21X

Figure 7.12b - Hardness of Embrittled Zone in Single-Edge Notched Bend Specimens

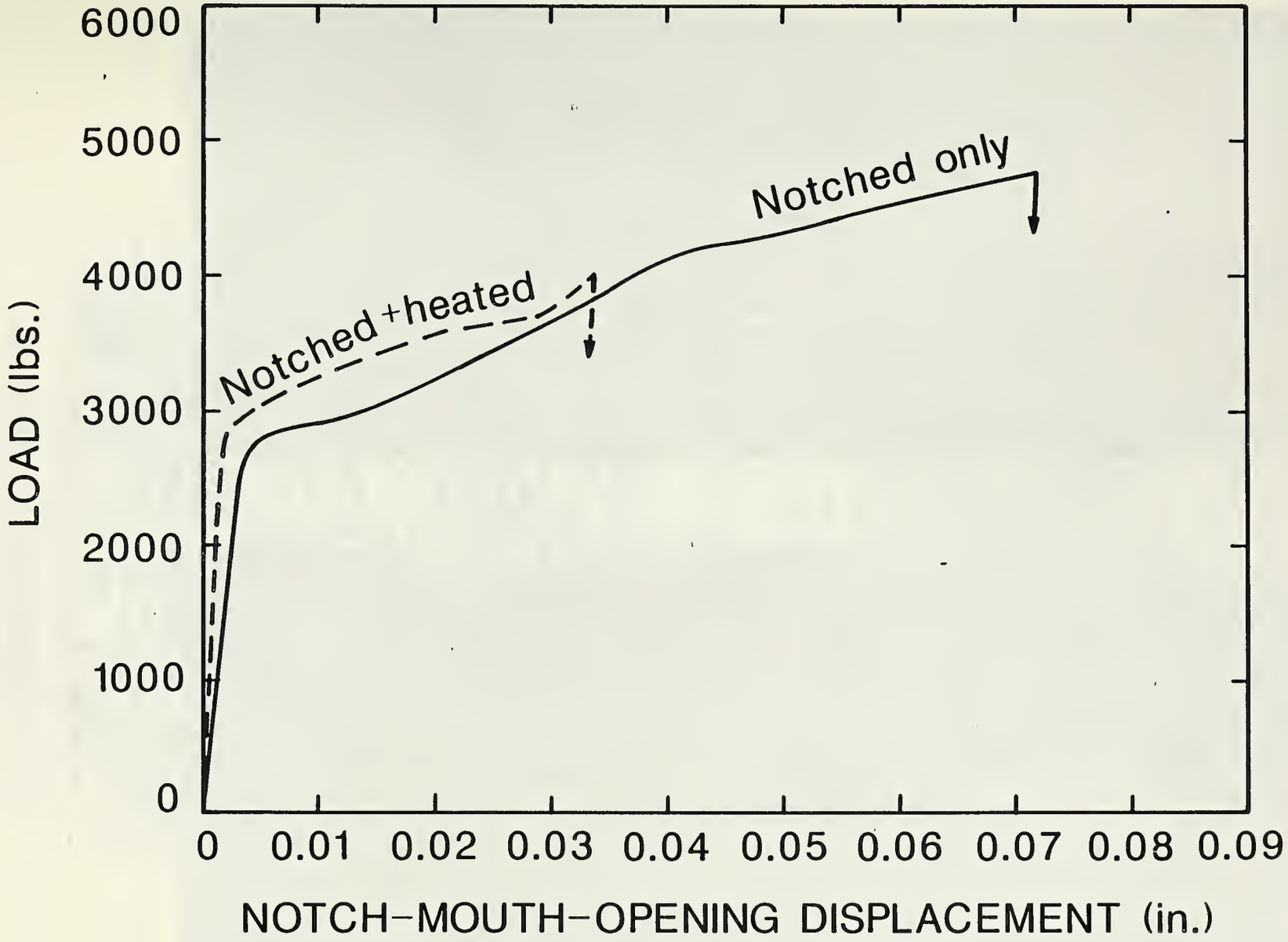

Figure 7.13 - Results of Notched-Bend Test

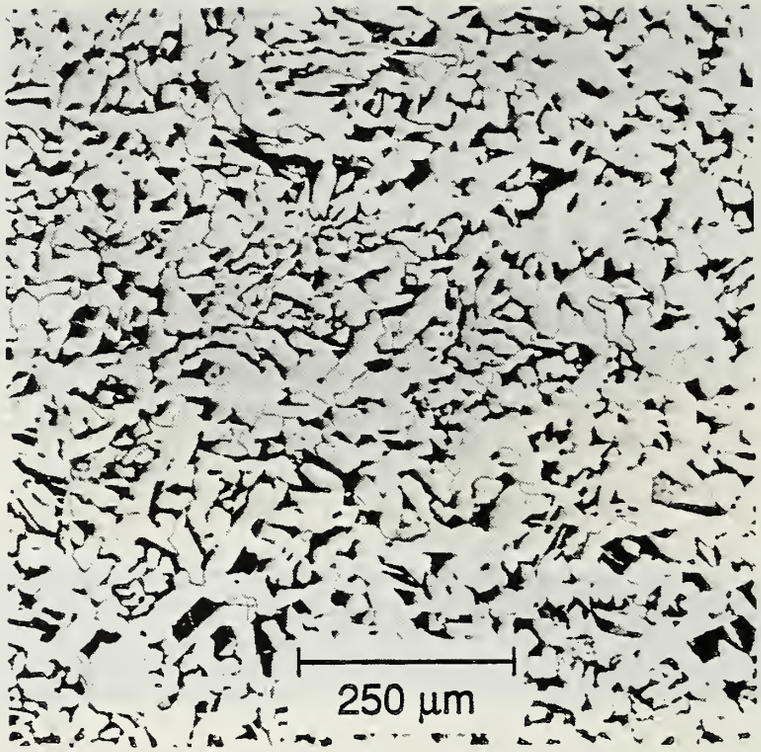

7.14a - Microstructure of First Shell Course Plate

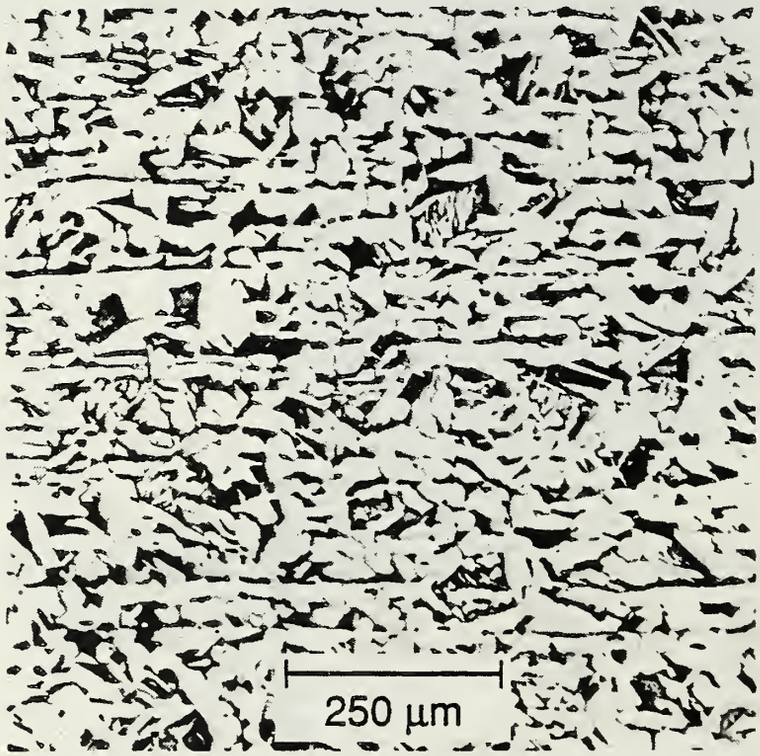

7.14b - Microstructure of Second Shell Course Plate

Figure 7.14 - Microstructure of Steel Plates
Magnification: 100X Etchant: 2% Nital

Figure 7.15 - X-ray Radiograph of Horizontal Weld after Surface Grinding

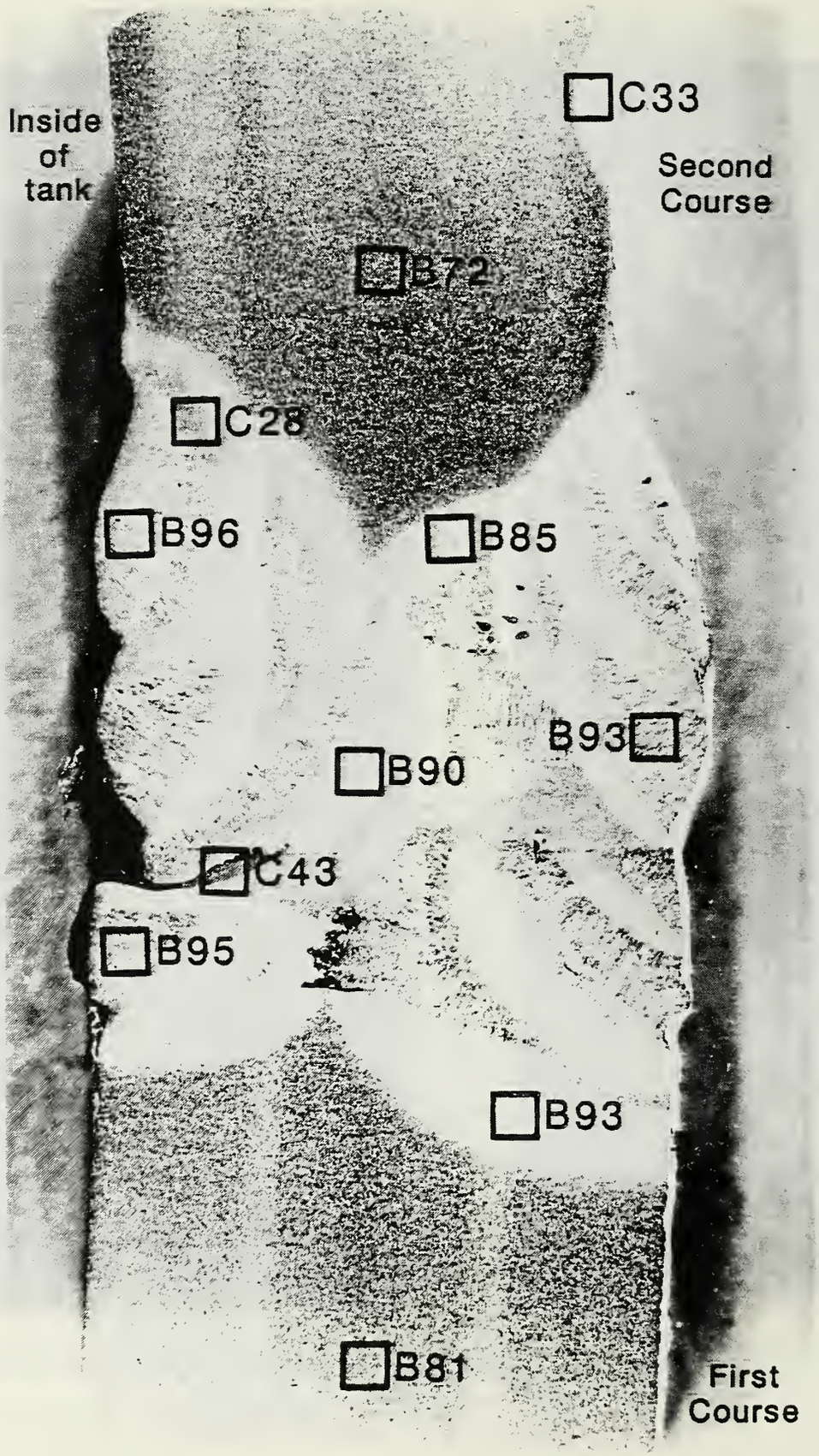

Figure 7.16 - Microstructure and Hardness of Horizontal Weld Metal

Rockwell B and C Scale Hardness Values are given for various Locations.

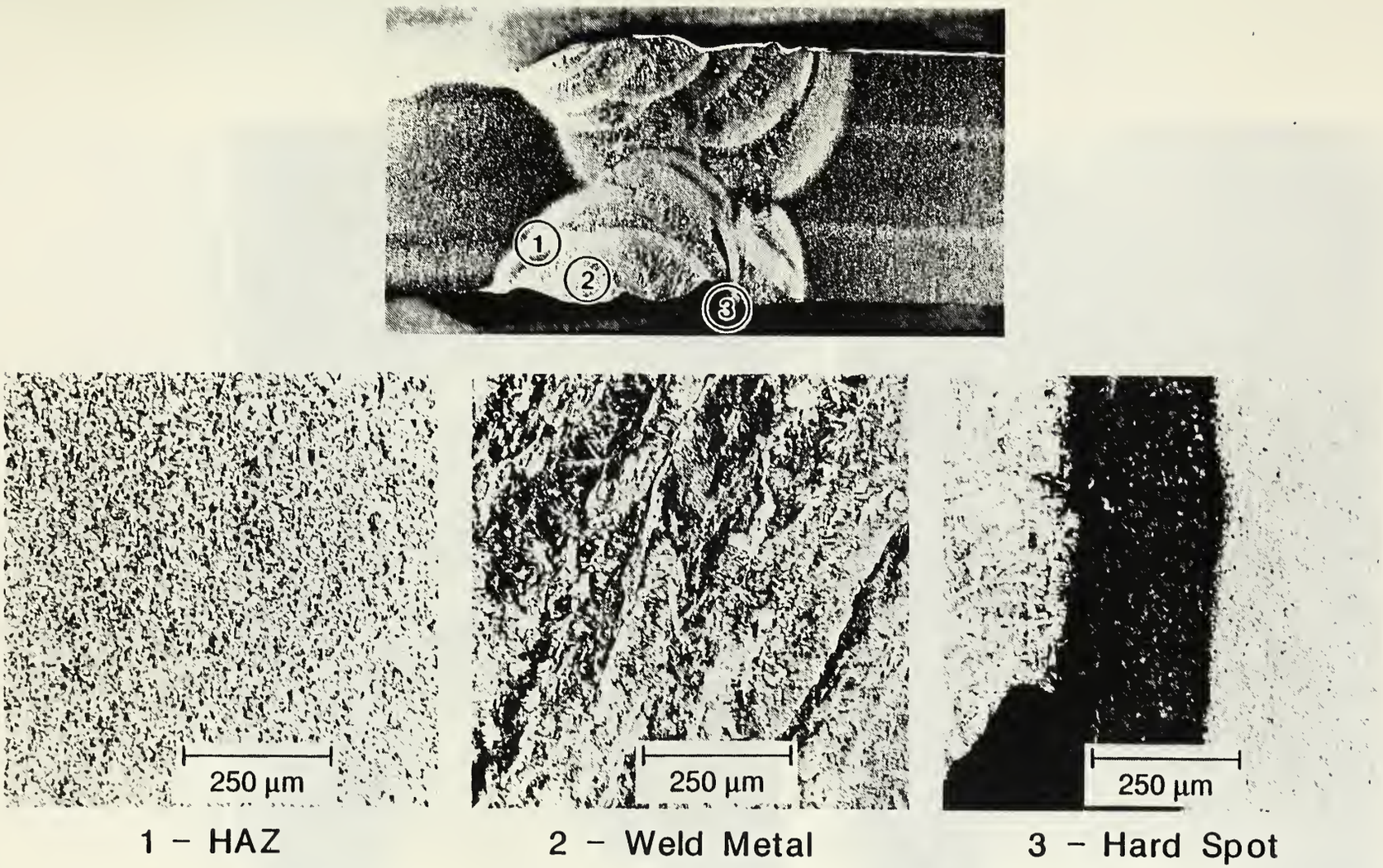

Figure 7.17 - Microstructure of Horizontal Weld Metal

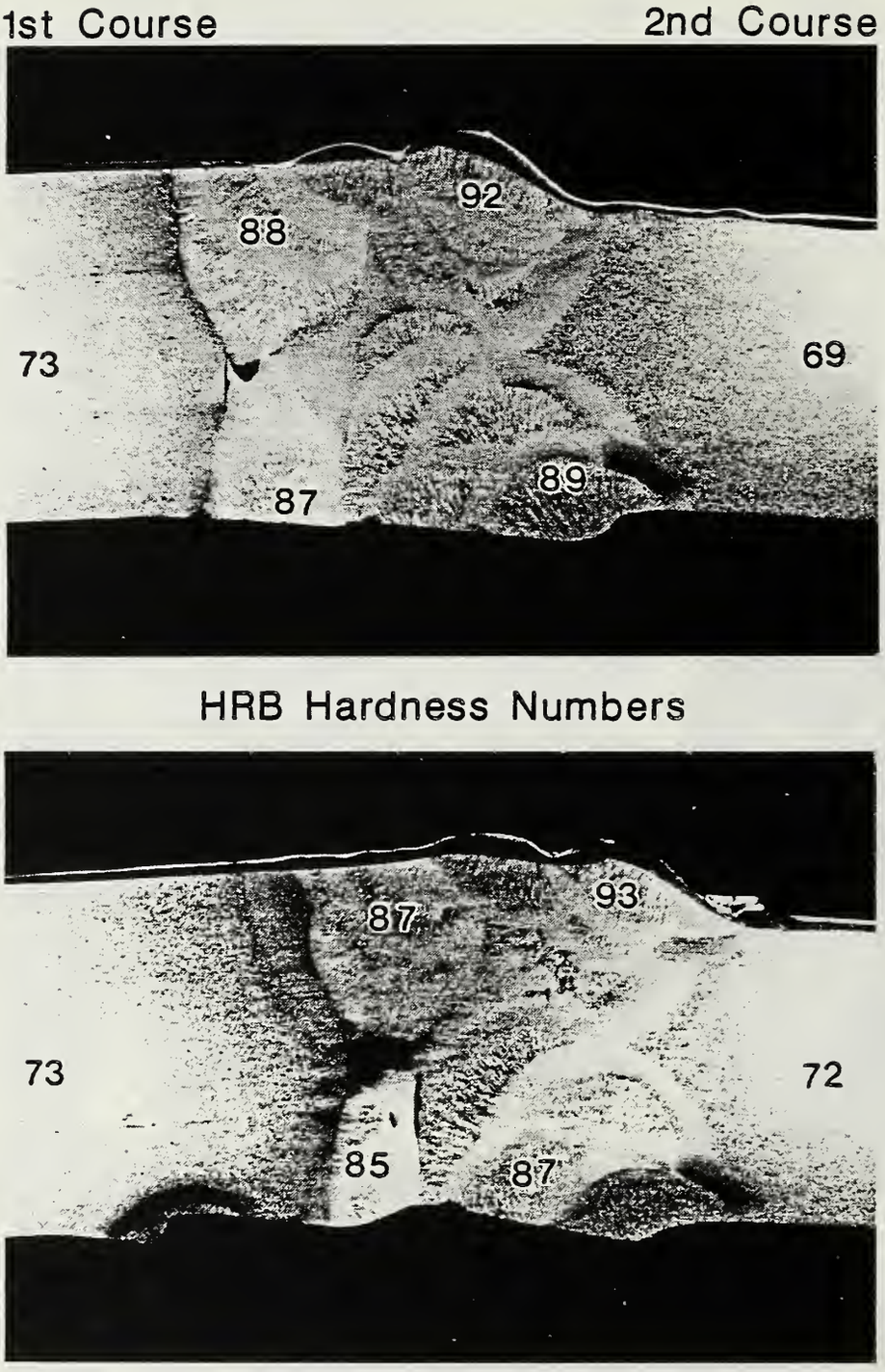

Figure 7.18 - Defects in Horizontal Weld Metal

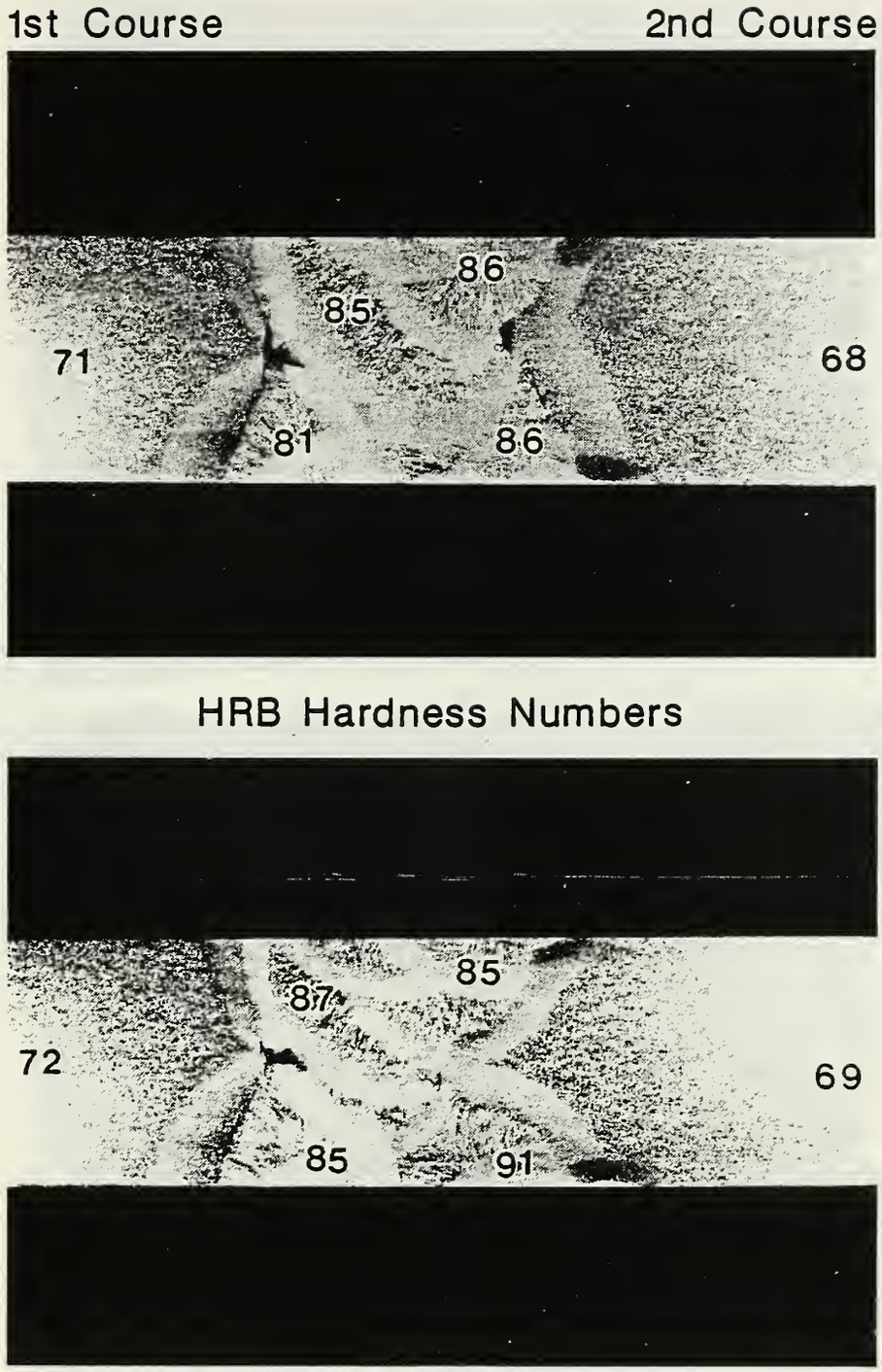

Figure 7.19 - Defects in Horizontal Weld Metal after Grinding Welds

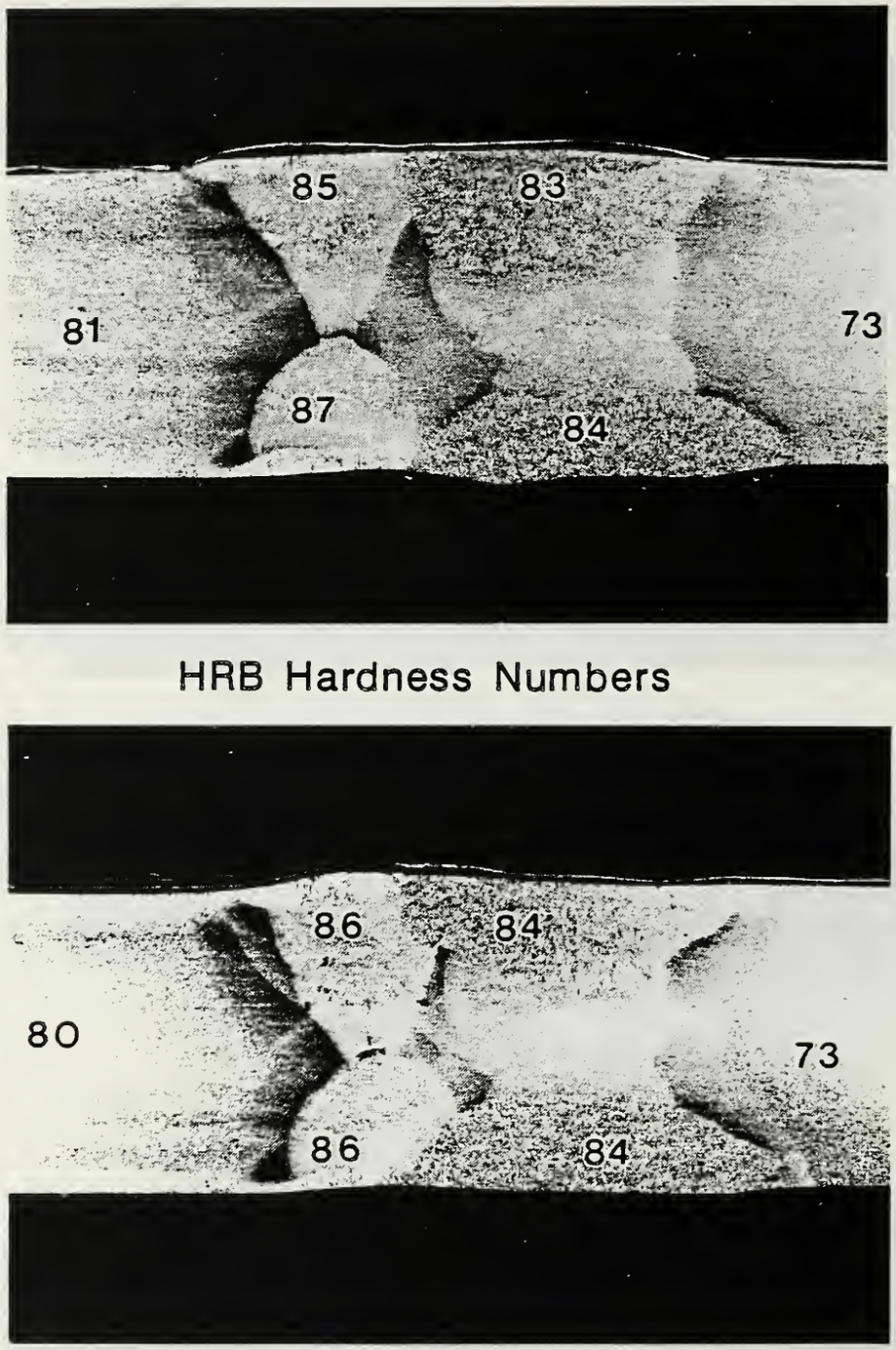

Figure 7.20 - Defects in Vertical Weld Metal

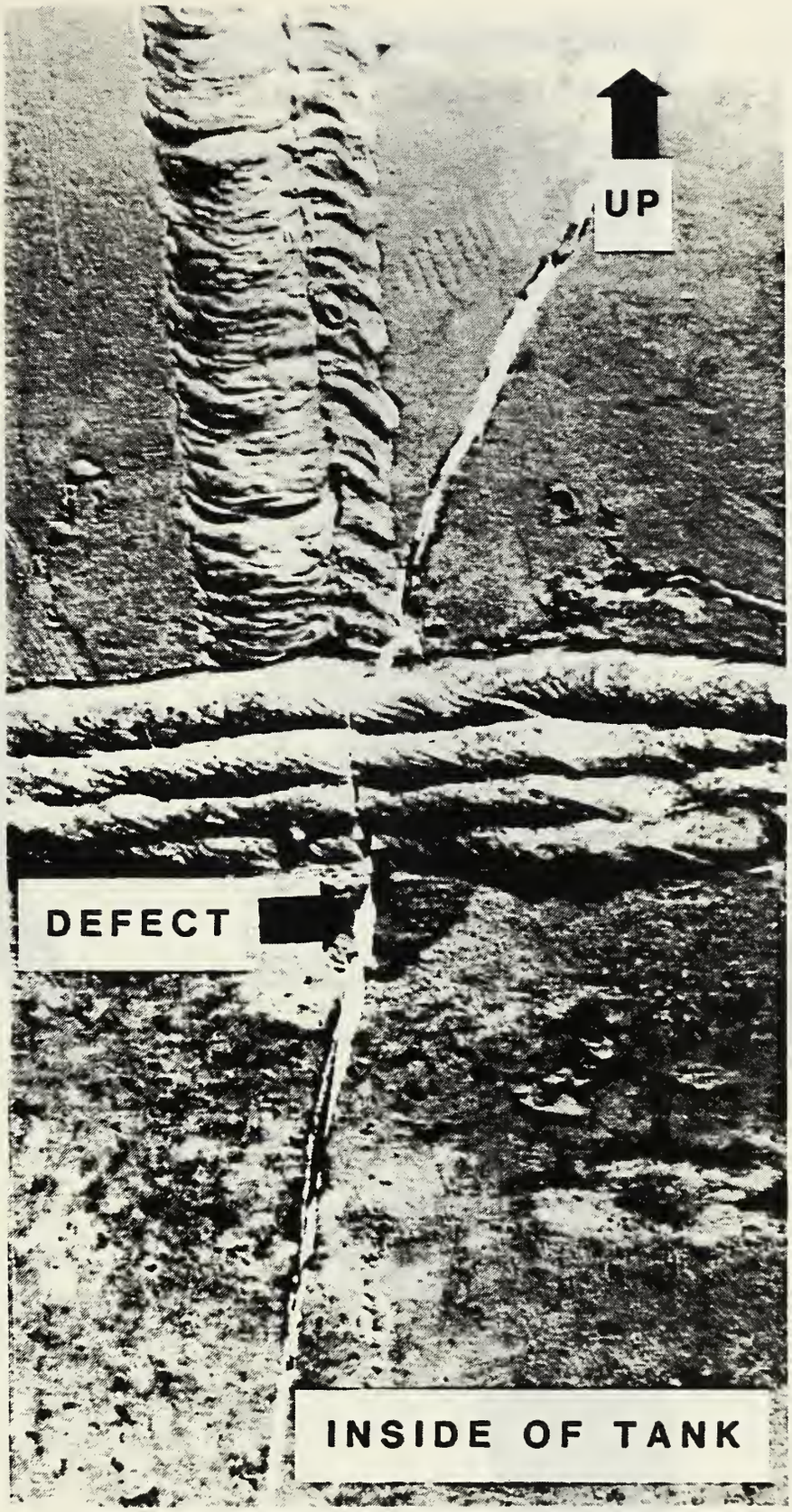

Figure 7.21 - Location of Fracture Surface Defect

Figure 7.22 - Fracture Surface Defect

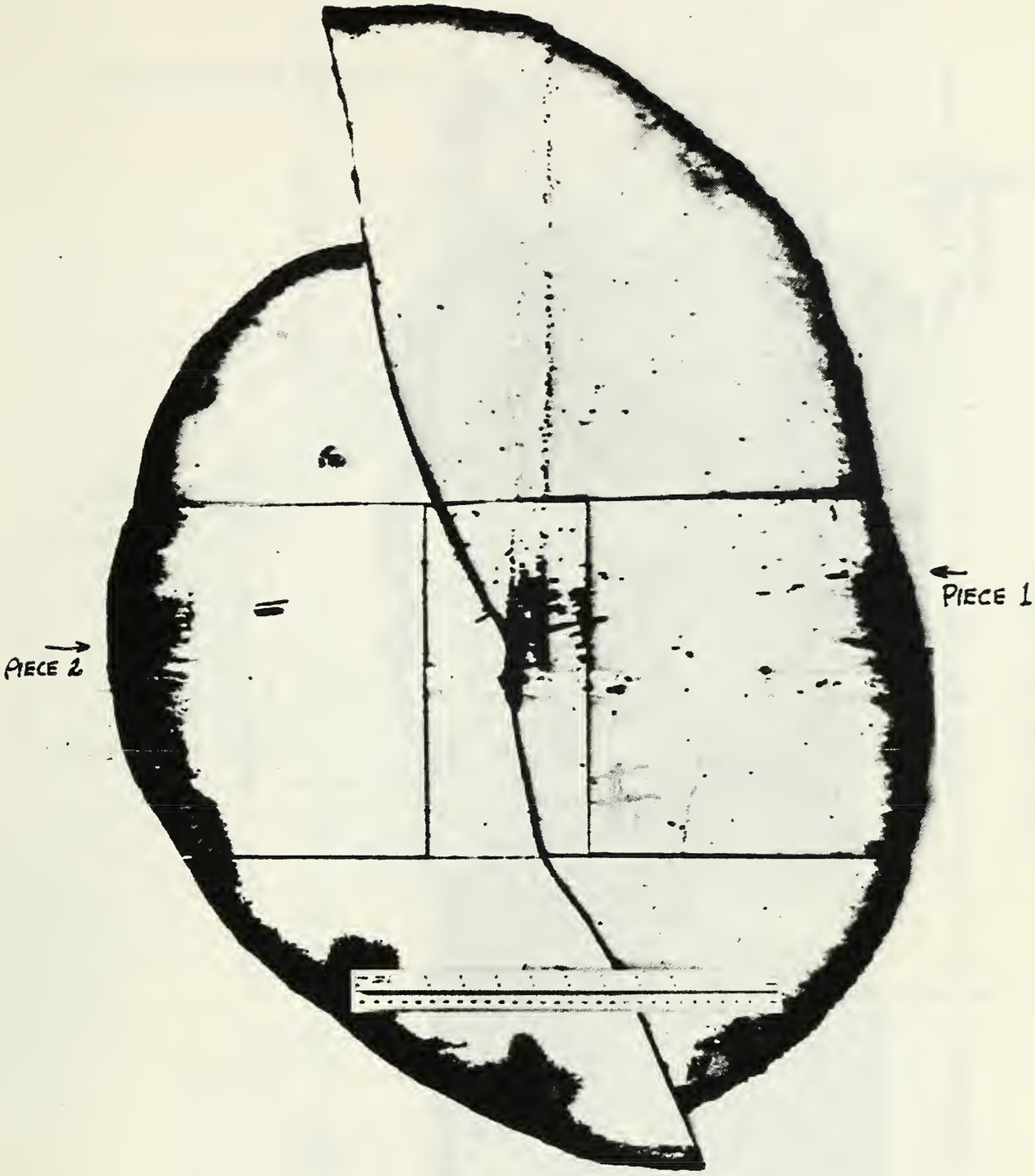

Figure 7.23 - Location of Fracture Surface Defect
From Outside of Tank

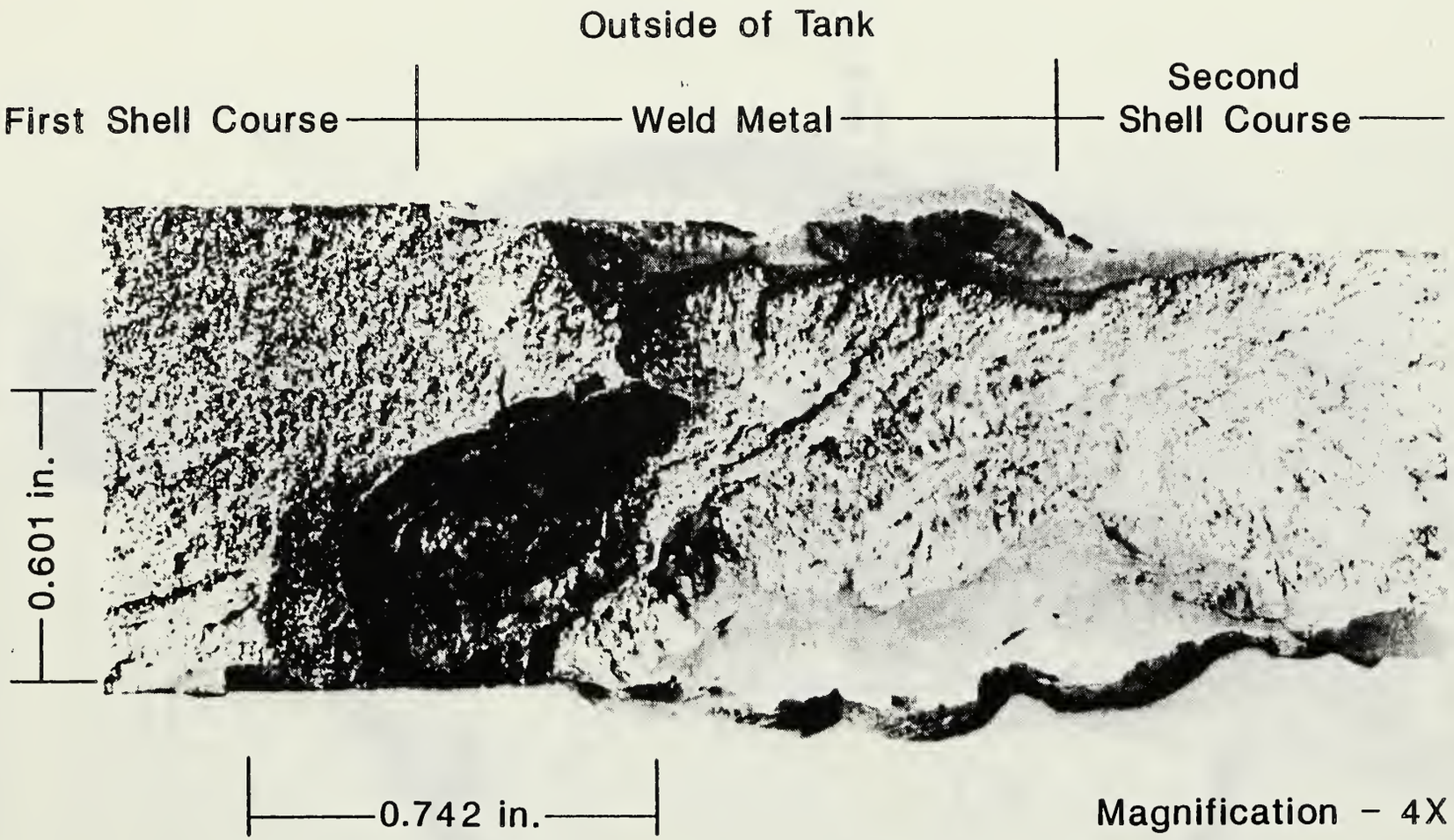

Figure 7.24 - Defect on Fracture Surface

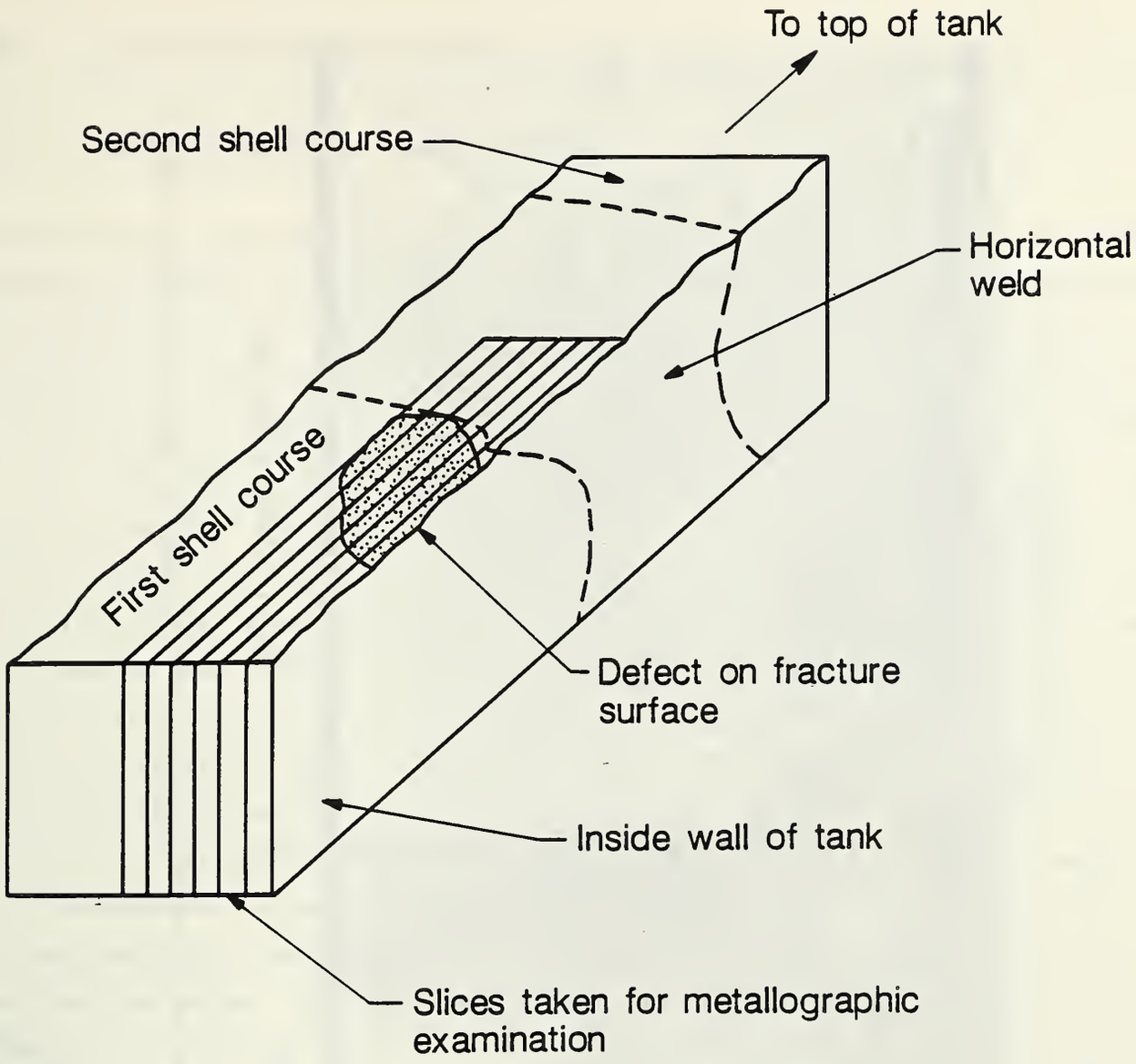

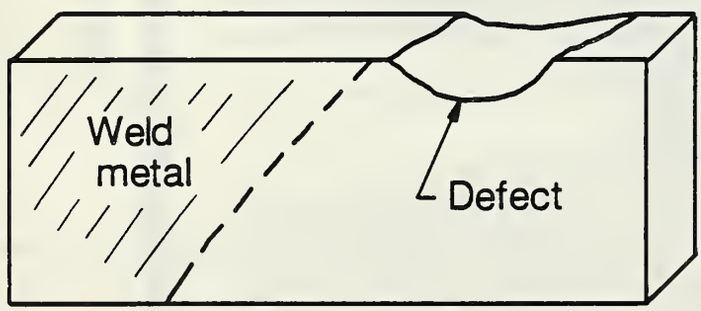

(Slice as shown in Fig. 7.26)

Figure 7.25 - Details of Sectioning to Determine Location of Defect

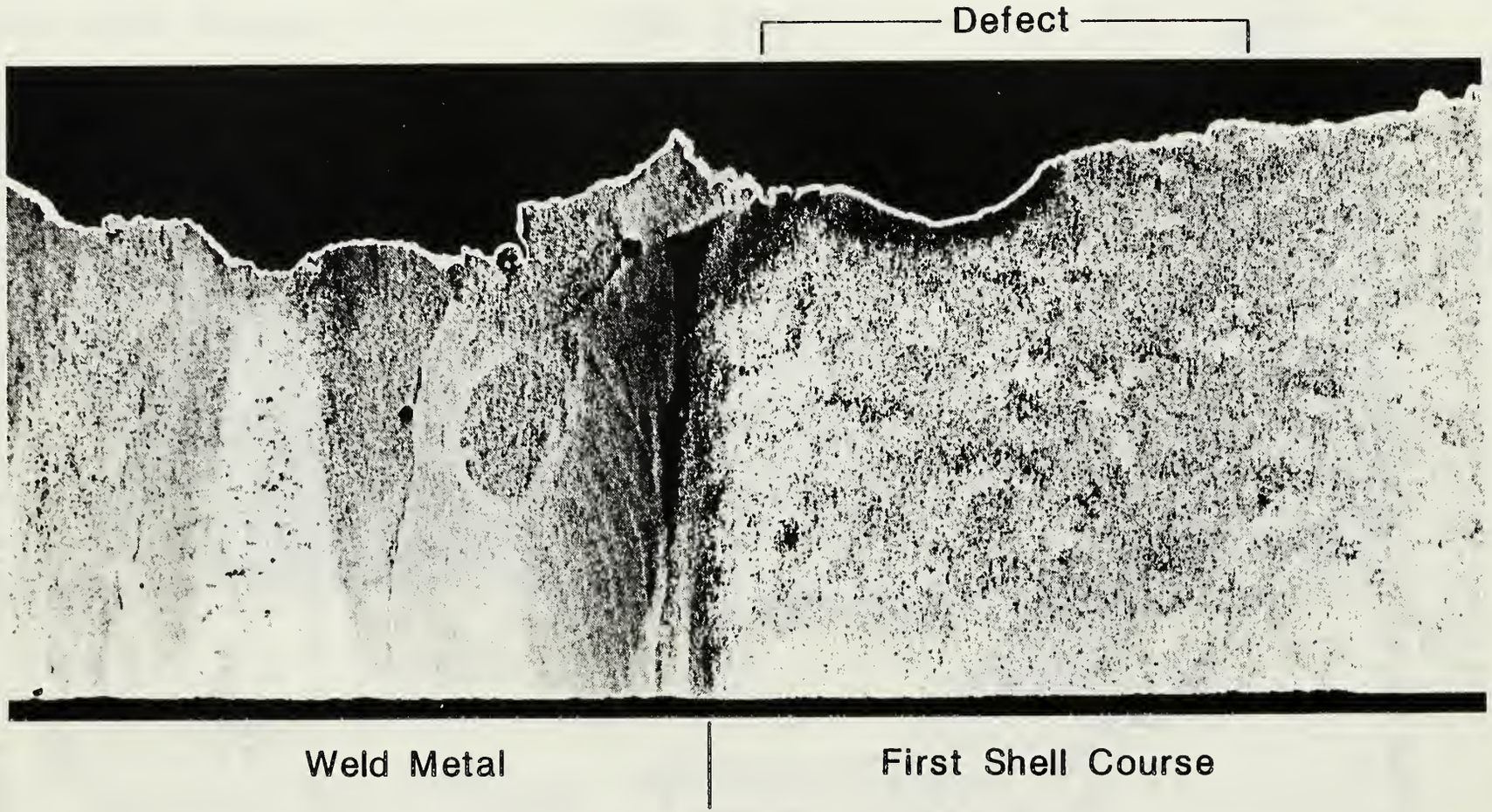

Figure 7.26 - Transverse Section of Fracture Surface Defect Showing Exact Location of Defect

8.0 ANALYSIS OF TANK FAILURE

8.1 Scope of Tank Failure Analysis

The tank was analyzed to determine (1) if the defect found on the fracture surface initiated the fracture and (2) why the fracture propagated and caused the tank to rupture instead of arresting and only causing the tank to leak. To predict if the defect found on the fracture surface could be expected to initiate fracture with the stresses determined to be present in the tank and at the operating temperature of the tank, several established failure assesment methods were used. These included predictions based on ductile-to-brittle transition temperature methods using Charpy-V-notch tests or the nil-ductility (NDT) temperature, and analyses based on linear-elastic fracture mechanics principles to predict quantitively if the defect found on the fracture surface was responsible for fracture initiation. The linear-elastic fracture mechanics analyses were performed to compare the applied stress intensity factor calculated from the applied stress and defect size with the fracture toughness of the material. The analyses were done in sequence by first making the assumption that the defect found on the fracture was a part-through-surface defect and next by assuming that the part- through-surface flaw was converted (by failure of the uncracked ligament below the surface defect) to a through-thickness defect. To predict if fracture propagation is to be expected once the fracture had initiated, an assessment of fracture propagation and arrest based on the measured nil-ductility-transition (NDT) temperature was made. A determination of the most probable cause of the failure was made and an assessment was made of possible means to reduce or prevent similar failures from occurring in other storage tanks.

8.2 Assessment of Fracture Initiation and Arrest

The simplest assesssment of the tendency for fracture initiation in the steel plates of the tank is based on the transition temperature of the steel. Extensive service experience with fracture in mild steel structures, particularly welded ships, and correlations with Charpy-V-notch tests has shown that fracture initiation is likely for steel plates that have an energy

absorbed in the Charpy-V-notch test of less than 10 foot-pounds at the temperature at which they are being used. Fracture arrest does not occur for steel plates that have a Charpy-V-notch energy of less than 20 foot-pounds [8.1].

It has become common practice to specify that mild steel plates must have a minimum Charpy-V-notch energy of 15 foot pounds at the lowest operating temperature at which the steel will be used [8.2]. The temperature at which the steel has a minimum Charpy-V-notch energy of 15 foot-pounds has been accepted as the definition of the ductile to brittle transition temperature for low to medium strength structural steels. This is considered a conservative definition of the highest temperature at which fracture initiation can occur in steel. The current requirement for selecting steels for oil tanks constructed as specified in the API Standard 650 requires that the steel have a minimum Charpy-V-notch energy of 15 foot-pounds at the design metal temperature which is +5° F for this tank. For these tanks, this minimum Charpy-V-notch energy is considered to be sufficient to prevent fracture initiation and to arrest any propagating fractures.

As can be seen from Table 7.7, the 15 foot-pound transition temperature of the steel plates used in both the first and second shell course plates was well above (80° F to 100° F) the operating temperature (32° F) at the time of failure of the tank. Therefore, fracture initiation and propagation is predicted to be possible.

A second, empirically determined, definition of the transition temperature below which fracture initiation is expected to occur is the temperature at which the lateral expansion in the Charpy-V-notch specimen is 15 mils [8.3]. This definition is also considered a conservative estimate of the lowest service temperature at which the steel can be used without risk of fracture initiation. For higher strength steels, the 15 mils lateral expansion criterion has been found to be a more suitable definition of the transition temperature than the 15 foot pound definition [8.2]. The 15 mils lateral expansion criteria is less conservative (defines a lower transition temperature) for the low strength structural steel such as that used in this tank. As can be seen from Table 7.7, the 15 mil lateral expansion transition

temperatures of the steel plates used in this tank (55° F to 68° F) were also substantially above the operating temperature (32° F) at failure of this tank and therefore this method predicts that fracture initiation is possible.

A more exact, but still empirically based, procedure to assess the probability of fracture initiation and arrest is the determination of the drop-weight nil-ductility transition (NDT) temperature. This NDT temperature is used in conjunction with the generic Fracture Analysis Diagram (FAD), shown in Figure 8.1, to make an assessment of the probability of fracture initiation and arrest [8.4]. The Fracture Analysis Diagram provides a generalized description of the relationships between the crack size, relative stress, and operating temperature relative to the NDT. At temperatures below the NDT, the Fracture Analysis Diagram predicts that fracture will initiate from small defects (typically less than 1-inch in length) at stress levels below the yield strength of the steel and that the fracture will be brittle in nature. As seen in Table 7.8, the NDT for the first and second shell course steel plates was 20° F to 40° F above the operating temperature of the tank at the time of the failure. Based on the measured NDT and the Fracture Analysis Diagram, fracture initiation is predicted to be likely to occur in this tank at the operating temperature of 32° F.

The NDT temperature also can be used to make a qualitative assessment of the probability of fracture propagation or arrest once fracture has been initiated. A crack arrest temperature (CAT) curve is defined by the Fracture Analysis Diagram and shows that fracture propagation is expected to occur at and below the NDT temperature even when the stress levels present are very low (<10 per cent of the yield strength). Fracture propagation is predicted at stress levels of approximately one half the yield strength level at temperatures about 30° F above the NDT temperature. Fracture arrest is not expected at stress levels equal to the yield strength of the steel until a temperature of approximately 50° F above the NDT temperature is reached.

8.3 Fracture Analysis

8.3.1 Basis for Fracture Analysis

A more quantitative and deterministic analysis to predict fracture initiation can be made on the basis of linear elastic fracture mechanics principles. The objective of this analysis is to calculate the applied stress intensity in the structure due to the presence of a defect and the known applied stresses and then to determine if this applied stress intensity exceeds the critical value stress intensity (K_{IC}) for initiating fracture in the material. The data used for this fracture analysis came from the measured materials properties, the measured size of the identified surface defect, the stress and thermal analyses done by the NBS, and the residual stress measurements conducted by Battelle. The values of all parameters used in the analyses that follow are summarized in Table 8.1. The fracture analysis was done using materials properties values measured at 40° F. The actual temperature of the metal in the tank was calculated to be 32° F but the small difference in temperature between the tank temperature and the temperature at which the materials properties were measured was not found to significantly affect the values of the materials properties. For the following fracture analyses, the three specific stress levels that were analyzed are: (1) stress only from the hydrostatic pressure of the oil (2) stress from the hydrostatic stress plus the measured residual stress, and (3) stress equal to yield strength of the steel plates.

The fracture analysis conducted here was based on linear elastic fracture mechanics principles. The analyses were done only for the defect located in base metal in the first shell course and the stresses used were those calculated at the position of this defect and all materials properties were those measured for the base metal in the first shell course. For a plane strain stress state to exist, the following relationship must be satisfied [Reference 8.5]:

$$t > 2.5 \left(\frac{K_C}{\sigma_y} \right)^2$$

where

K_C = Toughness

σ_y = yield strength

t = thickness

Using the thickness of the steel plate as 0.875-inch, the toughness of the steel plate as 47.7 ksi$\sqrt{in}$, and the yield strength as 34.0 ksi, it was determined that the shell of the tank was not in plane strain but should be analysed as a plane stress problem.

For purposes of the fracture analysis, it was determined that the curvature of the tank could be ignored and that the tank could be assumed to be a flat plate. This conclusion was reached because the tank radius to tank wall thickness ratio (R/t) was very large (>820). It has been determined that under some conditions, a part-through-wall or through-wall defect may cause a local increase in the stress in a thin walled, pressurized structure due to small amount of bulging of the wall in the vicinity of the defect. This increase in local stress is accounted for using a stress magnification factor (M_F) based on an analysis by Folias [8.6]. The stress magnification factor is calculated by the following relationship:

$$M_F = \sqrt{1 + \frac{1.62C^2}{R\ t}}$$

where

C = half defect length

R = radius of the tank

t = thickness of the tank wall

For the size of defect in the tank being analyzed here the stress magnification factor was calculated to be 1.0002. This indicates that the increase in local stress due to the defect causing bulging of the tank wall is insignificant. Because the curvature of the tank could be ignored and no significant stress magnification occurred due to bulging of the tank wall in the vicinity of the defect, the stress intensity in the tank wall due to the defect can be accurately calculated by modeling the problem as a defect in a flat plate.

8.3.2 Analysis of Part-Through-Surface Defect

The stress intensity for a part through wall defect was calculated based on a stress intensity formulation developed by Raju and Newman [8.7] for part-through-surface defects in a flat plate. This calculation is based on the following equation:

$$K_I = \sigma_H \, F \sqrt{\frac{\pi C}{Q}}$$

where

σ_H = hoop stress

Q = defect shape factor = $1 + 1.464 \, (a/c)^{1.65}$,

C = defect half length

F = stress magnification factor

$$F = \left[M_1 + \left\{ \left(\frac{QC}{a} \right)^{1/2} - M_1 \right\} \left(\frac{a}{t} \right)^{\sqrt{\pi}} + \left(\frac{QC}{a} \right)^{1/2} (M_2 - 1) \left(\frac{a}{t} \right)^{\sqrt{\pi}} \right] f_W$$

where

t = plate thickness

$M_1 = 1.13 - 0.1 \, (a/c)$

$M_2 = \sqrt{\pi/4}$

$f_W = \left[\sec \left(\frac{\pi C a}{W t} \right) \right]^{1/2}$

W = plate width

a = defect depth

As shown in Table 8.2 the applied stress intensity calculated from stresses created by the hydrostatic pressure was only 10.7 ksi$\sqrt{\text{in}}$ for the size of defect found in the tank. When residual stresses were taken into account and added to the hydrostatic pressure stresses the calculated applied stress intensity was increased to 22.7 ksi$\sqrt{\text{in}}$. Even if it is assumed that stresses from all other undocumented sources could be as high as the yield strength of the steel plate, the calculated applied stress intensity is increased only to 27.2 ksi$\sqrt{\text{in}}$. The critical stress intensity (K_C) for the first shell course steel plate was 47.7 ksi$\sqrt{\text{in}}$. For fracture initiation to occur the calculated

applied stress intensity must be larger than the critical stress intensity (Kc) for the steel plate. Therefore, it is concluded that even if stresses up to the level of the yield strength of the steel plates were present at the location of the defect, fracture would not be expected to have initiated from a surface defect of this size. This analysis predicts that, at most, the ligament of metal in the tank wall below the defect might be expected to break and a through-the-wall defect would be formed that would result in leaking of the tank without rupture of the tank occurring.

8.3.3 Analysis of Through-the-Wall Defect

The second stage of the fracture analysis was to determine, that if the part-through-wall defect became a through-the wall-defect as described above, whether fracture would be initiated. The applied stress intensity for the defect in the tank wall was calculated by using procedures for cracks in hypothetical structures that are available in the technical literature.

The defect was first modeled as a center-cracked-plate stressed in tension. This analysis gives results of acceptable accuracy when the curvature of the tank can be ignored because the tank radius to thickness ratio (R/t) is large. This condition was met for the problem analyzed here. Analytical solutions for both the case of an infinite plate and for the case of a wide plate of finite dimensions were used. The stress intensity factor for the center cracked plate is calculated from the following relationship given in reference [8.8]:

$$K_I = \sigma_H \sqrt{\pi C}$$

where

C = defect half length

For this case, because the tank is very large relative to the size of the defect, the stress intensity calculated using both the infinite plate and finite plate analyses gave the same answers. The results for these calculations of the stress intensity are shown in Table 8.2.

As shown in Table 8.2 the applied stress intensity calculated from stress created by the hydrostatic pressure alone was 14.5 ksi$\sqrt{in}$ for the size of defect found in the tank. When residual stresses were taken into account and added to the hydrostatic pressure stresses the calculated applied stress intensity was increased to 30.7 ksi$\sqrt{in}$. Even if it is assumed that stresses from all other undocumented sources could be as high as the yield strength of the steel plate, the calculated applied stress intensity is increased only to 36.7 ksi$\sqrt{in}$. The calculated applied stress intensity was the same for the infinite plate analysis as for the finite width plate. The critical stress intensity (K_C) for the first shell course steel plate was 47.7 ksi$\sqrt{in}$. For fracture initiation to occur the calculated stress intensity must be larger than the critical stress intensity (K_C) for the steel plate. Therefore, it is concluded that even if stresses up to the level of the yield strength were present at the location of the defect fracture would not be expected to have initiated from a through-wall defect of this size.

The stress intensity factor for the through-wall defect was calculated by an alternate method that models a defect in a thin walled, pressurized tank [Reference 8.9]. This analysis models the actual defect in a more rigorous manner and should give a more accurate value of the actual applied stress intensity in the tank. The stress-intensity factor for a through-wall defect in a thin walled pressurized structure is calculated from the following equation:

$$K_I = M_F \sigma_H \sqrt{\pi C}$$

where

M_F = stress magnification factor (defined previously)

As shown in Table 8.2 the applied stress intensity calculated by modeling the defect as being in a thin walled pressurized structure was exactly the same as for modeling the defect as being in a flat plate. The applied stress intensity from stress created by the hydrostatic pressure alone was 14.5 ksi$\sqrt{in}$. When residual stresses were taken into account and added to the hydrostatic pressure stresses the calculated applied stress intensity was increased to 30.7 ksi$\sqrt{in}$. Even if it is assumed that stresses from all other undocumented sources could be as high as the yield strength of the steel

plate, the calculated applied stress intensity is increased only to 36.7 ksi$\sqrt{in}$. The calculated stress intensity was the same for the infinite plate analysis as for the finite width plate. The critical stress intensity (K_C) for the first shell course steel plate was 47.7 ksi$\sqrt{in}$. For fracture initiation to occur the calculated stress intensity must be larger than the critical stress intensity (K_C) for the steel plate. Therefore, it is concluded that even if stresses up to the level of the yield strength were present at the location of the defect fracture would not be expected to have initiated from a through-wall defect of this size.

Because the steel plates in this tank had a relatively low yield strength and some plasticity is expected to be present in the vicinity of the defect, an additional calculation of the applied stress intensity was made to account for the size of the plastic zone at the edge of the defect. The analytical solution for the stress intensity factor that takes into account the plasticity is given by the following equation from reference [8.10]:

$$K_I = \left[\frac{8}{\pi} \bar{\sigma}^2 \, C \, \ell n \sec \left(\frac{\pi \, M_F \, \sigma_H}{2 \, \bar{\sigma}} \right) \right]^{1/2}$$

where

$$\bar{\sigma} = \text{flow stress} = \frac{\text{yield strength + tensile strength}}{2}$$

As can be seen from table 8.2, the applied stress intensity is increased slightly when the plasticity correction is added to the analysis. However, even at stress levels equal to the yield strength of the steel plate, the applied stress intensity is still only 41.4 ksi$\sqrt{in}$ which is still well below the critical stress intensity (47.7 ksi$\sqrt{in}$) required to initiate fracture.

8.4 Discussion of the Fracture Analysis Results

For all cases considered in the fracture analysis, the calculated applied stress intensity for the defect identified as the fracture origin was substantially below the stress intensity required to initiate fracture and cause rupture of the tank. This can readily be shown by the stress-flaw size curve shown in Figure 8.2. For the measured toughness (47.7 ksi$\sqrt{in}$) the

relationship between the nominal applied stress and the length of a through-thickness defect is calculated. Combinations of nominal stress and defect size that lie above the line shown in Figure 8.1 are predicted to cause fracture initiation and any combination of defect size and nominal stress that lies below the curve is not expected to result in fracture initiation. As can be seen from the points plotted in Figure 8.1, fracture is not expected to be initiated from a through-thickness defect of the length of the defect found on the fracture surface (0.742 inch.) even if the stresses in the vicinity of the defect are equal to the yield strength of the steel plates. Therefore, additional causes must be identified to determine why the tank ruptured. For the fracture analysis to predict rupture of the tank, either the defect must be significantly larger than the size identified on the fracture surface or the fracture toughness of the steel plate must be lower than that measured in this investigation.

The defect from which the fracture originated was clearly identified by corrosion products on the fracture surface of the defect. Detailed fractographic examination of the fracture surface in the vicinity of the defect by scanning electron microscopy (SEM) that was done by Battelle did not reveal any features that would indicate that the defect was significantly larger that the size used in this analysis.

Therefore, it was concluded that the measured fracture toughness determined on representative samples of the steel plates from the first shell course was not representative of the fracture toughness of the metal in the vicinity of the defect. This conclusion was supported by the microstructural examination of the defect area, shown in Figure 7.26, and by the microhardness measurements made near the defect. These results indicate that the metal in the vicinity of the defect was altered by heating, probably during the initial fabrication or during at the time of disassembly of the tank, and that a hard spot was created around the defect. It is likely that the fracture toughness of this hard spot was lower than the fracture toughness of the unaffected steel. This lower fracture toughness in the vicinity of the defect could cause fracture to initiate in this hardened area and to propagate without arresting through the tougher steel plates.

Previous studies [8.11]. have shown that the stress required to initiate a fracture at a defect in steels of the type used in this tank that has been altered by heating, such as by welding, is considerably reduced from the stress required to initiate fracture in unaltered steel. Heating the metal surrounding an existing defect, such as by a torch cut or welding over the defect may reduce the stress to initiate fracture very significantly.

It was not possible to determine directly the fracture toughness of the altered metal in the vicinity of the defect and therefore, it was not possible to do a quantitative fracture analysis to predict the fracture stress and critical defect size. To demonstrate that it was feasible for the stress required to initiate a fracture from a defect in a region of heat altered metal to be substantially reduced, the series of notched bend tests described in section 7.2 was conducted. This series of tests was conducted to determine the notch sensitivity of the steel at room temperature and 40° F when 1) a weld was deposited, then a notch machined into the weld, 2) a weld deposited over a prexisting notch, and 3) no weld was present near the notch.

In this investigation, the effect of the heat-affected zone on the steel is determined from the load/displacement curve. It is seen in Figure 7.13 that the notch mouth-opening displacement at the maximum load (point of fracture initiation) for the heat affected (embrittled) specimen was 0.032-inch compared with a value of 0.072-inch for the notch mouth-opening displacement for the normal steel plate. The area under the load-displacement curve, (Figure 7.13) which can be expressed in terms of energy, can also be taken as a measure of the tendency to fracture. For example, two specimens that were tested at 40° F with just a notch in the base metal had energy values at maximum load equal to 21.4 and 21.7 foot-pounds. A similar specimen tested at 40° F, in which the metal had been embrittled by heating before cutting the notch had an energy at maximum load of 9.0 foot-pounds and a specimen that was heated after cutting the notch had an energy at maximum load of 9.7 foot-pounds. It was found that the energy to initiate fracture in the notched and heat embrittled specimens at 40° F was less than one half the energy to initiate fracture in the steel base metal that had not been embrittled by heating.

The notched bend specimens did not meet all the requirements to permit determination of the fracture toughness using the crack-tip-opening-diplacement (CTOD) method described in reference [8.11]. However, the results of the notched bend tests indicate that fracture will initiate from a defect in a heat affected and embrittled region at a lower stress than from a defect in the unaltered base metal. If the notch-opening displacement at maximum load or the energy derived from the area under the load-displacement curve for the notch-bend tests is used to compare the fracture initiation of the heat affected and unaltered specimens, it is estimated that the toughness of the material in the heat affected region is less than 1/2 of the toughness of the unaltered base metal. That is, the toughness of the heat affected region surrounding the defect found on the fracture surface could be expected to be less than 25 ksi$\sqrt{\text{in}}$, that is, less than the stress intensity factor of 30.7 ksi$\sqrt{\text{in}}$ due to the combination of the hydrostatic and residual stresses in the tank.

This supports the conclusion that although the defect found on the fracture surface was not large enough to cause fracture initiation in the unaltered base metal, the defect was large enough to initiate the fracture when it was embedded in a hardened region of reduced toughness.

8.5 Evaluation of Fracture Propagation and Arrest

The objective of the fracture analysis described in section 8.4 was only to predict if fracture initiation could occur with the stress, defect size, and fracture toughness present in the tank. Once it has been predicted that fracture can be initiated, it is necessary to determine if the fracture will propagate to an unlimited extent and a complete rupture occur or if fracture arrest will occur, resulting in only a leak. The limited scope of this investigation did not permit a complete and quantitative fracture analysis to be made to predict the conditions under which fracture propagation and arrest could occur. A complete investigation of this type requires the determination of dynamic fracture toughness (K_D) and arrest fracture toughness (K_a) before a quantitative fracture analysis could be made to predict fracture propagation and arrest.

A qualitative assessment of the tendency for fracture propagation and arrest can be made from the results of the drop-weight nil-ductility-transition (NDT) temperature tests. The test results on the steel plates from the first and second shell course plates showed that the NDT temperature of these steel plates was 60° F to 70° F, or about 30° F to 40° F above the operating temperature of the tank. The predictions made from the NDT temperature in conjunction with the Crack-Arrest Curve on the Fracture Analysis Diagram [8.4] show that fracture arrest would not be expected to occur in structures operated at temperature below the NDT temperature of the steel plates, even for stress levels well below the level of the yield strength. A crack arrest temperature (CAT) is defined on the Fracture Analysis Diagram, Figure 8.1, which shows that fracture propagation is expected to occur at and below the NDT temperature even when the stress levels present are very low (<10 per cent of the yield strength). Fracture propagation is predicted at stress levels of approximately one half the yield strength level at temperatures about 30° F above the NDT temperature. Fracture arrest is not predicted for stress levels equal to the yield strength of the steel until a temperature of approximately 50° F above the NDT temperature.

On the basis of the NDT temperature tests alone, unlimited fracture propagation without fracture arrest is predicted to occur once fracture had initiated in the tank. Fracture arrest would not be expected even at stress levels due only to the hydrostatic pressure of the oil. This assessment agrees with the observed complete rupture of this tank.

Table 8.1 - Summary of Values Used in the Fracture Analysis

Property	Value
Tank Temperature	32° F
Defect Size	
Length	0.742 inch
Depth	0.601 inch
Plate Thickness	0.875 inch
Hydrostatic Stress	+ 13.7 ksi
Residual Stress	+ 15.0 ksi
Yield Strength[1] (σ_Y)	34.0 ksi
Tensile Strength[1] (σ_T)	67.1 ksi
Flow Stress[2] (σ_F)	50.6 ksi
Elastic Modulus	30,000 ksi
Fracture Toughness[1]	
K_C at 40° F	47.7 ksi$\sqrt{in}$
J_C at 40° F	75.7 in-lb/in^2

(1) Average value from measured properties at first shell course

(2) $\sigma_F = \frac{\sigma_Y + \sigma_T}{2}$

Table 8.2 - Summary of Calculated Stress - Intensity Factors

Source of Stress	Applied Stress	Stress-Intensity, K_I ksi$\sqrt{in}$			
		For Surface(1) Defect	For Through(2) Defect (Flat Plate)	For Through(3) Defect (Thin Walled vessel)	For Through(4) Defect (Thin walled vessel with plasticity Correction)
Hydrostatic	13.4	10.7	14.5	14.5	14.7
Hydrostatic (σ_H) and Residual (σ_R)	28.4	22.7	30.7	30.7	33.1
Yield Strength Level	34.0	27.2	36.7	36.7	41.4

(1) Based on Raju and Newman Formulation [8.7]

(2) Based on Infinitely wide Flat Plate [8.8]

(3) Based on thin-walled vessel [8.9]

(4) Based on thin-walled vessel with plascity correction [8.10]

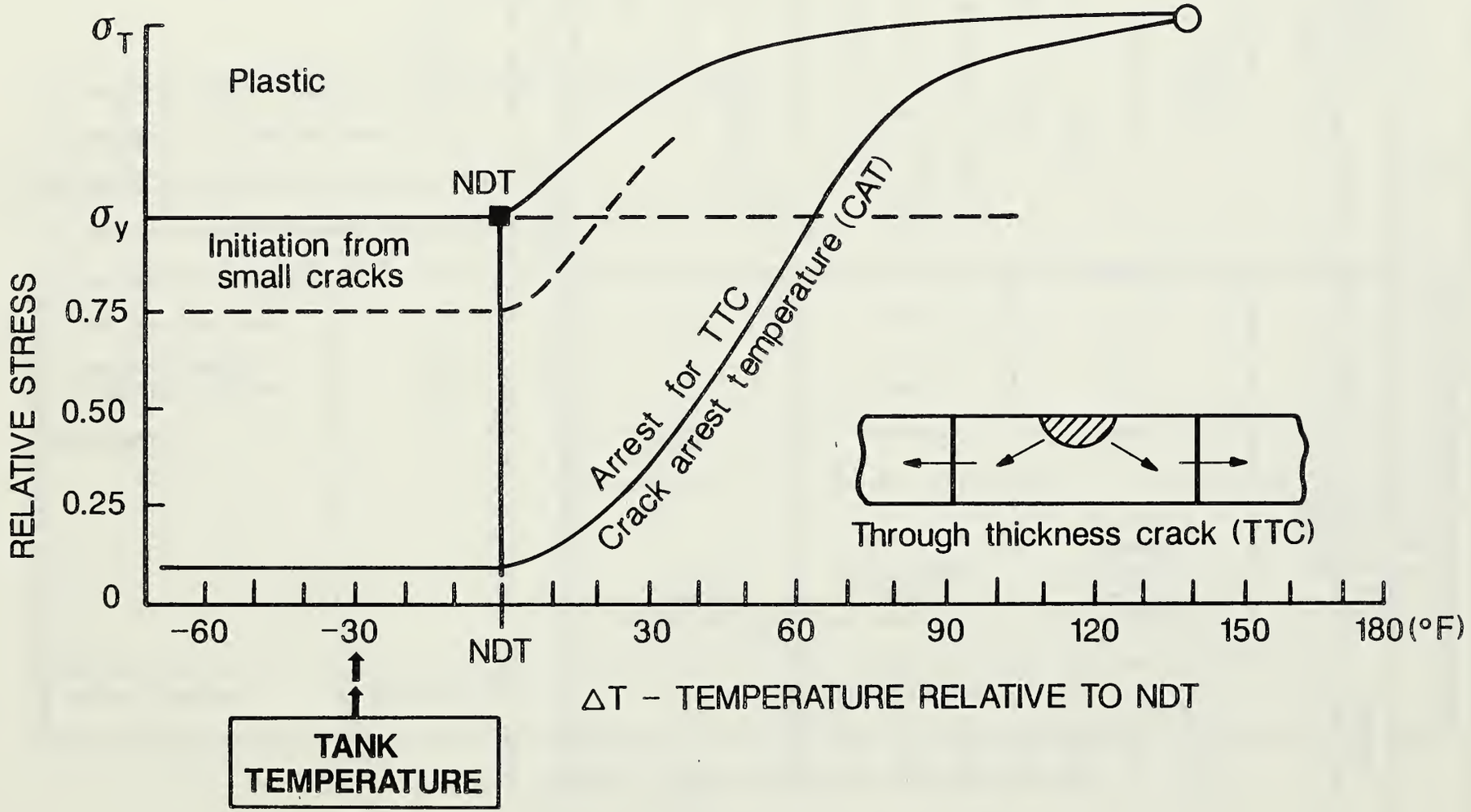

Figure 8.1 - Fracture Analysis Diagram (FAD)

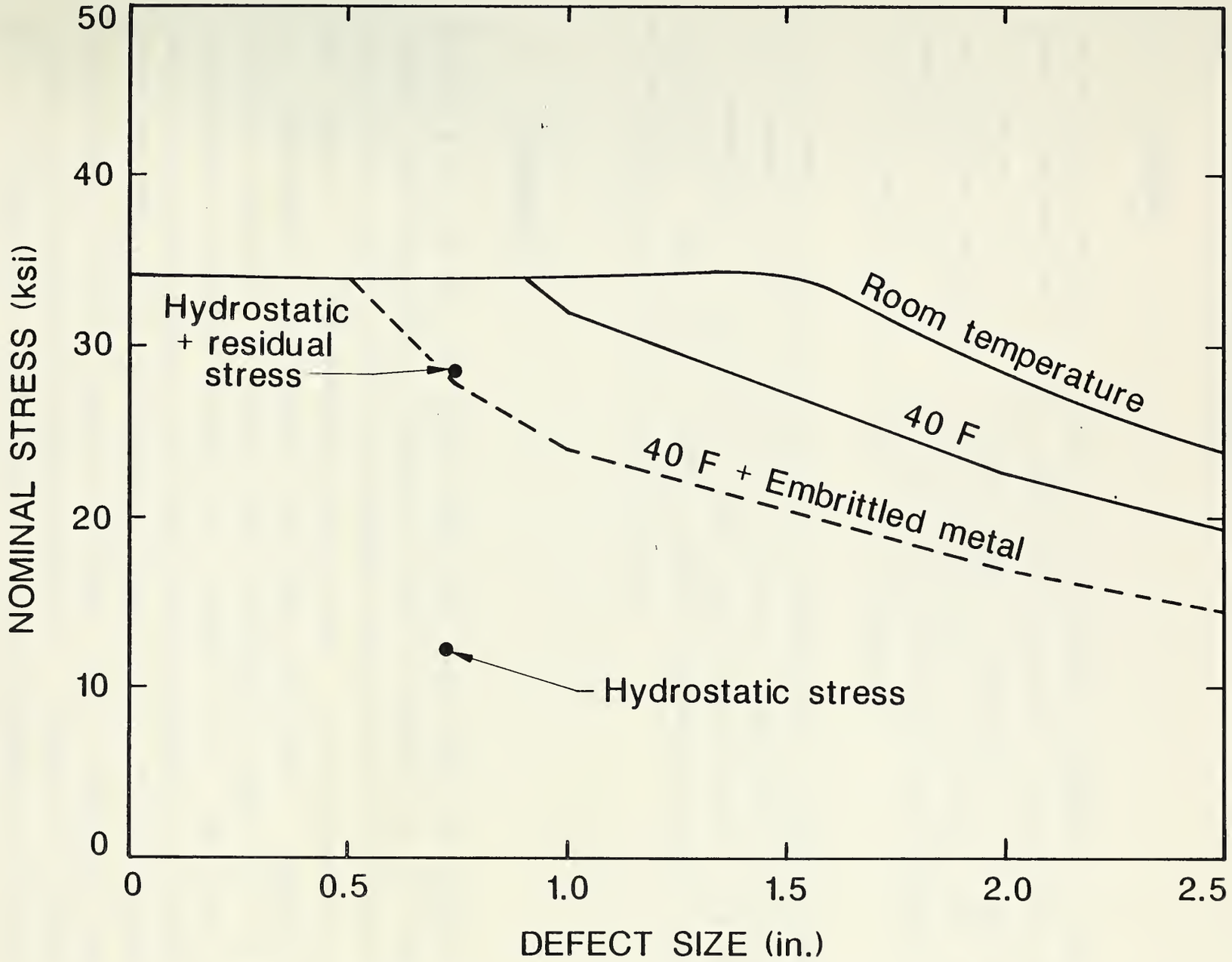

Figure 8.2 - Calculated Stress - Defect Size Relationship for Through-Wall Defect

9.0 CONFORMANCE WITH STANDARDS

9.1 General

The nationally recognized standard for above-ground, atmospheric, welded steel tanks is the American Petroleum Institute Standard 650, *Welded Steel Tanks for Oil Storage*, 1984 [9.1]. In this chapter a comparison will be made between the practices employed in the reconstruction of Tank No. 1338 and the provisions of API 650. Only those provisions which are relevant to the structural performance of the tank will be addressed.

API 650 does not explicitly address the reconstruction of existing tanks. It does, however, include provisions for the use of "materials on hand which are not identified as complying with any listed specification" (see API 650, Appendix N). Thus API 650 can be used for reconstruction of a tank when documentation is not available for the steel.

9.2 Materials

Section N.1.2 of API 650 states that each plate shall be subject to the chemical check analysis and physical tests as required in the designated specification, and the carbon and manganese content shall be determined in all check analyses. It also requires tensile tests. In this instance no record of a "designated specification" was found for review. Appendix N is, therefore, interpreted to require that the material comply with one of the specifications listed in Sections 2.2.2 through 2.2.5. The plate material used in this tank, because of its age, was not fabricated in accordance with any of the ASTM, CSA, or ISO standards listed. However, it complies with ASTM Specification A 283-84, listed in Section 2.2.2. Mechanical properties obtained for the plates are listed in Table 7.2. These can be compared with Table 1 in ASTM A 283. The comparison indicates conformance with Grade D.

Carbon contents for the plates, listed in Table 7.1, ranged from 0.207% to 0.299% and averaged 0.238%. ASTM A 283 does not specify carbon content. However, the steel should be considered weldable without pre-heating in

accordance with presently accepted criteria [9.2].

Section 2.2.9 of API 650 specifies toughness requirements. Section 2.2.9.2 states that when used at design metal temperatures below the design metal temperature specified for the material in Figure 2-2 of the standard "...the material shall demonstrate adequate notch toughness at the design metal temperature..."(in use). In accordance with Table 2-3 of the standard, the material of the plates used does not fit any of the groups listed, because it was not killed or semi-killed. However, for the pupose of assessing conformance with the toughness requirements the material is placed in Group I (A 283 Grade C is listed in Group I, but A 283 Grade D is not listed. However, as noted in Section 9.3 of this report, the design stress does not exceed the working stress allowed for A 283 Grade C). For a plate thickness of 7/8 inches, the specified design metal temperature for Group I materials is 42° F. However, in accordance with Figure 2-1 and Section 2.2.9.3 of API 650, the design metal temperature for Pittsburgh, Pennsylvania is +5° F. Thus adequate notch toughness must be demonstrated by testing. Table 2-2 of API 650 specifies a minimum absorbed energy requirement for the Charpy V-notch Test (ASTM A 370). For Group I material an absorbed energy of 15 ft-lb is specified for longitudinal orientation (parallel to the direction of rolling). The absorbed energy measured for specimens taken from the plates (Table 7.4) was 6 ft-lb or less for temperatures below 40° F. Thus the toughness of the material is seriously deficient in respect to the standard.

In addition to the base metal, the plates also included old welds which were not removed prior to the reconstruction of Tank No. 1338. Thus these old welds were part of the material and therefore must comply with the materials provisions of the standard. In accordance with a radiography report prepared by Progress Services, Inc. of Monroeville, PA and submitted to Ashland Oil Company on November 25, 1986, the old welds were not of acceptable quality per Paragraph UW-51(b) of the ASME *Boiler and Pressure Vessel Code*, Section VIII, Division 1 [9.3]. Figure 9.1 shows defects in old and new welds.

In summary, a comparison with of the test results of the plate material with the provisions in Section 2 and Appendix N of API 650 indicates that the plate material does not comply with the toughness requirements of API 650 and is

seriously deficient in this respect. In accordance with the standard, the material used was inappropriate for the climatic conditions of Pittsburgh, Pennsylvania.

9.3 Shell Design

The original plans and design calculations for Tank #1338, if they exist, were not available for review. Also, no design calculations were found for the reconstructed tank. The inspection report for the Whiskey Island Tank #16 indicates that the wall thickness for all shell courses was satisfactory. Presumably this determination was based on calculations made for the measured wall thicknesses, specific gravity of the product, corrosion allowance, allowable stress of the steel, and design metal temperature. These data, while required by API 650 to be supplied by the purchaser, were not available.

One can compute the required shell thickness using the "one-foot method" (API 650, Section 3.6.3.1) in which the design thickness, t, is given by,

$$t = \frac{2.6\ D\ (H-1)\ G}{S_d} + C.A.$$

where,

H = height from the bottom of the shell course to the top of the shell

D = tank diameter = 120 ft

G = specific gravity = 0.87

S_d = design allowable stress = 20,000 psi

C.A. = Corrosion allowance = 0

These values are reported in Table 9.1 for a specific gravity of 0.87 and a design stress of 20,000 psi. The wall thicknesses measured by NBS are also shown in Table 9.1. By subtracting the required thickness from the measured thickness, one obtains the available corrosion allowance. It is seen that, in all cases, the shell plate thickness provided either meets or exceeds the required thickness, but the available corrosion allowance is only approximately 1/16 in.

9.4 Inspection

Section 6 of API 650 requires that butt-welded joints of the shell plates, both vertical and horizontal, be spot radiographed. The spot radiographs are to be taken as the welding progresses (Section 6.1.2.7) and are intended to determine if a welder is making good quality welds. The acceptance criteria for welds examined by radiography are contained in Paragraph UW-51(b) of the ASME *Boiler and Pressure Vessel Code*, Section VIII, Division 1 [9.3] and are adopted by reference (API 650, Section 6.1.5).

The number and location of spot radiographs are described in Section 6.1.2.1 for vertical joints and Section 5.1.2.2 for horizontal joints. In the lowest shell course, for example, API 650 requires two spot radiographs in each vertical joint and a radiograph at all junctions of vertical and horizontal joints. Tank #1338 was radiographed on one occasion, after completion of construction. A total of 39 radiographs were taken; 26 in a vertical joint, 9 at the intersection of a horizontal and vertical joint, and 4 in a horizontal joint. The radiographer reported that, out of the 39 radiographs, 22 did not meet the acceptance criteria. There is no record that any repairs were made.

Several provisions of API 650 regarding radiographic inspection were not met: fewer radiographs were taken than were required; the radiographs were not taken during construction, but rather after the tank was completed; and, although 22 radiographs failed to meet the acceptance criteria, no repairs were made. In the letter of transmittal which accompanied the radiography report, the following comment was made:

> "It is my opinion that the areas which are rejectable are in the old weld and not in the weld recently done."

Had API 650 been followed, there would have been a radiograph at the location of the flaw that initiated the fracture of the shell that might have revealed the presence of the flaw.

9.5 Testing

Requirements for testing are included in Section 5 of API 650 which deals with erection. Section 5.3.6 deals with testing of the tank shell. Part 1 of this section requires that, if water is available, the tank shall be filled with water to the maximum design level or to a level 2 inches above the weld connection of the roof plate. Part 2 of the section permits an alternate method of testing for joint leakage if sufficient water is not available.

The availability of sufficient water at the Floreffe site is not questioned. Thus, in accordance with API 650, the tank should have been filled with 46 ft of water and carefully inspected during the filling, before external oil piping was connected.

It was reported that the tank was filled with only 5 ft of water rather than 46 ft. Thus the erection procedures specified by API were not followed. Had the test been carried out as specified, the tank might have failed during the water test preventing the severe environmental damage that occured. However, abrupt failure of a water-filled tank would itself be hazardous. It is also possible that a water test at a temperature higher than that at the time of the failure would have resulted in no leak at all or a slow leak, rather than a rapid crack propagation.

9.6 Foundation

Section 3.3.1 of API 650 specifies that site selection and foundation design and construction "shall be given careful consideration as outlined in Appendix B". This statement implies that Appendix B is a recommendation rather than a provision.

Section B.2.1 deals with subsurface exploration and settlement control. No data were available to NBS to indicate the nature and extent of subsurface exploration prior to construction of the tank. The statement in the standard on settlement is non-specific. However, an analysis of the foundation indicates that the maximum anticipated settlements would be within tolerable

limits.

Sections B.2.2 and B.2.3 do not apply because the underlying soil is considered competent to support the tank without special remedial measures.

Section B.2.4 deals with fill materials, but the degree of required compaction is not specified. The foundation analysis indicates that the compaction specified in the foundation construction contract was adequate and that the compacted fill was constructed in accordance with the specifications.

Section B.3 deals with the grading of the foundation surface supporting the tank bottom and the subgrade supporting the bottom plate. The tank foundation complies with these provisions.

Section B.4 deals with foundation design. The foundation analysis indicates that the design criteria in Section B.4.1 are satisfied. The recommended design detail for a tank which is not supported by a concrete ring foundation is shown in Figure B-2 of the Standard. The design of the tank foundation, shown in Figure 4.1 deviates from this detail. However, the gravel pad as a whole was 1 to 1 1/2 ft thick thereby eliminating the need for the crushed stone ringwall shown in Figure B-2. In addition, a geotextile sheet was inserted between the crushed-stone pad and the compacted fill, which could inhibit radial spreading of the crushed-stone pad and erosion caused by potential leaks.

In summary, on the basis of construction drawings and records and subsurface data supplied by the Pennsylvania Task Force and the foundation analysis presented in Section 4, it is concluded that the tank foundation complies with the provisions and recommendations in Section 3.3.1 and in Appendix B of API Standard 650.

Table 9.1 - Design Shell Plate Thicknesses

	Plate Thickness (in)		Computed Corrosion Allowance
	Measured by NBS (nearest 1/16")	Design Minimum (next 1/16")	
Shell Course 1	7/8	11/16	3/16
Shell Course 2	11/16	9/16	1/8
Shell Course 3	1/2	7/16	1/16
Shell Course 4	3/8	5/16	1/16
Shell Course 5	1/4	1/4	-
Shell Course 6	3/16	1/8	1/16

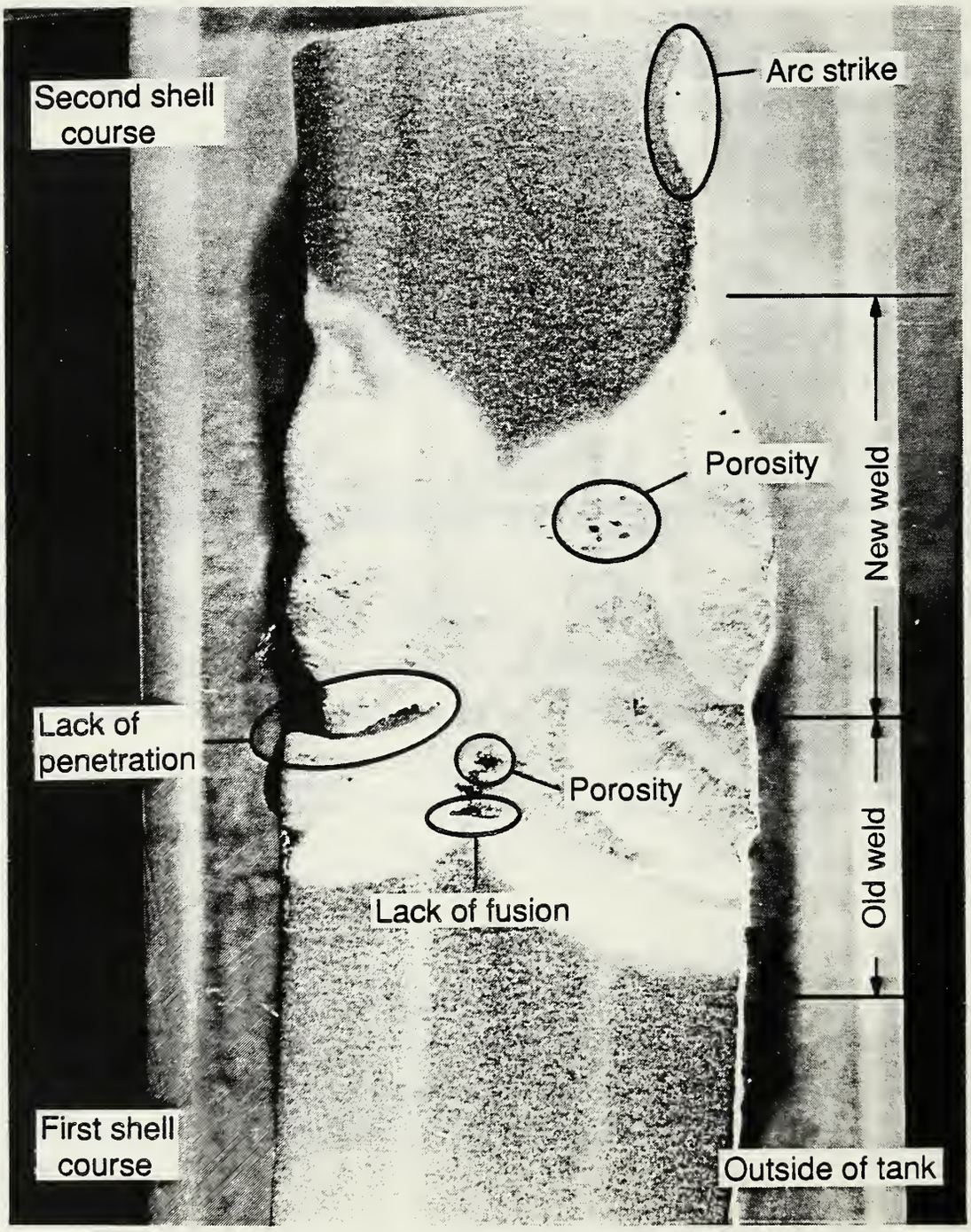

Figure 9.1 - Defects in a Horizontal Weld between the First and Second Shell Courses

10. CONCLUSIONS

10.1 Cause of Tank Collapse

The failure of the tank was caused by a brittle fracture that initiated at a flaw in the tank shell about 8 ft above the base and just below the horizontal weld between the first and second courses of steel. The fracture propagated to complete rupture of the tank shell because the steel lacked sufficient toughness to arrest a propagating fracture at the temperature and stresses existing in the tank shell.

Failure was reported to have occurred as the tank was being filled to capacity for the first time at the Floreffe site. The temperature of the shell was about 32° F, and the calculated stress at the initiating flaw about 13.7 ksi. These conditions are fully consistent with initiation and complete propagation of brittle fracture considering the flaw size, embrittlement of adjacent steel, presence of residual stresses, and the low fracture toughness of the shell steel at 32° F. The shell steel did not meet the fracture toughness requirements of API 650.

The flaw at which the fracture initiated was determined by Battelle to be present prior to the reconstruction of the tank at the Floreffe site. Deposits on the surface of the flaw indicate it was formed during a cutting operation.

Although the weld quality did not conform to API 650, the weld quality was not a contributing factor in the initiation or propagation of this fracture. However, welding adjacent to the flaw contributed to embrittlement of the metal.

Foundation conditions were investigated to determine if instability or irregular settlement of the foundation might have increased stresses in the shell. No evidence was found of foundation instability or excessive settlement.

10.2 Lessons Learned

This study focused on the tank that collapsed at the Floreffe Terminal on January 2, 1988, and on the standards applicable to its dismantling and reconstruction. In spite of this limited scope, lessons of general significance have been learned from this failure, and relearned from earlier, similar failures.

The catastrophic failure of the Ashland tank resulted from a flaw that might have been, but was not, detected in tests for welding quality, and the use of steel that did not possess sufficient fracture toughness to arrest a fracture that initiated at a localized flaw. While there are many reasons for control of weld quality, it is not feasible to guarantee the absence of localized defects by control of fabrication and detailed inspection for defects during fabrication. Neither is it feasible to guarantee the absence of localized defects during service by recurrent inspections. Therefore, it is advisable to use steel of adequate toughness to provide "leak before break" fail-safe behavior. If a crack is initiated, due to a flaw or local damage in service, in a tank with steel of adequate fracture toughness, the crack will arrest, the tank will leak, normal spill-control measures will confine the spread of contents, and the tank can be repaired all without catastrophic consequences.

Available standards should be reviewed to identify those calling for sufficient fracture toughness to prevent catastrophic brittle fracture at design stresses and temperatures. This study found the provisions of API 650 (1984) to be sufficient for the structural steels in its Materials Group I. Compliance with sufficient fracture toughness provisions should be required for steel to be used in construction or reconstruction of tanks, or for changes in service conditions.

There is concern for the safety of existing tanks whose catastrophic failure would cause unacceptable human, environmental or economic losses. If documentation exists to show that the steel of an existing tank meets sufficient fracture toughness provisions, the concern will be alleviated. If documentation shows inadequate fracture toughness, remedial actions should be taken. Possible remedial actions include conversion to adequately high

temperature service, retirement, or installation of crack arresters.

Test and assessment protocols should be developed for assessing the fracture safety of potentially hazardous existing tanks that lack adequate documentation for definition of the fracture toughness of their steel.

REFERENCES

2.1 ASME *Boiler and Pressure Vessel Code*, Section VIII - Rules for Construction of Pressure Vessels, Division 1, 1986 Edition, The American Society of Mechanical Engineers, New York, 1986.

4.1 Duncan, M.J. and D'Orazio, T.B., "Stability of Steel Oil Storage Tanks", *Journal of Geotechnical Engineering*, ASCE, Vol. 110, No. 9, September 1984.

4.2 Bjerrum, L. and Overland, A., "Foundation Failure of an Oil Tank in Fredrikstad, Norway", *Proceedings of the 4th Internalional Conference on Soil Mechanics and Foundation Engineering*, Vol. 1, pp. 287-290, 1957.

4.3 D'Orazio, T.B. and Duncan, M.J., "Differential Settlements in Steel Tanks", *Journal of Geotechnical Engineering*, ASCE, Vol. 113, No. 9, September 1987.

4.4 Langeveld, J.M.,"The Design of Large Storage Tanks for Crude Oil and Natural Gas", *Proceedings of the Annual Meeting of International Institute of Welding*, 1974.

4.5 Malik, Z. et al., "Ovalization of Cylindrical Tanks as a Result of Foundation Settlements", *Journal of Strain Analysis*, Vol. 12, No. 4, April 1977.

4.6 Penman, A.D.M.,"Soil-Structure Interaction and Deformation Problems with Large Oil Tanks", *Proceedings of the International Symposium on Soil-Structure Interaction*, Vol. 1, Roorkee, India, January 1977.

4.7 Marr, W.A., Ramos, A.J., and Lambe, T.W., "Criteria for Settlement of Tanks", *Journal of the Geotechnical Engineering Division*, ASCE, Vol. 108, No. GT8, August 1982.

5.1 *PATRAN Plus User Manual*, PDA Engineering, Costa Mesa, California, 1987.

5.2 *Stress Analysis Module Primer*, PDA Engineering, Costa Mesa, California, 1985.

6.1 Jakob, M., *Heat Transfer*, vol. 1, John Wiley & Sons, Inc., New York, 1949.

6.2 Spiers, H.M., *Technical Data on Fuel*, Fifth Edition, The British National Committee, World Power Conference, London, 1955.

6.3 McAdams, W.H., *Heat Transmission*, 3rd ed., McGraw-Hill, New York, 1954.

6.4 Holman, J.P., *Heat Transfer*, 5th ed., McGraw-Hill, New York, 1981.

6.5 *Wind Loading and Wind-Induced Structural Response*, ASCE, New York, 1987.

7.1 ASTM E-415-85, Standard Method for Optical Emission Vacuum Spectrographic Analysis of Carbon and Low Alloy Steel, published by the American Society for Testing and Materials, 1916 Race St. Philadelphia, PA. U.S.A.

7.2 ASTM A10-39, Standard Specification for Mild Steel Plates. published by the American Society for Testing and Materials, 1916 Race St. Philadelphia, PA. U.S.A.

7.3 ASTM A283-84, Standard Specification for Low and Intermediate Tensile Strength Carbon Steel Plates, Shapes and Bars, published by the American Society for Testing and Materials, 1916 Race St. Philadelphia, PA. U.S.A.

7.4 *Welded Steel Tanks for Oil Storage*, API Standard 650, Seventh Edition, November 1980, Revision 1, February 1984, American Petroleum Institute, Washington, D.C.

7.5 Barr, W. and Honeyman, A.J.K., "Some Factors Affecting Notched-Bar Impact Properties of Mild Steel," J. Iron & Steel Inst., Vol.157, pp.242-246 (1947).

7.6 ASTM E-8-86, Standard Methods of Tension Testing of Metallic Materials, published by the American Society for Testing and Materials, 1916 Race St. Philadelphia, PA. U.S.A.

7.7 ASTM E-23-86, Standard Methods for Notched Bar Impact Testing of Metallic Materials, published by the American Society for Testing and Materials, 1916 Race St. Philadelphia, PA. U.S.A.

7.8 Johnson, H.H. and Stoudt, R.D., "Comparison and Analysis of Notch Toughness Tests for Steels in Welded Structures," pp1-28. WRC Bulletin 62, July 1960.

7.9 ASTM E-208-85, Standard Method for Conducting Drop-Weight Test to Determine Nil-Ductility Transition Temperature for Ferritic Steels, published by the American Society for Testing and Materials, 1916 Race St. Philadelphia, PA. U.S.A.

7.10 ASTM E-813-87, Standard Test Method for J_{IC}, A Measure of Fracture Toughness, published by the American Society for Testing and Materials, 1916 Race St. Philadelphia, PA. U.S.A.

7.11 ASTM E-399-83, Standard Test Method for Plane-Stain Fracture Toughness of Metallic Materials, published by the American Society for Testing and Materials, 1916 Race St. Philadelphia, PA. U.S.A.

7.12 Rosenfield, A.R., and Shetty, D.K., "Cleavage Fracture of Steel in the Ductile-Brittle Transition Region," *Elastic-Plastic Fracture Test Methods: The User's Experience*, ASTM STP 856, E.T. Wessel and F.J. Loss eds., American Society for Testing and Materials, 1985, pp.196-209.

7.13 Barsom, J.M. and Rolfe, S.T., *Fracture and Fatigue Control in Structures*, Second Edition, Prentice-Hall, Englewood Cliffs, New Jersey, 1987, pp.569.

7.14 Private Communication--R.Mesloh, Battelle, April, 1988.

7.15 Micrographs supplied by R.Mesloh, Battelle.

7.16 Letter from Kirkpatrick & Lockhart Attorneys at Law, March 14, 1988, reporting results of tests by Battelle.

7.17 Masubuchi, K. *Analysis of Welded Structures*, Pergamon Press, Oxford, England, pp. 209.

8.1 Pellini, W.S., *Guidelines for Fracture-Safe and Fatigue-Reliable Design of Steel Structures*, The Welding Institute, Cambridge, England, 1983, pp.12-18.

8.2 Williams, M.L. and Ellinger, G.A., "Investigation of Structural Failures of Welded Ships," Welding Journal, Vol.32 (10), Research Supplement, pp.498s--528s, 1953.

8.3 Gross, J.H. and Stout, R.D., "Ductility and Energy Relations in Charpy Tests of Structural Steels", Welding Journal, Vol.37 (4), Research Supplement, pp.151s--159s, (1958)

8.4 Pellini, W.S. and Puzak, P.P., "Fracture Analysis Diagram Procedures for the Fracture-Safe Engineering Design of Steel Structures," Welding Research Council Bulletin No.88, May 1963.

8.5 Barsom, J.M. and Rolfe, S.T., *Fracture and Fatigue Control in Structures*, Second Edition, Prentice-Hall, Englewood Cliffs, New Jersey, 1987, pp.109.

8.6 Folias, E.S., "A Finite Line Crack in a Pressured Cylindrical Shell," International J. of Fracture Mechanics, Vol. 1, (1965), pp.104-113.

8.7 Raju, I.S. and Newman J.C., "Analyses of Surface Cracks in Finite Plates Under Tension or Bending Loads," NASA TP-1578, National Aeronautics and Space Administration, Dec. 1979.

8.8 Broek, D. *Elementary Engineering Fracture Mechanics*, Martinus Nordhoff Publ., The Hague, Holland, (1982), pp.12.

8.9 ibid. pp.379

8.10 Hahn, G.T., Sarrente,M. and Rosenfield, A.R., "Criteria for Crack Extension in Cylindrical Pressure Vessels," International J. Fracture Mechanics, Vol.5 (1969), pp.187-210.

8.11 Hall, W.J., Nordell, W.J. and Munse, W.H., "Studies of Welding Procedures", Welding Journal, Research Supplement Vol. 41 (11), (1962).

8.12 ASTM Draft Standard "Test Method for Crack-Tip Opening Displacement (CTOD) Fracture Toughness Measurements, August (1987).

9.1 *Welded Steel Tanks for Oil Storage*, API Standard 650, Seventh Edition, November 1980, Revision 1, Febryary 1984, American Petroleum Institute, Washington, D.C., 1984.

9.2 Ricker, D.T., "Field Welding of Existing Structures," *Engineering Journal*, AISC, Vol.25, No.1, 1988.

9.3 ASME *Boiler and Pressure Vessel Code*, Section VIII - Rules for Construction of Pressure Vessels, Division 1, 1986 Edition, The American Society of Mechanical Engineers, New York, 1986.

APPENDIX

SUBSURFACE EXPLORATION DATA

Boring Logs

Oedometer Tests from Boring B-4 and B-5

Unconsolidated Undrained Compression Tests

ENGINEERS FIELD BORING LOG

SHEET 1 OF 3
BORING NO. B-1

ASHLAND TANK COLLAPSE
PROJECT NO. _____ PROJECT LOCATION: L.R. _____; SEC. _____; CTY. _____
TEST PIT NO. _____ STATION _____ OFFSET _____ ELEVATION 180.2
DATE 2/25-3/2/88 EQUIPMENT USED 140# HAMMER W/30" DROP - 2 1/2" I.D. S.S. SPOON
ENGINEER GANNETT FLEMING ENGINEERS REP. BILL FRANZ
DRILLING METHODS HSA w/ 7 1/4" O.D. & 3 1/4" I.D.
WATER LEVEL DEPTH: _____ FEET ⊖ _____ HRS.; _____ FEET ⊖ _____ HRS.;

DEPTH (FT)	SAMPLE NO./TYPE OR RUN NO.	BLOWS/0.5 FT. ON SOIL SAMPLER	RECOVERY (IN)	RECOVERY (%) / ROD (%)	POCKET PENETROMETER (TSF)	DESCRIPTION	REMARKS
1.5	S-1	1 2	5			LIGHT BROWN & BROWN SILTY CLAY (CL); SOFT; MOIST	BORING ADVANCED AT TOP OF DIKE; DIKE IS ± 5 FT HIGH
3	S-2	1-2 2	3½				
4.5	S-3	1-1 1	4½				POOR RECOVERY FROM 0 TO 6 FT; WOOD TRAP BELOW 3 FT
6	S-4	2-2 5	0				
7.5	S-5	2-4 8	14		1.2	LIGHT BROWN & BROWN SILTY CLAY (CL); STIFF; MOIST	J. SCHMOL OF ENGINEERING SCIENCES TOOK HNU READINGS OF THE HEAD SPACE IN THE JARS; SHE REPORTED NO UNUSUAL READINGS
9	S-6	9-15 23	18		3.2		
10.5	S-7	5-7 10	13		3.6		
12	S-8	8-11 12	13		3.9		
13.5	S-9	3-5 7	18		3.2		
15	S-10	5-7 10	13		3.5		
Kas	S-11	5-9 8	18		3.8		
18	S-12	4-4 8	18		2.9		18
19.5	S-13	5-8 4	18		3.0	LIGHT BROWN & BROWN SANDY, SILTY CLAY (CL); SAND IS FINE; STIFF; MOIST	
21	S-14	4-7 7	18		1.6		
22.5	S-15	3-7 10	18		1.5		22.5
24	S-16	3-7 7	13		1.1	LIGHT BROWN & BROWN SANDY, CLAYEY SILT (CL/ML) MOIST	
	S-17	4-6 7	18		—		

25.5

NOTES:
STRATIFICATION LINES REPRESENT THE APPROXIMATE BOUNDRY BETWEEN SOIL OR ROCK TYPES AT THE BOREHOLE LOCATION ONLY.

ENGINEERS FIELD BORING LOG

SHEET 2 OF 3
BORING NO. B-1

ASHLAND TANK COLLAPSE

PROJECT NO. _____ PROJECT LOCATION: L.R. _____; SEC. _____; CTY. _____

TEST PIT NO. _____ STATION _____ OFFSET _____ ELEVATION 730±

DATE 1/25- EQUIPMENT USED _____

ENGINEER GARNETT FLEMING ENGINEERS REP. BILL FRANZ

DRILLING METHODS HSA W/ 7½" O.D & 3½" I.D.

WATER LEVEL DEPTH: _____ FEET @ _____ HRS.; _____ FEET @ _____ HRS.;

DEPTH (FT)	SAMPLE NO./TYPE OR RUN NO.	BLOWS/0.5 FT. ON SOIL SAMPLER	RECOVERY (IN)	RECOVERY (%) / ROD (%)	POCKET PENETROMETER (TSF)	DESCRIPTION	REMARKS
25.5						LIGHT BROWN & BROWN SANDY, CLAYEY SILT (ML) MOIST, BUT WET BELOW 32 FT.	
27	S-18	5-5 10	10 0		—		
28.5	S-19	5-6 7	12		—		
30	S-20	9-35 12	12		—		SAMPLE NO. 20 HAD A ½ INCH SHALE ROCK FRAGMENT.
31.5	S-21	4-4 6	14		1.7		
33	S-22	5-5 4	18		0.6		SAMPLE NO. 22 WAS WET
34.5	S-23	8-8 9	15		—	BROWN SANDY, CLAYEY SILT (ML); WET	33
36	S-24	4-6 8	18		0.2		
37.5	S-25	9-11 2	13		0.7		
39	S-26	9-11 10	10		—	BROWN SILTY SAND (SM) WITH SHALE & SANDSTONE ROCK FRAGMENTS, WET	37.5
40	S-27	3-4 2	10		—		
42	S-28	9-16 41	13		—	GRAY GREEN VERY WEATHERED SILTSTONE (CLAYSTONE) (CL) MOIST, VERY STIFF	41
43.5	S-29	9-35 25	12		—		
44.3	S-30	29-50/3	9		—		WATER LEVEL ~1 HOUR AFTER TAKING S-20 = 32.5 M. HARTLEY OF PADER TOOK A WATER SAMPLE FOR LAB TESTING (1/26/05)
49.3	R-1		(2.9')	58%/0.0	—	VERY WEATHERED AND VERY BROKEN BROWN AND GRAY SILTSTONE; CLAY SEAMS PRESENT	DRILLER REPORTED CIRCULATION PRESSURE DURING DRILLING => NO VOIDS
50							49.7
54.3	R-2		4.6'	1/3			

NOTES:
STRATIFICATION LINES REPRESENT THE APPROXIMATE BOUNDRY BETWEEN SOIL OR ROCK TYPES AT THE BOREHOLE LOCATION ONLY.

ENGINEERS FIELD BORING LOG

SHEET 3 OF 3
BORING NO. 3-1

ASHLAND TANK COLLAPSE
PROJECT NO. _____ PROJECT LOCATION: L.R. _____; SEC. _____; CTY. _____
TEST PIT NO. _____ STATION _____ OFFSET _____ ELEVATION 780.2
DATE 1/25- EQUIPMENT USED 2 INCH SPLIT-SPOON; NX DOUBLE CORE BARREL
ENGINEER GANNETT FLEMING ENGINEERS REP. BILL FINN
DRILLING METHODS HSA
WATER LEVEL DEPTH: 2 FEET @ 0 HRS.; _____ FEET @ _____ HRS.;
5.9 " 23 "

DEPTH (FT)	SAMPLE NO./TYPE OR RUN NO.	BLOWS/0.5 FT. ON SOIL SAMPLER	RECOVERY (IN)	RECOVERY (%) / ROD (%)	POCKET PENETROMETER (TSF)	DESCRIPTION	REMARKS
	R-2		(+6")	92.3/20.0	-	GRAY, MEDIUM HARD SILTSTONE; STAINING ON JOINTS	
54.3							54.3 END OF BORING @ 54.3

NOTES:
STRATIFICATION LINES REPRESENT THE APPROXIMATE BOUNDRY BETWEEN SOIL OR ROCK TYPES AT THE BOREHOLE LOCATION ONLY.

ENGINEERS FIELD BORING LOG

SHEET ___ OF 3
BORING NO. B-2

ASHLAND TANK COLLAPSE
PROJECT NO. _____ PROJECT LOCATION: L.R. _____; SEC. _____; CTY. _____
TEST PIT NO. _____ STATION _____ OFFSET _____ ELEVATION 775.5
DATE 1/23-24/18 EQUIPMENT USED 2 INCH SPLIT-SPOON; NX DOUBLE CORE BARREL
ENGINEER [illegible] ENGINEERS REP. [illegible]
DRILLING METHODS HSA
WATER LEVEL DEPTH: _____ FEET ⊕ _____ HRS.; _____ FEET ⊕ _____ HRS.;

DEPTH (FT)	SAMPLE NO./TYPE OR RUN NO.	BLOWS/0.5 FT. ON SOIL SAMPLER	RECOVERY (IN)	RECOVERY (%) / ROD (%)	POCKET PENETROMETER (TSF)	DESCRIPTION	REMARKS
1.5	S-1	3-4 6	9		-	BROWN & GREEN GRAY SILTY SAND & GRAVEL; MOIST (ROADWAY EMBANKMENT MATERIAL)	BORING DRILLED OUTSIDE ASHLAND'S FENCE LINE IN A SMALL BERM THAT IS ABOUT HALFWAY UP AN 8 FOOT HIGH ROAD EMBANKMENT
3	S-2	8-12 8	9		-		
4.5	S-3	3-6 3	11		—		
6	S-4	3-7 4	13		>4.5	LIGHT BROWN & BROWN SILTY CLAY (CL); VERY STIFF; MOIST	
7.5	S-5	4-8 15	18		>4.5		
	S-6	4-7 11	17		4.1		
	S-7	4-6 8	18		3.5		
10.5	S-8	6-7 11	18		3.6		
12	U-1		0.8'			LIGHT BROWN & BROWN SANDY, SILTY CLAY (CL); SAND IS FINE; STIFF; MOIST	12
14	U-2		1.7'				ATTEMPTED TO PUSH U-2, BUT COULD NOT PUSH BLADES FULLY INTO THE SOIL
16	S-9	5-6 9	18		1.0		
17.5	S-10	3-4 6	18		0.6		
19	S-11	3-4 6	17		0.4	LIGHT BROWN & BROWN SANDY SILT & CLAY (CL/ML) MOIST	19
20.5	S-12	2-3 6	14		0.5		
22	S-13	4-4 7	13		0.3		
23.5	S-14	2-5 8	18		0.3	BROWN SANDY SILTY CLAY (CL/ML); WET	S-14 WAS WET, ALSO HAD AN ODOR
25							

NOTES:
STRATIFICATION LINES REPRESENT THE APPROXIMATE BOUNDRY BETWEEN SOIL OR ROCK TYPES AT THE BOREHOLE LOCATION ONLY.

ENGINEERS FIELD BORING LOG

SHEET 3 OF 3
BORING NO. 3-2

Ashland Tank Collapse

PROJECT NO. ________ PROJECT LOCATION: L.R. ______; SEC. ______; CTY. ______

TEST PIT NO. ________ STATION ________ OFFSET ________ ELEVATION 775.5

DATE 1/28-29/88 EQUIPMENT USED 2 inch split-spoon, NX Double Core Barrel

ENGINEER Gannett Fleming ENGINEERS REP. Bill Franz

DRILLING METHODS HSA

WATER LEVEL DEPTH: ______ FEET @ ______ HRS.; ______ FEET @ ______ HRS.;

DEPTH (FT)	SAMPLE NO./TYPE OR RUN NO.	BLOWS/0.5 FT. ON SOIL SAMPLER	RECOVERY (IN)	RECOVERY (%) / RQD (%)	POCKET PENETROMETER (TSF)	DESCRIPTION	REMARKS
26.5	S-15	6-4 3	18		0.2	Brown sandy silt & clay (CL-ML); wet	Pushed a Shelby tube from 26.5-28.5, but had no recovery due to sample too low in clay content
27 – 28.5	S-16	2-4 4	13		0.2		
30	S-17	2-4 6	18		0.2		
31.5	S-18	4-5 7	18		0.9		
33	S-19	4-6 9	18		0.2		33
34.5	S-20	5 37 53	12		—	Brown & gray clayey, silty sand (SM) with shale & sandstone rock fragments. Rock frags can be larger than 1/2 inch, wet	
36	S-21	9-27 23	14		—		
37.2	S-22	21-32 30/.2	7		—		
37.5 – 40.4	S-23	24-50/.4	8		—		
39 – 40.5	S-24	13-17 21	10		—		M. Pavilonis (DER) took a water sample @ 40.5 the end of the day 1/28, & the beginning of the day 1/29; water level after sampling ~ 15-25.0'
42	S-25	13-15 21	4		—		
43.4	S-26	25-34 50/.4	14		—		
43.5 – 45	S-27	20-32 36	10		—		
45.6	S-28	19-50/.1	6		—		
46.5 – 47.4	S-29	41-50/.4	5		—		
48 – [illegible]	S-30	51 50/.4	6		—		
49.5 – [illegible]	S-31	50/.3	4		—	Gray green very weathered siltstone (claystone) moist; very stiff	49.5

NOTES:
STRATIFICATION LINES REPRESENT THE APPROXIMATE BOUNDRY BETWEEN SOIL OR ROCK TYPES AT THE BOREHOLE LOCATION ONLY.

ENGINEERS FIELD BORING LOG

SHEET 3 OF 3
BORING NO. B-2

ASHLAND TANK COLLAPSE

PROJECT NO. _____ PROJECT LOCATION: L.R. _____; SEC. _____; CTY. _____

TEST PIT NO. _____ STATION _____ OFFSET _____ ELEVATION 775

DATE 1/28-29/98 EQUIPMENT USED [illegible]

ENGINEER [illegible] ENGINEERS REP. [illegible]

DRILLING METHODS HSA

WATER LEVEL DEPTH: _____ FEET ⊖ _____ HRS.; _____ FEET ⊖ _____ HRS.;

DEPTH (FT)	SAMPLE NO./TYPE OR RUN NO.	BLOWS/0.5 FT. ON SOIL SAMPLER	RECOVERY (IN)	RECOVERY (%) / ROD (%)	POCKET PENETROMETER (TSF)	DESCRIPTION	REMARKS
51.2	R-1		0.7'	50.0 / 0.0	—		RUN CONTAINED A FEW ½ TO 1 INCH ROUNDED ALLSTONE PEBBLES
	R-2		4.7'	94 / 0.0	—	GRAY, MEDIUM HARD SILTSTONE	
56.2							56.2 END OF BORING

GROUT MIX
- 1 LB CEMENT
- 6 LB BENTONITE
- 6 GAL WATER

USED 2 TYPES OF
½ BAG OF [illegible]
[illegible]

CAVED NOT REMOVE BOTTOM 25' OF AUGERS FROM BORING.

NOTES:
STRATIFICATION LINES REPRESENT THE APPROXIMATE BOUNDRY BETWEEN SOIL OR ROCK TYPES AT THE BOREHOLE LOCATION ONLY.

ENGINEERS FIELD BORING LOG

SHEET 1 OF 1
BORING NO. B-3

ASHLAND TANK FAILURE
PROJECT NO. _____ PROJECT LOCATION: L.R. _____; SEC. _____; CTY. _____
TEST PIT NO. _____ STATION _____ OFFSET _____ ELEVATION 771.96
DATE 2/29/88 EQUIPMENT USED SIMCO TRUCK B-6
ENGINEER GOULET FLEMING ENGINEERS REP. D. FRANCIS
DRILLING METHODS HSA
WATER LEVEL DEPTH: _____ FEET ⊖ _____ HRS.; _____ FEET ⊖ _____ HRS.;

DEPTH (FT)	SAMPLE NO./TYPE OR RUN NO.	BLOWS/0.5 FT. ON SOIL SAMPLER	RECOVERY (IN)	RECOVERY (%) / RQD (%)	POCKET PENETROMETER (TSF)	DESCRIPTION	REMARKS
							CASING 2.3' STICKUP GROUT INSIDE OF CASING WAS 5.2' FROM TOP OF CASING
6	S-1	1-3 3-3			0.6	BROWN AND GRAY SILTY CLAY (CL); MOIST 6-10' WAS MEDIUM STIFF; BELOW 10' STIFF	S-1,-2,-3 WERE MATRO WITH VOLCLAY GROUT
8	S-2	1-2 3-4			1.4		
10	S-3	1-4 8-12			3.0		
12	S-4	5-8 11-13			3.7		
14	S-5	1-3 5-9			2.2	BROWN [illegible] SAND [illegible]; MOIST [illegible]	14
16	S-6	3-6 6-11			1.9		
18							END OF BORING AT 18' HAD A DRY BOREHOLE DID NOT ENCOUNTER WATER TABLE IN B-3

NOTES:
STRATIFICATION LINES REPRESENT THE APPROXIMATE BOUNDRY BETWEEN SOIL OR ROCK TYPES AT THE BOREHOLE LOCATION ONLY.

ENGINEERS FIELD BORING LOG

SHEET 2 OF 2
BORING NO. B-4

Ashland Tank Failure
PROJECT NO. _____ PROJECT LOCATION: L.R. _____; SEC. _____; CTY. _____
TEST PIT NO. _____ STATION _____ OFFSET _____ ELEVATION 769.43
DATE _____ EQUIPMENT USED _____
ENGINEER _____ ENGINEERS REP. _____
DRILLING METHODS _____
WATER LEVEL DEPTH: _____ FEET @ _____ HRS.; _____ FEET @ _____ HRS.;

DEPTH (FT)	SAMPLE NO./TYPE OR RUN NO.	BLOWS/0.5 FT. ON SOIL SAMPLER	RECOVERY (IN)	RECOVERY (%) / ROD (%)	POCKET PENETROMETER (TSF)	DESCRIPTION	REMARKS
26						BROWN SILTY SAND & SANDY SILT (SM/ML); WET; LOOSE	
	U-2						
28							
	S-11	WOR 17-9					29
30						BROWN SILTY SAND AND GRAVEL (SM); WET; DENSE; SOME ROUNDED GRAVEL PARTICLES	
	S-12	13-13 13-13					
32							
	S-13	6-9 24-50					
34							
35	S-14	50/6					END OF BORING AT 35'. DRILLED & GROUTED HOLE IN SAME DAY

NOTES:
STRATIFICATION LINES REPRESENT THE APPROXIMATE BOUNDRY BETWEEN SOIL OR ROCK TYPES AT THE BOREHOLE LOCATION ONLY.

ENGINEERS FIELD BORING LOG

SHEET 1 OF 2
BORING NO. 35

ASHLAND TANK FAILURE

PROJECT NO. ________ PROJECT LOCATION: L.R. ______; SEC. ______; CTY. ______

TEST PIT NO. ________ STATION ________ OFFSET ________ ELEVATION 772.5

DATE 3/1 /88 EQUIPMENT USED SIMCO TRACK RIG

ENGINEER [illegible] ENGINEERS REP. [illegible]

DRILLING METHODS HSA, 2 INCH SPLIT SPOON

WATER LEVEL DEPTH: ~21.9 FEET @ ______ HRS.; ______ FEET @ ______ HRS.;

DEPTH (FT)	SAMPLE NO./TYPE OR RUN NO.	BLOWS/0.5 FT. ON SOIL SAMPLER	RECOVERY (IN)	RECOVERY (%) / RQD (%)	POCKET PENETROMETER (TSF)	DESCRIPTION	REMARKS
6 – 7.65	U-1					BROWN & GRAY SILTY CLAY (CL); MOIST [illegible]	SHELBY REC=1.6'=100%
7.65 – 9.65	S-1	9-16 20-34			4.8		3 TURNS OF ROPE AROUND CATHEAD.
10 – 12	S-2	10-18 23-26			4.5		
12 – 14	S-3	4-8 12-16			3.8		
14 – 16	S-4	3-5 7-9			2.9		
16 – 18	S-5	4-9 11-36			3.0	BROWN & GRAY SANDY SILTY CLAY (CL/ML), ALSO NUMEROUS THIN (~1 INCH) SILTY SAND LENSES; MOIST TO 22 FT & WET BELOW.	16
18 – 20	S-6	31-12 15-26			—		S-6 HAD POOR RECOVERY ~3 INCHES
20 – 22	S-7	12-7 8-12			1.6		BOTTOM 0.1' OF S-7 WET WITH A STRONG PETROLEUM ODOR
22 – 24	S-8	2-5 7-8			1.1		
24 – 26	S-9	2-4 6-6					

NOTES:
STRATIFICATION LINES REPRESENT THE APPROXIMATE BOUNDRY BETWEEN SOIL OR ROCK TYPES AT THE BOREHOLE LOCATION ONLY.

ENGINEERS FIELD BORING LOG

SHEET 2 OF 2
BORING NO. B-5

ASHLAND TANK FAILURE

PROJECT NO. _____ PROJECT LOCATION: L.R. _____; SEC. _____; CTY. _____

TEST PIT NO. _____ STATION _____ OFFSET _____ ELEVATION 772.5

DATE 3/1/88 EQUIPMENT USED _____

ENGINEER _____ ENGINEERS REP. _____

DRILLING METHODS _____

WATER LEVEL DEPTH: _____ FEET ⊖ _____ HRS.; _____ FEET ⊖ _____ HRS.;

DEPTH (FT)	SAMPLE NO./TYPE OR RUN NO.	BLOWS/0.5 FT. ON SOIL SAMPLER	RECOVERY (IN)	RECOVERY (%) / RQD (%)	POCKET PENETROMETER (TSF)	DESCRIPTION	REMARKS
26							
	U-2						
27.9							EOB AT 27.9
							DRILLED & GROUTED HOLE ON OLDE DAY

NOTES:
STRATIFICATION LINES REPRESENT THE APPROXIMATE BOUNDRY BETWEEN SOIL OR ROCK TYPES AT THE BOREHOLE LOCATION ONLY.

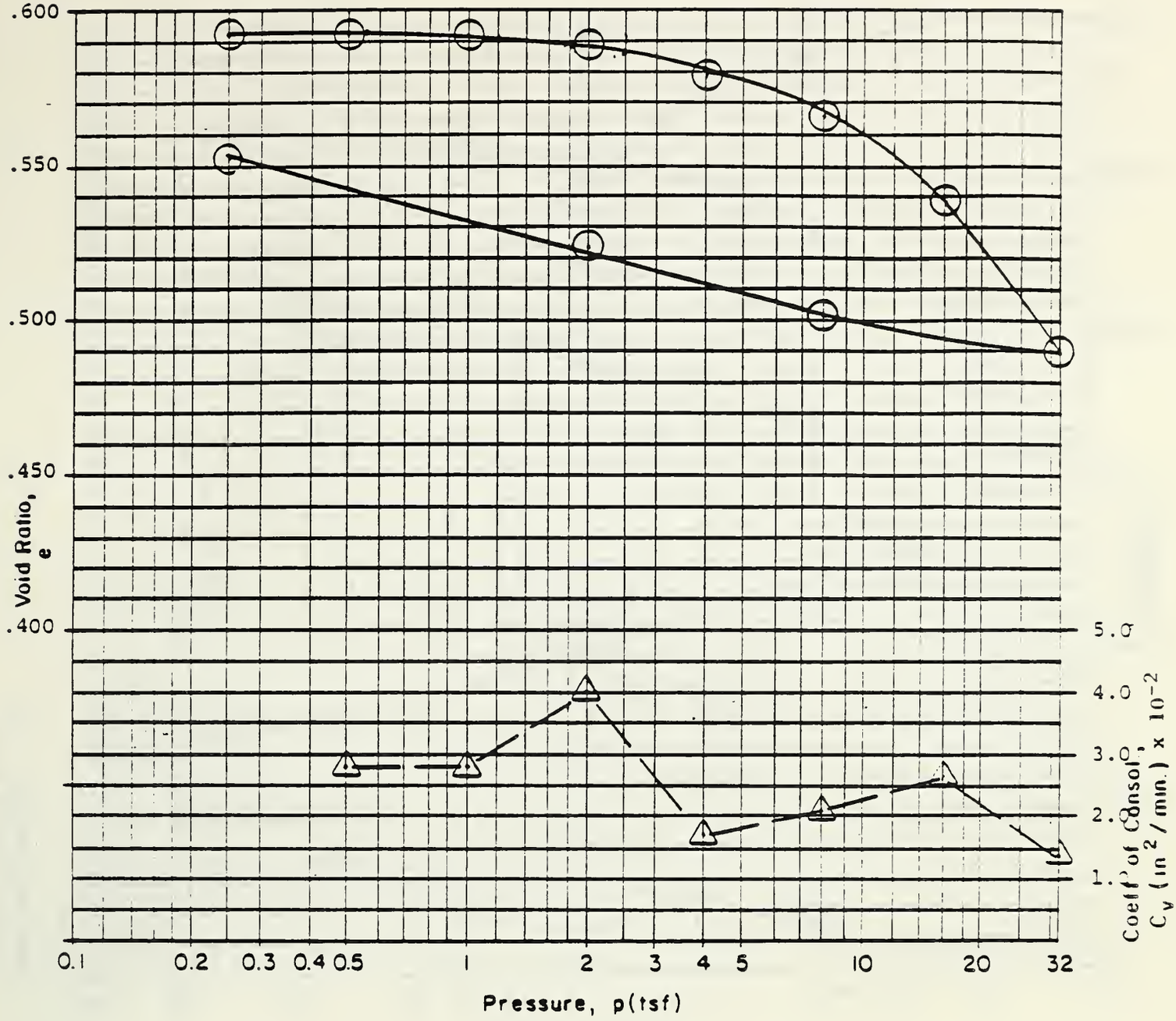

Type of Specimen	Shelby			Before Test			After Test
Dia 2.50 in	H_T	0.75 in		Water Content	w_o	18.9	w_f 20.1
Compression Index	C_c	0.16		Void Ratio	e_o	0.592	e_f 0.553
Classification	CL			Saturation	S_o	87.7	S_f 100.0
w_l 48.6	I_p	25.5		Project	ASHLAND TANK FAILURE		
w_p 23.1	LI	-0.16		Boring No	B-5	Sample No	U-1
Remarks Wet Unit Wt. = 128.2 PCF. Specimen required a seating load of 0.20 TSF to prevent swelling.				Depth	6.0'-7.6'	Date	4/88

GANNETT FLEMING GEOTECHNICAL LABORATORY
CONSOLIDATION TEST REPORT

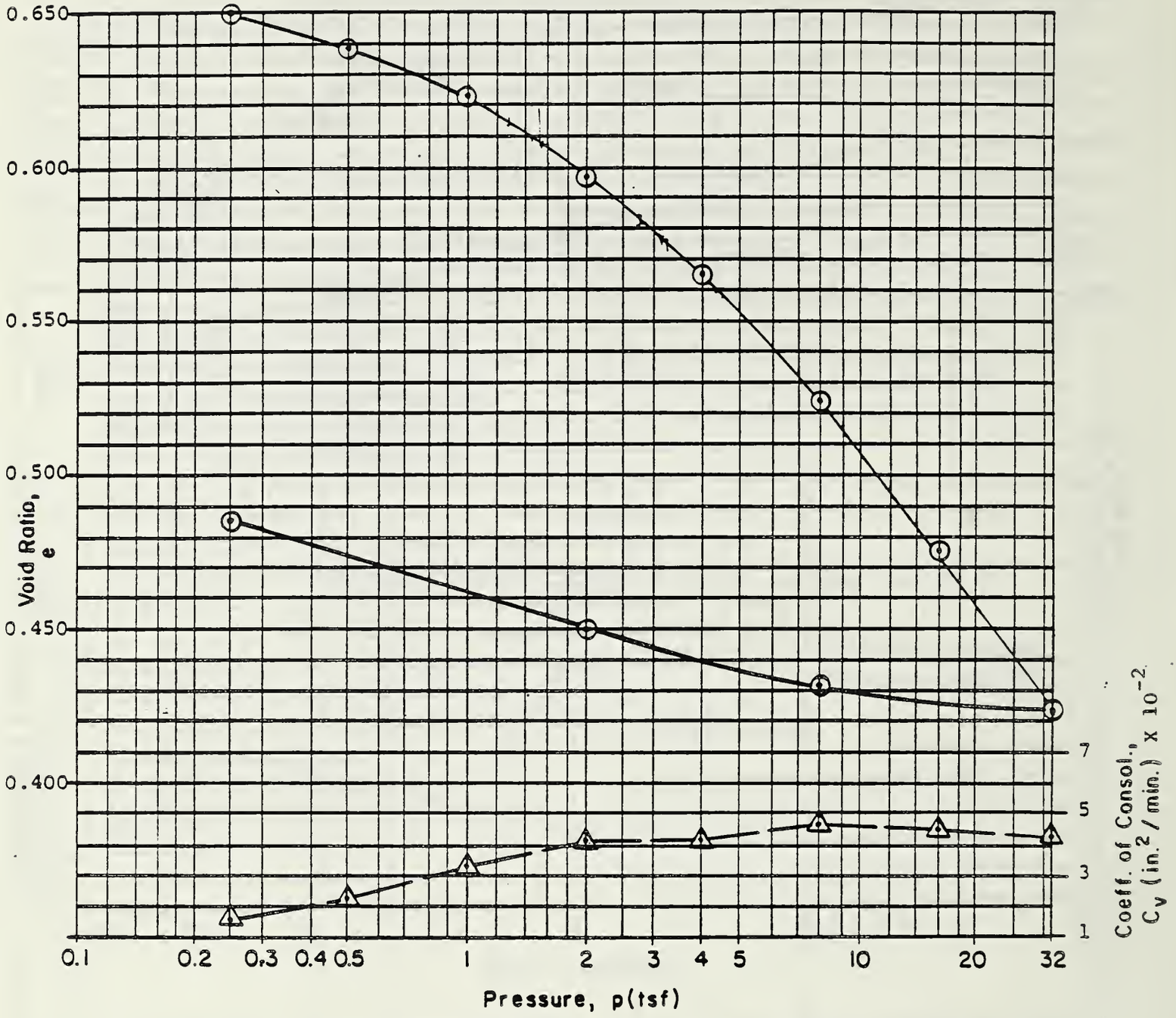

Type of Specimen			Shelby	Before Test				After Test	
Dia	2.50 in	H_T	0.75 in	Water Content	w_o	23.6		w_f	17.9
Compression Index		C_c	0.17	Void Ratio	e_o	0.668		e_f	0.487
Classification		CL		Saturation	S_o	96.0		S_f	100
w_l	25.2	I_p	7.5	Project	ASHLAND TANK FAILURE				
w_p	17.7	LI	0.79	Boring No	B-5		Sample No	U-2	
Remarks	Wet density= 125.8pcf			Depth	26-27.9'		Date	4/88	

GANNETT FLEMING GEOTECHNICAL LABORATORY
CONSOLIDATION TEST REPORT

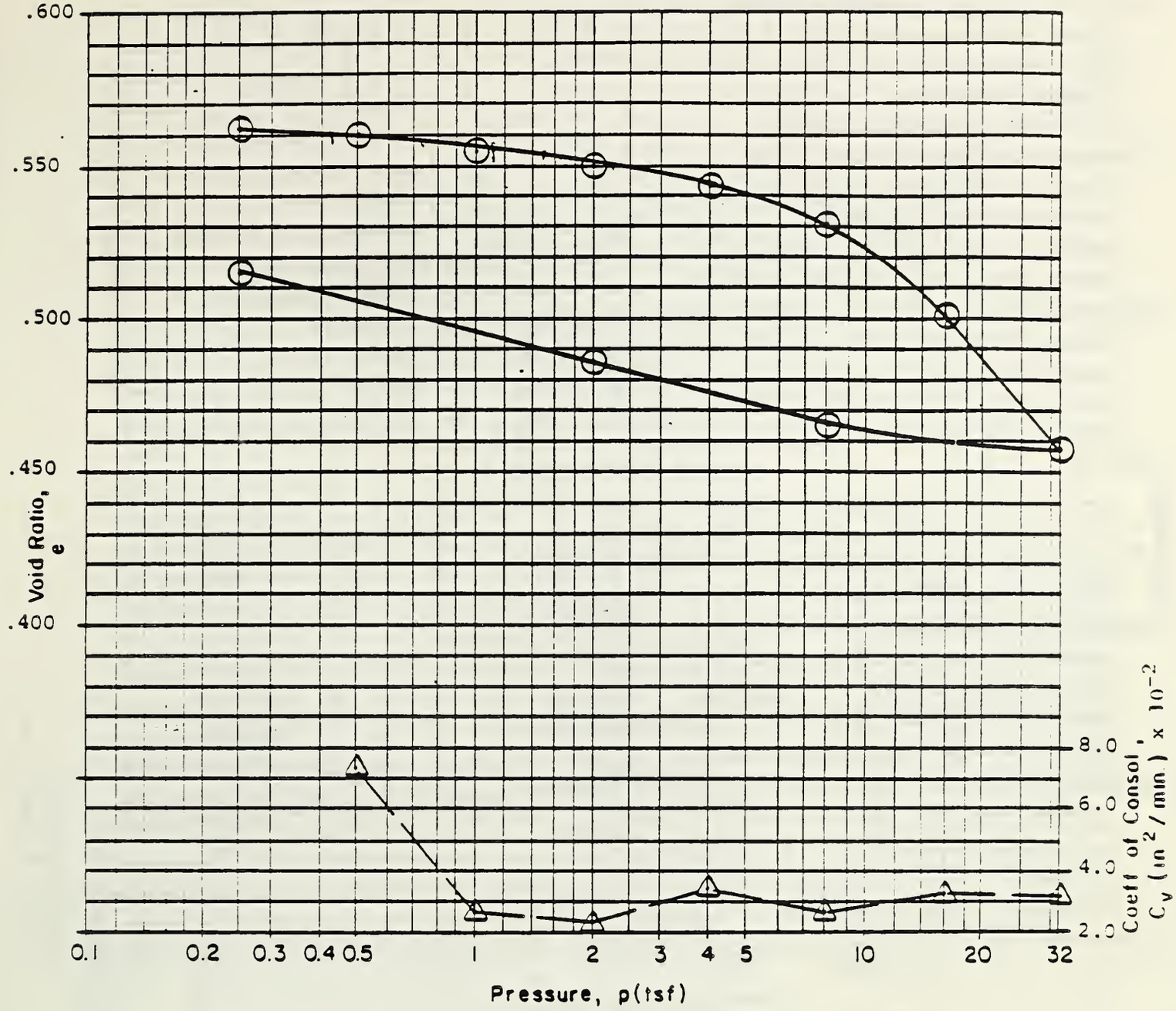

Type of Specimen	Shelby			Before Test			After Test	
Dia	2.50 in	H_T	0.75 in	Water Content	w_o	17.8	w_f	18.8
Compression Index	C_c	0.14		Void Ratio	e_o	0.566	e_f	0.516
Classification	CL			Saturation	S_o	86.7	S_f	100.0
w_l	48.5	I_p	23.2	Project	ASHLAND TANK FAILURE			
w_p	25.3	LI	-0.32	Boring No	B-4		Sample No	U-1
Remarks				Depth	4.0'-6.0'		Date	4/88
Wet Unit Wt. = 129.2 PCF				GANNETT FLEMING GEOTECHNICAL LABORATORY CONSOLIDATION TEST REPORT				

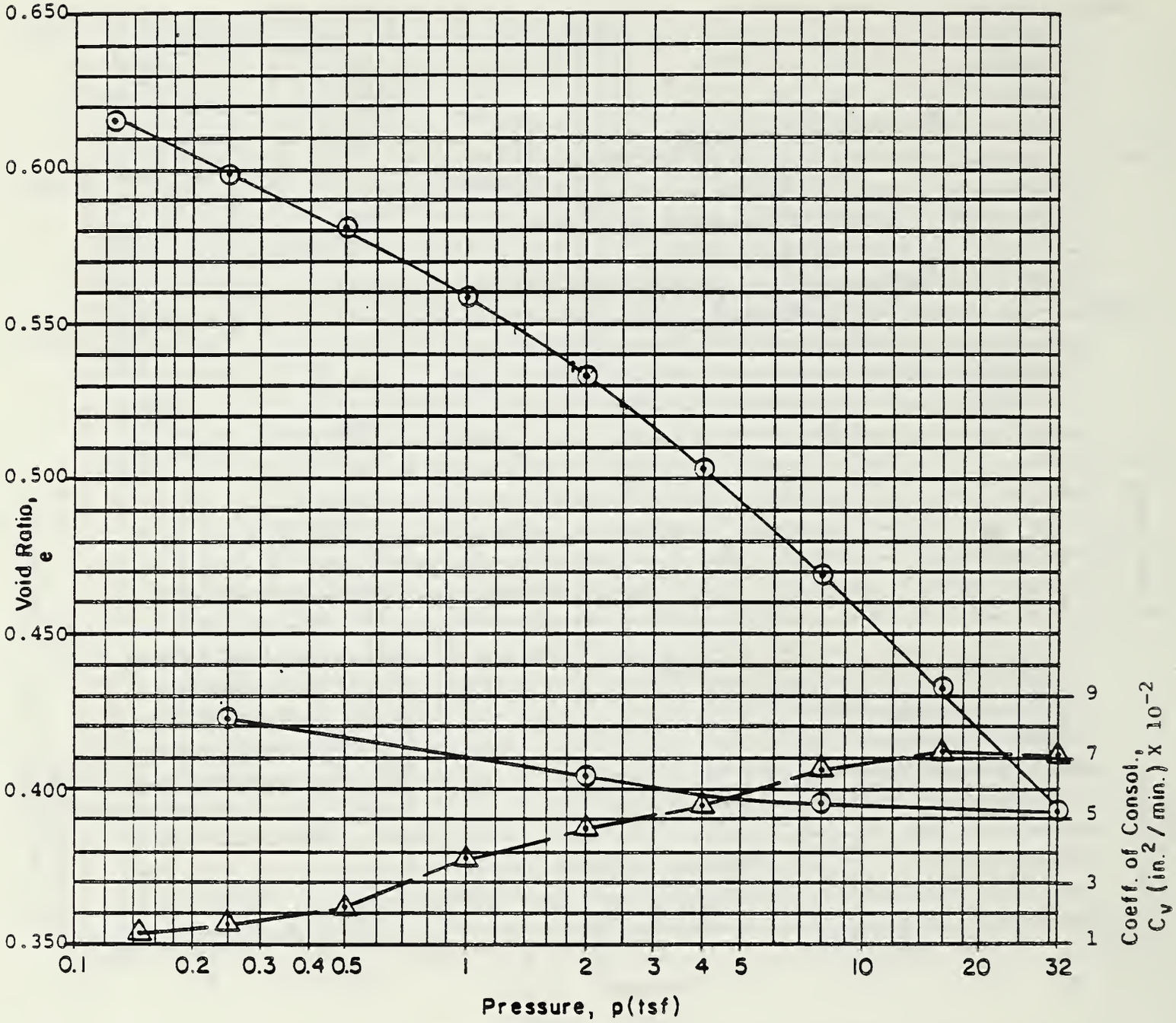

Type of Specimen		Shelby			Before Test			After Test	
Dia	2.50 in	H_T	0.75 in		Water Content	w_o	23.1	w_f	14.8
Compression Index		C_c	0.13		Void Ratio	e_o	0.646	e_f	0.423
Classification		ML			Saturation	S_o	97.2	S_f	95.3
w_l	22.9	I_p	5.3		Project	ASHLAND TANK FAILURE			
w_p	17.6	LI	1.2		Boring No	B-4		Sample No	U-2
Remarks	Wet density= 127.0pcf				Depth	26-28'		Date	4/88

GANNETT FLEMING GEOTECHNICAL LABORATORY
CONSOLIDATION TEST REPORT

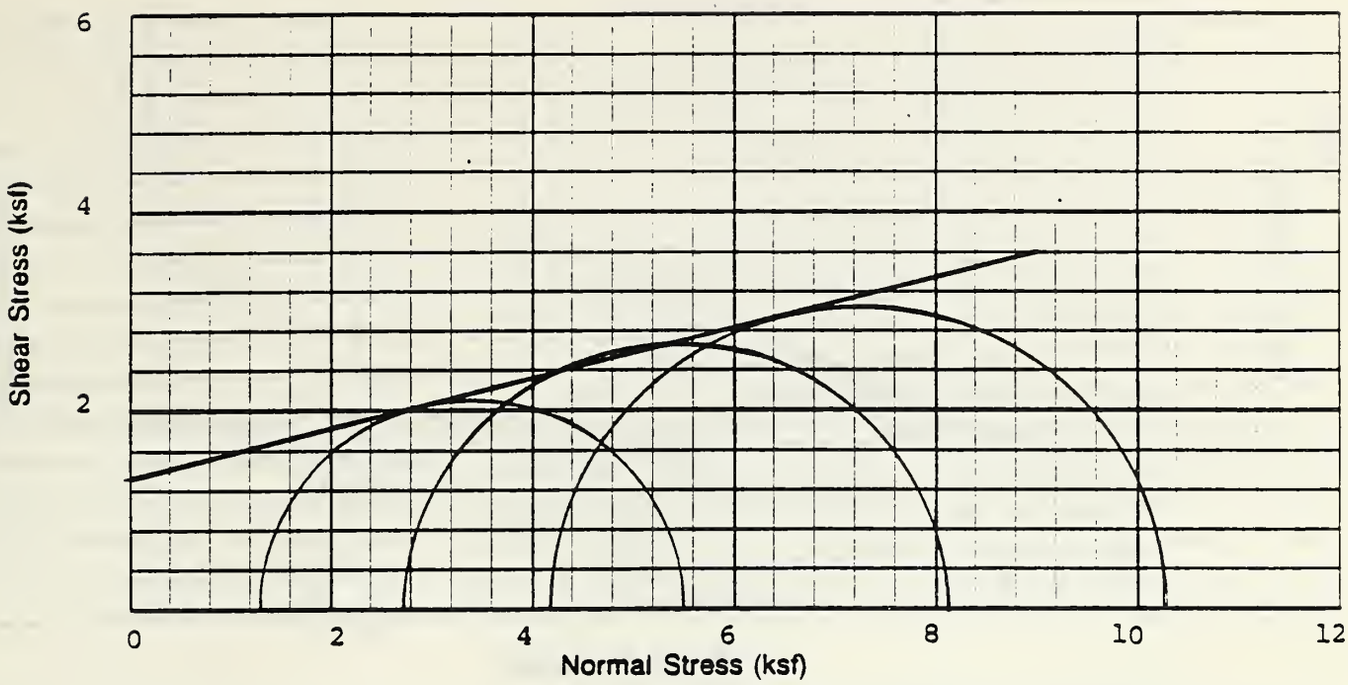

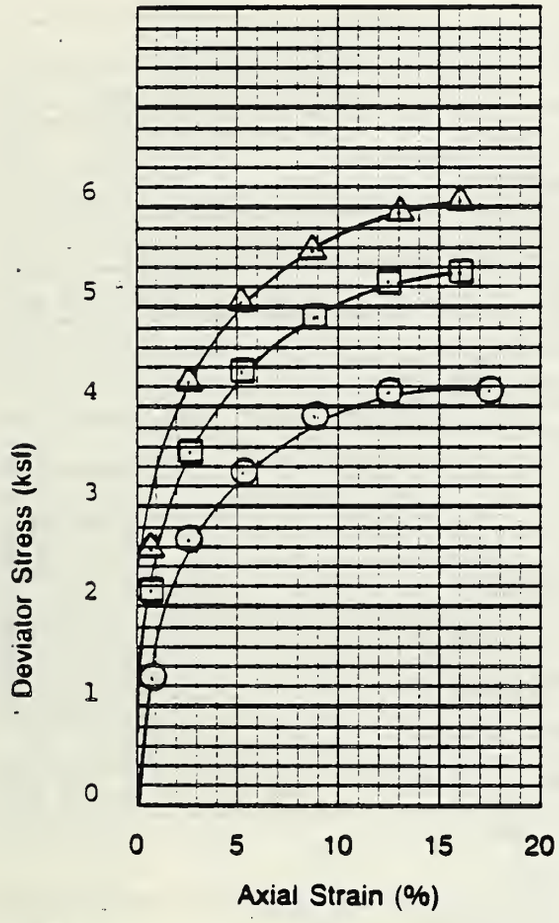

Remarks: _____

Specimen No			1	2	3
Diameter (in)		D_o	2.82	2.82	2.82
Height (in)		H_o	5.59	5.60	5.59
Initial	Water Content (%)	w_o	16.8	16.2	16.5
Initial	Dry Density (pcf)	γ_{do}	111.9	112.3	111.8
Initial	Void Ratio	e_o	0.534	0.528	0.535
Initial	Saturation (%)	S_o	86.6	84.4	84.8
Before Test	Water Content (%)	w_c	—	—	—
Before Test	Dry Density (pcf)	γ_{dc}	—	—	—
Before Test	Void Ratio	e_c	—	—	—
Before Test	Saturation (%)	S_c	—	—	—
Before Test	Back Pressure (ksf)	μ_B	0	0	0
Total Minor Princ Stress (ksf)		σ_3	1.27	2.71	4.15
Maximum Deviator Stress (ksf)		P/A	4.16	5.34	6.02
Time Max Deviator Stress		t_f	21	21	21
Total Major Princ Stress (ksf)		σ_1	5.43	8.05	10.17
Pore Pressure at Max Deviator Stress (ksf)		μ	—	—	—
Eff Minor Princ Stress (ksf)		σ_3'	—	—	—
Eff Major Princ Stress (ksf)		σ_1'	—	—	—

Project ASHLAND TANK FAILURE	Boring No D-1,2,3	Sample No
Type of Test: Unconsolidated-Undrained		Sample Type: Remolded
c = 1.3 ksf	ϕ = 14.5 °	c' = — ksf	ϕ' = — °

GANNETT FLEMING GEOTECHNICAL LABORATORY
TRIAXIAL COMPRESSION TEST REPORT

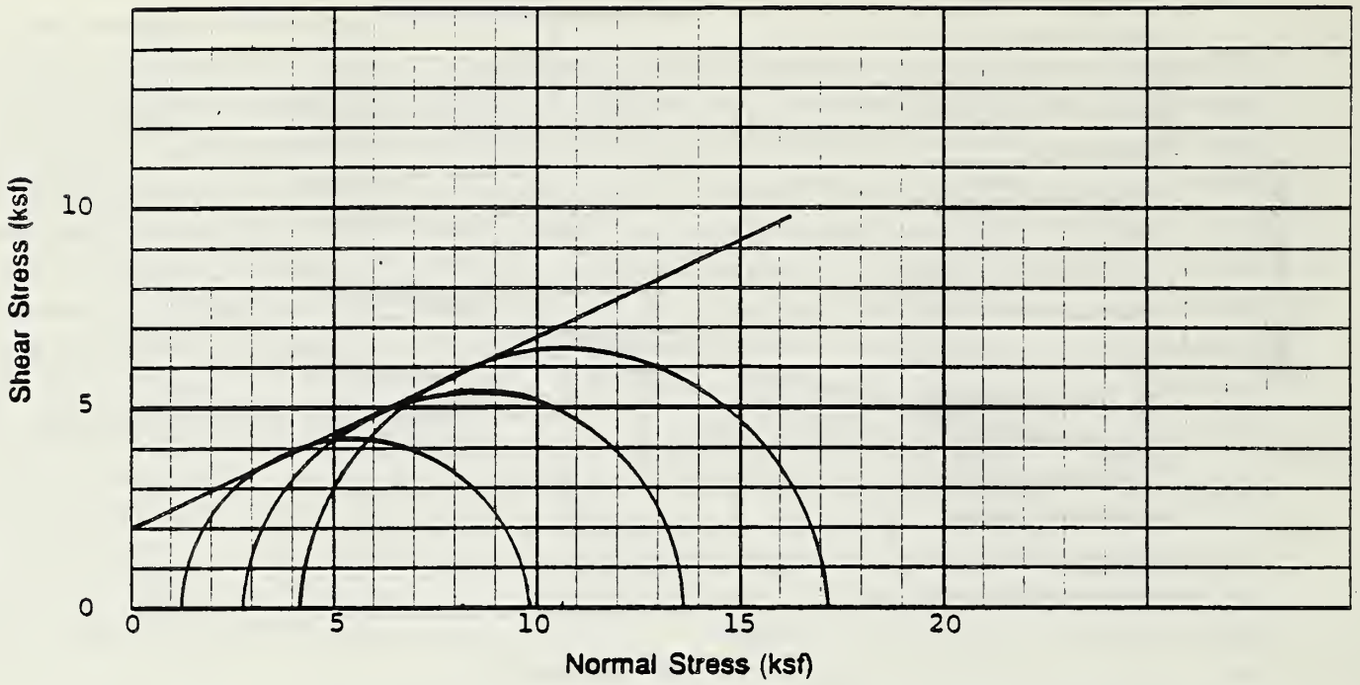

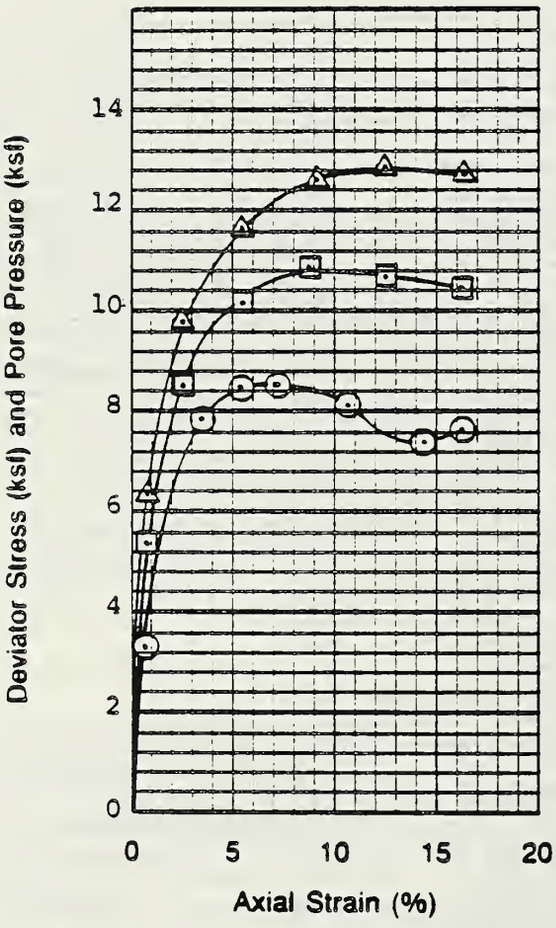

Remarks: _____

Specimen No			1	2	3
Diameter (in)		D_o	2.83	2.83	2.83
Height (in)		H_o	5.60	5.60	5.60
Initial	Water Content (%)	w_o	14.3	14.3	13.7
Initial	Dry Density (pcf)	γ_{do}	116.4	116.2	117.4
Initial	Void Ratio	e_o	0.474	0.477	0.463
Initial	Saturation (%)	S_o	82.9	82.4	81.3
Before Test	Water Content (%)	w_c	-	-	-
Before Test	Dry Density (pcf)	γ_{dc}	-	-	-
Before Test	Void Ratio	e_c	-	-	-
Before Test	Saturation (%)	S_c	-	-	-
Before Test	Back Pressure (ksf)	μ_B	-	-	-
Total Minor Princ Stress (ksf)		σ_3	1.27	2.71	4.15
Maximum Deviator Stress (ksf)		P/A	8.53	10.85	12.89
Time Max Deviator Stress		t_f	10	13	18
Total Major Princ Stress (ksf)		σ_1	9.80	13.56	17.04
Pore Pressure at Max Deviator Stress (ksf)		μ	-	-	-
Eff Minor Princ Stress (ksf)		σ_3'	-	-	-
Eff Major Princ Stress (ksf)		σ_1'	-	-	-

Project ASHLAND TANK FAILURE	Boring No D-1,2,3	Sample No	
Type of Test: Unconsolidated-Undrained		Sample Type: Remolded	
c = 2.00 ksf	ϕ = 26.0 °	c' = - ksf	ϕ' = - °

GANNETT FLEMING GEOTECHNICAL LABORATORY
TRIAXIAL COMPRESSION TEST REPORT

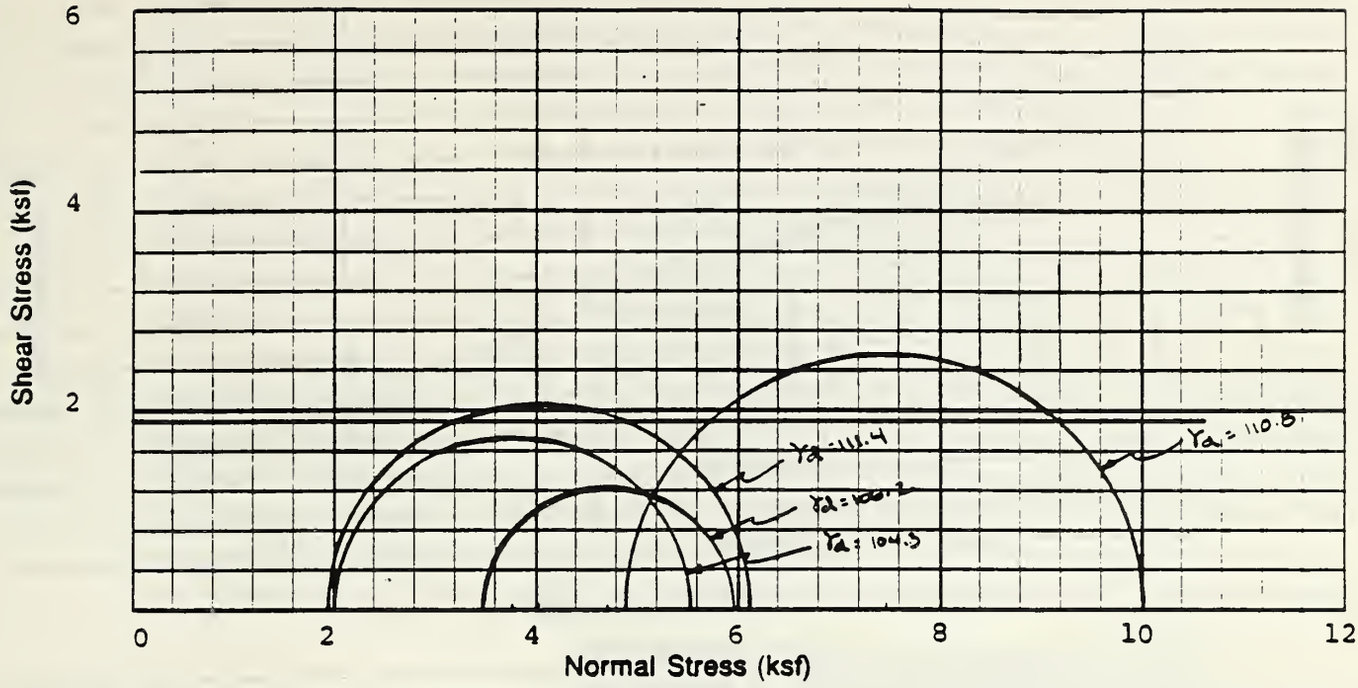

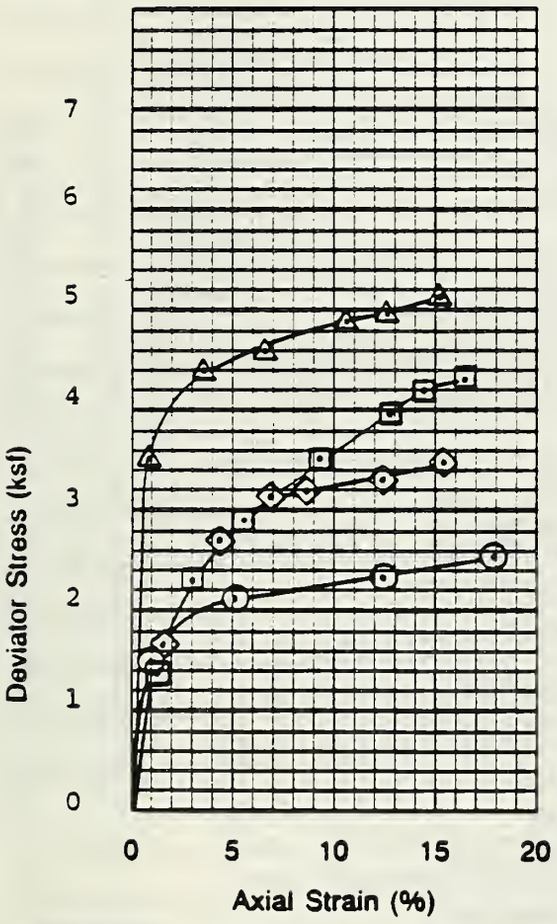

Specimen No			1	2	3
Diameter (in)		D_o	2.83	2.83	2.85
Height (in)		H_o	5.60	5.59	5.60
Initial	Water Content (%)	w_o	19.3	19.4	20.0
	Dry Density (pcf)	γ_{do}	106.2	111.4	104.3
	Void Ratio	e_o	0.617	0.540	0.645
	Saturation (%)	S_o	86.1	98.7	85.1
Before Test	Water Content (%)	w_c	—	—	—
	Dry Density (pcf)	γ_{dc}	—	—	—
	Void Ratio	e_c	—	—	—
	Saturation (%)	S_c	—	—	—
	Back Pressure (ksf)	μ_B	11.52	11.61	11.52
Total Minor Princ Stress (ksf)		σ_3	3.43	1.90	1.99
Maximum Deviator Stress (ksf)		P/A	2.45	4.24	3.45
Time Max Deviator Stress		t_f	120	120	120
Total Major Princ Stress (ksf)		σ_1	5.88	6.14	5.44
Pore Pressure at Max Deviator Stress (ksf)		μ	2.36	0.38	0.49
Eff Minor Princ Stress (ksf)		σ_3'	—	—	—
Eff Major Princ Stress (ksf)		σ_1'	—	—	—

Remarks: Max. Deviator Stress taken at 15% strain; Specimens 1 & 2 taken from S-4, and 3 & 4 from S-5

Project ASHLAND TANK FAILURE		Boring No S-4, S-5	Sample No U-1
Type of Test: Saturated-Unconsolidated-Undrained		Sample Type: Shelby	
c = 1.9 ksf	ϕ = 0.0 °	c' = - ksf	ϕ' = - °

GANNETT FLEMING GEOTECHNICAL LABORATORY
TRIAXIAL COMPRESSION TEST REPORT

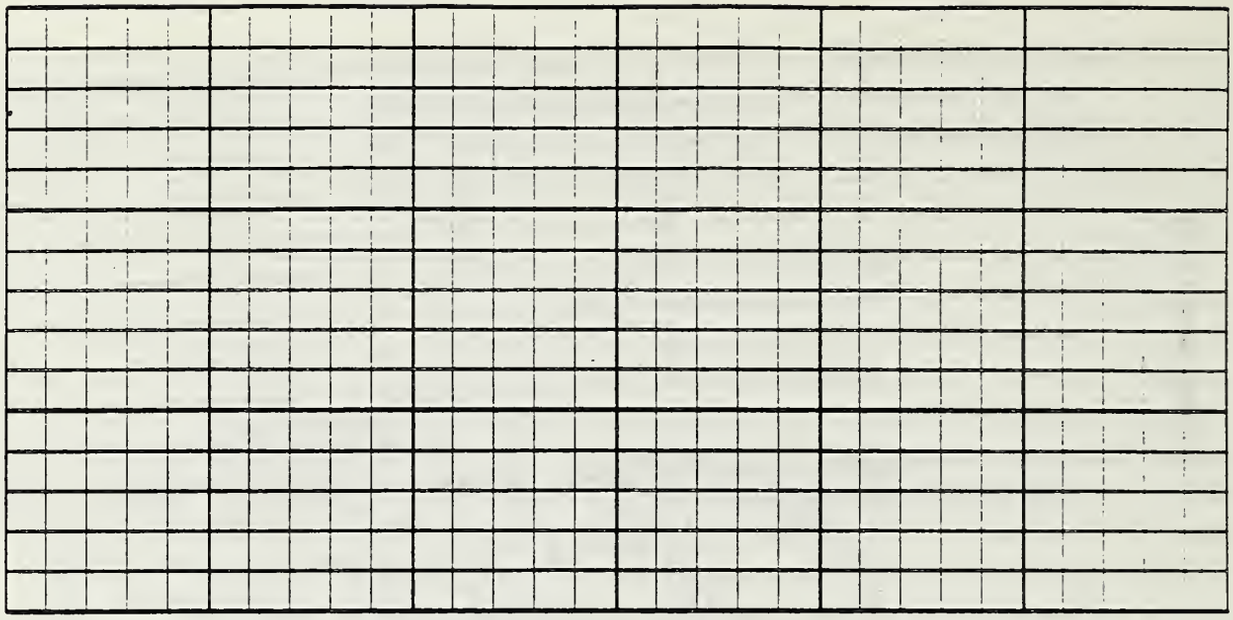

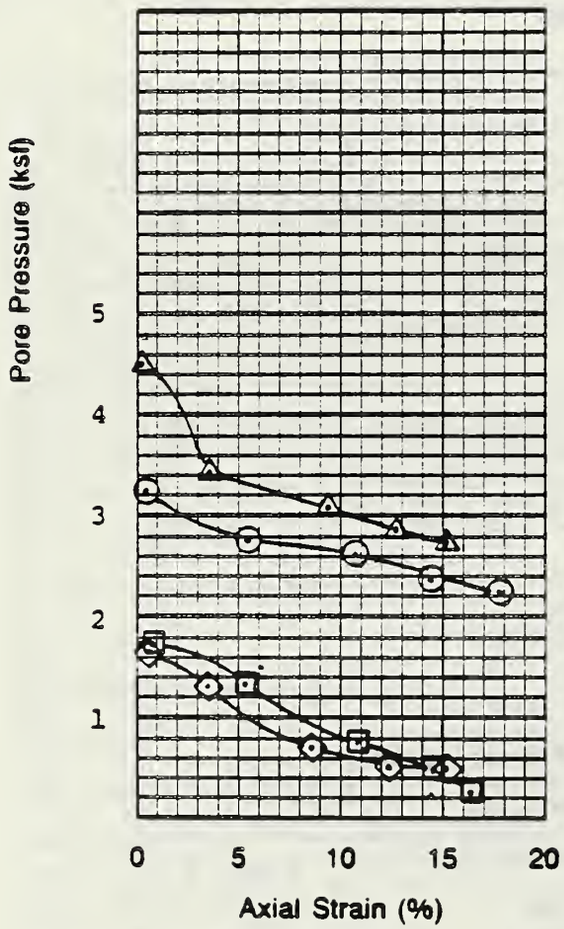

Remarks: Max. Deviator Stress taken at 15% strain

Specimen No			4		
Diameter (in)		D_o	2.83		
Height (in)		H_o	5.60		
Initial	Water Content (%)	w_o	17.4		
	Dry Density (pcf)	γ_{do}	110.8		
	Void Ratio	e_o	0.549		
	Saturation (%)	S_o	87.2		
Before Test	Water Content (%)	w_c	—		
	Dry Density (pcf)	γ_{dc}	—		
	Void Ratio	e_c	—		
	Saturation (%)	S_c	—		
	Back Pressure (ksf)	μ_B	11.52		
Total Minor Princ Stress (ksf)		σ_3	4.87		
Maximum Deviator Stress (ksf)		P/A	5.05		
Time Max Deviator Stress		t_f	120		
Total Major Princ Stress (ksf)		σ_1	9.92		
Pore Pressure at Max Deviator Stress (ksf)		μ	2.75		
Eff Minor Princ Stress (ksf)		σ_3'	—		
Eff Major Princ Stress (ksf)		σ_1'	—		

Project ASHLAND TANK FAILURE	Boring No S-4, S-5	Sample No U-1	
Type of Test: Saturated-Unconsolidated-Undrained		Sample Type: Shelby	
c = _____ ksf	ϕ = _____ °	c' = _____ ksf	ϕ' = _____ °

GANNETT FLEMING GEOTECHNICAL LABORATORY

TRIAXIAL COMPRESSION TEST REPORT

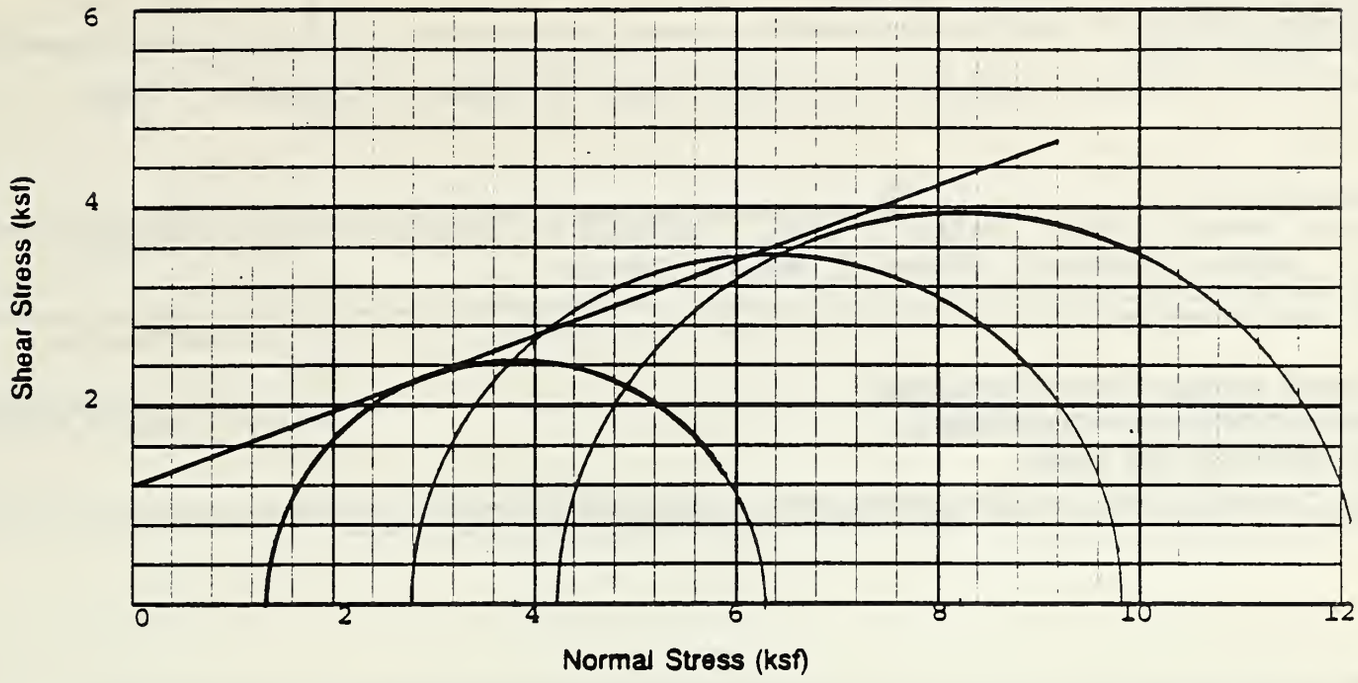

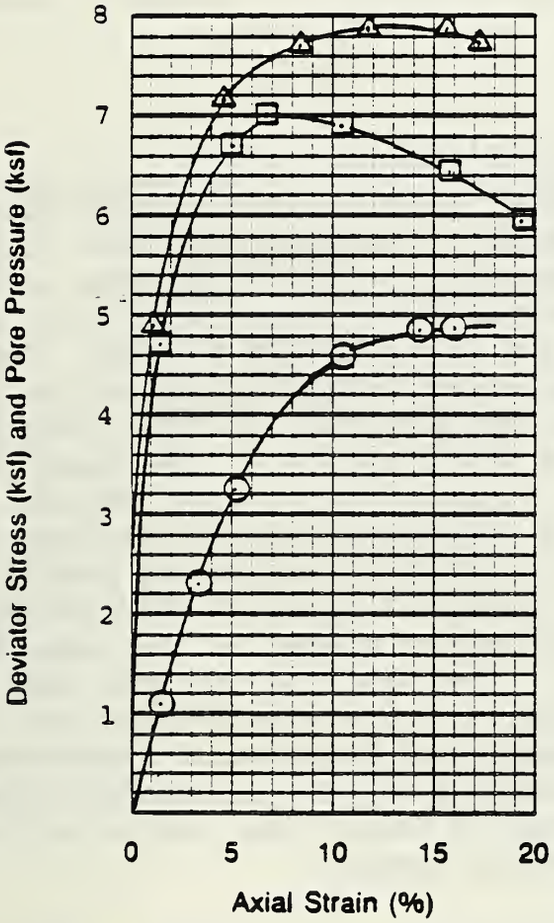

Remarks: _____

Specimen No			1	2	3
Diameter (in)		D_o	2.83	2.85	2.83
Height (in)		H_o	5.60	5.60	5.60
Initial	Water Content (%)	w_o	21.1	19.9	20.6
Initial	Dry Density (pcf)	γ_{do}	104.7	105.1	104.2
Initial	Void Ratio	e_o	.640	.633	.647
Initial	Saturation (%)	S_o	90.7	86.4	87.6
Before Test	Water Content (%)	w_c	--	--	--
Before Test	Dry Density (pcf)	γ_{dc}	--	--	--
Before Test	Void Ratio	e_c	--	--	--
Before Test	Saturation (%)	S_c	--	--	--
Before Test	Back Pressure (ksf)	μ_B	1.44	1.44	1.44
Total Minor Princ Stress (ksf)		σ_3	1.31	2.71	4.19
Maximum Deviator Stress (ksf)		P/A	4.87	7.00	7.88
Time Max Deviator Stress		t_f	45	19	33
Total Major Princ Stress (ksf)		σ_1	6.19	9.71	12.07
Pore Pressure at Max Deviator Stress (ksf)		μ	—	—	—
Eff Minor Princ Stress (ksf)		σ_3'	--	—	—
Eff Major Princ Stress (ksf)		σ_1'	--	--	--

Project ASHLAND TANK FAILURE	Boring No S-5a		Sample No U-1
Type of Test: Unconsolidated-Undrained		Sample Type: Shelby	
c = 1.20 ksf	ϕ = 21.0 °	c' = - ksf	ϕ' = - °

GANNETT FLEMING GEOTECHNICAL LABORATORY
TRIAXIAL COMPRESSION TEST REPORT

NBS-114A (REV. 2-8C)

U.S. DEPT. OF COMM. BIBLIOGRAPHIC DATA SHEET (See instructions)	1. PUBLICATION OR REPORT NO. NBSIR 88-3792	2. Performing Organ. Report No.	3. Publication Date JUNE 1988

4. TITLE AND SUBTITLE

Investigation into the Ashland Oil Storage Tank Collapse on January 2, 1988

5. AUTHOR(S) John L. Gross, Felix Y. Yokel, Richard N. Wright, A. Hunter Fanney, John H. Smith, George E. Hicho, T. Robert Shives

6. PERFORMING ORGANIZATION (If joint or other than NBS, see instructions)

NATIONAL BUREAU OF STANDARDS
U.S. DEPARTMENT OF COMMERCE
GAITHERSBURG, MD 20899

7. Contract/Grant No.

8. Type of Report & Period Covered

9. SPONSORING ORGANIZATION NAME AND COMPLETE ADDRESS (Street, City, State, ZIP)

10. SUPPLEMENTARY NOTES

☐ Document describes a computer program; SF-185, FIPS Software Summary, is attached.

11. ABSTRACT (A 200-word or less factual summary of most significant information. If document includes a significant bibliography or literature survey, mention it here)

On January 2, 1988, a four million gallon capacity oil storage tank at the Ashland Petroleum Company Floreffe Terminal near West Elizabeth, Pennsylvania, collapsed as it was being filled to capacity for the first time since it was reconstructed at the site. The tank had been dismantled in Cleveland, Ohio, after more than 40 years of service and reconstructed at the Floreffe Site in 1986. The National Bureau of Standards (NBS) conducted an independent investigation of the physical causes of the Ashland Tank collapse. Data were obtained from NBS field observations, laboratory and analytical studies, from the investigation of the Pennsylvania Tank Collapse Task Force appointed by the Governor of Pennsylvania, and from the Battelle Columbus Division investigation sponsored by the Ashland Petroleum Company. The cause of the failure was determined to be brittle fracture, initiating from a flaw existing prior to the reconstruction of the tank. Complete rupture of the tank shell occurred because the steel of the shell was of inadequate toughness at the operating temperature to prevent brittle fracture propagation. The steel did not meet the fracture toughness requirements of the American Petroleum Institute Standard 650, 1984, "Welded Steel Tanks for Oil Storage," which was effective at the time of reconstruction of the tank. The collapse shows the importance of using steel with sufficient fracture toughness to prevent propagation of a brittle fracture in tanks whose sudden failure would mean unacceptable human, environmental or economic losses.

12. KEY WORDS (Six to twelve entries; alphabetical order; capitalize only proper names; and separate key words by semicolons)
Brittle fracture; collapse; failure investigation; fracture analysis; steel; tanks; welded steel tanks

13. AVAILABILITY

☒ Unlimited

☐ For Official Distribution. Do Not Release to NTIS

☐ Order From Superintendent of Documents, U.S. Government Printing Office, Washington, D.C. 20402.

☒ Order From National Technical Information Service (NTIS), Springfield, VA. 22161

14. NO. OF PRINTED PAGES
204

15. Price
$24.95

USCOMM-DC 6043-P80